Defective Iron Homeostasis in Lysosomal Storage Diseases

Chun-Wu (Oscar) Chen

Balliol College, Department of Pharmacology

Trinity Term, 2013

A Thesis Submitted to the Board of the Faculty of Medical Science, University of Oxford, in Partial Fulfilment of the Requirements for the Degree of Doctor of Philosophy

Defective Iron Homeostasis in Lysosomal Storage diseases

Oscar C.W Chen, Balliol College, D.Phil Thesis, Trinity Term, 2013

ABSTRACT

Niemann-Pick type C1 (NPC1) disease is a neurodegenerative lysosomal storage disorder characterized by the accumulation of multiple lipids in the late endosome/lysosomal system and reduced acidic store calcium levels. Since the lysosomal system is involved in regulating aspects of transition metal ion homeostasis and its intracellular compartmentalization, we have investigated whether there are metal ion metabolism defects and haematological abnormalities in NPC1 disease. We have identified multiple haematological changes, including decreased haematocrit, haemoglobin and mean corpuscular haemoglobin volume in *Npc1*$^{-/-}$ mice. Similar haematological changes with low normal serum iron levels as well as low normal haematocrit, haemoglobin, mean corpuscular volume and mean corpuscular haemoglobin were observed in NPC1 patients, suggesting that NPC1 patients are at risk of iron deficiency. Furthermore, decreased levels of serum iron, transferrin saturation, elevated levels of serum copper and ceruloplasmin and up-regulated expression of soluble transferrin receptor (s-TfR), ferritin levels in *Npc1*$^{-/-}$ mice and NPC1 patients were observed. Additionally, up-regulation of hepatic transferrin receptor, down-regulation of hepatic hepcidin and altered expression of multiple copper and zinc transporters were also found in *Npc1*$^{-/-}$ mice. These data demonstrate that systemic metal dyshomeostasis, intracellular metal compartmentalization defects and impaired erythropoiesis occur in NPC1 disease. As transition metal dyshomeostasis may be involved in the pathogenesis of NPC1 disease, we hypothesized this may represent a novel therapeutic intervention point for adjunctive therapy. To test this hypothesis, we have evaluated several metal manipulation treatments, including metal supplementation, metal chelation and metal ionophore treatments, in *Npc1*$^{-/-}$ mice. Our results revealed that (i) iron supplementation, (ii) reduced copper absorption reagent (iii) and copper/zinc ionophore therapies significantly either improved haematological abnormalities, neurological/motor functions or survival in *Npc1*$^{-/-}$ mice. These data suggest that metal-targeted therapies may be useful adjunctive therapies in NPC1 disease patients.

Abbreviations

ALAS	δ-aminolevulinate synthase
ASM	Acid sphingomyelinase
β-gal$^{-/-}$	β-galactosidase, GM1 gangliosidosis
BMP	Bone morphogenetic protein
CHS	Chediak-Higashi syndrome
CRP	Collagen related peptide
CSF	Cerebrospinal fluid
DAPI	4',6-diamidino-2-phenylindole
DFO	Deferoxamine
DMT-1	Divalent metal transporter -1
EPO	Erythropoietin
Epo-R	Erythropoietin receptor
FAC	Ferric ammonium citrate
FPN	Ferroportin
Fe-S	Iron-Sulfur
GPN	Gly–Phe–β-naphtylamide
Gpx3	Glutathione peroxidase 3
GSH	Glutathione
HCT	Hematocrit
HF	Human fibroblast
HIFs	Hypoxia-inducible factors
HPS	Hermansky-Pudlak syndrome
HGB	Hemoglobin
IRP	Iron regulatory protein
IL-6	Interleukin-6
IL-1β	Interleukin-1 beta
IL-1α	Inteleukin-1 alpha
ICP-MS	Inductively Coupled Plasma Mass Spectrometry
LROs	Lysosome-related organelles
LSDs	Lysosomal storage diseases
MCH	Mena corpuscular hemoglobin
MCHC	Mean corpuscular hemoglobin concentration
MCV	Mean corpuscular volume

MLIV	Mucolipidosis type IV
MNK	Menke's disease
MPV	Mean platelet volume
MT	Metallothionein
NAADP	Nicotinic acid-adenine dinucleotide phosphate
NPA	Niemann-Pick type A
NPB	Niemann-Pick type B
NPC1	Niemann-Pick type C1
NPC2	Niemann-Pick type C2
NSM	Neutral sphingomyelinase
PBS	Phosphate buffered saline
PCT	Plateletcrit
PLT	Platelet count
PRP	Platelet rich plasma
qRT-PCR	Quantative real time polymerase chain reaction
RBC	Red blood cell
RND	Resistance-Nodulation-Cell Division
S1P	Sphingosine-1-phosphate
SDS	Sodium dodecyl sulfate
SOD	Superoxide dismutase
SPHKs	Sphingosine kinases
s-TfR	Soluble form transferrin receptor
TfR-1	Transferrin Receptor-1
TfR-2	Transferrin Receptor-2
TIBC	Total iron-binding capacity
TMPRSS6	Transmembrane protease, serine 6
TNF-α	Tumor necrosis factor alpha
TPCs	Two Pore Channels
UIBC	Unbound iron-binding capacity
vWF	von Willebrand factor
WND	Wilson's disease
WPBs	Weibel-Palade bodies

Table of Contents

Chapter 1: General Introduction

1.1.1 General introduction 1
1.1.1 The lysosome 2
1.1.2 The function of lysosome related organelles 3
1.1.2.1 The function of lysosome related organelles in platelets 4
1.1.2.2 Lysosome related organelles and lysosome related organelles disorders 5
1.1.3 Lysosoaml storage diseases 5
1.1.4 Niemann-Pick type C1 disease 7

1.1.2 Systemic iron homeostasis 8
1.1.2.1 Iron absorption 9
1.1.2.2 Iron recycling 9

1.1.3 Systemic iron homeostasis: the iron regulator hormone hepcidin 11
1.1.3.1 Regulation by systemic iron availability 11
1.1.3.2 Regulation by inflammatory and stress signals 13
1.1.3.3 Regulation by erythropoietic signals 13

1.2 Cellular Iron regulation 14
1.2.1 Lysosome mediated iron-related metabolism 16
1.2.2 Mitochondria-mediated subcellular iron homeostasis 18

1.3 Systemic and cellular copper regulation 19
1.3.1 Regulation of copper transport via trafficking 19
1.3.2 Intestinal copper absorption 21
1.3.3 Hepatic copper storage and excretion 22

1.4 Aim of this thesis 24

Chapter 2: Defective iron homeostasis and hematological abnormalities in Niemann-Pick type C1 disease mice and their clinical implications

2.1 Introduction 26
2.1.1 Systemic iron regulation 26
2.1.2 The role of the lysosome in cellular iron metabolism 26
2.1.3 The pathogenesis of Niemann-Pick type C disease 26
2.1.4 Inflammation, hypoxic stress and iron metabolism 27
2.1.5 Systemic regulation of hepcidin expression and its related iron homeostasis 27
2.1.6 Aims of this chapter 28

2.2 Patients, Materials and Methods 29
2.2.1.1 Patients blood analysis 29
2.2.1.2 Clinical specimen collection 29
2.2.1.3 Patients plasma soluble-transferrin receptor, C-reactive protein and ferritin levels analysis 29
2.2.2 Animals 30

2.2.3 Administration of iron supplementation therapy on *Npc1*$^{-/-}$ mice 30
2.2.4.1 Mice hematological analysis 30
2.2.4.2 Mice blood smears preparation 31
2.2.4.3 Mice serum samples preparation 31
2.2.4.4 Mice serum/plasma iron levels and transferrin saturation levels analysis 31
2.2.5.1 Neurological behavioral analysis – open field 31
2.2.5.2 Neurological behavioral analysis - tremor 32
2.2.6.1 Antibodies for Westeern blotting/immunoblotting 32
2.2.6.2 SDS-PAGE/immunoblotting analysis 32
2.2.7 Immunohistochemistry/Immunofluorescence analysis 33
2.2.8 Flow cytometric analysis of spleen erythroid lineage cells 33
2.2.9 Enzyme Linked Immunosorbent Assay (ELISA) for human serum TNF-α analysis 34
2.2.10 Tissue isolation, RNA extraction and microarray hybridization an data analysis 34
2.2.11 Statistical analysis 35

2.3 Results 36
2.3.1 Decrease hematocrit (HCT), mean corpuscular volume (MCV), hemoglobin (HGB) and mean corpuscular hemoglobin (MCH) in *Npc1*$^{-/-}$ mice 36
2.3.2 Decreased serum iron levels, altered serum iron regulators expression, down-regulation of hepatic hepcidin and up-regulation of hepatic transferrin receptor levels in *Npc1*$^{-/-}$ mice. Clinical specimen collection 38
2.3.3 Abnormal hepatic iron metabolism-related pro-inflammatory cytokines in *Npc1*$^{-/-}$ mice 40
2.3.4 Increased splenic red blood cell frequency and diminished splenic F4/80^{+} macrophage numbers in *Npc1*$^{-/-}$ mice 41
2.3.5 Improved hematological abnormalities, motor function and survival in *Npc1*$^{-/-}$ mice in response to iron supplementation 47
2.3.6 Hematological abnormalities and decreased serum iron and transferrin saturation levels in NPC1 patients 51

2.4 Discussion 55

Chapter 3: Defective Systemic and Cellular Iron Homeostasis in Niemann-Pick type C1 Disease

3.1 Introduction 64
3.1.1 The biological function of iron and its systemic homeostasis 64
3.1.2 Cellular iron homeostasis and its regulation 64
3.1.3 The role of lysosomes in iron homeostasis 65
3.1.4 The biological function of mitochondria in iron regulation and its utilization 65
3.1.5 Systemic and cellular regulation of hepcidin and ferroportin interaction 65
3.1.6 Lysosomal storage diseases 66
3.1.7 Aims of this chapter 67

3.2 Patients, Materials and Methods 68
3.2.1 Animals 68
3.2.2 Administration of iron supplementation therapy 68
3.2.3 Mice serum samples preparation 68
3.2.4 Cell culture 68
3.2.5 Immunofluorescence analysis 68
3.2.6 Antibodies 69
3.2.7 Collection of CSF from NPC1 patients 69
3.2.8 CSF transferrin and ferritin levels analysis 70

3.2.9 Proteomic analysis (2D-gels) 70
3.2.10 Perl's Prussian blue iron histochemistry 71
3.2.11 Electron microscopy analysis 71
3.2.12 Assessment of intracellular/tissue levels of lipid peroxidation 72
3.2.13 Quantification of tissue glutathione (GSH) levels 72
3.2.14 Double immunofluorescence analysis 72
3.2.15 Image analysis 73
3.2.16 Tissue isolation, RNA extraction and microarray hybridization an data analysis 74
3.2.17 In vitro erythrophagocytosis assay by RAW 264.7 murine macrophage cell line 74
3.2.17.1 Cell culture 74
3.2.17.2 Preparation of CFSE-labeled mouse erythrocytes 74
3.2.17.3 In vitro erythrophagocytosis assay 74
3.2.17.4 Immunofluorescence microscopy 75
3.2.18 Statistical analysis 75

3.3 Results 76
3.3.1 Altered expression of iron regulators in tissues from *Npc1*$^{-/-}$ mice and an in vitro model of NPC1 disease 76
3.3.2 Down-regulation of hepatic mitochondrial iron transporters, heme metabolism and [Fe-S] clusters biosynthesis gene expression in *Npc1*$^{-/-}$ mice. 82
3.3.3 Increased mRNA levels of endosomal/lysosomal divalent metal transporter-1 (DMT-1) and mucoln (MCOLN-1) in *Npc1*$^{-/-}$ liver 88
3.3.4 Altered iron metabolism and up-regulation of iron regulator protein-1 (IRP-1) in *Npc1*$^{-/-}$ brain 89
3.3.5 Impaired erythrophagocytosis and heme metabolism in U18666A induced NPC1 disease RAW 264.7 cells 90
3.3.6 Abnormal gastrointestinal bleeding in *Npc1*$^{-/-}$ mice 93
3.3.7 Iron dysregulation induced tissue reactive oxygen species production, decreased intracellular glutathione (GSH) levels and elevated lipid peroxidation in *Npc1*$^{-/-}$ mice 95
3.3.8 Increased circulating and tissue iron contents in iron-dextran treated *Npc1*$^{-/-}$ mice 97
3.3.9 Iron supplementation improves motor function and activity in *Npc1*$^{-/-}$ mice 100
3.3.10 Iron supplementation does not protect against neuro-inflammation or Purkinje cells loss in *Npc1*$^{-/-}$ mice 103
3.3.11 Abnormal cellular ferritin synthesis and storage in NPC1 human fibroblasts 106
3.3.12 Abnormalities in CSF concentration of ferritin in NPC1 patients 110

3.4 Discussion 111

Chapter 4: Defective Copper and Zinc Homeostasis in Niemann-Pick C1 Disease

4.1 Introduction 120
4.1.1 Copper/zinc dyshomeostasis and its related diseases 120
4.1.2 Systemic and cellular copper homeostasis 120
4.1.3 Systemic and cellular zinc homeostasis 121
4.1.4 Metallothioneins and copper, zinc homeostasis 121
4.1.5 Copper and zinc dyshomeostasis disorders 121
4.1.6 The biological function of lysosomes and metal homeostasis 122
4.1.7 Acid sphingomyelinas and NPC1 disease 122
4.1.8 Niemann-Pick type C1 disease 123
4.1.9 Aim of this chapter 123

4.2 Materials and Methods 124
4.2.1 Animals 124
4.2.2 Administration of copper/zinc manipulation therapies on *Npc1*$^{-/-}$ mice.....124
4.2.3 Mouse serum samples preparation 124
4.2.4 ICP-MS metal analysis for tissue and serum copper and zinc levels.....124
4.2.5.1 Behavioural analysis - open field 124
4.2.5.2 Neurological behavioural analysis – tremor.....124
4.2.5.3 Locomotor activity: AmLogger and open field rearing 125
4.2.5.4 Gait analysis 125
4.2.6 Tissue copper staining (rhodanine staining).....125
4.2.7 Tissue isolation, RNA extraction, and Microarray hybridization and data analysis…126
4.2.8 Cell culture.....126
4.2.9 Immunocytochemistry analysis – cytosolic copper transporters, MNK ATP7A and WND ATP7B, subcellular localization analysis 126
4.2.10 Fluorescence imaging and flow cytometric analysis of free intracellular zinc 126
4.2.11 Statistics.....127

4.3 Results.....128
4.3.1 Defective systemic copper regulation in *Npc1*$^{-/-}$ mice.....128
4.3.2 Altered hepatic copper metabolism gene expression in *Npc1*$^{-/-}$ mice.....129
4.3.3 Impaired hepatic cytosolic copper transport in *Npc1*$^{-/-}$ mice 131
4.3.4 Hepatic subcellular copper metabolism defects in *Npc1*$^{-/-}$ mice.....132
4.3.5 Mislocalization of endogenous WND ATP7B copper transporter in U18666A-treated HepG2 cells 133
4.3.6 Mislocalization of exogenous GFP-tagged WND ATP7B copper transporter in NPC1-null CHO-M12 cells 138
4.3.7 Transfected exogenous GFP-tagged WND ATP7B copper transporter is not co-localized with LAMP-1 in CHO-H1 and CHO-M12 cells.....143
4.3.8 Cytosolic copper accumulation in NPC1-null CHO cells 147
4.3.9 Mislocalization of the MNK ATP7A copper transporter in U18666A-treated RAW cells and NPC1 human fibroblasts 151
4.3.10 Up-regulation of hepatic metallothioneins (MT-1 & MT-2) in *Npc1*$^{-/-}$ mice 158
4.3.11 Subcellular zinc compartmentalization defects in vitro in NPC1 disease cells 158
4.3.12 Down-regulation of cellular metallothioneins in primary mouse *Npc1*$^{-/-}$ astroglial cells.....164
4.3.13 The copper chelator D-Penicillamine, has limited therapeutic effects in *Npc1*$^{-/-}$ mice.....165
4.3.14 Copper/zinc metal ionophore, clioquinol, treatment significantly improved gait and extended life expectancy in treated *Npc1*$^{-/-}$mice.....168
4.3.15 Reduced copper absorption therapy improved motor coordination, gait and extended survival in *Npc1*$^{-/-}$ mice 172

4.4 Discussion.....176

Chapter 5: Investigating the function of lysosome-related organelles in megakaryocytes and platelets in NPC1 disease

5.1 Introduction.....184
5.1.1 The biological functions of lysosomes and lysosome-related organelles 184
5.1.2 The development and function of lysosome-related organelles in megakaryocytes and platelets.....184

5.1.3 The biological functions of sphingolipids during megakaryopoiesis and thrombopoiesis 185
5.1.4 The role of cholesterol in megakaryopoiesis and thrombopoiesis 186

5.1.5 Acidic compartments calcium signaling in megakaryocytes and platelets 186
5.1.6 Niemann-Pick type C1 disease 187
5.1.7 Aims of this chapter 187

5.2 Patients, Materials and Methods 189
5.2.1 Patients for hematological analysis 189
5.2.2 Animals 189
5.2.3 Administration of substrate reduction therapy using miglustat on *Npc1*$^{-/-}$ mice 189
5.2.4 Mice hematological analysis 189
5.2.5 Immunohistological analysis of tissue sections 189
5.2.6 Isolation of murine platelets 189
5.2.7 Flow cytometry analysis of granules release 190
5.2.8 Bleeding assay 190
5.2.9 Platelet Aggregation 190
5.2.10 Ferric chloride carotid injury model 191
5.2.11 Cell culture 191
5.2.12 Immunofluorescence analysis of human megakaryoblastic MEG-01 cell line 191
5.2.13 Flow cytometric analysis for the measurements of the numbers and volume of platelet acidic compartments 192
5.2.14 Isolation and culture murine megakaryocytes 192
5.2.15 Megakaryocyte pro-platelet formation assay 192
5.2.16 Statistics 193

5.3 Results 194
5.3.1 Increased number of platelets (PLT), plateletcrit (PCT) in *Npc1*$^{-/-}$ mice 194
5.3.2 Impaired *Npc1*$^{-/-}$ platelets aggregation in response to thrombin stimulation 195
5.3.3 Impaired α-granules release in *Npc1*$^{-/-}$ platelets in response to thrombin stimulation 197
5.3.4 Increased tail bleeding time in *Npc1*$^{-/-}$ mice 199
5.3.5 *In vivo* thrombus formation defect in *Npc1*$^{-/-}$ mouse 200
5.3.6 Abnormal ultra-structure in *Npc1*$^{-/-}$ platelets 201
5.3.7 Increased LysoTracker-Green fluorescence intensity in *Npc1*$^{-/-}$ platelet 202
5.3.8 Increased LysoTracker-Green fluorescence intensity in U18666A-treated human megakaryoblastic MEG-01 cell line 203
5.3.9 Abnormal intracellular storage bodies in U18666A-treated MEG-01 cells 204
5.3.10 NPC1 is co-localized with α-granules marker, P-selectin (CD-62P) and δ- and late endosome/lysosome marker, CD63 (LAMP-3), in U18666A treated MEG-01 cells206
5.3.11 Defects in acidic compartments calcium flux in U18666A-treated MEG-01 cells in response to GPN stimulation 209
5.3.12 Miglustat (NB-DNJ) treatment improved abnormal circulating platelet count in treated *Npc1*$^{-/-}$ mice 210
5.3.13 NPC1 patients present with mild thrombocytopenia 212

5.4 Discussion 213

Chapter 6: General Discussion, Future Prospects and Concluding Remarks

6.1 General discussion 219
6.2 Future work and implications 219
6.3 Concluding remarks 233

Chapter 7: References

7 References 237

Chapter 1: General Introduction

Chapter 1: General Introduction

1.1 General Introduction

1.1.1 *The lysosome*

Lysosomes play a crucial role in intracellular catabolic pathways to degrade/ redistribute intracellular macromolecules (1, 2). However, there is growing evidence that they also mediate plasma membrane repair, intracellular nutrient sensing, cellular signalling and energy metabolism (2, 4).

Figure 1.1. The biological function of lysosomes. Lysosomes are involved in the degradation and recycling of macromolecules. Lysosomes can fuse with autophagosomes and with late endosomes. The lysosomal-mediated breakdown products can be used to generate new cellular components and for energy production in response to nutrient requirements. Lysosomes also undergo Ca^{2+} regulated exocytosis to secrete their contents into the extracellular space and to repair plasma membrane damage. Upon plasma membrane injury, lysosomes can rapidly migrate to the damaged site and fuse with the plasma membrane to allow efficient resealing. In addition, lysosomes have been recently identified as signalling organelles that can sense nutrient status and activate a lysosome-to-nucleus signalling pathway that mediates the starvation response and regulates energy metabolism. This figure was adapted from Saftig et al., 2009.

1.1.2 The function of lysosome-related organelles

Lysosome related organelles **(**LROs) are a group of heterogeneous cytosolic vesicles, which share several common features with conventional lysosomes, including acidic pH, specific lysosomes/LROs membrane proteins, and convergent biogenesis (5). Despite sharing several features with lysosomes, LROs have further specialized and have distinct morphologies, composition and contents (6). Lysosomes/LROs biogenesis and functional defects have been identified in rare human genetic disorders, such as Hermansky-Pudlak syndrome (HPS) and Chediak-Higashi syndrome (1), which suggests a close relationship between lysosomes and LROs (7, 8). In addition, certain specialized cell types, such as melanocytes and platelets, lysosomes and LROs co-exit, which suggested the presence of distinct biogenesis and sorting pathways (6, 9) **(Fig 1.2)**.

Figure 1.2. Comparison of the biogenesis of lysosomes and LROs (e.g., melanosomes and Weibel–Palade bodies). This figure presents the differences, such as origin in the TGN versus origin in the EE for melanosomes and Weibel-Palade bodies, and the similarities, such as continued receipt of content after initial formation (tyrosinase versus CD63) and recruitment of Rabs. Gold coating, AP-1; purple coating, AP-3; grey coating on stage I melanosome, bilayered clathrin/Hrs coat. TGN, trans-Golgi network; EE, early endosome; MVB, multivesicular body/late endosome; Tyr, tyrosinase; Tyrp1, tyrosinase-related protein-1. This figure was adapted from Raposo et al., 2007.

1.1.2.1 The function of LROs in platelets

Platelets deliver pro-hemostatic proteins and other mediators to sites of vessel injury (10). In addition to lysosomes, α- and δ-granules are major platelet LROs, which release mature secretory proteins and small molecules, such as ADP and serotonin upon stimulation (9). α-granules are the most abundant vesicles in platelets, which store proteins that promote platelet adhesiveness and wound healing (11, 12). δ-granules number only three to eight per platelet and store non-protein small molecules e.g. calcium, serotonin, ADP, ATP, and polyphosphates (13); their membranes contain the lysosomal membrane proteins LAMP2 and CD63/LAMP3, but not LAMP1. The high calcium content of δ-granules gives them an intrinsic electron density and their highly osmophilic properties cause them to appear dark on transmission electron microscopy (13) **(Fig 1.3)**. However, unlike other secretory cells, circulating platelets do not form their own vesicles. Instead, bone marrow megakaryocytes create the granules and transport them into developing pro-platelets via microtubule and actin networks (14). During megakarocytopoiesis, α- and δ-granules arise from the Golgi complex, with Multivesicular bodies (MVBs) as intermediate structures (15). Immature megakaryocytes contain numerous MVBs but few α- and δ-granules (15). As the development of megakaryopoiesis, the number of MVBs decreases, the number of α- and δ-granules increases, a demarcating membrane system develops, and the granules enter nascent pro-platelets (14). Pro-platelets released from the megakaryocyte fragments to form individual platelets (16).

Figure 1.3. Schematic diagram of a platelet. The platelet contains two different types of LROs, including α-granules, δ-granules in addition to conventional lysosomes. δ-granules containing ADP or ATP, Ca^{2+} and serotonin. α-granules containing several growth factors, platelet factor 4, fibronectin, von Willebrand factor, fibrinogen and coagulation factors V and XIII. Lysosomes contain multiple hydrolytic enzymes. The figure was adapted from Flaumenhaft et al., 2013.

1.1.2.2 LROs and LRO-related disorders

In addition to melanosomes in pigmented cells and α- & δ-granules in platelets, several other specialized types of LROs have been identified including; (i) lamellar-bodies in pulmonary type II cells, (ii) azurophilic granules in neutrophils, (iii) basophil granules in basophils, (iv) MHC class II compartment in B lymphocytes, dendritic cells and other antigen presenting cells (v) and Weibel-Palade bodies in endothelial cells (5). LROs dysfunction causes pathological features, including hypo-pigmentation, abnormal bleeding, immune deficiency, lung dysfunction/fibrosis and osteopetrosis (7). However, limited LROs disorder animal models are available (8, 17). Insights into LROs biogenesis and trafficking defects could help elucidate the complex pathways involved and also identify therapeutic intervention strategies for these LROs disorders (6).

1.1.3 Lysosomal Storage Disease (LSDs)

It is known that defects in genes encoding lysosomal proteins/enzymes can lead to the accumulation of substrates that are not degraded in the lumen of the lysosome, leading to storage of macromolecules that cause severe progressive disease (18).

These disorders are termed lysosomal storage diseases (LSDs) and are a relatively large group of inherited diseases (>60 known) (19). They collectively affect 1:5000 live births (18). The common feature of all LSDs is the initial accumulation of specific macromolecules, such as lipids and carbohydrates, within the endosomal/lysosomal system (18). The age of clinical symptom onset and clinical spectrum exhibited amongst different LSDs can be highly variable depending on the severity of genetic mutations, the biochemical features of the stored substrates and the specific cell types where storage occurs (19). The clinical features and

storage substrates of several LSDs are summarized in **Table 1.1** (19).

* This table was adapted from Platt et al., 2012.

1.1.4 Niemann-Pick type C (NPC) Disease

When compared with other LSDs, Niemann-Pick type C (NPC) disease is relatively unique as it is caused by genetic mutations in either the NPC1 or NPC2 genes (20). Since the similarity of clinical symptoms/phenotypes are identical, irrespective of whether NPC1 or NPC2 dysfunction, it has been proposed that these NPC proteins may function in a common cellular pathway (21). In addition to the neurodegenerative phenotypes, the other clinical symptoms of NPC disease include learning difficulties, psychiatric problems, changes in sleep patterns, epilepsy, loss of speech, vertical gaze palsy and respiratory dysfunction (20). When compared with other LSDs, the biochemical features of NPC disease is also relatively unique as the storage substrates within the endosomal/lysosomal system are highly complex, including sphingosine, cholesterol, sphingomyelin and glycosphingolipids (20). In addition, NPC disease is unique in having reduced acidic stored calcium levels (22).

Around 95% of cases of NPC disease are caused by mutations in the NPC1 gene (23). NPC1 is a 1278 amino acid integral membrane protein of the late endosome/lysosome with a sterol-sensing domain (SSD) and belongs to the resistance-nodulation-cell division (RND) permease superfamily **(Figure 1.4)** (24). The NPC1 protein has a cysteine-rich loop with zinc binding activity (24). It has been suggested that the cysteine-rich loop is crucial for the function of NPC1 protein for the transport of lysosomal cargos (24). Although the biological functions of NPC1 remain controversial, NPC2 is generally accepted to function as soluble lysosomal cholesterol binding protein (25).

Figure 1.4. Predicted topology of NPC1. NTD = N-termianl domain and SSD – sterol sensing domain. This figure was adapted from Scott et al., 2004.

1.1.2 Systemic iron homeostasis

Iron is an essential trace element involved in multiple biological processes/reactions and serves as a co-factor for the biosynthesis of iron-porphyria (heme) groups and iron-sulfur [Fe-S] clusters for functional hemoglobin and cytochrome family molecules, such as cytochrome c and cytochrome P450s. For example, iron helps (i) maintain systemic oxygen supply, (ii) regulate mitochondrial electron transport chain respiration (iii) and is involved in the regulation of the biosynthesis of lipids, such as steroid hormones, and drug detoxification reactions (26). In mammalian systems, systemic iron homeostasis is tightly regulated via complex mechanisms and is involved at least four different cells types, including iron absorption via duodenal enterocytes, iron storage in hepatocytes, iron utilization for erythropoiesis by erythroid precursors and iron recycling through hepatic and splenic reticuloendothelial macrophages (27, 28) **(Fig 1.5)**.

Figure 1.5. Systemic iron regulation and its homeostasis. Dietary iron is absorbed by enterocytes before being exported into plasma where it binds to transferrin (Tf). Tf-bound iron is then delivered to tissues and cells (primarily to reticulocytes) where it is incorporated into heme. Senescent erythrocytes are phagocytosed by macrophages, which degrade hemoglobin and recycle iron back into plasma where it again binds Tf. If iron is absorbed or released into the plasma at a higher level than the iron-binding capacity of Tf, then the excess, non-Tf-bound iron is deposited in parenchymal tissues. This figure was adapted from Kaplan et al., 2008.

1.1.2.1 Iron absorption

Dietary iron uptake is mainly mediated by the divalent metal transporter 1 (DMT-1) at the brush border of duodenal enterocytes (29). After uptake, iron is reduced by the membrane-associated ferrireductase DcytB (30). Cytosolic iron can be exported into the circulation by the basolateral iron exporter, ferroportin (30). In addition, enterocytic iron export through ferroportin requires hephaestin, a multicopper oxidase homologous to ceruloplasmin, which oxidases ferrious iron (Fe^{2+}) to ferric iron (Fe^{3+}) for loading onto Tf (31) **(Fig 1.6)**. Enterocyte mediated iron absorption can be up-regulated when physiological demand increases, such as in pregnancy or when there is increased erythropoiesis (29).

Figure 1.6. Enterocyte iron transporters mediate iron absorption. Fe^{3+} can be reduced to Fe^{2+} in the intestinal lumen by ferrireductase. Fe^{2+} then can be transported across the enterocytes by divalent metal transporter-1 (DMT-1). Fe^{2+} is transported across the basolateral membrane of the enterocyte by the iron exporter, ferroportin. The transported Fe^{2+} is oxidized back to the Fe^{3+} form by ferroxidase. Fe^{3+} is then incorporated into transferrin in the serum. Cytosolic iron can be stored as ferritin inside the enterocytes. This figure was adapted from Scohen et al., 2011.

1.1.2.2 Iron recycling

Hepatic and splenic reticuloendothelial macrophages are responsible for the phagocytosis of senescent erythrocytes and they catabolize heme using hemoxygenase to facilitate iron recycling (32). Natural resistance-associated macrophages protein 1 (NRAMP-1), a divalent metal transporter homologous to DMT-1, is expressed within phagolysosomal membranes and participates in iron export from phagocytic vesicles (32). Export of ferrous iron from macrophages occurs via iron exporter, ferroportin (26) **(Fig 1.7)**. Reflecting its central role in systemic iron homeostasis, ferroportin expression in macrophages is regulated at multiple levels: ferroportin transcription is induced by erythrophagocytosis and heme iron, its translation is regulated by the IRE/IRP system, and its protein stability by hepcidin (26).

Figure 1.7. Macrophage mediated iron recycling via erythrophagocytosis Following erythrophagocytosis, hemoglobin derived from senescent erythrocytes can be degraded and ferrous iron is released from the heme upon oxidation of the organic ligand (porphyrin) by heme oxygenase. The heme can then either be exported to the cytosol and undergo degradation by heme oxgyenase, or can be degraded in the phagolysosome followed by export of ferrous iron to the cytosolic compartments through DMT-1 or NRAMP-1. Iron is then transported into the plasma by ferroportin, oxidized by ceruloplasmin, bound to Tf, and reutilized for hemoglobin synthesis. This figure was adapted from Hamza et al., 2013.

1.1.3 Systemic iron homeostasis: the iron regulator hormone hepcidin

Recent studies have indicated that hepatic hepcidin is the main regulator of systemic iron homeostasis (28). Hepcidin is a 25-amino acid peptide, which can modulate intestinal

iron absorption and systemic iron distribution and utilization. Hepcidin is mainly synthesized by the liver and secreted into plasma to regulate circulating iron levels and the cell surface expression of the iron exporter, ferroportin, via binding and inducing ferroportin internalization and degradation in lysosomes (28, 31, 33). Ferroportin is mainly expressed on the surface of (i) duodenal enterocytes, which regulate iron absorption, (ii) hepatocytes, which is the place for system iron storage (iii) and reticulendothelial macrophages, which recycle iron from senescent erythrocytes (34). Dysregulation of hepcidin/ferroportin complex could cause systemic iron dyshomeostasis and lead to the development of various iron related diseases, such as iron deficiency anemia and iron overload disorders (28). Hepatic hepcidin levels can be regulated by several pathophysiological factors, including system iron status, systemic inflammation, hypoxic stress and erythropoiesis (35-37). These different regulatory inputs are integrated transcriptionally (38) **(Fig 1.8)**.

Figure 1.8. Hepcidin is a key regulator of systemic iron homeostasis. Hepatic hepcidin levels can be regulated by different stimuli. Systemic iron content and inflammation can stimulate hepatic hepcidin expression, whereas increased erythropoietic activity inhibits hepatic hepcidin expression. In turn, hepatic hepcidin can regulate cell surface ferroportin expression on iron-exporting cells, including duodenal enterocyte, hepatic and splenic macrophages and hepatocytes, and further modulate circulating iron concentrations. Figure was adapted from Ganz & Nemeth, 2012.

1.1.3.1 Regulation by systemic iron availability

Iron bounded Tf complex can stimulate hepatic hepcidin expression via the bone morphogenic protein-6 (BMP-6)/SMAD signalling pathway. This includes hemojuvelin (HJV), the hemochromatosis protein (HFE) and transferrin receptor -2 (TfR-2), that regulate hepatic iron mediated induction of hepatic hepcidin expression (37, 39). Conversely, iron deficiency leads to low hepatic hepcidin levels (35). A liver transmembrane serine protease, TMPRSS6 or matriptase-2, is required to suppress the hepatic hepcidin expression under such conditions (39). This protease can cleave and solubilize HJV, down regulating the signaling

of the BMP-6/SMAD pathway mentioned above (34).

1.1.3.2 Regulation by inflammatory and stress signals

The inflammatory cytokines, such as interleukin-6 (IL-6) and interleukin-1β (IL-1β), can induce hepatic hepcidin expression and further regulate systemic iron homeostasis (38). Several studies have indicated that the hepatic pro-inflammatory cytokine, IL-6, is the major pro-inflammatory cytokine mediating increased hepatic hepcidin expression, which can activate the JAK/STAT-3 signalling pathway, to activate hepcidin transcription (40). Other studies also indicated that the BMP signalling pathway also contributes to the inflammatory response via SMAD4 (40) **(Fig 1.9)**.

Figure 1.9. Signaling pathways regulate hepatic hepcidin expression. Expression of hepatic hepcidin in response to iron status is regulated by the levels of Fe-bound Tf and BMP-6 and involves the membrane proteins HFE, hemojuvelin (HJV) and transferrin receptor-2 (TfR-2). The increased hepatic hepcidin expression under inflammatory conditions is triggered by IL-6, which activates the JAK/STAT-3) signalling pathway. Figure was adapted from Coyne, 2011.

1.1.3.3 Regulation by erythropoietic signals

Erythropoiesis requires considerable quantities of iron, and the inhibition of hepcidin expression by erythropoietic signals is of great physiological importance. However, the molecular mechanisms of how hepcidin levels are regulated by erythropoietic signalling are still poorly understood (41). Hepcidin suppression in response to phlebotomy or hemolysis depends on intact erythropoietic activity in mouse models: irradiation and cytotoxic inhibition of erythropoiesis prevent hepcidin suppression, GDF15 and TWSG1 are both released by erythroid precursors (26). High doses of GDF15 are detectable in the serum of patients with ineffective erythropoiesis, such as β-thalassemia (26).

1.2 Cellular iron regulation

Cellular iron uptake is predominately mediated by the interaction of iron-bound transferrin (Tf) and cell surface transferrin receptor-1 (TfR-1) via the cellular endocytosis pathway. After receptor-mediated endocytosis, iron-bound Tf/TfR-1 complex is acidified in endosomes to facilitate the release of bound-iron from the Tf/TfR-1 complex and export to the cytosol (26). Cytosolic iron is then either transported to (i) nucleus to facilitate DNA synthesis, (ii) mitochondria via mitoferrin to facilitate mitochondrial electron transport chain respiration and to support other mitochondrial functions (iii) and excess intracellular iron is stored into the cytosolic iron storage protein complex, ferritin (42).

Cellular iron homeostasis is regulated at transcriptional and post-transcriptional levels to coordinate cellular iron metabolism-related gene expression to facilitate cellular iron acquisition, distribution, utilization and storage (26). Although both the transcriptional and post-transcriptional regulatory mechanisms have been suggested to be involved in the regulation of cellular iron homeostasis, post-transcriptional regulation via the IRPs/iron regulatory machinery is the predominant system to regulate cellular iron homeostasis (26). The IRPs/iron regulatory machinery mainly consists of RNA biding proteins, IRP-1 & IRP-2, and a numbers of iron-responsive element (IRE) containing proteins, such as TfR-1 and ferritin (43). Under conditions of iron deficiency, IRPs can interact directly with the IREs containing mRNA transcripts and modulate mRNAs translation. In iron-deficient cells, IRPs bind to IREs found in the mRNAs of ferritin, TfR-1 and other iron metabolism transcripts, enhancing iron uptake and decreasing iron sequestration (26) **(Fig 1.10)**. In addition to response to cellular iron levels, IRPs/IRE iron regulatory machinery have also been suggested to be regulated by other physiological and pathophysiological factors, including, hypoxia, oxidative stress, nitric oxide, hormone and xenobiotics, through distinct molecular mechanisms (26).

Figure 1.10. Regulation of cellular iron metabolism gene expression. In iron-depletion condition, iron regulatory proteins (IRPs), either IRP-1 or IRP-2, can bind to iron-responsive elements (IREs), which are present in the untranslated regions of mRNAs encoding proteins involved in cellular iron metabolism. The binding of IRPs to single IREs in the 5′ UTRs of target mRNAs inhibits their translation, whereas IRPs interaction with multiple 3′ UTR IREs in the transferrin receptor-1 (TfR-1) transcript increases its stability. As a consequence, TfR-1 mediated iron uptake increases whereas iron storage in ferritin and export via ferroportin decrease, thereby increasing the labile iron pool (LIP). On the other hand, in iron-replete condition, the FBXL5 iron-sensing F-box protein interacts with IRP-1 and IRP-2 and recruits the SKP1-CUL1 E3 ligase complex that promotes IRP ubiquitination and degradation by the proteasome. IRP-1 is primarily subject to regulation via the assembly of a [Fe-S] clusterS, which triggers a conformational switch precluding IRE-binding and conferring aconitase activity to the holoprotein. This figure was adapted from Camaschella et al., 2010.

1.2.1 Lysosome-mediated iron-related metabolism

Recently, several lines of evidence have highlighted the crucial functions of lysosomes in maintaining systemic and cellular iron homeostasis, including iron acquisition, intracellular distribution, storage, recycling and utilization (44, 45). For example, impaired intracellular endocytic pathway and receptor recycling defects have been implicated in some lysosomal storage diseases, such as NPC1 disease, and these defects could be involved in intracellular iron uptake/acquisition and receptor recycling defects (46). Further, in terms of intracellular iron storage and utilization, cellular iron storage protein complex, ferritin, can be targeted to lysosomes to be degraded and ferritin-stored iron is released for further utilization (47). It has been recently demonstrated that ferritin can be degraded via lysosomal degradation when iron was scarce, and autophagy contributes to this process, which suggested that lysosomal degradation of ferritin plays a crucial role in the utilization of ferritin-stored iron (48) **(Fig 1.11)**. Moreover, lysosomes are also the intracellular organelles where hepcidin/ferroportin complex and erythrophagocytosis mediated heme complex degradation/recycling occurs (32). While lysosomes dysfunction, the lysosomal-mediated ferritin iron release, hepcidin/ferropeotin complex degradation and heme complex recycling could be affected and impair down-stream systemic and cellular iron utilization (2). Lysosome could also be involved in intracellular iron re-distribution into other subcellular

compartments (44). Indeed, it has been indicated that lysosomes can help facilitate intracellular iron transport into mitochondria via a kiss and run model (49). Although the precise molecular mechanisms of lysosome mediated intracellular iron metabolism remain to be established, some lysosomal transporters, including MCOLN-1, DMT-1, have been suggested to be involved in lysosome-mediated iron transport (50, 51).

Figure 1.11. The role of lysosomes in cellular iron metabolism. Circulating iron is mainly bound in a Tf-iron complex that binds to cell surface TfR-1, which results in receptor-mediated endocytosis inside clathrin-coated vesicles. In the lowered pH of late endosomes, iron is released and transported to the cytosol, while the Tf/TfR-1 complexes are recycled to the plasma membrane. Cytosolic iron can be either transported to the nucleus for DNA synthesis, mitochondria for electron chain protein function or stored in ferritin complexes. Figure was adapted from Brunk et al., 2008.

1.2.2 Mitochondria-mediated subcellular iron homeostasis

Mitochondria are another crucial subcellular organelle involved in various aspects of cellular iron metabolism (52). Mitochondria are the main site of biosynthesis of (i) heme groups for hemoglobin and cytochrome production and (ii) cytosolic [Fe-S] clusters required for mitochondrial, cytosolic and nuclear [Fe-S]-containing enzymes (52). When cytosolic iron homeostasis is disrupted, it affects the content of mitochondrial iron and the function of the heme biosynthetic pathway (53). Friedreich's ataxia is caused by a genetic defects in the mitochondrial protein frataxin and is characterized by progressive neurological/cardiological symptoms and mitochondrial iron loading phenotypes (54). Although the biological function of frataxin remains unclear, several studies have suggested that frataxin is involved in the regulation of mitochondrial iron metabolism, especially mitochondrial iron-sulfur clusters biosynthesis, heme metabolism and mitochondrial iron storage (52). Indeed, mitochondrial frataxin deficiency led to (i) cytosolic iron deficiency with increased RNA-binding activity of IRP-2, increased expression of TfR-1, decreased cytosolic ferritin expression, (ii) impaired heme metabolism and [Fe-S] cluster biosynthesis gene expression (iii) and decreased expression levels of mitochondrial storage protein, mitoferritin (Ftmt) in Friedreich's ataxia

disease mouse model. In addition, impaired mitochondrial respiratory chain complex I–III activity and lower rates of ATP production have also been documented in Friedreich's ataxia (55).

1.3 Systemic and cellular copper regulation

Copper is another crucial trace element in biological system and is required as a co-factor for many metalloproteins, which are involved in intestinal iron mobilization, biosynthesis and release of neurotransmitters, neuron myelination, blood clotting, melanin formation, mitochondrial function and protect against intracellular reactive oxygen species production (56). Imbalanced copper homeostasis is considered a contributing factor to neuropathology in several severe hepatic and neurodegenerative diseases, such as Wilson's syndrome, Menke's disease and Alzheimer's disease (57, 58). Therefore, systemic and cellular copper homeostasis is maintained through delicate mechanisms, which regulate extracellular copper uptake, intracellular distribution, subcellular compartmentalization and export (59).

1.1.3.1 Regulation of copper transport via trafficking

Copper absorption is mainly regulated by a plasma membrane transporter, CTR-1, which facilitates copper uptake and delivery/distribution to intracellular copper chaperones, such as ATOX1, CCS, that facilitate copper delivering to *trans*-Golgi (TGN) P-type ATPase transporters, MNK ATP7A and WND ATP7B, and help copper incorporate into apo-cuproproteins for holo-cuproproteins, such as holo-ceruloplasmin or tyrosinase. Besides, cytosolic copper can also be either (i) incorporated into Cu/Zn superoxide dismutases to help against cellular superoxide damages, (ii) or delivered into mitochondrial cytochrome c oxidase to help maintain mitochondrial functions (59) **(Fig 1.12)**. However, the molecular mechanisms of how intracellular copper trafficking and its subcellular compartmentalization remain poorly understood (59). Due to lack of suitable molecular probes for *in vitro* studies of intracellular copper trafficking, most of our current knowledge of systemic and cellular

copper regulation mainly relies on (i) certain copper metabolism genetic knock-out animal models or (ii) inborn errors of copper dysregulation metabolism in the human population, such as MEDNIK syndrome (60).

Figure 1.12. Subcellular copper trafficking and distribution. Cellular copper uptake is primarily mediated by cell surface copper transporter-1 (CTR-1), and cytosolic copper chaperone proteins. COX17 and other mitochondrial copper transporters can facilitate incorporation of subcellular copper into cytochrome c oxidase for mitochondrial function. CCS can help deliver copper to cytosolic Cu/Zn superoxide dismutases. Copper can also be transported to cytosolic WND ATPBA or MNK ATP7A and delivered to cupro-enzymes or excess cytosolic copper content exported. The figure was adapted from Dmitriev et al., 2007. COX17, Copper chaperone for cytochrome c oxidase; CCS, copper chaperone for superoxide dismutase; ATOX1, antioxidant 1 copper chaperone; SOD-1, superoxide dismutase-1.

1.3.2 Intestinal copper absorption

Most copper absorption appears to take place in the duodenum suggesting enterocytes CTR-1 mediates the acquisition of dietary copper at the apical membrane (59). In addition, DMT-1 has also been suggested as a candidate for copper uptake (59). However the molecular pathways through which dietary copper is absorbed by the intestinal epithelium remains poorly understood and controversial (61). After copper uptake, cytosolic copper is delivered to cytosolic metallochaperones (59). The cytosolic copper transporter MNK ATP7A accepts copper from ATOX1 and facilitates copper export from enterocytes to blood and to other tissues (59) **(Fig 1.13).** Mutations of MNK ATP7A result in intestinal accumulation of copper, impaired efflux of copper from enterocytes and pathologies resulting from diminished activity of copper-dependent enzymes (62). Recently, the WND ATP7B was detected in mouse intestine and in CaCo-2 cells; however, the exact physiological functions of WND ATP7B in the intestine remain unclear (61, 63).

Figure 1. 13. Enterocyte-mediated copper absorption. CTR-1 and a putative metalloreductase can help dietary copper import and its mobilization into the cytosol and endosomal compartments. Cytosolic copper is pumped into the secretory compartments for either loading onto copper-dependent enzymes, or out across the basolateral membrane by the P-type ATPase copper transporter MNK ATP7A. In the bloodstream, copper is transported via the portal vein to the liver. Copper can also be transported to peripheral tissues via the systemic circulation in a complex with one or more ligands, which have not yet been identified. Meanwhile, excess copper is excreted in the bile and eliminated from the body. In addition, in the secretory compartment, copper is loaded onto hephaestin, a multi-copper ferroxidase, which functions in concert with ferroportin at the basolateral membrane in iron efflux into the portal circulation. Figure adapted from Thiele et al., 2008.

1.3.3 Hepatic copper storage and excretion

The major homeostatic control of copper takes place in the liver (59). Copper enters the liver from the blood via CTR-1 (59). Copper is then used in the liver for many physiological functions. For examples, hepatic copper can be used to synthesize holo-ceruloplasmin, an abundant secreted copper ferroxidase. Excess hepatic copper contents can be exported from hepatocytes by WND ATP7B (64). Copper ATPases sequester copper into vesicles that subsequently fuse with the plasma membrane, and copper is extruded (61). In Menke's disease, MNK ATP7A is inactivated and copper export from the enterocytes is greatly impaired (61). As a result, copper accumulates in intestinal cells and less copper is delivered to the blood, resulting in restricted copper supply to other tissues (62). It has been suggested that there is a close relationship between iron and copper. Under conditions of iron deficiency in rats, DMT-1 expression is increased and could be responsible for the increase in absorption of both iron and copper at the brush border (65). The expression of MNK ATP7A in duodenum is also markedly elevated in iron deficiency, most likely contributing to the overall increase of copper transport across intestinal epithelium (66). The majority of copper that emerges form the intestinal epithelium into the blood is delivered to the liver and less to kidney and other tissues. In Wilson's disease, both WND ATP7B mediates cytosolic copper transport to the secretory pathway and cytosolic copper release into the bile are greatly impaired, resulting in marked accumulation of cooper in the liver, very low levels of copper bound ceruplasmin in the serum, and low biliary copper (62). Copper, when delivered to

various organs, is utilized to produce copper-dependent enzymes with general and tissue specific regions (62). Some organs, though, express only one copper ATPases in hepatocytes, and in these tissues one single copper ATPase appears to perform both biosynthetic and copper export functions. Many other tissues, however, such as brain, developing kidney, placenta, mammary gland, eye, and lung express both copper ATPase transporters, MNK ATP7A and WND ATP7B **(Fig. 1.14**). The cell specificity of copper ATPase expression can be associated with different functional characteristics of MNK ATP7A and WND ATP7B, their distinct developmental regulation, or different targeting and trafficking behavior in polarized epithelia (62).

Figure 1.14. Simplified scheme of systemic copper transporters MNK ATP7A and WND ATP7B distribution in the body. The figure was adapted from Dmitriev et al., 2007.

In addition to being regulated during development, recent studies also indicated that the trafficking of MNK ATPA7 and WND ATP7B copper transporters could also be coupled to hormone-mediated signaling, changes in Ca^{2+} flux and kinase-mediated phosphorylation (62, 67). These findings suggest that systemic copper homoeostasis can also be regulated by complicated physiological responses, such as neuronal activity and hypoxia (68).

1.4 Aim of this thesis

The aims of this thesis were to **(i)** investigate the underlying molecular mechanism of metal dysregulation in the murine model of NPC1 disease due to the structural homology that NPC1 shares with bacterial transporters the substrates of which include metals, **(ii)** identify novel metal-related cerebrospinal fluid (CSF) and peripheral blood biomarkers for monitoring disease progression and evaluating treatment effects in patients with NPC1 disease and **(iii)** evaluate clinically approved metal manipulation therapies in a mouse model of NPC1 disease as pre-clinical proof of concept.

Chapter 2: Defective iron homeostasis and hematological abnormalities in Niemann-Pick type C1 disease mice and their clinical implications

Chapter 2: Defective iron homeostasis and hematological abnormalities in Niemann-Pick type C1 disease mice and their clinical implications

2.1 Introduction.

2.1.1 Systemic iron regulation

Iron is an essential element, required as a cofactor for many metalloproteins, including hemoglobin, myoglobin and cytochromes. Systemic iron levels are regulated by the demand for erythropoiesis and by inflammation/infection (27, 69, 70). Dysregulation of systemic iron homeostasis could impair erythropoiesis and systemic oxygen utilization (71), therefore, mammals have evolved complex mechanisms to regulate systemic iron metabolism at the levels of absorption, recycling, distribution and storage (26).

2.1.2 The role of the lysosome in cellular iron metabolism

The lysosome plays a crucial role in intracellular catabolic pathways by degrading and redistributing/recycling intracellular macromolecules and metal ions (2). This is accomplished in part by being the site where iron regulators, transporters and storage proteins are degraded, including hepcidin, ferroportin, iron regulatory proteins-2 (IRP-2), ferritin and heme complexes (31, 40, 72). Lysosomes have also been suggested to regulate intracellular iron release and transport to other subcellular organelles, e.g., mitochondria (47, 48, 73-75).

2.1.3 The pathogenesis of NPC disease

NPC disease is a lysosomal storage disorder, caused by mutations in either the *NPC1* (95% of cases) or *NPC2* genes and occurs at a frequency of approximately 1:120,000 live births (23). It is characterized by reduced acidic store calcium levels and the accumulation of un-esterified cholesterol and sphingolipids within the late endosomal/lysosomal system (20, 22). Clinically, it presents as a lethal and progressive neurodegenerative disease of infancy/childhood and also in adults with variable degrees of transient hepatosplenomegaly

involvement (23). The exact biological functions and molecular interactions of NPC1 and NPC2 proteins remain elusive and require further study (76, 77).

2.1.4 Inflammation, hypoxic stress and iron metabolism

Inflammation is involved in the pathogenesis of many hepatic and neurodegenerative diseases, including Wilson's, Alzheimer's, Parkinson's and NPC1 disease (78, 79). Pro-inflammatory cytokines, including TNF-α, IL-6 and IL-1β, have been reported to regulate systemic iron homeostasis via activation of JAK/STAT-3 and related signaling pathways (34). In response to inflammatory stimuli, systemic iron homeostasis could be linked with hypoxic stress via the hypoxia-inducible factors (HIFs) regulatory pathways (36)-(80). During hypoxic stress, HIFs pathways would be activated and stimulate expression of genes involved in iron-metabolism and erythropoiesis (36).

2.1.5 Systemic regulation of hepcidin expression and its related iron homeostasis

Hepcidin, a small iron regulatory hormone, is mainly produced by hepatocytes and secreted into the circulation to maintain systemic iron homeostasis (34). Hepatic hepcidin levels are regulated by various factors, including cytosolic iron contents, inflammation, erythropoiesis and hypoxia. In iron deficiency, low erythropoiesis and hypoxic stress conditions, the hepatic hepcidin levels are supressed (34). Conversely, hepatic hepcidin levels are induced by inflammation (34). Circulating hepcidin can regulate the expression of the transmembrane iron transporter, ferroportin, at the post-translational level, which results in the internalization and degradation of hepcidin/ferroportin complex within lysosomes (28). Dysregulation of hepcidin/ferroportin complex has been suggested to be involved in the pathogenesis of various diseases, such as hemochromatosis, anaemia of chronic disease and β-thalassemia, which underlines the importance of the interaction of hepcidin and ferroportin in the regulation of systemic iron homeostasis (28).

2.1.6 Aims of this chapter

In this chapter, we aimed to investigate whether hematological changes and iron metabolism defects occur in NPC1 disease. We have found hematological abnormalities and iron metabolism defects in the murine model of NPC1 disease and in NPC1 patients. We observed low levels of serum iron, transferrin saturation, hemoglobin and mean corpuscular hemoglobin in *Npc1*$^{-/-}$ mice and low normal levels in NPC1 patients. Further, we demonstrated that the decreased serum iron levels in *Npc1*$^{-/-}$ mice may be linked with abnormal systemic inflammation and contribute to hypoxic stress in *Npc1*$^{-/-}$ mice. These observations were further confirmed via microarray analysis, which revealed age-dependent up-regulation of hepatic transferrin receptor-1 (TfR-1) throughout the lifespan of *Npc1*$^{-/-}$ mice. In addition, hepatic hepcidin (HAMP-1) mRNA levels were also significantly inhibited from the pre-symptomatic stage to the late-symptomatic stage of *Npc1*$^{-/-}$ mice. Therefore, we have evaluated the effects of iron supplementation therapy on *Npc1*$^{-/-}$ mice, which partially corrected hematological abnormalities, improved motor function and extended survival. These studies suggested serum iron deficiency may induce multiple hematological changes in NPC1 disease that impact the disease course. NPC1 patients appear to be at risk of iron deficiency and should be closely monitored. Supplementation of iron in the setting of iron deficiency anemia, has clear clinical benefit that impacts survival in *Npc1*$^{-/-}$ mice and may merit clinical studies in NPC1 patients with anemia or bordering on anemia.

2.2 Patients, materials and methods.

2.2.1 Patient blood analysis

NPC1 patients in this study were enrolled in an ongoing longitudinal observational study at the National Institutes of Health in Bethesda, Maryland, USA. This study and collection of age-matched control samples were approved by the NICHD Institutional Review Board. Informed consent was obtained for all subjects as well as assent, when appropriate. The diagnosis was established by biochemical testing/mutation analysis. Twenty of the patients (38%) were taking off-label miglustat (Zavesca). Eighteen of the NPC1 patients (34%) were taking a multi-vitamin containing iron. Exclusion of these subjects yielded similar results to inclusion. The clinical samples and hematological analysis were provided by Dr. Denny Porter (NIH, USA)

2.2.1.2 Clinical specimen collection

Serum samples were obtained from 59 of the NPC1 patients and from 39 age-matched, healthy controls. Blood for iron analyte analysis was collected in serum separator tubes (SST) and analyzed immediately in the NIH Clinical Center Department of Laboratory Medicine (DLM). Control serum was collected in SST, frozen, and shipped to the NIH on dry ice. Control samples were stored at -80^{o}C prior to analysis. Iron, transferrin and percent saturation were measured using *in vitro* diagnostic test for the quantitative measurement of iron in human serum and plasma on the Dimension Vista® System in the NIH DLM.

2.2.1.3 Patients plasma soluble-transferrin receptor, C-reactive protein and ferritin levels analysis

Plasma samples were obtained from 20 of the NPC1 patients and from 20 healthy controls into EDTA-treated tubes and stored at -80^{o}C before analysis. Plasma hepcidin levels were quantified by competition ELISA using the human hepcidin-25 enzyme immunoassay kit (Bachem, USA) according to the manufacturer's protocol. Plasma soluble-transferrin receptor (s-TfR) levels were measured by using Human sTfR Quantikine IVD ELISA kit

(R&D systems, UK). Plasma C-reactive protein (CRP) and ferritin levels were analyzed in the Birmingham Heartlands hospital (Birmingham, UK).

2.2.2 Animals

Niemann-Pick type C1 mice (BALB/cNctr-*Npc1m1N*/J, *Npc1*$^{-/-}$ mice) were from an established colony (81). All mice were bred under sterile conditions, with food and water available *ad lib*. All animal studies were conducted using protocols approved by the UK Home Office for the conduct of regulated procedures under license (Animal scientific Procedures Act, 1986). The *Npc1*$^{-/-}$ mice have a lifespan of 10-12 weeks (average 10.5 weeks) with neurological symptoms presenting from 5-6 weeks of age. In this study, we examined mice at three time points: early pre-symptomatic (3-week-old), pre-symptomatic (5-weeks-old), early-symptomatic (7-week-old), late-symptomatic (9-weeks-old) stage and late end stage (11-week-old). Pups were weaned 3 weeks after birth and subsequently had free access to water and normal mouse chow.

2.2.3 Administration of iron supplementation therapy on Npc1$^{-/-}$ *mice*

Npc1$^{-/-}$ mice were injected intraperitoneally with iron-dextran (50 mg/kg body weight, twice per week) or vehicle (PBS solution) alone. Injections began at 3 weeks of age. The total iron concentration in the commercial diet was 200 mg Fe/kg (Teklad global 16% protein rodent diet - 2016, Harlan Laboratories, UK).

2.2.4.1 Mice hematological analysis

Blood samples were obtained by cardiac puncture using an EDTA rinsed – needle/syringe, and collected into EDTA rinsed tubes. Multiple hematological parameters, including erythrocyte related parameters (RBC, MCV, HCT), hemoglobin related parameters (HGB, MCH, MCHC), were determined using automatic blood analyzer (ABX Pentro 60 system, HORIBA-ABX, UK).

2.2.4.2 Mice blood smears preparation

Blood smears were prepared from fresh blood on glass slides and air dried at room temperature. For blood cell morphology analysis, blood smears were stained with Wright-Giemsa reagent (Sigma-Aldrich, St. Louis, MO, USA) according to the manufacturer's instructions. Stained samples were mounted with DePex mounting medium (VWR International Ltd, Poole, UK) and analyzed with a Zeiss Axioplan 2 fluorescence microscope. Images were acquired using a Zeiss charge-coupled digital camera and edited using Axiovision 2.0 software.

2.2.4.3 Mice serum samples preparation

Blood samples were collected by cardiac puncture, clotted for 1-2 hours at room temperature spun at 3,000 rpm for 15 minutes at 4^{o}C. The serum was collected and stored at -20^{o}C.

2.2.4.4 Mice serum/plasma iron levels and transferrin saturation levels analysis

Serum iron levels were quantified using Inductively Coupled Plasma Mass Spectrometer (ICP-MS). Serum samples were diluted 200-fold with 1% nitric acid at 70°C overnight. Samples were measure iron isotope (Fe-56) by Agilent 7500 Series ICP-MS (Department of Chemistry, University of Sussex), and Ge-72 was used as internal standard. Calibration solution for iron measurement was prepared between 0 and 1.0 ug/ml.

2.2.5.1 Neurological behavioral analysis - open field

Open field analysis was performed as previously described (82). In brief, the spontaneous activity of each mouse was recorded individually. After at least 20~30 minutes acclimatization in the room, the mouse was placed into the open field. Rearing was recorded manually for 5 minutes (the number of times the mouse reared on its hind legs), either without support (center rearing) or against the cage wall (rearing).

2.2.5.2 Neurological behavioral analysis - tremor

Tremor analysis was performed as previously described (82). Briefly, tremor was measured with a commercial tremor monitor (San Diego Instruments) according to the manufacturer's instructions. The tremor monitor was connected to a computer via a National Instruments PCI card and the output (amplitude/time) was analyzed using LabView software, to give a measurement of power at each frequency (0-64 Hz).

2.2.6.1 Antibodies for Western blotting/Immunoblotting

Primary antibodies, goat anti-mouse serum albumin (HRP-conjugated), rabbit anti-mouse light chain ferritin (L-ferritin), rabbit anti-mouse EPO, were obtained from Abcam**;** Rat anti-mouse soluble transferrin receptor (s-TfR) antibody was purchased from AbD Serotec. All primary antibodies were diluted in PBS-Tween (1:1000).

Secondary antibodies, Peroxidase-AffiniPure goat anti-rabbit and goat anti-rat IgG were purchased from Jackson ImmunoResearch Laboratories. Both secondary antibodies were diluted in PBS-Tween solution (1:10000).

2.2.6.2 SDS-PAGE/immunoblotting analysis

Serum protein concentration was determined by bicinchoninic acid (BCA) assay (Sigma-Aldrich, St. Louis, MO, USA) with bovine serum albumin (BSA) standard. Equal amounts of reduced serum protein (20 ug/well) were loaded onto 10% sodium dodecyl sulfate (SDS) polyacrylamide gels and separated using XCell SureLock^{TM} mini-cell system (Invitrogen, Paisley, UK) then transblotted using XCell blot module (Invitrogen, Paisley, UK) onto Hybond-P polyvinylidene difluoride (PVDF) membranes (GE healthcare, Chalfont St. Giles, UK). PVDF membranes were stained with 1% Ponceau S solution to demonstrate equivalent protein loading. Primary antibodies were incubated overnight at 4^{o}C, PVDF membranes were washed with DPBS-Tween (0.02%) solution (3x15 minutes) then incubated with horseradish peroxidase (HRP) conjugated secondary antibodies and visualized using SuperSignal West Pico Chemiluminescent Substrate (Thermo Scientific, Rockford, USA).

The optical density of immunoreactive bands was analysed and quantified using the Molecular Imager ChemiDoc^{TM} XRS with software Image Lab (version 3.0, Bio-Rad Laboratories, UK).

2.2.7 Immunohistochemistry/Immunofluorescence analysis

Age-matched control (*Npc1*$^{+/+}$) and *Npc1*$^{-/-}$ mice (9 weeks of age) were deeply anaesthetized with CO_2 and trans-cardially perfused with 4% paraformaldehyde. Tissues were removed and fixed for at least another 48 hours then dehydrated in 30% sucrose-DPBS solution. For immunofluorescence staining, 30 μm thick lung sections were cut, and blocked with 10% horse serum in DPBS for 1 hour. Sections were incubated with primary antibodies, either rat anti-mouse CD68 mAb (1:3000, AbD Serotec, UK) or rabbit anti-mouse HIF-1α pAb (1:1000, Novus, UK), in 10% horse serum in DPBS-Triton (0.3%) overnight at 4 ^{o}C. Sections were washed with DPBS solution, then incubated with secondary antibodies either Dylight-594 Red, rabbit anti-mouse (1:3000, Vector Laboratories, UK) or Dylight-488 Green, donkey anti-rat secondary antibodies (1:2000, Invitrogen, UK) for 2 hours at room temperature. Sections were counterstained with DAPI (100 ng/ml, 4'-6-diamidino-2-phenylindole; Sigma-Aldrich, UK). Images were captured and processed with a Zeiss Axioskop 2 Plus fluorescence microscope.

2.2.8 Flow cytometric analysis of spleen erythroid lineage cells

For analysis of erythrocytes in spleen, a single-cell suspension was generated from 9-week-old *Npc1*$^{-/-}$ and age-matched control (*Npc1*$^{+/+}$) mice, followed by washing with HBSS solution with 1% FBS, filtered through a cell strainer to generate single-cell suspensions and incubated on ice for 30 minutes with PE-conjugated anti-mouse TER-119, (BD Bioscience, UK) and FITC-conjugated anti-mouse CD71 antibodies (Biolegend, UK) in HBSS-1% FBS solution. Stained splenocytes were subsequently labelled using LIVE/DEAD cell viability assay kit. (Invitrogen, Paisley, UK). Samples were washed and data were acquired on a FACSCalibur flow cytometer (BD Biosciences, UK). FACS experiments shown are

representative experiments in which littermate controls were directly compared to age-matched *Npc1*$^{-/-}$ mice. Data were analysed using FlowJo v8.7.1 (TreeStar, OR).

2.2.9 Enzyme Linked Immunosorbent Assay (ELISA) for human serum TNF-α levels

Serum samples were obtained from 22 of the NPC1 patients participating in a Natural History study (06-CH-0186) and 14 of the control individuals of similar age and gender distribution. Mean age of patients and controls were 11.6 ± 7.9 years old and 12.7 ± 5.8 years old respectively (p = 0.66). Phenotypic severity was determined using the severity scale developed by Yanjanin et al. (83), and ranged from 1 to 35 (max severity on this scale is 50). 11 of the patients (55%) were being treated off-label with miglustat, an inhibitor of glycosphingolipid synthesis. Human serum levels of TNF-α were measured in triplicate by ELISA kit (Thermo Scientific), following the manufacturer's instructions. Standards ranging from 2 to 20,000 pg/mL were prepared following manufacturer's instructions. A standard curve was generated by linear regression. Serum TNF-α levels could not be precisely determined for 2 patients and 1 control, as their luminescence values were below the limit of detection.

2.2.10 Tissue isolation, RNA extraction, and Microarray hybridization and data analysis

Microarray analysis was performed by Cluzeau *et al.* as described (84). Female pups were sacrificed at 1, 3, 5, 7, 9 and 11 weeks of age. Only female mice were used for microarray analysis to avoid increasing variability due to potential gender effects on iron related metabolism genes expression. Livers were collected from both mutant and control animals, and immediately frozen on dry ice. Four livers were collected corresponding to each age and genotype, for a total of 48 samples. Microarray experiments were performed using standard Affymetrix protocols (Affymetrix, Inc.). Briefly, 200 ng of total RNA was reverse-transcribed to obtain labeled cDNA as recommended by the manufacturer. The hybridization cocktail containing the fragmented and labeled cDNAs was hybridized to Affymetrix Mouse GeneChip 1.0 ST chips, and the chips were washed and stained using standard protocols for

the Affymetrix Fluidics Station. Probe arrays were stained with the streptavidin phycoerythrin solution (Molecular Probes) and enhanced using an antibody solution containing 0.5 mg/ml of biotinylated anti-streptavidin (Vector Laboratories). Arrays were scanned using the Affymetrix Gene Chip Scanner 3000, and gene expression intensities were calculated using the Affymetrix GeneChip Command Console software. Affymetrix. CEL files were normalized using the RMA (robust multi-array analysis) algorithm within the Partek Genomics Suite software, version 6.5 (Partek, Inc.). Analysis of variance (ANOVA) and linear contrasts were used to identify DEGs, using a larger set of samples, including additional controls. Lists of genes differentially expressed between *Npc1*$^{-/-}$ and control mice were generated at each time point, using a combination of thresholds for both uncorrected *P*-value and FC (*p*-value ≤ 0.05, and FC ≤ -1.3 or ≥ 1.3). This gene selection method combining *P*-value and FC cutoff was previously demonstrated to result in higher concordance degree of DEGs between different platforms, when compared with genes selected only on *p*-value ranking. The microarray data were provided by Dr. Denny Porter (NIH, USA).

2.2.11 Statistical analysis

Data were expressed as the mean ± SEM. Statistical analysis was performed using the software package Prism 5 (GraphPad software). An unpaired 2-tailed Student's *t* test was used to determine the significant differences. For microarray analysis, analysis of variance (ANOVA) and linear contrasts were used to identify DEGs, using a larger set of samples, including additional controls. *P* values less than 0.05 were considered statistically significant.

2.3 Results.

2.3.1 Decreased hematocrit (HCT), mean corpuscular volume (MCV), hemoglobin (HGB) and mean corpuscular hemoglobin (MCH) in *Npc1*$^{-/-}$ mice.

To investigate the pathophysiological impact of lysosomal storage on hematopoiesis in NPC1 disease, we first evaluated erythrocyte-related parameters in *Npc1*$^{-/-}$ mice. Mean corpuscular volume (MCV) showed decreased and reached statistical significance by 7 weeks of age (-15.2%, $P = 0.0037$, 9 weeks, -12.9%, $P < 0.0001$) **(Fig. 2.1A)** while, hematocrit (HCT) followed a similar trend, reaching significance at 9 weeks of age (-15%, $P = 0.0002$) **(Fig. 2.1B)**. However, *Npc1*$^{-/-}$ red blood cell counts (RBC) and red cell distribution width (RDW) did not significantly differ between control (*Npc1*$^{+/+}$) and *Npc1*$^{-/-}$ mice **(Fig. 2.1C-D)**. Levels of hemoglobin (HGB) in *Npc1*$^{-/-}$ mice showed a decreased trend while compared to age-matched controls (*Npc1*$^{+/+}$) and reached statistical significance by 9 weeks of age in (-15.5%, $p = 0.0008$) **(Fig. 2.1E)**. Mean corpuscular hemoglobin (MCH) was also significantly reduced from 5 weeks of age in *Npc1*$^{-/-}$ mice (5 weeks, -5.6%, $p = 0.0010$, 7 weeks, -6.4%, $p < 0.0001$, 9 weeks, -12.6%, $p < 0.0001$) **(Fig. 2.1F)**. However, mean corpuscular hemoglobin concentration (MCHC) and circulating number of red blood cells (RBC) remained unchanged **(Fig. 2.1G)**. Furthermore, consistent with the hematological findings, Wright-Giemsa staining revealed that *Npc1*$^{-/-}$ erythrocytes appear microcytic and irregularly shaped by 9 weeks of age (**Fig. 2.1H-I**).

Figure 2.1. Decreased hematocrit (HCT), mean corpuscular volume (MCV), hemoglobin (HGB) and mean corpuscular hemoglobin (MCH) in *Npc1*$^{-/-}$ mice. (A-G) Whole Blood from 5, 7 & 9 week old control (*Npc1*$^{+/+}$) and *Npc1*$^{-/-}$ mice were analysed using an automated blood analyser as described in "Materials and Methods", which included erythrocyte and hemoglobin-related parameter analysis, red blood cell count (RBC), hematocrit (HCT), mean corpuscular volume (MCV), red cell distribution width (RDW), hemoglobin (HGB), mean corpuscular hemoglobin (MCH) and mean corpuscular hemoglobin concentration (MCHC). Data shown are mean ± SEM, n = 5 ~ 7, per group. ** $p < 0.005$, *** $p < 0.0005$, **** $p < 0.0001$, calculated by an unpaired *t* test using GraphPad Prism v5. **(H-I)** Wright-Giemsa stain of peripheral blood smears from control (*Npc1*$^{+/+}$) and *Npc1*$^{-/-}$ mice. Peripheral blood smears were prepared from 9-week-old control (*Npc1*$^{+/+}$) and *Npc1*$^{-/-}$ mice. Bars represent 5 μm.

2.3.2 Decreased serum iron levels, altered serum iron regulators expression, down-regulation of hepatic hepcidin and up-regulation of hepatic transferrin receptor-1 levels in *Npc1*$^{-/-}$ mice.

To further characterize the underlying mechanistic defects responsible for the hematological abnormalities in *Npc1*$^{-/-}$ mice, we evaluated circulating iron status, transferrin saturation and measured serum ferritin and soluble-form transferrin receptor (s-TfR) levels in *Npc1*$^{-/-}$ mice. Compared with the age-matched control littermates, 9-week-old *Npc1*$^{-/-}$ mice had significantly lower serum iron levels (reduced by approximately 25%) (9 weeks, -25%, $p = 0.047$) **(Fig. 2.2A).** Serum ferritin and soluble-transferrin receptor (s-TfR), were examined by immunoblotting analysis from 9-week-old *Npc1*$^{-/-}$ mice. Markedly increased levels of serum s-TfR were found in 9-week-old *Npc1*$^{-/-}$ mice (**Fig. 2.2B**), together with slightly elevated levels of serum L-ferritin **(Fig. 2.2B).** Considering the decreased serum iron status and evidence of microcytic anemia, we examined hepatic iron metabolism-related gene expression in *Npc1*$^{-/-}$ mice. Microarray experiments indicated that there was progressive and significant up-regulation of hepatic transferrin receptor-1 (TfR-1) mRNA expression from 3-weeks of age in *Npc1*$^{-/-}$ mice (3 weeks, 1.5 fold, $p = 0.038$, 5 weeks, 1.7 fold, $p = 0.010$, 7 weeks, 2.1 fold, $p < 0.0005$, 9 weeks, 2.1 fold, $p < 0.0005$; 11 weeks, 3.4 fold, $p < 0.00005$). Furthermore, significant up-regulation of relative hepatic transferrin (Tf) expression from 5-week-old *Npc1*$^{-/-}$ mice was also observed (5 weeks, 1.2 fold, $p < 0.005$, 7 weeks, 1.1 fold, $p < 0.05$, 9 weeks, 1.2 fold, $p < 0.0005$, 11 weeks, 1.1 fold, $p < 0.05$) **(Fig. 2.2D)**. In addition, there was a significant down-regulation of hepatic hepcidin mRNA expression at different

stages of disease in *Npc1*$^{-/-}$ mice (3 weeks, -1.6 fold, $p = 0.026$, 5 weeks, -1.7 fold, $p < 0.050$, 9 weeks, -1.9 fold, $p < 0.005$) **(Fig. 2.2E)**. However, it should be noted *Npc1*$^{-/-}$ hepatic hepcidin mRNA levels did not show significant down-regulation at 7 & 9 weeks of age, which could be associated with the initiation of systemic inflammation. The molecular target of hepcidin, ferroportin, was also examined; however, there were no significantly altered hepatic ferroportin mRNA expression throughout the lifespan of *Npc1*$^{-/-}$ mice, except for the late end stage time point (11 weeks, 1.17 fold, $p < 0.05$) **(Fig. 2F)**. The microarray data were consistent with hepatic cytosolic iron deficiency in *Npc1*$^{-/-}$ mice. This hypothesis was further supported by the significant down-regulation of hepatic hepcidin expression in *Npc1*$^{-/-}$ mice.

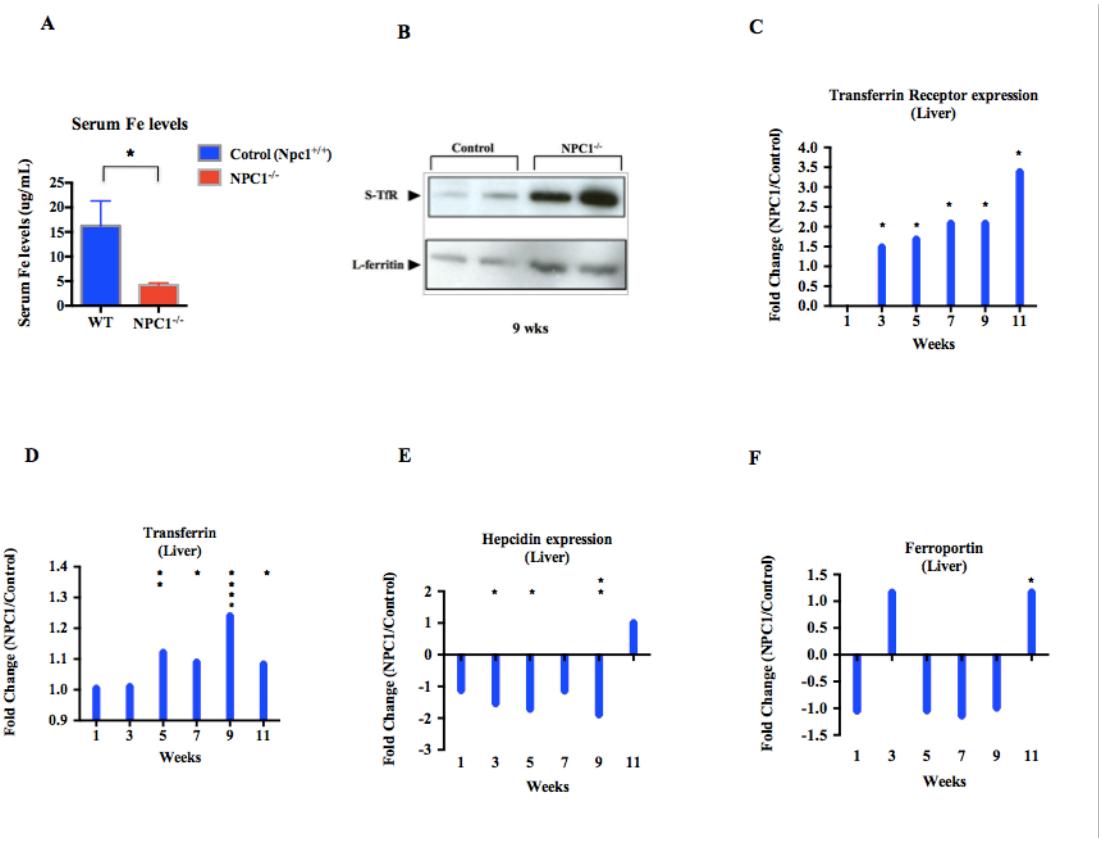

Figure 2.2 Decreased serum iron levels, altered expression of hepatic iron regulators in *Npc1*$^{-/-}$ mice. (A) For serum iron level analysis, equal volumes of serum samples were analyzed using ICP-MS technique as described in "Materials and Methods". Compared with the 9-week-old controls, the levels of total serum iron in *Npc1*$^{-/-}$ mice were significantly decreased by 25 %, n = 5 per group, * $p < 0.05$. **(B)** For serum soluble transferrin receptor and ferritin levels analysis, equal amount of serum samples (protein contents) were analyzes using Western blotting **(C-F)** For hepatic iron-related metabolism genes expression, hepatic microarray examination were analyzed from *Npc1*$^{-/-}$ mice and age-matched controls. ANOVA analysis was used to analyze microarray genes expression change. Data shown are mean ± SEM, n = 4 ~ 6, per group.

2.3.3 Abnormal hepatic iron metabolism-related pro-inflammatory cytokines in *Npc1*$^{-/-}$ mice.

Systemic iron status, hematological changes and hepatic hepcidin expression levels could be regulated by various pathophysiological factors, including systemic inflammation, hypoxic stress and abnormal erythropoiesis (26). In order to further characterize the underlying mechanisms, we investigated hepatic pro-inflammatory cytokines profile by microarray examination. Strikingly, the microarray examination indicated that there was significant down-regulation of *Npc1*$^{-/-}$ hepatic IL-1β mRNA expression as early as the early pre-symptomatic stage (1 week, -1.7 fold, $p = 0.04$, 7 weeks, -1.4 fold, $p = 0.02$, 9 weeks, -1.5 fold, $p < 0.05$) until late end-stage (11 weeks, -1.5 fold, $p = 0.01$) **(Fig. 2.3A)**. Other *Npc1*$^{-/-}$ hepatic pro-inflammatory cytokines, such as IL-1α, were markedly elevated in *Npc1*$^{-/-}$ liver with for example, elevations in IL-1α mRNA observed from 7 weeks (7 weeks, 1.9 fold, $p < 0.0005$, 9 weeks, 1.4 fold, $p < 0.05$, 11 weeks, 2.1 fold, $p < 0.0005$) **(Fig. 2.3B)**. However, there were no significant changes of *Npc1*$^{-/-}$ hepatic IL-6 mRNA expression from the early pre-symptomatic stage (1-week-old) till the late end–stage (11-weeks-old) *Npc1*$^{-/-}$ mice **(Fig. 2.3C)**. In addition, there were significantly elevated of hepatic TNF-α levels from 7-week-old *Npc1*$^{-/-}$ mice (unpublished observation, Platt *et.al.*,). These results, therefore, indicated that there were atypical hepatic pro-inflammatory cytokines profiles, in *Npc1*$^{-/-}$ mice, especially IL-1β-related ones that may impair *Npc1*$^{-/-}$ hepatic hepcidin expression and affect systemic iron homeostasis in *Npc1*$^{-/-}$ mice.

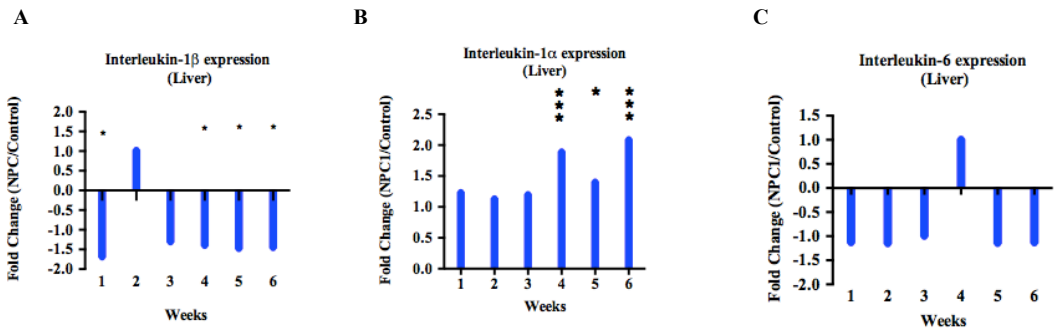

Figure 2.3 Atypical hepatic pro-inflammatory cytokines profile in *Npc1*$^{-/-}$ mice. (A-C) For hepatic pro-inflammatory cytokines levels, hepatic microarray examination were analyzed from *Npc1*$^{-/-}$ mice and age-matched controls. ANOVA analysis was performed to analyze microarray genes expression change. Data shown are mean ± SEM, n = 4, per group.

2.3.4 Increased splenic red blood cell frequency and diminished splenic F4/80^{+} macrophage numbers in *Npc1*$^{-/-}$ mice.

To determine whether the abnormal hematological changes and hepatic iron metabolism defects could be associated with abnormal erythropoiesis in *Npc1*$^{-/-}$ mice, we examined spleen morphology in *Npc1*$^{-/-}$ mice and measured spleen weights. Striking, 9-week-old *Npc1*$^{-/-}$ spleen exhibited splenomegaly compared with age-matched controls **(Fig. 2.4Ai)**. Further, *Npc1*$^{-/-}$ spleens weights were measured and revealed with an approximately 70% increase in wet weight compared with age-matched controls **(Fig. 2.4B)**. Similarly, an enlarged pale liver was noted in 9-week-old *Npc1*$^{-/-}$ mice with a wet weight increase of approximately 40% **(Fig. 2.4Aii,C)**. The percentage of *Npc1*$^{-/-}$ erythroid lineage cells was measured in spleen and maturation stages were examined (erythroid lineage-specific marker Ter119 and with CD71 (transferrin receptor) by flow cytometry **(Fig. 2.4D-F)**. By 9-weeks of age, *Npc1*$^{-/-}$ spleens displayed a significant increase in the total number of Ter119^{+} erythroblasts, suggesting enhanced erythropoiesis **(Fig. 2.4D)**. Moreover, the levels of Ter119^{+} erythroblasts were increased by approximately 54% **(Fig 2.4D)**. Further, flow cytometric analysis indicated that 9-week-old *Npc1*$^{-/-}$ spleen had a significantly greater number of orthochromatic erythroblasts (Region IV). However, the maturation from splenic proerythroblasts to chromatophilic erythroblasts (Region I-III) was not significantly different between 9-week-old *Npc1*$^{-/-}$ and control mice **(Fig. 2.4F)**. These results suggested that the altered pattern of splenic erythroblasts maturation may reflect the response to erythropoietin (EPO) or to changes induced by the splenic microenvironment. As altered splenic structure and increased erythropoiesis was observed in *Npc1*$^{-/-}$ mice, the observations of impaired systemic iron homeostasis and hematological abnormalities could be associated with *Npc1*$^{-/-}$ splenic red pulp macrophages (F4/80^{+})-mediated erythrocyte-derived iron recycling (unpublished observation, Dr. Aruna Jeans). Therefore, these results suggested that the abnormal diminished splenic red pulp F4/80^{+} macrophages in *Npc1*$^{-/-}$ mice (from 5-week-old) could impair splenic macrophages-mediated red cell clearance/iron recycling and affect systemic iron homeostasis in *Npc1*$^{-/-}$ mice.

Epo and its receptor (EpoR) are crucial for promoting cell survival, proliferation and differentiation of mammalian erythroid progenitors (85). To evaluate whether NPC1 deficiency induced iron deficiency and abnormal erythropoiesis could affect EPO/EPO-R mediated signaling, *Npc1*$^{-/-}$ hepatic microarray analysis was examined and indicated that (i) EPO-induced MAPK pathways, (ii) EPO-induced PI3K-AKT and calcium influx pathway were significantly altered from the early pre-symptomatic (1-week-old) till the late end stage (11-week-old) of *Npc1*$^{-/-}$ mice **(Table 2.1)**. Furthermore, the microarray examination indicated that EPO/EPO-R mediated PI3K-AKT and Ras/Raf/MEK/ERK pathway exhibited significantly altered gene expression of down-streamed signaling molecules from 1-week-old (P7) of *Npc1*$^{-/-}$ liver. In addition, we also found that EPO-mediated calcium influx signaling pathways were markedly altered in *Npc1*$^{-/-}$ liver, which could be associated with lysosomal acidic store calcium efflux defects in NPC1 disease (22) **(Fig. 2.5-6)**. These results, therefore, suggested that hepatic EPO/EPO-R mediated signaling defects might be associated with the abnormal erythropoiesis in *Npc1*$^{-/-}$ mice.

Table 2.1 Activation of hepatic EPO/EPO receptor-induced MAPK pathway in *Npc1*$^{-/-}$ mice

		1-week-old	3-week-old	5-week-old	7-week-old	9-week-old	11-week-old
1	Btk			1.53946	1.53946	1.85571	2.08049
2	Rapgef1					-1.33341	
3	Mapk3		1.40326	1.59157	1.59157	1.36674	1.5492
4	Gnb1		1.37154	1.35319	1.35319	1.65304	1.617
5	Gnb4					1.66608	1.46341
6	Gng13					-1.43208	
7	Gng2			1.34889	1.34889		1.75681
8	Gngt2		1.72684	1.96596	1.96596	2.48332	2.00605
9	Itpr1						
10	Kras		1.3936			1.38608	1.39738
11	Lyn			1.32408	1.32408		
12	Lyn			1.32408	1.32408		
13	Lyn			1.32408	1.32408		
14	Kitl						1.54462
15	Nras			1.42038	1.42038	1.32737	
16	Pak1	1.45546	2.06705	2.44469	2.44469	2.26699	2.56281
17	Cdkn1a		2.13559			2.05571	
18	Pik3cg					1.46191	1.59994
19	Pik3cg					1.46191	1.59994
20	Pik3cg					1.46191	1.59994
21	Pik3cg					1.46191	1.59994
22	Plcg1					-1.37103	
23	Plcg2			1.33859	1.33859	1.69593	1.63037
24	Plcg1					-1.37103	
25	Inpp5d		1.32247	1.97571	1.97571	2.07795	2.69478
26	Hgf					1.30941	
27	Sykb		1.92475	2.93093	2.93093	2.91221	3.93363
28	Vav1		1.5302	2.18373	2.18373	2.60996	2.99469
29	Cbl			1.86769	1.86769	1.88295	2.28284
30	Jun	1.68381	1.63895	3.39399	3.39399	2.1607	2.46005
31	Sco1					-1.40688	-1.54905

Normalized expression

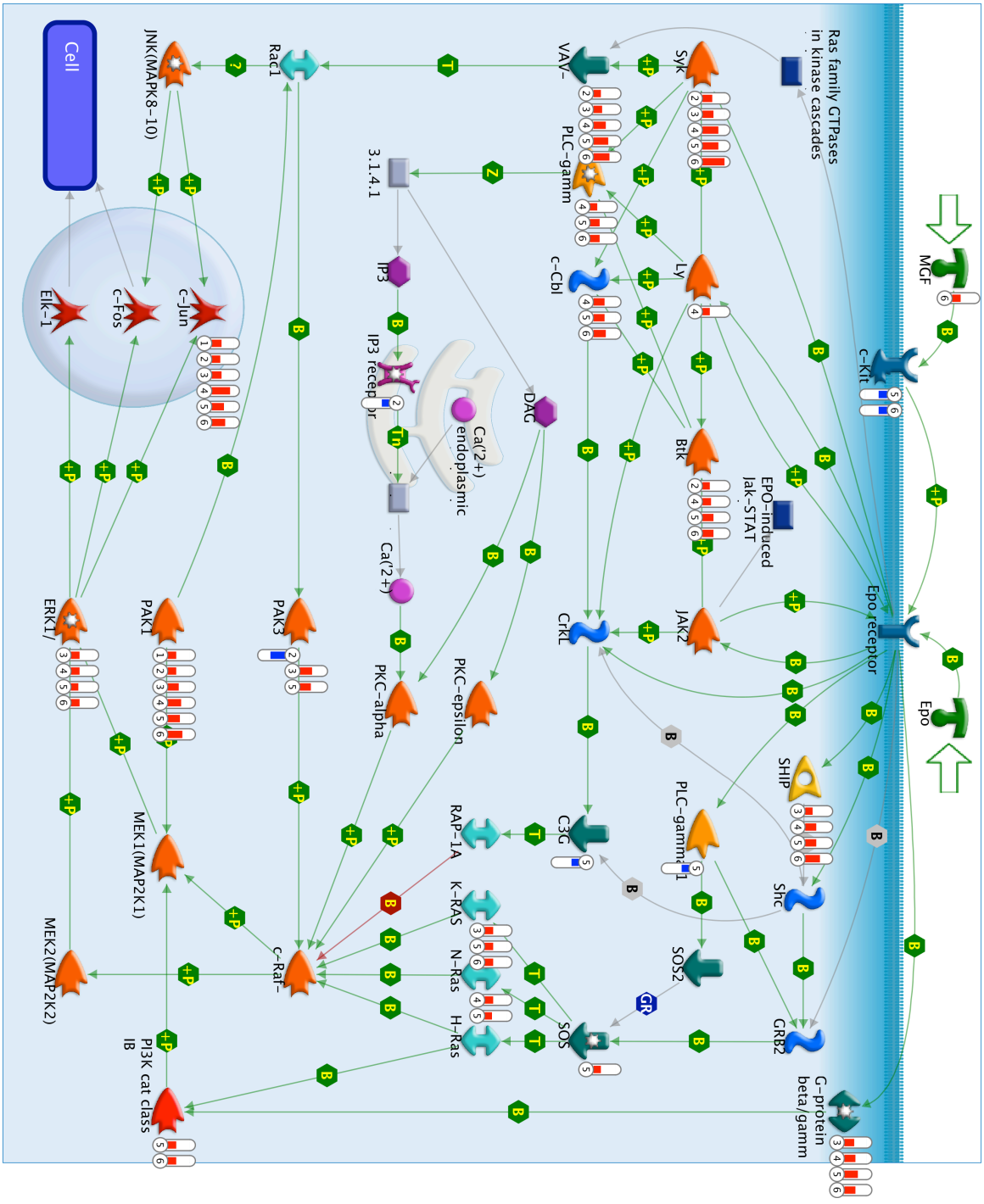

Figure 2.5 Activation of hepatic EPO/EPO-receptor mediated MAPK pathway in *Npc1*$^{-/-}$ mice.

In addition, hypoxic stress and macrophage activation status were evaluated, our results indicated a marked increase of HIF-1α levels and the macrophage activation marker CD68 in 9-week-old *Npc1*$^{-/-}$ lung section **(Fig. 2.7)**.

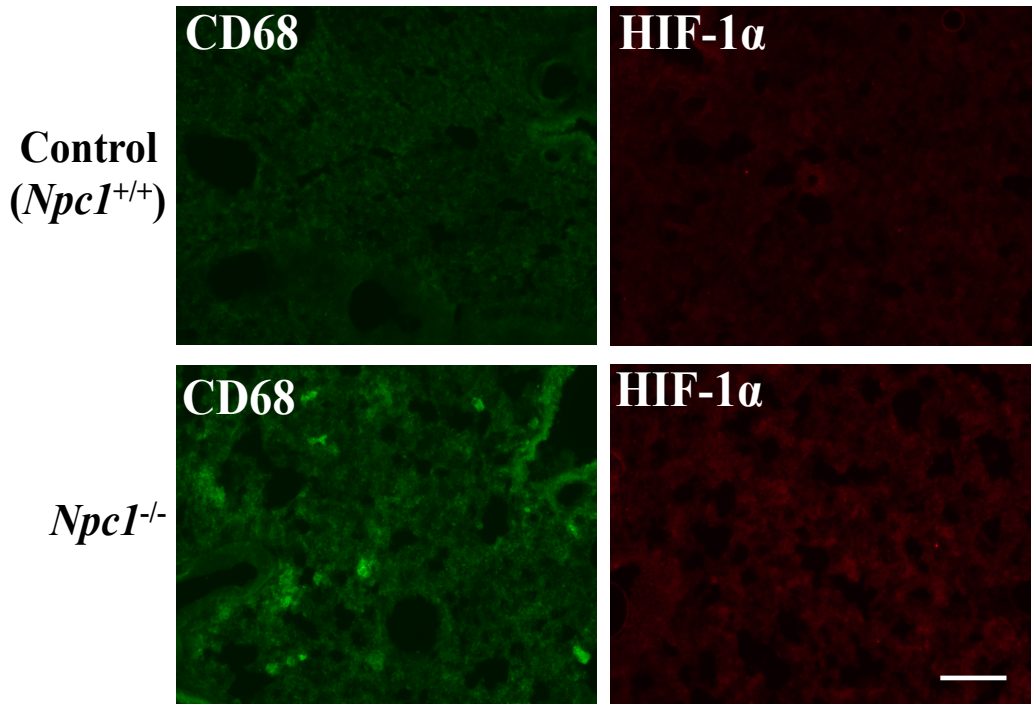

Figure 2.7. Increased expression of macrophage activation marker (CD68) and hypoxia-inducible factor-1α (HIF-1α) in *Npc1*$^{-/-}$ mouse lung. Representative images of immunofluorescence analysis on macrophage activation marker (CD68, green) and hypoxia-inducible factor 1α (HIF-1α, red) on lung sections of 9-week-old control (*Npc1*$^{+/+}$) and *Npc1*$^{-/-}$ mice. Scale bar = 1 μm.

2.3.5 Improved hematological abnormalities, motor function and survival in *Npc1*$^{-/-}$ mice in response to iron supplementation.

To test the hypothesis that iron supplementation may be of therapeutic benefit, we treated *Npc1*$^{-/-}$ mice with iron supplementation initiated at 3 weeks of age, and continued twice per week until the animals reached the humane endpoint (loss of 1g in body weight in 24 hours when feeding is compromised in late stage disease). Treatment of *Npc1*$^{-/-}$ mice with iron-dextran (50 mg/kg/body weight, IP, twice per week) had a modest effect on weight maintenance of *Npc1*$^{-/-}$ relative to *Npc1*$^{-/-}$ mice treated with vehicle alone **(Fig. 2.8A).** Interestingly, the survival of vehicle-treated *Npc1*$^{-/-}$ mice was significantly increased compared with untreated littermates (14.3%, $p < 0.005$), probably due to partial correction of dehydration in end stage *Npc1*$^{-/-}$ mice **(Fig. 2.8B)**. Furthermore, vehicle-treated *Npc1*$^{-/-}$ mice had an average life span of 84 days whereas the iron-dextran treated *Npc1*$^{-/-}$ mice lived up to 95 days, with an average of 89 days, resulting in a significant increase in survival (8.3%, $p <$

0.05) **(Fig. 2.8C-D)**. No significant difference in fine tremor was observed between iron-dextran or vehicle-treated *Npc1*$^{-/-}$ mice at 9 weeks of age **(Fig. 2.8E)**. However, center rearing, an indicator of muscle strength, motor coordination and motivation, showed a significant and marked increase compared to vehicle-treated *Npc1*$^{-/-}$ mice at 6, 8 and 10 weeks of age (6 weeks, 4.8 v.s. 19.8, $p < 0.05$, 8 weeks, 3.6 v.s. 11.5, $p < 0.05$, 10 weeks, 0.8 v.s. 8, $p < 0.05$) **(Fig. 2.8F)**. In addition, there were significantly elevated levels of serum ferritin and s-TfR in iron-dextran treated *Npc1*$^{-/-}$ mice (9 weeks, $p < 0.0005$) while compared with vehicle treated controls **(Fig. 2.8G-H)**.

Figure 2.8 Effects of iron supplementation therapy on body weight, survival and neurological function of *Npc1*$^{-/-}$ mice. Mice were injected (I.P.) with iron-dextran (50 mg/kg), twice per week. Iron supplementation therapy was started at 3 weeks of age. Age-matched control animals were injected with saline solution as a vehicle control group. **(A)** Average body weight over time. **(B)** Average survival days, $p < 0.05$. **(C)** Kaplan-Meier survival curve (%), $p < 0.05$. **(D)** Average survival days, $p < 0.05$. **(E)** Average tremor at 9 weeks**. (F)** Center rearing at 4, 6, 8 and 10 weeks. Data shown are mean ± SEM, n = 6 ~ 12, per group. * $p < 0.05$. **(G-H)** Representative image of Western blotting analysis of serum ferritin and soluble-form transferrin receptor in vehicle and iron-dextran treated *Npc1*$^{-/-}$ mice. Quantitative analysis of serum levels of ferritin and s-TfR in vehicle and iron-dextran treated *Npc1*$^{-/-}$ mice. Data are representative of 2 independent experiments.

In addition, hematological abnormalities, including MCV, HGB and HCT, in *Npc1*$^{-/-}$ mice were markedly improved after treatment with iron-dextran **(Fig. 2.9A-F).** Interestingly, the circulating RBC showed a significant increase in iron-dextran treated *Npc1*$^{-/-}$ mice compared with vehicle (PBS)-treated animals, which could reflect the stimulatory effects of parental iron supplementation on erythropoiesis.

2.3.6 Hematological abnormalities and decreased serum iron and transferrin saturation levels in NPC1 patients.

Altered levels of erythrocyte-related parameters, including low normal range values for HCT, MCV and MCH, were observed in NPC1 patient blood samples (**Fig. 2.10A-D**). There were no significant differences in absolute lymphocyte, neutrophil, basophil, eosinophil or monocyte counts in NPC1 patients compared with age-appropriate reference ranges (**data not shown**).

Figure 2.9 Improved hematological abnormalities in *Npc1*$^{-/-}$ mice in response to iron supplementation treatment. **(A-F)** Hematological parameters in vehicle or iron-dextran treated *Npc1*$^{-/-}$ mice. RBC, red blood cell count; HCT, hematocrit; RDW, red blood cell distribution width; MCV, mean corpuscular volume; HGB, hemoglobin; MCH, mean corpuscular hemoglobin; and MCHC, mean corpuscular hemoglobin concentration. Data shown are mean ± SEM, n = 3 ~ 4, per group, ** $p < 0.005$, for the comparison of age-matched vehicle-treated *Npc1*$^{-/-}$ mice and iron-dextran treated *Npc1*$^{-/-}$ mice, calculated by an unpaired *t* test using GraphPad Prism v5.

NPC1 patients had significantly lower levels of serum iron and transferrin saturation as compared to control group (-22.2%, p = 0.0020 and -17.1%, p = 0.0446, n = 38~39 and n = 59, respectively) (**Fig. 2.11A-B**). However, serum transferrin levels remained unchanged compared with controls (**Fig. 2.11C**). No significant correlation between serum iron levels and disease severity were observed (**data not shown**). Levels of serum ferritin in NPC1 patients were significantly elevated **(Fig. 2.11D)**, and again there was no statistically significant correlation between serum ferritin levels and disease severity (**data not shown**). In addition, despite the slightly elevated levels of serum TNF-α measured in NPC1 patients, no significant difference was observed compared with controls **(Fig. 2.11E)**. In addition, no significant correlation was observed between serum TNF-α levels, or liver function parameters (AST, ALT) and disease severity (data not shown). Finally, plasma CRP and sTfR levels were not significantly changed compared to controls **(Fig. 2.11F-G)**.

2.4 Discussion.

We have documented multiple abnormal hematological changes in *Npc1*$^{-/-}$ mice, including altered erythrocyte and hemoglobin-related parameters, which are consistent with anemia (**Table. 2.3**) (68).

Anemia could be caused by multiple pathophysiological factors, including inflammatory processes and it is interesting that the profile in *Npc1*$^{-/-}$ mice includes elements of both inflammatory and non-inflammatory anemia (**Table. 2.3**). For instance, the reduced levels of serum iron, hemoglobin, elevated levels of hepatic transferrin receptor and hypoxic stress suggest that all these factors may contribute to pathogenesis in NPC1 disease. This hypothesis was supported by the improved hematological abnormalities, greatly improved motor function and modest increase in survival in *Npc1*$^{-/-}$ mice receiving iron supplementation therapy. Relative to *Npc1*$^{-/-}$ mice, NPC1 patients only exhibited mild symptoms of anemia and hematological abnormalities with low serum iron and transferrin saturation levels presumably because partially functional NPC1 protein may exist in NPC1 patients. However, these data suggest that NPC1 patients are at risk of iron deficiency anemia and monitoring of both serum iron and complete blood counts is important in NPC1 patients. Should iron deficiency anemia become an issue, iron supplementation may be a useful adjunctive therapy for NPC1 patients based on the studies conducted in mice showing neurological benefit of iron supplementation therapy.

The involvement of hypoxic stress has been implicated in the pathogenesis of multiple diseases, including amyotrophic lateral sclerosis, cystic fibrosis, heart failure and chronic obstructive pulmonary disease (86, 87). The connections between iron homeostasis and hypoxia have been extensively studied and have revealed that hepcidin and hypoxia inducing factors (HIFs) are regulated by both systemic iron homeostasis and oxygen supply (88) . Chronic lung dysfunction has also been shown to occur in *Npc1*$^{-/-}$ mice (89-91). Therefore, it

is possible that systemic iron deficiency induces systemic hypoxic stress, including lung hypoxia, resulting in macrophage activation, a systemic inflammatory responses and lung dysfunction in NPC1 disease (92). Indeed, our microarray analysis revealed that hypoxic and EPO-related pathways were significantly modified in *Npc1*$^{-/-}$ liver (84). Furthermore, it also raised the intriguing possibility that abnormal erythropoiesis may induce systemic hypoxic stress in the early stages of development of *Npc1*$^{-/-}$ mice, and it could possibly contribute to the pathogenesis cascades in NPC1 disease, especially in *Npc1*$^{-/-}$ brain and liver. Therefore, it would be of interest to further determine the pathophysiological impacts of abnormal erythropoiesis induced hypoxic stress and brain erythropoietin expressions in *Npc1*$^{-/-}$ mice.

In this study, we found significant changes in *Npc1*$^{-/-}$ mouse erythrocytes with decreased MCV and HCT, suggesting that *Npc1*$^{-/-}$ erythrocytes are microcytic. Interestingly, microcytic erythrocytes are often observed in iron deficiency anemia, thalassemia and anaemia of chronic diseases (93). Furthermore, we observed abnormal erythrocyte morphology in *Npc1*$^{-/-}$ peripheral blood smears, which are consistent with our finding of low MCV in hematological analysis of *Npc1*$^{-/-}$ mice. However, we still cannot exclude the possibility that altered lipid compositions of erythrocyte plasma membranes, especially cholesterol and sphingolipids-enriched domains (lipid rafts), could lead to the defects in *Npc1*$^{-/-}$ erythrocytes production, morphology changes and also impair the contents of HGB in *Npc1*$^{-/-}$ erythrocytes (94, 95).

Observations of low serum iron and low Tf saturation levels in *Npc1*$^{-/-}$ mice could be related to the pathophysiological effects of systemic iron dysregulation and abnormal systemic inflammatory signalling in NPC1 disease. This hypothesis was supported by the microarray examination indicating that atypical hepatic IL-1β inflammatory signalling is a major pathophysiological feature of the NPC1 disease (84). In addition, we also observed up-regulation of hepatic TfR-1 in *Npc1*$^{-/-}$ mice, suggesting that hepatic cytosolic iron deficiency in *Npc1*$^{-/-}$ mice. Another crucial regulator of systemic iron homeostasis, hepcidin, was observed to be significantly down-regulation from the early pre-symptomatic (P21) stage in *Npc1*$^{-/-}$ mice, despite no-significant difference in hepatic ferroportin mRNA levels. However,

it should be noted that ferroportin expression is mainly regulated at the post-transcriptional and post-translational levels by the iron regulatory proetein-1 (IRP-1) and hepcidin (31). The dynamic changes of *Npc1*$^{-/-}$ hepatic hepcidin expression could be associated with different factors, e.g., anemia, hypoxia, inflammation, involved in the underlying pathogenesis of NPC1 disorder (34). For example, inflammation and hypoxic stress, which have been demonstrated to be involved in the regulation of hepcidin expression, may only start to be involved in NPC1 pathogenesis from the early symptomatic (6/7-week-old) stage. Interestingly, an atypical hepatic pro-inflammatory cytokines profile has been observed in *Npc1*$^{-/-}$ mice, which could be associated with lysosomal calcium dysregulation in *Npc1*$^{-/-}$ mice (Platt et., al unpublished observation). Therefore, it would be crucial to investigate further the underlying mechanisms of iron metabolism defects in NPC1 disease to get a better understanding of the underlying pathogenesis of NPC1 disease **(Fig. 2.12)**.

The causes of the decreased serum iron levels and abnormal hematological changes in *Npc1*$^{-/-}$ mice and patients could be linked to (i) defective iron absorption in the duodenum (34), (ii) the disturbance of the Tf uptake and TfR recycling (96, 97), (iii) systemic hypoxic stress and unusual inflammatory responses (86) (iv) and/or altered distribution of intracellular iron in subcellular compartments. Interestingly, mis-localization of intracellular iron has been recently reported in the lysosomal storage disease, *TRPML1*$^{-/-}$ type IV mucolipidosis (MLIV) in human fibroblast (98). Therefore, it will be crucial to determine the intracellular and tissue iron distribution *in vitro* and *in vivo* in NPC1 disease models. In addition, GI tract iron absorption defects could be one of the causes of the abnormal iron-related hematological changes in NPC1 disease. Interestingly, it has been suggested the there are potentially mechanistic links between the inflammatory bowel disease, Crohn's disease, NPC1 disease and other related lysosomes or LROs dysfunctional diseases, such as Tangier disease and Chediak-Higashi Syndrome (99-101). One of the common pathogenesis features

of inflammatory bowel disease and Crohn's disease is iron deficiency anemia with abnormal low hemoglobin levels. The anemia related symptoms of inflammatory bowel disease (IBD) and Crohn's disease have been demonstrated to be ameliorated when patients were treated with iron supplementation therapy (68). Although the underlying pathogenesis of iron dysregulation phenotypes in NPC1 disease remain to be further investigated and the molecular mechanisms could be quite complicated, our current studies highlight the importance of lysosome-mediated iron homeostasis and could provide some potential mechanistic links of lysosome/LROs dysfunctional disorders and iron absorption defect-related diseases.

This study also has practical implications as it has identified a number of potential clinical biomarkers, including inflammatory and iron-related proteins. Serum ferritin and s-TfR have been extensively measured as iron-related biomarkers to evaluate systemic iron levels and erythropoietic activity in patients with various iron related disorders, such as iron deficiency anaemia and iron overload disorders, e.g., hemaochromatosis (68, 102-104). The levels of serum ferritin have been suggested to be regulated by various factors (age, gender) and different pathological conditions, including inflammation, infection and chronic diseases (105). Another common iron indicator that changes in NPC1 disease is the s-TfR. Unlike other iron-related biomarkers, the levels of serum s-TfR are up-regulated in response to iron deficiency anaemia, but are not affected by chronic inflammation and infection (102). In this study, we screened both of these biomarkers and found that the levels of serum ferritin were slightly elevated, but the levels of s-TfR were markedly up-regulated in *Npc1*$^{-/-}$ mice. Moreover, after administrating of iron supplementation, the levels of serum ferritin and s-TfR were both markedly increased, which could be the effects of iron supplementation treatment on increasing tissue/circulating iron contents and stimulating erythropoiesis activity in iron-dextran-treated *Npc1*$^{-/-}$ mice. These results, therefore, suggested that both serum s-TfR and ferritin could serve as potentially useful biomarkers for clinical monitoring of iron deficiency, erythropoiesis activity and evaluation of the effects of iron supplementation on NPC1 disease.

In a previous study, we identified systemic iron dysregulation induced hematological changes in another subgroup of lysosomal storage disorder, mouse models of the GM1 and GM2 gangliosides (106). In these mice, there was progressive depletion of tissue iron, including in the brain, and iron supplementation therapy was also of benefit (106). Furthermore, our findings revealed that the hematological profiles of GM1/GM2 gangliosidosis mice also included elements of iron deficiency as well as inflammatory associated microcytic and macrocytic anemia with (i) progressive systemic iron deficiency, (ii) elevated levels of pro-inflammatory cytokine, e.g., IL-6 (iii) and up-regulation of hepatic hepcidin levels, while this seems not to be the case in *Npc1*$^{-/-}$ mice (106). While compared with the GM1/GM2 gangliosidesis mice, our current findings indicated that *Npc1*$^{-/-}$ mice showed much more severe hematological abnormalities, down-regulation of hepatic hepcidin and abnormal hepatic pro-inflammatory cytokines profiles, including IL-1β, TNF-α and IL-6. In addition, it should also be noted that peripheral tissue ferritin (ferritin light & heavy chain subunits) deficiency has been reported in a small number of clinical cases of NPC1 disease, but not in patients with other lysosomal storage diseases, including Gaucher, Batten and GM2 gangliosidosis, which may suggest a specific role for NPC1 protein in systemic iron homeostasis (107-109). Although the biological functions of the NPC1 protein still remain unclear, it has been suggested that NPC1 protein may be involved in the regulation of intracellular metal transportation, such as copper (110). NPC1 belongs to a member of the resistance-nodulation-cell division (RND) permease superfamily (24). In prokaryotic system, RND proteins are generally proton symporters involved in coupled efflux from the cell of substrates such as hydrophobic drugs, fatty acids, detergents, antibiotics and metals; however, most eukaryotic RND proteins remains uncharacterized (111). Therefore, it would be of interest to further investigate the biological functions of NPC1 protein on systemic iron homeostasis. However, in our current study, it still cannot be excluded that the dysregulation of systemic iron metabolism in *Npc1*$^{-/-}$ mice could be possible associated with lysosomal dysfunction in NPC1 disorder as the lysosome is involved in many aspects of systemic and cellular iron metabolism, including iron uptake, trafficking, storage, utilization and recycling

(45). Since systemic iron homeostasis is tightly regulated, dysfunction of lysosomal NPC1 protein could either directly or indirectly interact other lysosomal iron metabolism related proteins that impair systemic iron homeostasis and cause hematopoiesis defects (45). We are currently investigating whether *Npc1*$^{-/-}$ mice have similar tissue iron deficiency. Our current findings suggest that iron dysregulation is involved in the pathogenesis of NPC1 disease and may be a very tractable target for therapeutic intervention.

In conclusion, we have found that serum iron deficiency with elevated levels of hepatic TfR-1 and down-regulated hepatic hepcidin occurs in NPC1 disease and has functional consequences in the mouse model of NPC1 disease. Similarly, NPC1 patients have low normal serum iron and transferrin saturation levels and thus appear to be at risk of anemia. The serum iron deficiency and hematological changes may contribute to systemic/neurological hypoxic stress and may be influenced in part by systemic abnormal inflammation in NPC1 disease. Although the underlying molecular mechanisms of iron dysregulation in the pathogenesis of NPC1 disease remain to be further investigated, our findings have the potential to provide insights into the biological functions of the NPC1 protein in terms of systemic iron homeostasis and highlight multiple potential peripheral biomarkers for clinical monitoring. Finally, the functional improvement and hematological correction in *Npc1*$^{-/-}$ mice achieved with iron supplementation therapy suggests serum iron related parameters and hematological changes should be monitored carefully in NPC1 patients and it may represent a new approach to clinical management of NPC1 disease.

Chapter 3: Defective Systemic and Cellular Iron Homeostasis in Niemann-Pick type C1 Disease

Chapter 3: Defective Systemic and Cellular Iron Homeostasis in Niemann-Pick type C1 Disease

3.1 Introduction.

3.1.1 The biological function of iron and its systemic homeostasis

Iron is an essential trace element in multiple biological systems. For example, it serves as a co-factor in the biosynthesis of heme groups in hemoglobin and cytochrome family molecules, including cytochrome c and cytochrome P450s (CYPs), to help (i) maintain systemic oxygen supply, (ii) regulate mitochondrial electron transport chain respiration (iii) and is also involved in the regulation of the biosynthesis of lipids and steroid hormones and drug detoxification reactions (27, 71). In mammalian systems, systemic iron homeostasis is tightly regulated via complex mechanisms, including (i) iron absorption via duodenal enterocytes, (ii) iron storage via hepatocyte, (iii) iron utilization for erythropoiesis via erythroid precursors (iv) and iron recycling through splenic reticuloendothelial macrophages (41). Imbalances in systemic iron homeostasis could result in the generation of intracellular reactive oxygen species (ROS) and cause subcellular organelles dysfunction, increase lipid peroxidation and cellular apoptosis (48, 112).

3.1.2 Cellular iron homeostasis and its regulation

Cellular iron uptake is primarily mediated by the interaction of iron bound Tf and cell surface TfR-1 complex. Following receptor-mediated endocytosis, iron-bounded Tf and its receptor complex become mildly acidified in endosomal compartments facilitating the release of iron from the Tf/TfR-1 complex and is exported into the cytosol (79). Cytosolic iron is either transported to the nucleus to facilitate DNA synthesis or to mitochondria via mitoferrin to facilitate mitochondrial electron transport chain respiration (53). Excess cellular iron can be stored by the cytosolic iron storage protein complex, ferritin (113). In response to low cellular iron levels, cell surface TfR-1 is up-regulated to accelerate cellular iron uptake. Conversely, high cellular iron contents cause a down-regulation of cell surface TfR-1 expression and reduce cellular iron uptake (114).

3.1.3 The role of lysosomes in iron homeostasis

The lysosome plays a crucial role in catabolic pathways to redistribute and degrade intracellular macromolecules to maintain the balance of intracellular substrates use and storage (1, 2, 97). Several studies have suggested that lysosomes are involved in the synthesis and degradation of ferritin, an intracellular iron storage protein complex, and also regulate intracellular iron transport into other subcellular organelles, e.g., mitochondria via kiss and run model (44, 48, 115, 116). Lysosomes are also the sites of degradation of various iron regulators and transporters, such as hepcidin/ferroportin and heme complexes (28, 32, 72).

3.1.4 The biological function of mitochondria in iron regulation and its utilization

Mitochondria are crucial subcellular organelles involved in various aspects of cellular iron metabolism (53). Mitochondria are the main sites for the biosynthesis of (i) heme groups for hemoglobin and cytochrome production (ii) and cytosolic [Fe-S] clusters, which provide [Fe-S] clusters for mitochondrial, cytosolic and nuclear [Fe-S]-containing enzymes and its related cellular metabolic utilization (53). When cytosolic iron homeostasis is disrupted, it could alter the mitochondrial iron contents and impair the biological function of mitochondrial mediated (i) heme biosynthesis pathway, (ii) [Fe-S] clusters biogenesis and (iii) mitochondria iron homeostasis and utilization (52).

3.1.5 Systemic and cellular regulation of hepcidin and ferroportin interaction

Hepcidin is mainly synthesized in the liver (hepatocytes) and secreted into the plasma to regulate circulating iron levels and the cell surface expression of the iron exporter, ferroportin, via binding and inducing ferroportin internalization and degradation into lysosomes (40). Ferroportin is mainly expressed on the surface of (i) duodenal enterocytes, which regulates system iron absorption, (ii) hepatocytes, which is the site of systemic iron storage (iii) and reticulendothelial macrophages, which help iron recycle from senescent erythrocytes (114). Dysregulation of hepcidin/ferroportin complex causes systemic iron dyshomeostasis and leads to the development of various iron related disorders, such as iron

deficiency anaemia and iron overload disorders (93, 117). Hepatic hepcidin levels could be regulated by several pathophysiological factors, including (i) systemic iron status, (ii) systemic inflammation (iii) and hypoxic stress (36, 69, 80, 86). Increased hepcidin expression levels could be stimulated by systemic inflammatory responses, which result in duodenal ferroportin degradation and cause intestinal iron absorption defects (33, 118, 119). The expression of hepatic hepcidin-1 (*Hamp1*) is regulated by several physiological factors, such as erythropoiesis, inflammation, tissue iron contents, and requires the coordination of multiple essential signalling components, including TfR-2, hereditary hemochromatosis (HFE), TMPRS66, hemojuvelin (HJV) and bone morphogenic protein 6 (BMP-6), to maintain systemic iron homeostasis (120).

3.1.6 Lysosomal storage diseases

LSDs belong to a group of inherited metabolic diseases caused by lysosomal protein/enzyme defects leading to the intracellular storage of substrates, in the endosomal/lysosomal system (2, 121). However, the impact of dysfunctional lysosomes on systemic iron homeostasis remains largely unexplored. NPC disease is a lysosomal storage disease caused by mutations in either the NPC1 or NPC2 genes, and characterized by intracellular accumulation of un-esterified cholesterol and glycosphingolipid within the endolysosomal system and reduced acidic store calcium levels (21, 22, 25, 122, 123). Around 95% of cases of NPC disease are caused by mutations in the NPC1 gene. NPC1, a 1278 amino acid integral membrane protein of the late endosome/lysosome with a sterol-sensing domain (SSD) and belongs to the RND permease superfamily (124). The NPC1 protein has a cysteine-rich loop with zinc binding activity, which has been suggested to be crucial for the function of NPC1 protein to transport lysosomal cargos (124).

3.1.7 Aims of this chapter

Previously, we found evidence of iron dysregulation in a subgroup of lysosomal storage diseases, the GM1 and GM2 gangliosidoses (106). Our previous findings demonstrated system iron deficiency in the GM1 and GM2 gangliosidoses murine models, with evidence of anemia with inflammatory and iron deficiency elements. We also studied its potential impact on erythropoiesis, including altered serum iron-related parameters (TIBC/UIBC levels), and severe hematological changes (106). Although the molecular mechanism remains unclear, our previous study suggested that altered iron homeostasis may be a common element in the pathogenic cascades of multiple lysosomal storage disorders. Therefore, in this chapter, we extended the iron regulation studies to NPC1 disease and demonstrated the dysregulation of systemic and cellular iron homeostasis occurs *in vitro* and *in vivo* in NPC1 disease models and in NPC1 patients. In addition, systemic iron dysregulation could be linked to reactive oxygen species generation, mitochondria dysfunction with [Fe-S] clusters biosynthesis and heme metabolism defects, in *Npc1*$^{-/-}$ mice. Furthermore, iron supplementation of *Npc1*$^{-/-}$ mice improved motor coordination and increased tissue iron levels suggesting that iron supplementation therapy may be of potential clinical benefit.

3.2 Materials and Methods.

3.2.1. Animals

Niemann-Pick type C1 mice (BALB/cNctr-*Npc1m1N*/J, *Npc1*$^{-/-}$ mice) were from an established colony. All mice were bred under sterile conditions, with food and water available *ad lib* as described in **Chapter 2**. All animal studies were conducted using protocols approved by the UK Home Office for the conduct of regulated procedures under license (Animal scientific Procedures Act, 1986).

3.2.2 *Administration of iron supplementation therapy*

Npc1$^{-/-}$ mice were injected intraperitoneally with iron-dextran (50 mg/kg body weight, twice per week) or vehicle (DPBS solution) alone from the beginning of 3 weeks of age (P21). The total iron concentration in the commercial diet was 200 mg Fe/kg (Teklad global 16% protein rodent diet - 2016, Harlan Laboratories, UK) as described in **Chapter 2**.

3.2.3 Mice serum samples preparation

Blood samples were collected by cardiac puncture technique as described in **Chapter 2**.

3.2.4 Cell culture

Cells (human fibroblast and RAW 264.7 cells) were routinely passaged by trypsinization and maintained either in Dulbecco's modified Eagle's (DMEM) or Dulbecco's modified Eagle's-F12 (DMEM-F12) medium supplemented with 10% fetal bovine serum (FBS), 10% L-glutamine and 1% of penicillin G and streptomycin (Lonza).

3.2.5 Immunofluorescence analysis

Cells were fixed with 4% paraformaldehyde in DPBS solution (pH = 7.4) for 15 minutes, at 37 ^{o}C then washed with PBS solution at least 2~3 times. To avoid antibody non-specific binding, samples were incubated with 10 % horse serum in (3 uM) glycine/DPBS or DPBS-Triton X-100 (0.3%) solution for 1 hour. Samples were then incubated with the

appropriate primary antibodies in 10% horse serum in PBS/PBS-Triton X-100 solution at 4°C for overnight reaction. After washing samples with either PBST or PBS (for surface antigen detection only) several times, cells were incubated with secondary antibodies in 10% horse serum in DPBS/DPBS-Triton X-100 solution for 1 hour, at room temperature in dark. Then, cells were washed again with DPBST or DPBS solution for 3 times, each time at least 5 minutes. To counter stain nucleus, cells were incubated with 0.5 ug/ml DAPI solution for 30 minutes, and washed with PBS solution. Finally, the coverslips were mounted onto the slices with mounting medium and then samples were observed with fluorescence microscopy with suitable wavelength filters. Images were captured and processed with a Zeiss Axioskop 2 Plus fluorescence/light microscope and software.

3.2.6 Antibodies

Primary antibodies, rabbit anti-mouse light chain, rabbit anti-mouse heavy chain ferritin (L-& H- ferritin), antibodies were obtained from Abcam (anti-ferritin light chain pAb, ab69090; anti-ferritin heavy chain pAb, ab81444); Rat anti-mouse native, denatured and soluble-form transferrin receptor (TfR) antibody was purchased from AbD Serotec (MCA2396EL mAb). All primary antibodies were diluted in PBST (1:1000) as working conditions. Secondary antibodies, Peroxidase-AffiniPure goat anti-rabbit and goat anti-rat IgG (H+L chain, cat. No. 111-035-003 and 112-035-003, respectively) were purchased from Jackson ImmunoResearch Laboratories. Both secondary antibodies were diluted in PBST (1:10000) as working conditions.

3.2.7 Collection of CSF from NPC1 patients

NPC1 patients included in this study were enrolled in an ongoing longitudinal observational trial at the National Institutes of Health in Bethesda, Maryland as described in **Chapter 2**. The NICHD Institutional Review Board approved the study and the collection of age-matched control samples. The diagnosis was established by biochemical testing and/or mutation analysis. NPC1 diagnosis was established by fibroblast testing or molecular

analysis. CSF samples were collected by lumbar puncture performed under anesthesia in the L4/L5 interspace, after an age-appropriate overnight fast. CSF was collected in a polystyrene tube, and immediately transported to an on-site laboratory where it was aliquoted into polypropylene tubes. Samples were frozen on dry ice and stored at -80^{o}C prior to being sent to Medical Neurogenetics, LLC for assay. The CSF samples were kindly provided by Dr. Denny Porter (NIH, USA).

3.2.8 CSF ferritin levels analysis

CSF ferritin levels were measured using a commercial ELISA kit (Human Ferritin ELISA kit, Abnova, Taipei, Taiwan) according to the manufacture's instructions with minor modifications. Briefly, 20 µl of CSF samples were deposited on a microplate pre-coated with monoclonal antibody specific for ferritin and incubated at 4^{o}C overnight. After several washes with washing reagent, polyclonal anti-ferritin antibody conjugated to horseradish peroxidase was added and incubated for 2~3 hours at room temperature, followed by several wash and then chromogen substrate was added for 1 hour at room temperature. Finally, the stop reagent was added to stop the reaction. The optical density was measured at 450 nm using a FlurStar microplate reader (BMG LabTec, UK). Standard curves were also plotted from series concentration of ferritin standard reagent. All experimental results were calculated and averaged from duplicated experiment. The analytical accuracy of the ELISA kit is between 2% and 4% for the within-batch coefficient of variation and averages at 5% for the between batch CV.

3.2.9 Proteomic analysis (2D-Gels)

The protein pellet was resuspended in 375 µl IEF sample buffer. Carrier ampholytes were added at 0.9 % v/v Servalytes 3-10, 0.45% V.V servalyte 2-4 and 9-11 (Biowhitaker) for isoelectric focusing (IEF) on 3-10 non-linear pH gradient gels. Immobilised pH gradient (IPG) strips (Amersham Pharmacia Biotech) were rehydrated in the sample overnight and covered with mineral oil to prevent dehydration. IEF was carried out at 70kVh. Following

focusing the IPG strips were immediately equilibrated for 10 min in 2D samples buffer. The IPG strips were placed on top of the second dimension gels (Oxford GlycoScience) and embedded with 0.5 % melted agarose. Proteins were separated in the second dimension on SDS-PAGE gradient gels at run condition of 10^{o}C, 20 mA per gel for 1 hr, followed by 40 mA per gel for 4 4hrs. After electrophoresis, gels were fixed in 40% v/v ethanol: 10 % acetic acid and stained with the fluorescent dye OGT MP17 (Oxford GlycoScience). 16-bit monochrome fluorescence images were obtained at 200 um resolution by scanning gels with an Apollp II linear fluorescence scanner (Oxford Glycoscience). The 2D-proteomic analysis was performed by Dr. Annie Speak.

3.2.10 Perl's prussian blue iron histochemistry

Tissue iron distribution was analyzed using Perl's Prussian blue staining. Briefly, 9-week-old *Npc1*$^{-/-}$ and control (*Npc1*$^{+/+}$) mice were perfused with 4% paraformaldehyde in DPBS solution, pH 7.2. Tissue samples were harvested, dehydrated in 30% sucrose-DPBS solution for at least 24 hours at 4^{o}C. 20 μm thick fixed tissue sections were cut and then immersed in a potassium ferrocyanide mixture (Perl's solution, containing 1 part 10% aqueous, potassium ferrocyanide (Sigma, analytical grade) and 1 part of 10% hydrochloric acid) for 60 minutes, followed by washing with DPBS solution 3 times for 5 minutes and counterstained with 1% nuclear fast red (Sigma-Aldrich) for 5 minutes. Control sections were incubated with potassium ferrocyanide solution, but with distilled water in place of the hydrochloric acid. Images were captured and processed with a Zeiss Axioskop 2 Plus fluorescence/light microscope and software.

3.2.11 Electron microscopy analysis

Human fibroblasts were cultured with standard medium supplemented with 50 μM ferric ammonium citrate (FAC) for 72 hours. Followed by fixation with 4% paraformaldehyde in 0.2 M PHEM buffer (120 mM PIPES, 50 mM HEPES, 4 mM $MgCl_2$ and 20 mM EGTA) for 24 hours. Cells were washed twice with PBS+ (PBS containing 0.15

M glycine) and incubated with 1% gelatin for 30 min at 37^{o}C. After washing with PBS, cells were stored in 0.1 M PHEM buffer containing 4% paraformaldehyde. For electron microscopy, cells were re-fixed in PBS containing 2.5% glutaraldehyde, 2% paraformaldehyde, and 4% sucrose for 2 hours followed by 1% osmium tetroxide for 1 hour. After dehydrating in increasing concentrations of ethanol, cells were embedded in Epon 812 and examined using a JEOL 1200EX electron microscope.

3.2.12 Assessment of intracellular/tissue levels of lipid peroxidation

The tissue levels of lipid peroxidation products were determined using 4-hydroxynoneal (4-HNE) antibody and combined with tissue/cellular immunofluorescence techniques.

3.2.13 Quantification of tissue glutathione (GSH) levels

The total tissue GSH contents were analyzed using a commercial glutathione assay kit (Sigma-Aldrich, UK) according to the manufacture's instructions. Briefly, the protein concentration of prepared tissue homogenate was quantified using the BCA assay reagent. Equal amount of protein samples were de-proteinized using 5% 5-sulfosalicylic acid solution. After 10 minutes incubation on ice and subsequent centrifugation, the clear supernatant was collected and measured colormetrically at 405 nm using a FlurStar microplate reader (BMG LabTec, UK) The assay used a standard curve of reduced glutathione to quantify glutathione contents in the samples.

3.2.14 Double immunofluorescence anaysis.

8-week-old *Npc1*$^{-/-}$ mice and age-matched controls were deeply anaesthetized and trans-cardially perfused with 4% paraformaldehyde in 0.1 M PBS buffer, pH 7.2. Tissues (including brain, liver, spleen, kidney, lung and small intestine), were removed and further fixed for at least 48 hours then dehydrated in 30% sucrose-PBS solution. For immunofluorescence/immunohistochemistry staining, 10 μm thick sections were cut, and

blocked with 10% horse serum in DPBS for 1 hour. Brain sections were incubated overnight with a Rat anti-mouse CD68 primary antibody (1:100, Serotec) and then 2 hours with fluorescein-conjugated horse Anti-Rat IgG (1:200, Vector Labs) and counterstained with DAPI (100 ng/ml, 4'-6-diamidino-2-phenylindole; Sigma-Aldrich, UK).

3.2.15 Image analysis

To measure the levels of microglial activation (CD68) in the cerebellum of the mice, a series of images were taken using a Zeiss AXIO Imager A1 fluorescence microscope connected to a Zeiss AxioCamHRc digital camera. Images were taken from a minimum of 13 fields selected at random from several cerebellar sections per animal, including examples from both vermal and hemispheric regions of cerebellar tissue. For each field, images of the FITC channel and the DAPI channel were superimposed in Adobe Photoshop, then analysed using ImageJ (NIH). As the cell density and CD68 expression were not uniform across the cerebellum, each field was split into different zones, the deep cerebellar nuclei and surrounding parenchyma (DCN), the lobular white matter and internal granular layer (WM and IGL), and finally the molecular layer (ML). The area of these zones was calculated in mm^2, and the number of DAPI-labeled nuclei surrounded with a $CD68^+$ stain was counted in each area. For every animal, the areas and cell counts were pooled together and the total number of $CD68^+$ cells per mm^2 of molecular layer (ML) was calculated. The data set for each treatment consisted of three separate animals ($n = 3$). In order to assess the effect of iron supplementation on Purkinje cell survival, other sections from the same animals were stained with an antibody against calbindin, which in the cerebellum is a specific marker for Purkinje cells. As two of the cerebella in each data set were cut as transverse sections, (the other was cut parasagittaly) the crus1 zone of the ansiform lobule was chosen as a common area present in the remaining sections in which to count the surviving Purkinje cells. As this region is not in lobule IX or X it will therefore allow an unbiased representation of NPC-Purkinje cell loss. For each individual animal the number of Purkinje cells present in the crus1 zone was counted in multiple sections and the mean calculated.

3.2.16 Tissue isolation, RNA extraction, and Microarray hybridization and data analysis

Microarray related analysis was performed by Cluzeau *et al.* as described (84).

3.2.17 In Vitro Erythrophagocytosis Assay by RAW 264.7 murine macrophage cell line

3.2.17.1 Cell culture

The murine macrophage cell line RAW 264.7 was cultured in Dulbecco's Modified Eagle Medium F-12 (DMEM-F12, Sigma-Aldrich, UK) supplemented with 10% heat-inactivated fetal bovine serum (Atlanta Biologicals, Norcross, GA), 100 U/mL penicillin, and 100 μg/mL streptomycin at 37°C in 5% CO_2. For the erythrophagocytosis assay, the RAW 264.7 cells were pre-treated with U18666A (2 μg/mL) for 72 hours to induce Niemann-Pick type C1 disease cellular phenotypes. The control cells were incubated with 0.1% DMSO as a vehicle control groups.

3.2.17.2 Preparation of CFSE-labelled mouse erythrocytes.

9-week-old control (*Npc1*$^{+/+}$) mouse erythrocytes from were collected by cardiac puncture and washed with Hank's Balanced Salt solution (HBSS) solution, followed by labeling with a final concentration of 25 μM CFSE (Invitrogen, UK) for 30 minutes, according to the manufacturer's protocol. For opsonization of CFSE-labelled mouse erythrocytes, CFSE-labeled mouse erythrocytes were opsonized by incubating 1×10^9 red blood cells with rabbit anti-mouse red blood cell antibody, immunoglobulin G (IgG) fraction (1:50; Abcam, UK) for 30 minutes at room temperature and then washed twice with HBSS solution.

3.2.17.3 In vitro erythrophagocytosis assay.

Opsonized and CFSE-labelled mouse erythrocytes were added to the RAW 264.7 murine macrophage cell line monolayer and co-cultured for 2 hours at 37°C in 5% CO_2 incubator. Non-ingested opsonized CFSE-labelled erythrocytes were removed by incubating with mouse red blood cell lysing buffer (Sigma-Aldrich, UK) for 10 minutes, followed by

another 2 washes with DPBS solution. After incubation for the indicated times after erythrophagocytosis, RAW 264.7 cells were fixed with 4% paraformaldehyde.

3.2.17.4 Immunofluorescence microscopy.

After *in vitro* erythrophagocytosis assay, RAW 264.7 cells were fixed with 4% paraformaldehyde for 10 minutes at 37°C, as described earlier, then washed twice with DPBS solution and permeabilized with 0.2% Triton X-100 in DPBS+10% heat-inactivated goat serum for 1 hour at room temperature. Cells were incubated overnight at 4°C with 1:1000 primary anti-antibody. Cells were washed 3 times with DPBS followed by incubation with secondary antibody (either Dylight-594 Red, rabbit anti-mouse (1:3000, Vector Laboratories, UK) or Dylight-488 Green, donkey anti-rat secondary antibodies (1:2000, Invitrogen, UK)) for 2 hours at room temperature. After several wash with DPBS solution, cells were counterstained with DAPI (100 ng/ml, 4'-6-diamidino-2-phenylindole; Sigma-Aldrich, UK), mounted with anti-fading mounting medium and processed for immunofluorescence analysis.

3.2.18 Statistics

Data represent as mean ± SEM. Statistical analysis were performed by using GraphPad Prism software. An unpaired 2-tailed Student's *t* test was used to determine the significant differences. *p* values less than 0.05 were considered statistically significant.

3.3 Results

3.3.1. Altered expression of iron regulators in Npc1$^{-/-}$ peripheral organs

In **Chapter 2**, we found (i) up-regulation of hepatic TfR-1, (ii) down-regulation of hepatic hepcidin (*HAMP-1*) and (iii) atypical hepatic pro-inflammatory cytokines profile in *Npc1*$^{-/-}$ mice, which suggested hepatic cytosolic iron deficiency, inflammation and other pathophysiologcial factors may be involved in the regulation of *Npc1*$^{-/-}$ hepatic hepcidin-1 (*Hamp1*) expression. In order to further clarify the underlying mechanism of systemic iron dysregulation and its related hepcidin-1 regulation in *Npc1*$^{-/-}$ mice, we firstly examined microarray data and identified a number of genes with altered mRNA expression that are involved in cellular signaling involved in hepatic hepcidin-1 regulation, including (i) the BMPs-SMADs pathway, (ii) IL-6 mediated JAK-STAT3 pathway and (iii) HFE-TfR-2 mediated pathway, which modulates the expression of hepcidin levels in responses to different signals to maintain hepatic iron homeostasis. As shown in **Fig. 3.1A-B**, there were significant down-regulation of hepatic TfR-2 expressions from 1-week of age in *Npc1*$^{-/-}$ mice (1 week, -1.3 fold, $p < 0.0001$, 3 weeks, -1.2 fold, $p < 0.005$, 5 weeks, -1.2 fold, $p < 0.0001$, 7 weeks, -1.5 fold, $p < 0.0001$, 9 weeks, -1.4 fold, $p < 0.0001$, 11 week, -1.7 fold, $p < 0.0001$). Similar finding was observed with hepatic TMPRSS-6 expression, which showed significant down-regulation at 1,3, 7, 9 and 11-week of age in *Npc1*$^{-/-}$ mice (1 week, -1.3 fold, $p < 0.0001$, 3 weeks, -1.2 fold, $p = 0.0017$, 7 weeks, -1.4 fold, $p < 0.00001$, 9 weeks, -1.2 fold, $p < 0.00001$, 11 weeks, -1.5 fold, $p < 0.00001$). Furthermore, *Npc1*$^{-/-}$ hepatic hemochromatosis mRNA levels were significantly decreased at 7-weeks of age (7 weeks, -1.2 fold, $p = 0.01$) **(Fig. 3.1C)**. However, no significant change in relative BMP-6 mRNA expression was observed over the lifespan of *Npc1*$^{-/-}$ mice **(Fig. 3.1D)**. Interestingly, our microarray analysis also indicated that another murine hepcidin gene, hepcidin-2 (*Hamp2*), was significantly down-regulated from the early pre-symptomatic stage (3-week-old) of *Npc1*$^{-/-}$ mice (3 weeks, -2.0 fold, $p < 0.0001$, 7 weeks, -1.8 fold, $p < 0.005$, 9 weeks, -2.8 fold, $p < 0.0001$, 11 weeks,

-2.4 fold, $p < 0.0001$) **(Fig. 3.1E)**. The hepatic mRNA expression patterns of hepcidin-2 (*Hamp2*) were similar to hepcidin-1 (*Hamp1*) in *Npc1*$^{-/-}$ mice (**Chapter 2**).

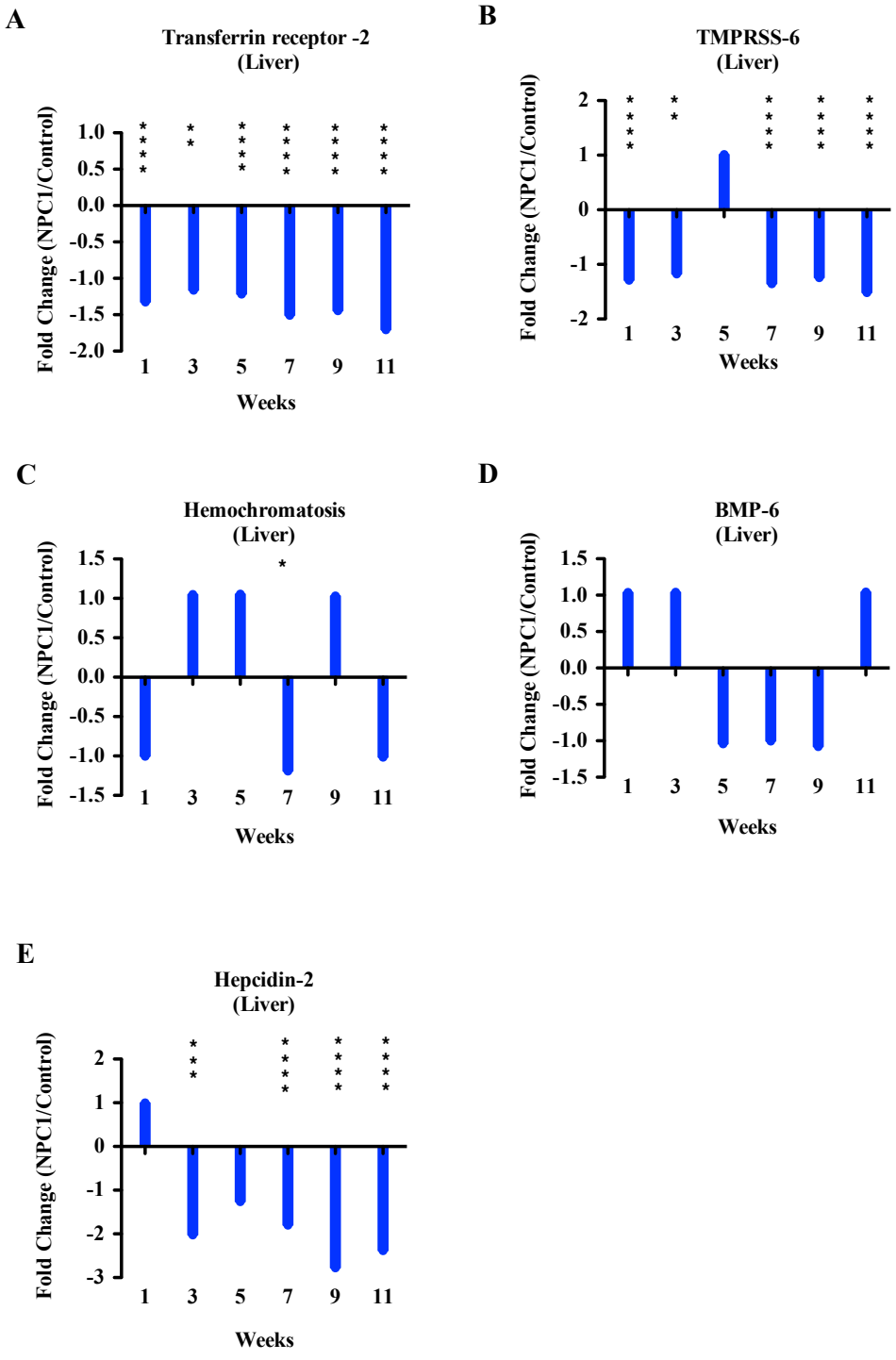

Figure 3.1. Altered genes expression of signaling molecules involved in the regulation of hepatic hepcidin expression in *Npc1*$^{-/-}$ mice. (A-E) For analysis of signaling components involved in the regulation of hepatic hepcidin expression, hepatic microarray examination were analyzed in *Npc1*$^{-/-}$ mice and age-matched control animals. ANOVA analysis was used to analyze microarray genes expression change. Data shown are mean ± SEM, n = 4, per group. * $p < 0.05$, ** $p < 0.005$, *** $p < 0.00005$, **** $p < 0.00001$.

In addition, our previous studies found atypical hepatic inflammation with down-regulated IL-1β, up-regulated TNF-α and unchanged IL-6 levels in *Npc1*$^{-/-}$ mice. Consistent with these findings, there were no significant changes in mRNA expressions of hepatic IL-6-related signalling molecules, including IL-6 receptor and STAT-3, in *Npc1*$^{-/-}$ mice (**data not shown**).

We then characterized systemic iron dysregulation phenotypes in liver from age-matched control and *Npc1*$^{-/-}$ mice using Perl's Prussian blue staining to detect hepatic ferric iron. As shown in **Fig. 3.2A**, ferric iron was readily detected in liver sections from 9-week-old control (*Npc1*$^{+/+}$) mice; however, there was little detectable ferric iron in age-matched *Npc1*$^{-/-}$ liver sections **(Fig. 3.2F)**. This observation suggested hepatic iron deficiency in *Npc1*$^{-/-}$ mice, which was consistent with hepatic TfR-1 levels progressively increasing in *Npc1*$^{-/-}$ mice. Besides, tissue ferric iron distributions from other peripheral organs were also analyzed. As illustrated in **Fig. 3.2 B-H**, there were markedly diminished of Prussian's blue stained ferric iron in 9-week-old *Npc1*$^{-/-}$ spleen, kidney and lung sections. These findings suggested that *Npc1*$^{-/-}$ mice have disrupted systemic iron homeostasis, which could be associated with the pathogenesis of NPC1 disorder.

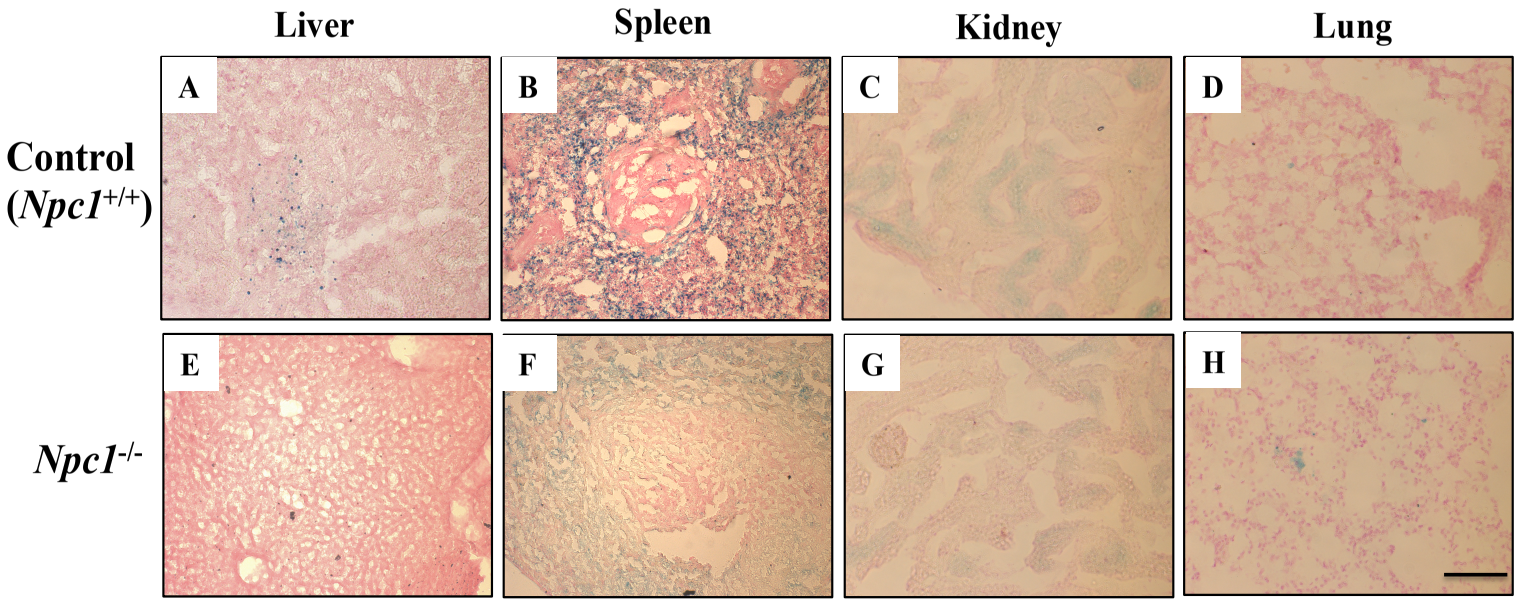
Liver
Spleen
Kidney
Lung
Control
(Npc1+/+)
Npc1-/-
A
B
C
D
E
F
G
H

Figure 3.2. Peripheral iron deficiency in *Npc1*$^{-/-}$ mice. (A-H) Representative images of peripheral tissues iron distribution in control (*Npc1*$^{+/+}$) and *Npc1*$^{-/-}$ mice. 9-week-old control and *Npc1*$^{-/-}$ mice liver, spleen, kidney and lung sections were collected and prepared as described in "Materials & Methods". Tissue iron distribution was detected by Perl's Prussian blue staining. The nucleus was counterstained with nuclear fast red reagent (red). Representative images were taken from three individual animals. Scale bar = 100 μm.

To further confirm the observation of peripheral iron deficiency phenotypes in *Npc1*$^{-/-}$ mice, peripheral tissues were collected and analyzed protein levels of several key iron metabolism regulators, including TfR-1 and ferritin. Consistent with microarray data, immunofluorescence and native-PAGE analysis indicated that there were markedly up-regulated hepatic TfR-1, down-regulated L-chain ferritin and native-form ferritin expressions in 9-week-old *Npc1*$^{-/-}$ mice **(Fig 3.3A-L)**. These observations were consistent with the Perl's Prussian blue tissue staining, which indicated *Npc1*$^{-/-}$ hepatic cytosolic iron deficiency. Similar results were also observed in *Npc1*$^{-/-}$ spleen and kidney and revealed up-regulation of TfR-1 and down-regulation of L-ferritin and native form ferritin. **(Fig 3.3M)**. Interestingly, the immunofluorescence and Perl's Prussian blue analysis indicated reduced ferric iron particles and L-ferritin positive signals in 9-week-old *Npc1*$^{-/-}$ spleen sections, which could be associated with the glycosphingolipids (GSLs) storage induced changes in splenic F4/80^{+} macrophage population in *Npc1*$^{-/-}$ mice **(Platt et., al, unpublished observations)**.

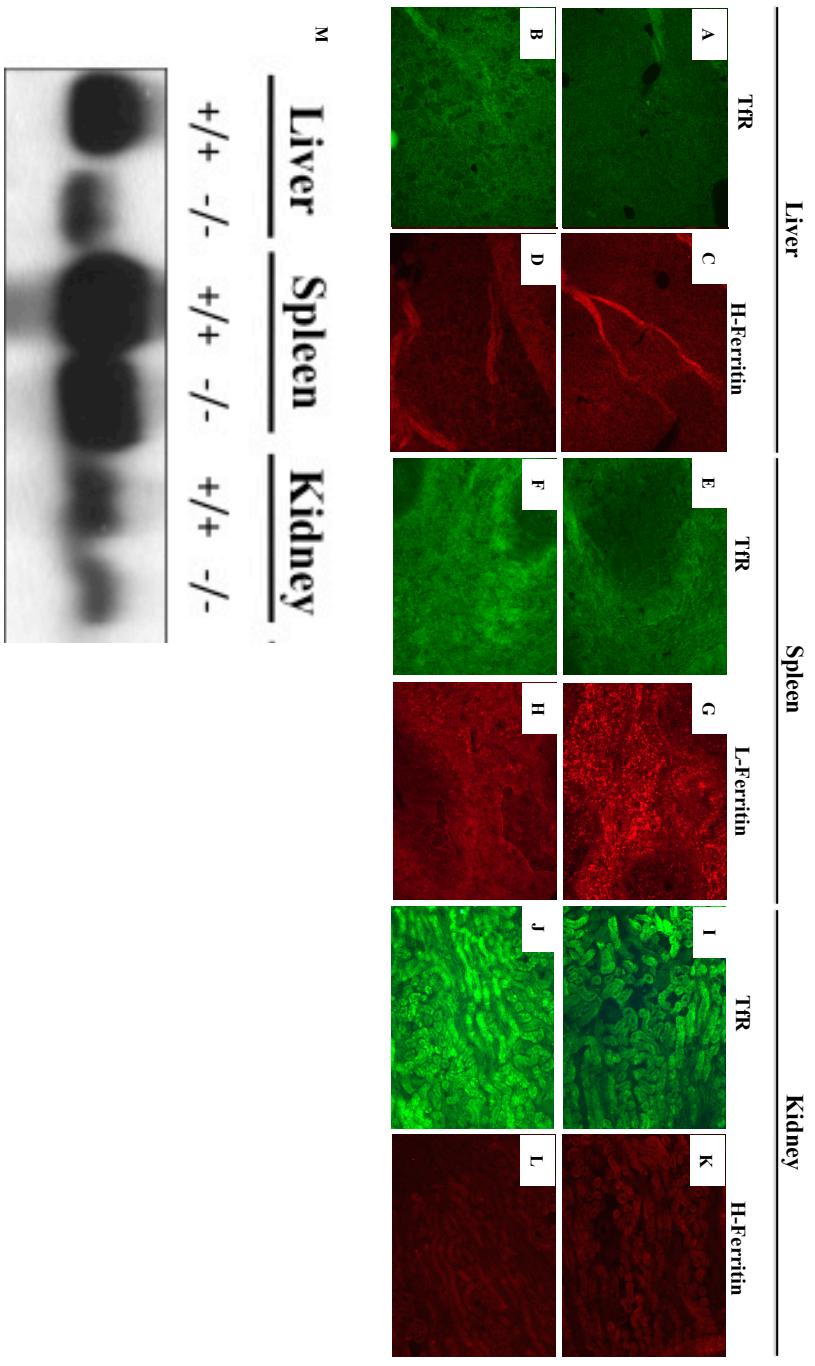

Figure 3.3. Up-regulation of TfR-1 and down-regulation of ferritin in *Npc1*$^{-/-}$ peripheral tissues. (A-H) Representative images of peripheral tissue TfR-1 and ferritin expressions in control and *Npc1*$^{-/-}$ mice. 9-week-old control and *Npc1*$^{-/-}$ mice liver, spleen, kidney and lung sections were prepared and analyzed as described in "Material & Methods". Tissues TfR-1 (green) and ferritin (red) expression were detected using immunofluorescence as described in "Material & Methods". **(M)** Native-PAGE/immunoblotting analysis of ferritin expression in control (*Npc1*$^{+/+}$) and *Npc1*$^{-/-}$ peripheral tissues. Representative images were taken from three individual animals. Original Magnification, x 100.

3.3.2 Down-regulation of hepatic mitochondrial iron transporters, heme metabolism and [Fe-S] clusters biosynthesis gene expressions in Npc1$^{-/-}$ mice.

Since iron is an essential co-factor for cytosolic and mitochondrial [Fe-S] clusters biosynthesis, *Npc1*$^{-/-}$ hepatic cytosolic iron deficiency could cause hepatic mitochondrial iron utilization defects in *Npc1*$^{-/-}$ mice. To evaluate the potential impact of *Npc1*$^{-/-}$ hepatic cytosolic iron deficiency on hepatic [Fe-S] clusters metabolism, the microarray data were examined. As shown in **Fig. 3.4 A-E**, there were significant down-regulation in mRNA levels of a number of [Fe-S] clusters biosynthesis, assembly and scaffolding proteins, including *Iscu, Isca-1, Nfs-1 and Nfu-1* from the early pre-symptomatic (1-week-old) until late end stage (11-week-old) *Npc1*$^{-/-}$ mice. These results suggested that defects in the [Fe-S] clusters biogenesis pathway occur in *Npc1*$^{-/-}$ liver.

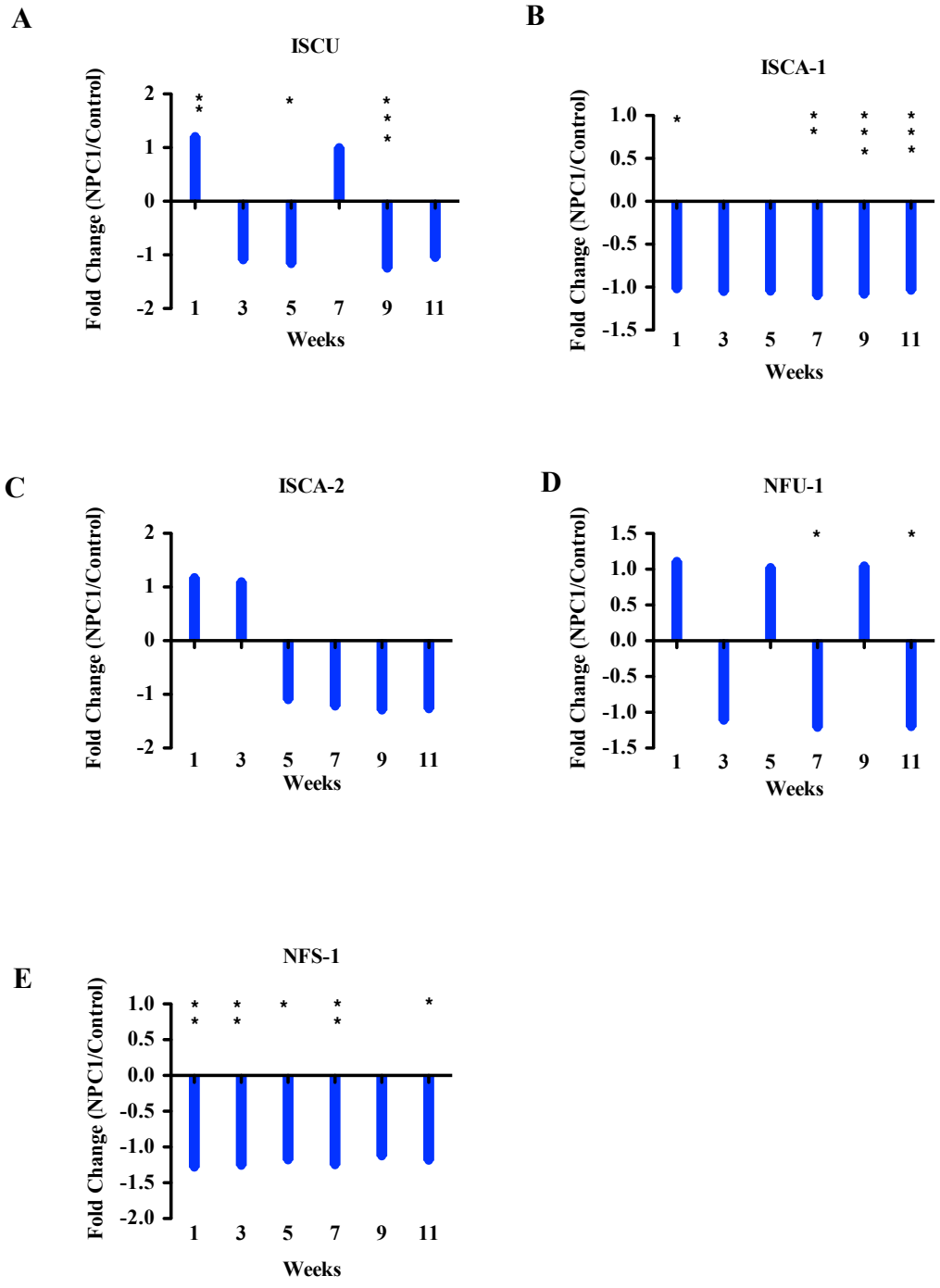

Figure 3.4 Impaired hepatic mitochondrial and cytosolic [Fe-S] clusters biosynthesis, transportation and metabolism genes in *Npc1*$^{-/-}$ mice. (A-E) Hepatic samples from age-matched of control (*Npc1*$^{+/+}$) and *Npc1*$^{-/-}$ mice were collected and analyzed through microarray analysis. ANOVA analysis was used to analyze microarray genes expression change. n = 4, per group, * $p < 0.05$, ** $p < 0.005$, *** $p < 0.00005$. **** $p < 0.00001$.

Next, since iron is also an essential co-factor for the biosynthesis of heme, dysregulation of systemic iron homeostasis in *Npc1*$^{-/-}$ mice could also cause systemic heme metabolism defects and impair heme-containing enzyme activities. Indeed, our microarray examination indicated that there were significantly altered mRNA levels of a number of cytosolic and mitochondrial heme transporters, including heme transporter-1, heme oxygenase-2, heme binding protein and delta-aminolevulinate synthase 2 (ALAS-2), in *Npc1*$^{-/-}$ mice **(Fig. 3.5).** Besides, we also observed that there were significant down-regulation of a series of genes involved in the regulation of hepatic heme biosynthesis, transport, metabolism and catabolism, including hemo-coproporphyrinogen oxidase (*Cpox*), hydroxyl-methylbilane synthase (*Hmbs*), 5-aminolevulinate dehydratase (*Alad*), uroporphyrinogen III synthase (*Uros*), and ferrochelatase (*Fech*) **(Fig 3.6)**. Therefore, these results suggested that impaired hepatic heme metabolism in *Npc1*$^{-/-}$ mice.

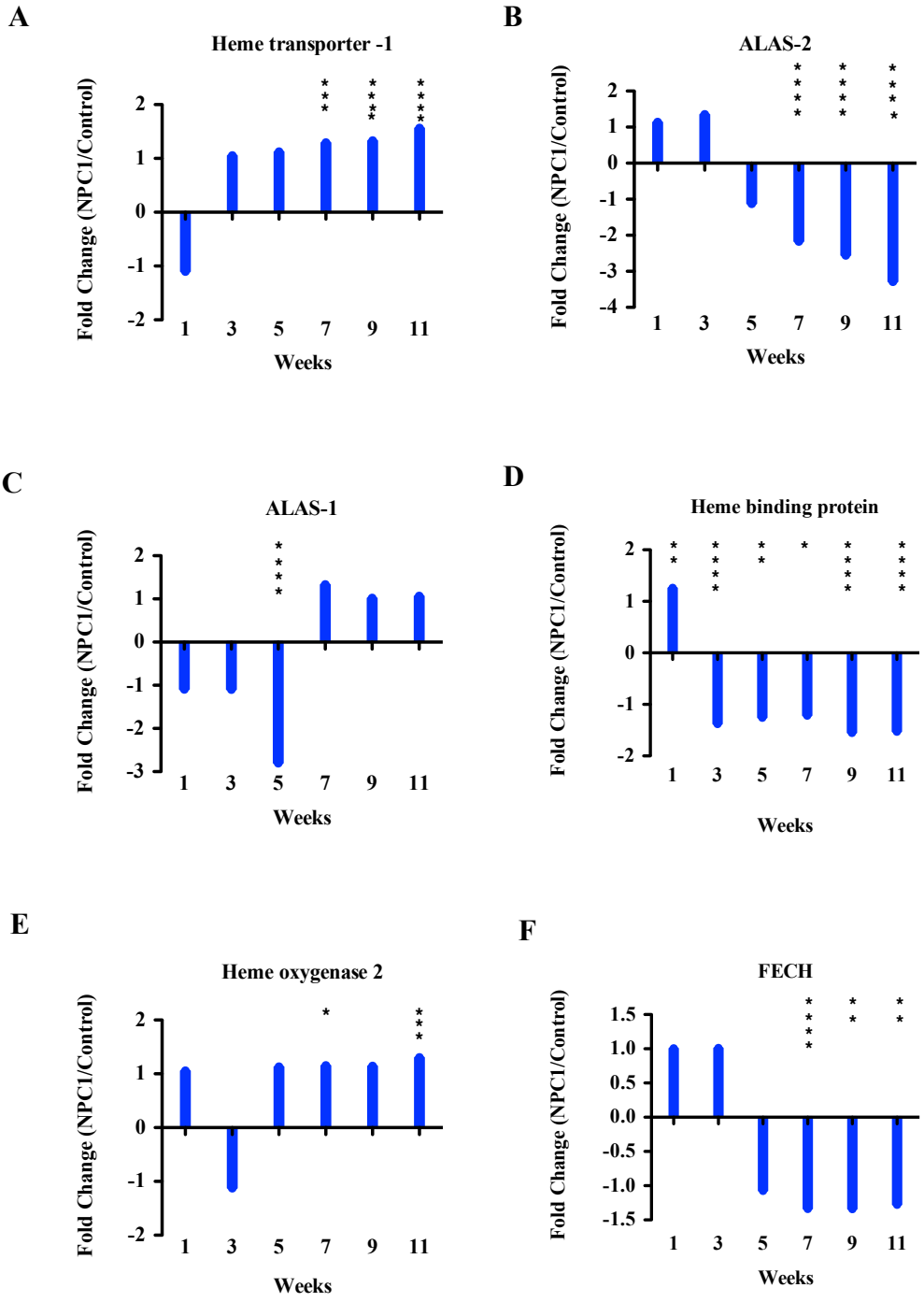

Figure 3.5. Impaired expression of genes involved in hepatic mitochondrial and cytosolic [Fe-S] clusters biosynthesis, transport and metabolism in *Npc1*$^{-/-}$ mice. (A-F) Hepatic samples from age-matched of control (*Npc1*$^{+/+}$) and *Npc1*$^{-/-}$ mice were collected and analyzed through microarray analysis. ANOVA analysis was used to analyze microarray genes expression change. n = 4, per group. * $p < 0.05$, ** $p < 0.005$, *** $p < 0.00005$. **** $p < 0.00001$.

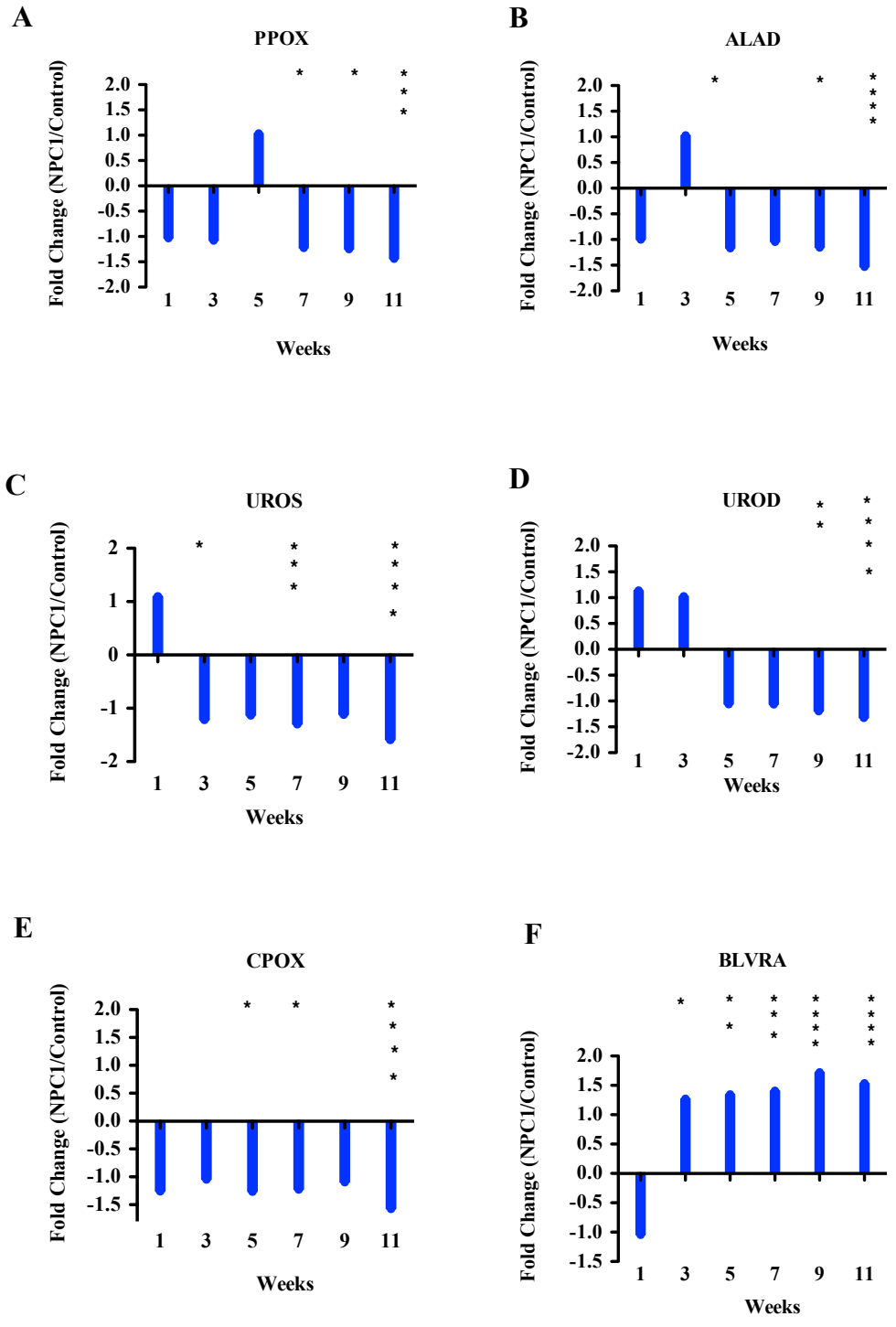

Figure 3.6 Altered expression of genes involved in hepatic, mitochondrial and cytosolic heme biosynthesis/metabolism in *Npc1*$^{-/-}$ mice. (A-F) ANOVA analysis was used to analyze microarray genes expression change. Data shown are mean ± SEM, n = 4, per group. * $p < 0.05$, ** $p < 0.005$, *** $p < 0.00005$, **** $p < 0.00001$.

3.3.3 Up-regulated mRNA levels of endosomal/lysosomal divalent metal transporter-1 (DMT-1) and mucoln-1 (MCOLN-1), in Npc1$^{-/-}$ liver.

Our studies so far have demonstrated the down-regulation of hepatic heme biosynthesis and impaired [Fe-S] clusters biosynthesis in *Npc1*$^{-/-}$ mice. These findings suggested mitochondria iron utilization defects in *Npc1*$^{-/-}$ mice. It has been suggested that lysosomal iron could be regulated by the (i) endosomal/lysosomal divalent metal transporter-1 (DMT-1) and (ii) Mucolin-1 (MCOLN-1), which modulate lysosomal iron uptake and release within the intracellular endosomal/lysosomal system (51, 125). Interestingly, our microarray analysis indicated that there were significantly progressive up-regulation of hepatic DMT-1 mRNA expressions from the early pre-symptomatic stage (3-week-old) until late stage disease (9-week-old) *Npc1*$^{-/-}$ mice (3 weeks, 1.2 fold, $p = 0.03$, 5 weeks, 1.3 fold, $p < 0.007$, 7 weeks, 1.4 fold, $p < 0.0005$, 9 weeks, 1.3 fold, $p < 0.005$) **(Fig. 3.7A)**. However, another potential lysosomal iron transporter, MCOLN-1, only showed significant increases at 1, 3 and 7-week-old *Npc1*$^{-/-}$ mice (1 week, 1.2 fold, $p = 0.017$, 3 weeks, 1.2 fold, $p < 0.005$, 7 weeks, 1.2 fold, $p < 0.0005$) **(Fig. 3.7B)**.

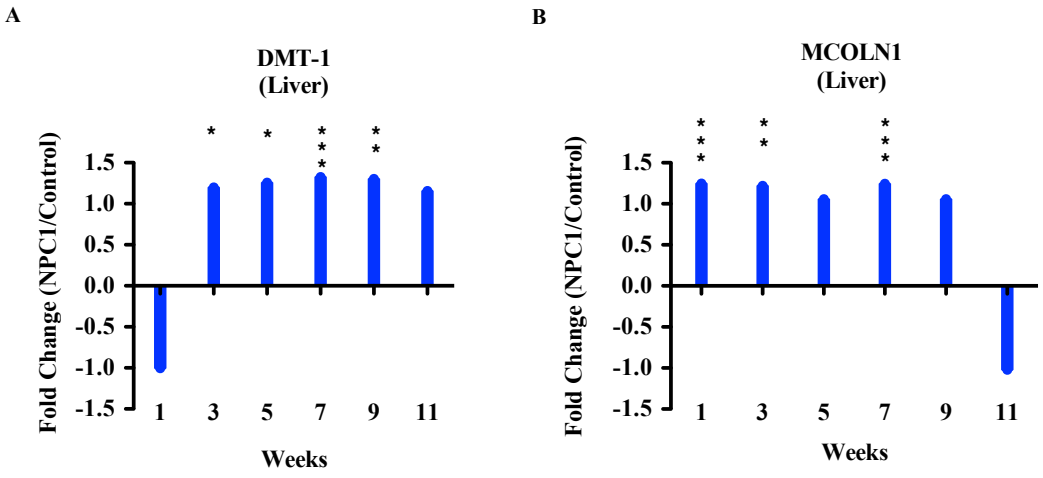

Figure 3.7 Increased hepatic DMT-1 and MCOLN-1 expressions in *Npc1*$^{-/-}$ mice. (A-B) Microarray data were analysed as described in "Materials & Methods". ANOVA analysis was used to analyze microarray genes expression change. Data shown are mean ± SEM, n = 4, per group.

3.3.4 Altered iron metabolism and up-regulation of iron regulatory protein-1 (IRP-1) in Npc1$^{-/-}$ *brain.*

To investigate whether peripheral iron metabolism defects and hematological abnormalities could affect the CNS iron metabolism in *Npc1*$^{-/-}$ mice, 2D-proteomic analysis was performed on 6-week-old *Npc1*$^{-/-}$ brain compared with age-matched controls (*Npc1*$^{+/+}$). As shown in **Fig. 3.8A-B**, the protein expression levels of IRP-1, which mainly functions to regulate iron metabolism related genes at the post-transcriptional and post-translational levels, were markedly up-regulated by 6-weeks of age in the *Npc1*$^{-/-}$ mouse brain compared with age-matched controls. In addition, the mitochondrial specific [Fe-S] clusters containing proteins, such as cytochrome c oxidase and other metal related proteins had altered expression levels in the brain by 6 weeks of age in *Npc1*$^{-/-}$ mice **(Table. 3.1**).

Figure 3.8A-B. Proteomic analysis of 6-week-old control (*Npc1*$^{+/+}$) and *Npc1*$^{-/-}$ brain aqueous fractions. Spots which were increased on the *Npc1*$^{-/-}$ relative to the controls (*Npc1*$^{+/+}$) are marked on the *Npc1*$^{-/-}$ gel with an O. Spots which were decreased on the *Npc1*$^{-/-}$ relative to the control (*Npc1*$^{+/+}$) are marked on the *Npc1*$^{+/+}$ with an O. These differences were validated by differential analysis before the spots were excised and sequenced via mass spectrometry. The proteomic analysis identified several iron-related regulators, such as the IRP-1, ALAS, [Fe-S] containing proteins (cytochrome c, ATP synthase α- and β-chain precursor) and other metalloproteins, altered expressions in *Npc1*$^{-/-}$ brain aqueous fraction. *Npc1*$^{-/-}$ means only present in *Npc1*$^{-/-}$ gels; Control * means present in both *Npc1*$^{-/-}$ and control (*Npc1*$^{+/+}$) gels, but to a higher extent in Control (fold is shown). The 2D-proteomic data were kindly provided by Dr. Annie Speak (unpublished observation).

Category	Examples	Expression (Fold)
Iron Metabolism	Iron response element binding protein-1 (IRP-1)	NPC1$^{-/-}$ only
	Delta aminolevulinic acid dehydratase	NPC1$^{-/-}$ only
Mitochondrial specific (Fe/S containing proteins)	Cytochrome c	NPC1$^{-/-}$ only
	ATP synthase alpha and beta chain precursor	NPC1$^{-/-}$ only
Metal ion binding	LIM and SH3 domain protein-1	NPC1$^{-/-}$ only
Neuronal specific (metal ion binding)	Calbindin (Pukinje cell specific)	WT* (-2.11)

Table 3.1. Summary of the 2-D proteomic analysis results from *Npc1*$^{-/-}$ mice brain aqueous fraction. The proteomic analysis identified that several iron related regulators, such as the IRP-1, ALAS, [Fe-S] clusters containing proteins (cytochrome c, ATP synthase α- and β-chain precursor) and other metalloproteins, altered expression in *Npc1*$^{-/-}$ brain aqueous fraction. *Npc1*$^{-/-}$ means only present in *Npc1*$^{-/-}$ gels; WT* means present in both *Npc1*$^{-/-}$ and control (*Npc1*$^{+/+}$, WT) gels, but to a higher extent in control (WT) (fold is shown). The 2D-proteomic data were provided by Dr. Annie Speak (unpublished observation).

3.3.5 Impaired erythrophagocytosis and heme metabolism in U18666A treated RAW 264.7 cells.

Since systemic heme/iron recycling is mainly regulated through splenic macrophage-mediated erythrophagocytosis, ineffective erythrophagocytosis or impaired phagolysosome formation could lead to systemic iron metabolism defects in *Npc1*$^{-/-}$ mice. Therefore, we hypothesized that defects in erythrophagocytosis by macrophages could be one of the potential mechanisms leading to the systemic iron metabolism defects that occur in *Npc1*$^{-/-}$ mice. In order to test this hypothesis, *in vitro* erythrophagocytosis assays were performed using a pharmacologically induced *in vitro* model of NPC1 disease (U18666A treated RAW mouse macrophage cell line). The *in vitro* erythrophagocytosis efficiency was evaluated by analyzing the protein expressions of a number of heme-metabolism genes. Immunofluorescence analysis indicated that L-chain ferritin and heme oxygenease-1 expressions were greatly increased in vehicle (DMSO)-treated RAW cells compared with U18666A-treated RAW cells. Therefore, these results suggest that U18666A-treated RAW 264.7 cells have less effective erythrophagocytosis and this defect could impair down-

streamed heme metabolism gene expression, such as heme oxygenase-1 and iron-storage protein, ferritin **(Fig 3.9C-I)**.

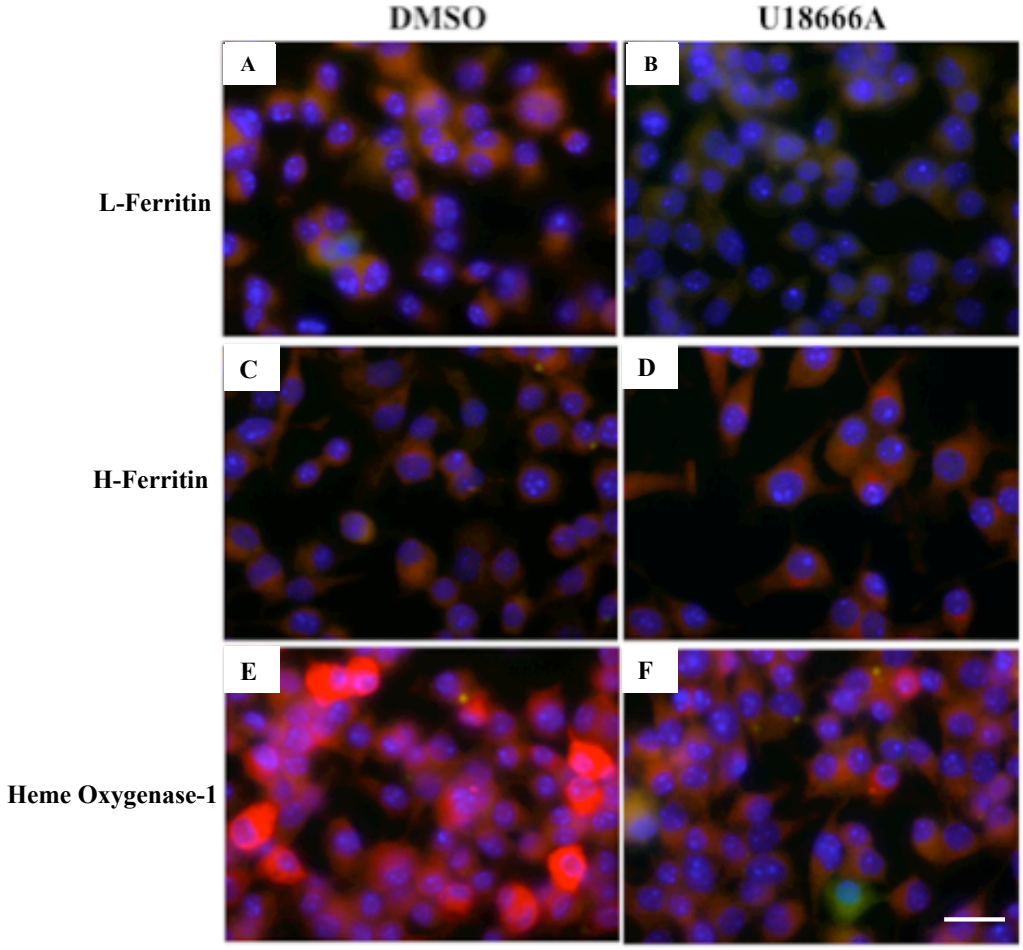

Figure 3.9 Impaired *in vitro* erythrophagocytosis and down-regulated heme metabolism gene expression in U18666A-treated RAW 264.7 cells. Adherent RAW 264.7 cells were treated either with U18666A or DMSO (vehicle control) for 72 hours and assayed for phagocytic responses to mouse IgG-opsonized CFSE-labeled RBCs from control ($Npc1^{+/+}$) donor mice. The phagocytic rate was determined after incubation of cells for 2 hours at 37°C. **(A-F).** Immunofluorescence staining of iron/heme metabolism genes (ferritin and heme-oxygenase-1) in U18666A or DMSO-treated RAW cells after erythrophagocytosis for 2 hours. Scale bar = 10 μm.

3.3.6 Abnormal gastrointestinal bleeding in late end stage $Npc1^{-/-}$ mice.

Since systemic iron homeostasis is regulated at the levels of absorption, storage, utilization and recycling, abnormal iron absorption and bleeding could also affect systemic

iron regulation in NPC1 disease. Interestingly, gastrointestinal bleeding is commonly (75%) observed in late end stage disease (10.5~11 weeks of age) *Npc1*$^{-/-}$ mice. In addition, enhanced vascularity at the ileo-colonic junction was also observed in 10.5~11-week-old *Npc1*$^{-/-}$ mice **(Fig 3.11 & 12A-F)**. The observation of Crohn's-like pathology in *Npc1*$^{-/-}$ mice suggested that abnormal gastrointestinal mediated nutrient absorption defects and abnormal bleeding could be another pathophysiological factors exacerbating iron dyshomeostasis phenotypes in late stage disease in *Npc1*$^{-/-}$ mice.

Figure 3. 11. Abnormal gastrointestinal bleeding in late end stage *Npc1*$^{-/-}$ mice. Representative image of gastrointestinal morphology from 11-week-old *Npc1*$^{-/-}$ mice.

Figure 3. 12. Abnormal gastrointestinal bleeding in late end stage *Npc1*$^{-/-}$ mice. (A-F) Representative images of different parts of gastrointestinal morphology from 11-week-old *Npc1*$^{-/-}$ mice.

3.3.7 Iron dysregulation induced tissue reactive oxygen species production, decreased intracellular glutathione (GSH) levels and elevated lipid peroxidation in Npc1$^{-/-}$ *mice.*

Iron dysregulation has been suggested to be involved in the generation of intracellular reactive oxygen species (ROS) via the Fenton reaction, which could cause cellular apoptosis and cell death. In order to assess the effects of iron dysregulation on *Npc1*$^{-/-}$ peripheral organs and CNS, we examined *Npc1*$^{-/-}$ tissue glutathione levels, which serve as an indicator of intracellular oxidative stress. As presented in **Fig 3.13A-C**, there were markedly decreased total glutathione (GSH) contents in *Npc1*$^{-/-}$ peripheral tissues, including liver, spleen and kidney, as well as brain. Furthermore, this finding was supported by the microarray data, which showed significant up-regulation of hepatic glutathione peroxidase-3 (Gpx3) (1 week, 1.31 fold, $p < 0.025$, 3 weeks, 1.63 fold, $p < 0.0005$, 5 weeks, 1.74 fold, $p < 0.0001$, 7 weeks,

2.64 fold, $p < 0.0001$, 9 weeks, 2.10 fold, $p < 0.0001$, 11 weeks, 4.40 fold, $p < 0.0001$) and glutathione peroxidase-4 (Gpx4) (1 week, 1.43 fold, $p < 0.0001$, 3 weeks, 1.39 fold, $p < 5$ weeks, 1.35 fold, $p < 0.0001$, 7 weeks, 1.42 fold, $p < 0.0001$, 9 weeks, 1.54 fold, $p < 0.0001$, 11 weeks, 1.79 fold, $p < 0.0001$) **(Fig 3.13D-E)**. In addition, the toxic effects of iron dysregulation were measured by analyzing the lipid peroxidation product, 4-HNE, in *Npc*1$^{-/-}$ mice. Immnuofluorescence analysis indicated that there was a marked increased of 4-HNE fluorescence intensity in *Npc1*$^{-/-}$ liver and kidney sections **(Fig. 3.13F-K)**. These results suggested that systemic iron dysregulation could be one of the causes of oxidative stress and lipid peroxidation in *Npc1*$^{-/-}$ mice.

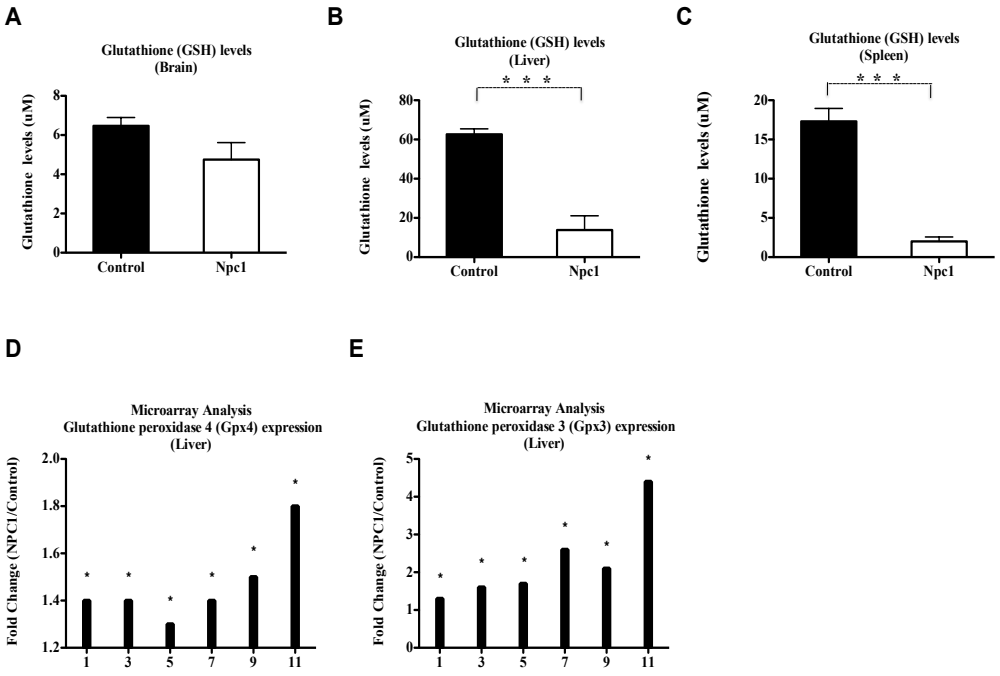

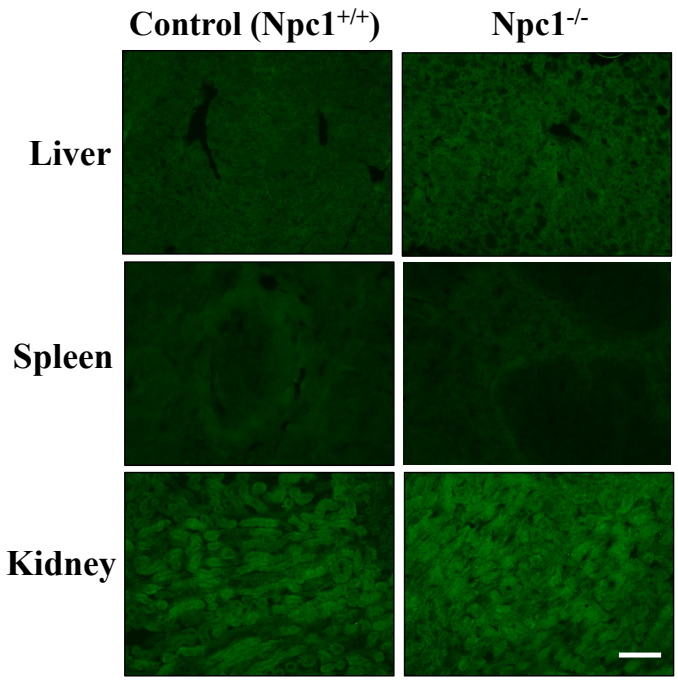

Figure 3.13 Systemic iron dysregulation induced tissue oxidative stress and lipid peroxidation in *Npc1*$^{-/-}$ mice. (A-C) 9-week old control and *Npc1*$^{-/-}$ tissue homogenates were prepared and tissue GSH levels analysed as described in "Material & Methods". **(D-E)** Hepatic samples were collected from *Npc1*$^{-/-}$ and age-matched control animals and analysed using microarray analysis as described in "Materials & Methods". **(F-K)** 9-week-old control (*Npc1*$^{+/+}$) and *Npc1*$^{-/-}$ liver, spleen kidney sections were prepared and stained using anti-4-hydroxy-2-nonenal (4-HNE), lipid peroxidation product, antibody to detect tissue lipid peroxidation levels. Scale bar = 100 μm.

3.3.8 Increased circulating and tissue iron contents in iron-dextran treated Npc1$^{-/-}$ *mice.*

In our previous studies, the hematological abnormalities with low hemoglobin and microcytic erythrocytes were identified in *Npc1*$^{-/-}$ mice and these hematological defects have been suggested to be associated with impaired erythropoiesis and hypoxic stress in *Npc1*$^{-/-}$ mice. Consistent with our earlier findings in **Chapter 2**, our current studies further indicated systemic iron dyshomeostasis in *Npc1*$^{-/-}$ mice and these defects could cause progressive peripheral iron deficiency, impair hepatic mitochondria [Fe-S] clusters biosynthesis and heme metabolism in *Npc1*$^{-/-}$ mice. In order to evaluate the potential impact of iron supplementation on *Npc1*$^{-/-}$ peripheral tissues and CNS, *Npc1*$^{-/-}$ mice were treated with parental iron supplementation using iron-dextran (i.p injection 50 mg/kg, twice per week) and started the treatment from 3-week-old (P21) *Npc1*$^{-/-}$ mice. Circulating iron levels and tissue iron

distribution were determined using inductively coupled plasma mass spectrometry (ICP-MS) and Perl's Prussian blue staining. After 6 weeks of iron supplementation treatment, ICP-MS analysis indicated that there were significant increase in serum iron contents (5.3 fold p = 0.002) in iron-dextran treated *Npc1*$^{-/-}$ mice compared with 9-week-old vehicle (PBS)-treated *Npc1*$^{-/-}$ mice **(Fig 3.14A)**. Intriguingly, the ICP-MS analysis revealed that serum manganese levels were also significantly increased (2.1 fold p = 0.047) in iron-dextran treated *Npc1*$^{-/-}$ mice. However, no significant difference of serum copper and zinc level between vehicle (PBS) and iron-dextran-treated *Npc1*$^{-/-}$ mice were observed **(Fig 3.14B-C)**. In addition, consistent with the ICP-MS analysis, Perl's Prussian blue iron staining also demonstrated that there were marked increases in peripheral tissue ferric iron contents, especially in the liver and spleen, of *Npc1*$^{-/-}$ mice administered parental iron **(Fig 3.15A-H)**.

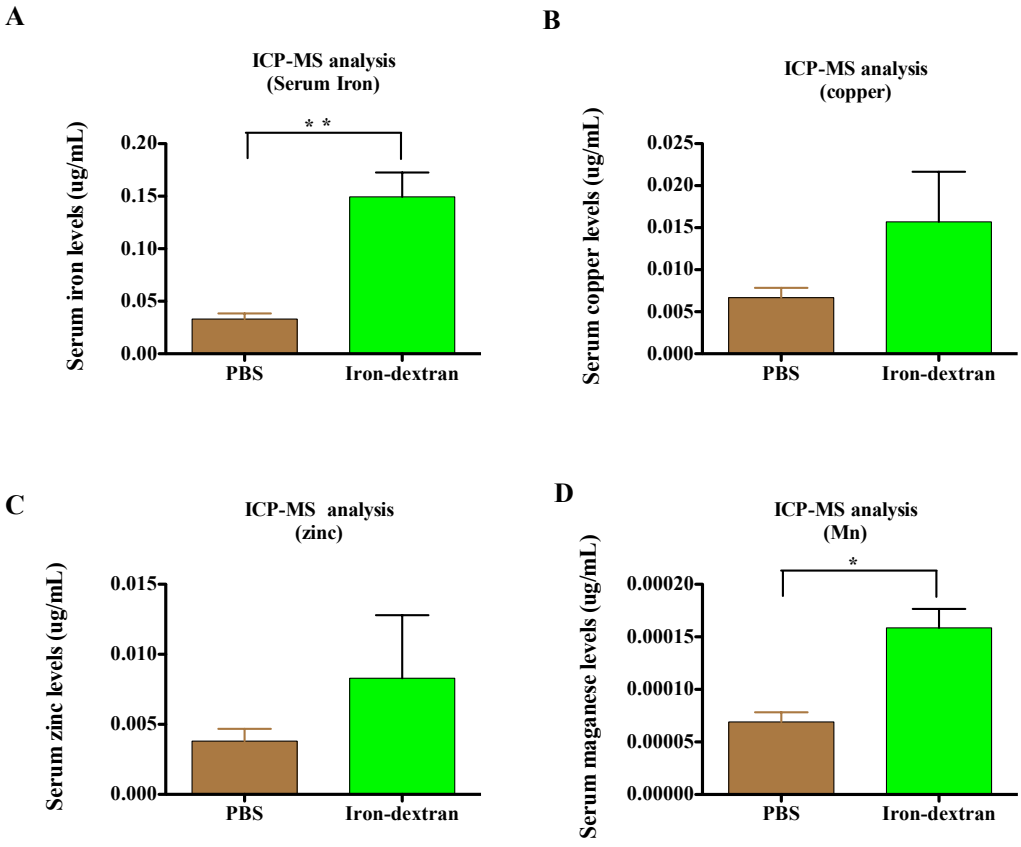

Figure 3.14 Increased serum iron levels in iron-dextran treated *Npc1*$^{-/-}$ mice. (A-D) Mice were injected (I.P.) with iron-dextran (50 mg/kg), twice per week. Iron supplementation started at 3 weeks of age. Blood samples were collected from 9-week-old vehicle-treated and iron-dextran-treated *Npc1*$^{-/-}$ mice. Serum metal contents were measured using ICP-MS as described in "Materials & Methods". Data shown are mean ± SEM, n = 3, per group. * $p < 0.05$, ** $p < 0.005$, calculated by an unpaired *t* test using GraphPad Prism v5.

Figure 3.15. Peripheral tissue iron distribution after treatment with iron supplementation in *Npc1*$^{-/-}$ mice. (A-H) Mice were injected (I.P.) with iron-dextran (50 mg/kg), twice per week. Iron supplementation treatment was started at 3 weeks of age. Age-matched control animals were injected with saline solution as a vehicle control group. Sections of peripheral organs (liver, spleen, kidney and lung) from vehicle-treated *Npc1*$^{-/-}$ and iron-dextran treated *Npc1*$^{-/-}$ mice (9-week old) stained for ferric iron with Perl's Prussian blue reagents. Images were viewed and captured as described in "Materials and Methods". Scale bar = 100 μm.

3.3.9 Iron supplementation improved motor function and activity in Npc1$^{-/-}$ *mice.*

The potential therapeutic effect of iron supplementation on motor function in iron-dextran treated-*Npc1*$^{-/-}$ mice was also examined. Automated activity measurements indicated that iron supplementation treated-*Npc1*$^{-/-}$ mice exhibited higher levels of activity parameters relative to age-matched vehicle treated *Npc1*$^{-/-}$ mice. When compared with vehicle-treated *Npc1*$^{-/-}$ mice, iron supplementation did not show any significant functional improvements in terms of exploratory activity or movement and mobility. However, the supported rearing counts were significantly improved in 6 and 7-week-old iron-dextran treated *Npc1*$^{-/-}$ mice compared with age matched vehicle-treated *Npc1*$^{-/-}$ mice (6 weeks, 120.30 ± 27.41 v.s 236.70 ± 37.31, $p = 0.03$, 7 weeks, 103.70 ± 16.04 v.s. 219.80 ± 21.74, $p = 0.0019$). The unsupported rearing counts were also significantly increased in 7 and 8-week-old iron-dextran treated *Npc1*$^{-/-}$ mice (7 weeks, 13.73 ± 4.464 v.s. 31.75 ± 2.810, $p = 0.0367$, 8 weeks, 4.125 ± 1.619 v.s. 25.63 ± 8.870, $p = 0.0318$).

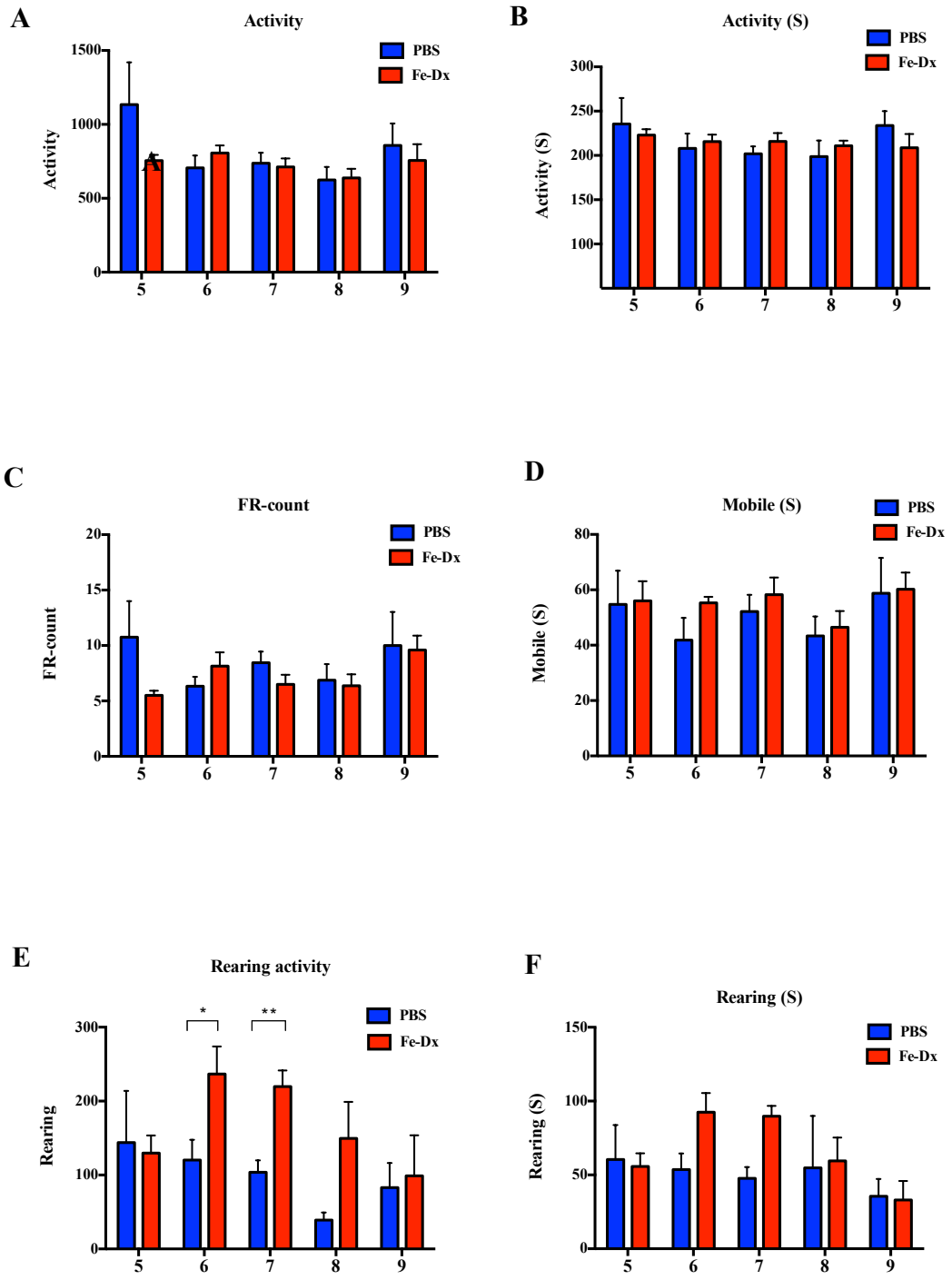

Figure 3.16A-I. **Iron supplementation treatment improved motor function in treated *Npc1*$^{-/-}$ mice.** Mice were injected (I.P.) with iron-dextran (50 mg/kg), twice per week. Iron supplementation therapy was started at 3 weeks of age. Age-matched control animals were injected with saline solution as a vehicle control group. The evaluations of motor function were measured weekly using the AmLogger as described in "Materials & Methods". Data represent mean ± SEM, n = 4 ~ 6, per group. * $p < 0.05$, ** $p < 0.005$, calculated by an unpaired t test using GraphPad Prism v5.

3.3.10 Iron supplementation does not protect against neuro-inflammation or Purkinje cell loss in Npc1$^{-/-}$ mice.

The potential effect of iron supplementation on Purkinje cells survival and neuro-inflammation was examined in iron-dextran treated 8-week-old *Npc1*$^{-/-}$ mice. The inflammatory marker CD68 was used to detect activated microglia/infiltrating macrophages, whilst Purkinje cells were identified by calbindin staining to asses patterns of neurodegeneration. Within the cerebellum, patterned neurodegeneration of Purkinje cells starts in lobules I and II and progresses to other lobules whereas lobule X is spared. Lobule III is a site of Purkinje cells loss early on in NPC1 disease progression and was therefore studied. Iron supplementation did not promote Purkinje cells survival (4.54 ± 0.08 av. PC/mm IGL v.s. 4.23 ± 1.39 av. PC/mm IGL) or protect against neuroinflammation **(Fig 3.17A-D)**.

Figure 3.17. Lack of benefit of iron supplementation on *Npc1*$^{-/-}$ cerebellar microglial activation and Purkinje cell survival. (A–B) Cerebellar sections (20 μm) were immunostained with anti-CD68 antibody and revealed with a FITC-conjugated secondary to label activated microglia (green). The tissues were counterstained with DAPI to outline cerebellar structure. Layers of dense blue staining correspond to the internal granular layer, while the arrows indicate the lobular white matter tracts. The cerebellum of untreated *Npc1*$^{-/-}$ mice **(A–B)** was compared to iron-dextran and vehicle (PBS) treated animals, $n = 3$ for each treatment group. The images illustrated the microglial activation in the deep cerebellar nucleus and surrounding parenchyma the lobular white matter and internal granular layer and the molecular layer. The number of $CD68^+$ cells was calculated per mm^2 of each cerebellar zone. The data is presented in **(C-D)** with each cerebellar zone colour-coded as before (all bars ± SEM). In other sections, the number of calbindin-labeled Purkinje cells in the crus1 zone was counted to assess the impact of iron supplementation on Purkinje cell survival. NS = not significant calculated by an unpaired *t* test using GraphPad Prism v5. Scale bar = 200 mm. These data were analyzed by Dr. Ian Williams (NIH, USA).

3.3.11 Abnormal celluler ferritin synthesis and storage in NPC1 human fibroblasts.

We evaluated the iron loading response of human skin fibroblasts derived from NPC1 patients. Human fibroblasts were grown in the medium supplemented with 50 μM FAC for 72 hours and the cellular responses were examined by electron microscopy. As illustrated in **Figure 3.18A-D**, electron microscopy (EM) examination indicated that several electron-dense ferritin-like structures (e.g., hemosiderin) were clearly observed within lysosome-like subcellular organelles in control human fibroblasts. However, in NPC cells, several cellular storage bodies were observed as anticipated but only relatively few electron dense ferritin-like structures were observed in the cytoplasm and subcellular organelle compartments in iron-loaded NPC1 fibroblasts **(Fig 3.19-23A-D)**.

Figure 3.19 Abnormal intracellular ferritin synthesis and storage in iron-loaded NPC1 human fibroblasts. (A-D) Human fibroblasts derived from NPC1 patients were cultured with standard medium supplemented with 50 uM ferric ammonium citrate (FAC) for 72 hours. Followed by processed electron microscopy analysis as described in Material & Methods. ← indicated electron dense ferritin-like complexes (hemosiderin) stored into intracellular membrane bound structure. ← indicate lysosomal storage bodies distributed over the cytosol. Scale bar = 1 μm.

Figure 3.20 Abnormal intracellular ferritin synthesis and storage in iron-loaded NPC1 human fibroblasts. **(A-B)** Human fibroblasts derived from healthy individual and NPC1 patients were cultured with standard medium supplemented with 50 μM ferric ammonium citrate (FAC) for 72 hours. Followed by processed electron microscopy analysis as described in "Materials & Methods". ← indicated electron dense ferritin-like complexes (hemosiderin) stored into intracellular membrane bound structure in fibroblasts derived from healthy individual. ← indicated electron dense cytosolic ferritin-like molecules distributed around the lysosomal storage bodies.

3.3.12 Abnormalities in CSF concentrations of ferritin in NPC1 patients.

Our *in vitro* and *in vivo* studies so far have demonstrated disruption of cellular and systemic iron homeostasis in peripheral organs and CNS of *Npc1*$^{-/-}$ mice. In this thesis **Chapter 2**, we found decreased circulating iron levels and hematological abnormalities with low haemoglobin and microcytic erythrocytes in NPC1 patients. In order to further evaluate whether our current observations of systemic iron dysregulation in *Npc1*$^{-/-}$ mice could be relevant to the clinic, cerebrospinal fluid (CSF) samples from patients with NPC1 disease were collected and CSF transferrin levels analysed. No significant differences in CSF transferrin levels were found between control individuals and NPC1 patients (1.127 ± 0.128 v.s. 1.354 ± 0.069, p = 0.089, n = 30 and n = 58, respectively) **(Fig 3.21A)**. Next, CSF ferritin levels from NPC1 patients were measured. The detection limit of the ELISA was 5 ng/ml. Intriguingly, the ferritin ELISA analysis indicated that the CSF ferritin levels from these 5 unrelated NPC1 patients were all in the undetectable range (n = 5, per group, detection limit = 5 ng/ml); however the CSF ferritin levels from control individuals were approximately 10.29 ± 2.748 ng/ml (n = 5, per group, detection limit = 5 ng/ml) **(Fig 3.21B)**. Therefore, these results suggested that CNS iron metabolism defects may occur in NPC1 patients.

Figure 3.21 CSF ferritin deficiency in NPC1 patients. **(A)** CSF transferrin levels were analysed using commercial anti-human Tf kit (n =30, and n = 58, for control group and NPC1 patients, respectively). **(B)** CSF ferritin levels were measured using anti-human ferritin kit (n = 5 of each, for control group and NPC1 patients). The dashed line indicates the detection limit (5 ng/mL) of the commercial anti-ferritin ELISA kit. CSF samples from NPC1 patients and control individuals were collected and analysed as described in "Materials & Methods". Data shown are mean ± SEM, calculated by an unpaired *t* test using GraphPad Prism v5.

3.4 Discussion

We have found systemic iron dysregulation in *Npc1*$^{-/-}$ mice including modified gene expression of a number of signaling molecules involved in the regulation of hepatic hepcidin expression, such as TMPRSS-6, TfR-2. Furthermore, Prussian blue iron staining indicated peripheral iron deficiency in *Npc1*$^{-/-}$ mice. This finding was supported by the observation of

up-regulation of peripheral TfR-1 and down-regulation of ferritin levels in *Npc1*$^{-/-}$ mice. Microarray analysis suggested that systemic iron dyshomeostasis could have pleiotropic effects including (i) impair mitochondrial and lysosomal iron trafficking, (ii) decreased mitochondrial iron utilization with impaired mitochondrial/cytosolic heme metabolism and [Fe-S] cluster biosynthesis (iii) and stimulate tissue reactive oxygen species generation and lipid peroxidation in *Npc1*$^{-/-}$ mice **(Fig. 3.22)**. Proteomic analysis also indicated that brain iron metabolism defects with up-regulation of IRP-1 and transferrin was detected in *Npc1*$^{-/-}$ mice. Defective cellular ferritin synthesis and storage were also observed in NPC1 disease cell line model. In addition, CSF ferritin deficiency was observed in NPC1 patients. The potential therapeutic effects of iron supplementation to correct iron deficiency were evaluated in *Npc1*$^{-/-}$ mice. Iron supplementation treatment was of benefit in terms of survival and function, with correction of peripheral tissue iron levels.

Figure 3.22. Proposed model of iron dysregulation induced oxidative stress, mitochondrial dysfunction, lipid peroxidation and DNA damage in Niemann–Pick type C1 disease. The schematic presents a model of iron dyshomeostasis related NPC1 pathogenesis based on evidence obtained in the murine and *in vitro* models of NPC1 disease. Lysosomal dysfunction due to mutations in NPC1 protein would cause impair endosomal/lysosomal pathway mediated Tf-iron uptake and TfR-1 recycling defect. This defect could further affect intracellular iron storage protein, ferritin, synthesis, trafficking and storage within lysosomes. Due to the lysosomal dysfunction in NPC1 disease, it could cause cellular iron dyshomeostasis and generate intracellular free radical via the Fenton reaction. The increased cellular oxidative stress could affect cellular anti-oxidative enzymes genes expression, activities, which would lead to increasing intracellular free radical levels, causing lipid peroxidation and DNA damage. The NPC1 lysosomal dysfunction could also affect mitochondrial iron uptake, transport and utilization and affect mitochondrial functions.

The microarray data indicated that the iron dysregulation in NPC1 disease could be associated with the defective regulation of subcellular iron trafficking and its compartmentalization. These findings were supported by the observation of impaired mitochondria-mediated heme metabolism, [Fe-S] clusters biosynthesis and cause mitochondrial dysfunction in *Npc1*$^{-/-}$ mice. Interestingly, we have very recently found hepatic CYPs functional defects in NPC1 disease animal models and NPC1 patients (**Platt et.,**

unpublished observations). Since iron is an essential cofactor for heme-containing enzymes, including hemoglobin, cytochromes, hepatic iron/heme metabolism defects in NPC1 disease could impair heme containing enzymes activities further as the disease progresses (52). Although the underlying mechanisms of hepatic CYPs defects in NPC1 disease remains to be explored, the observations of impaired hepatic heme biosynthesis and mitochondrial dysfunction could contribute to the functional defects of hepatic CYPs in NPC1 disease.

We also found that the postulated hepatic endosomal/lysosomal cation and iron transporters, DMT1-1 and MCOLN-1, were significantly increased from the early pre-symptomatic stage (3-week-old) *Npc1*$^{-/-}$ mice. Since DMT-1 and TRML-1 have both been suggested to be involved not only in the regulation of lysosomal iron transportation but also control lysosomal calcium flux, these observations therefore raised the possibilities whether the hepatic iron metabolism defects in NPC1 disease could be either directly or indirectly related to (i) lysosomal calcium flux defects, or (ii) the abnormal increase in the number and size of lysosomes in NPC1 disease (98, 125, 126). Since our previous studies have demonstrated that NPC1 disease is mainly characterized by lysosomal calcium flux defects, defective lysosomal calcium signalling would impair intracellular vesicles fusion and fission events and cause the abnormal increase of lysosome numbers and volume (22). Indeed, this hypothesis was supported by our microarray examination indicating significantly elevated levels of endosomal/lysosomal markers, LAMP-1 and LAMP-2, and the postulated endo/lysosomal two pore calcium channel, TPC-2, in *Npc1*$^{-/-}$ mice (**Platt et al., unpublished observation**) (127). These findings also suggested that the lysosomal calcium signaling defect is involved in the regulation of abnormal hepatic pro-inflammatory cytokines (IL-1β, IL6 and TNF-α), hepcidin expression and iron metabolism defects in *Npc1*$^{-/-}$ mice. This proposed model would need to be further investigated and it could potentially highlight the importance of lysosomal calcium-mediated signaling in the regulation of systemic inflammatory responses and iron homeostasis.

Cellular iron homeostasis is maintained by the coordinated regulation of cytosolic, mitochondria and lysosomal iron pools (47). Dysregulation in subcellular iron trafficking and

its compartmentalization could lead to imbalanced cellular iron distribution in all three compartments (49). Based on our microarray analysis, it is reasonable to assume lysosomal iron metabolism defects occur in NPC1 disease. However, although there is growing evidence that lysosomes might play a crucial role on maintaining systemic and cellular iron homeostasis, in terms of iron uptake, trafficking, subcellular compartmentalization, recycling and ferritin iron release, the biological function of lysosomes on systemic and cellular iron homeostasis still remains incompletely understood(45, 47). Most of our current knowledge on subcellular iron trafficking and compartmentalization relies on rare mitochondrial or lysosomal diseases, such as Friedreich's ataxia, siderocytic anemia and transient receptor potential cation channel mucolipin-1 disorder (75, 98). Friedreich's ataxia and Mucoln-1-deficienct human fibroblasts exhibited cytosolic iron deficiency as well as subcellular iron compartments accumulation phenotypes, which suggest a defect in intracellular iron transportation across either the cytosolic/mitochondrial compartment or the endsosomal/lysosomal system. The Friedreich's ataxia and Mucoln1-deficienct human fibroblasts exhibit either mitochondrial or lysosomal iron overload and concurrent cytosolic iron deficiency phenotypes (98, 128). This could lead to the misregulation of the cellular IRE-IRP regulatory system and cause systemic iron dysregulation and the development of hepatic dysfunction and neurodegenerative symptoms. Considering the potential therapeutic approaches for the subcellular iron compartmentalization defects in Friedreich's ataxia and Mucoln1 disorders, it has been proposed that therapies should either (i) replenish cytosolic iron levels or (ii) chelate subcellular compartmentalized iron (129). Indeed, *in vitro* studies have previously demonstrated that the iron chelator (DFO) has certain beneficial effects and rescues Friedreich's ataxia fibroblasts from oxidative stress (128). Furthermore, *in vivo* studies on muscle creatine kinase conditional frataxin knockout mouse model have recently demonstrated that either (i) iron chelating treatment with combination of iron chelators, pyridoxal isonicotinoyl hydrazone (130) and (DFO), can decrease cardiac iron accumulation and limits cardiac hypertrophy in mutant mice (55) and (ii) dietary iron supplementation can delay weight lost and limit cardiac hypertrophy (131). Interestedly, our previous and current

studies (described in this thesis **Chapter 2 and Chapter 3)** have also evaluated (i) parental iron supplementation with iron dextrin and (ii) iron chelating treatment using iron chelator, (deferoxamine, DFO), in *Npc1*$^{-/-}$ mice (**data not shown**). Our results indicated that iron supplementation treatment could (i) improve hematological abnormalities, (ii) correct peripheral tissue iron deficiency phenotypes (iii) and modestly prolong lifespan in treated *Npc1*$^{-/-}$ mice. However, our studies also indicated that the iron chelator defecroxamine did not show any functional improvements, in terms of survival and locomotor activity, on treated *Npc1*$^{-/-}$ mice **(data not shown)**. However, it should be noted that there are several possibilities to explain the limited therapeutic effects of deferoxamine on treated *Npc1*$^{-/-}$ mice. One possibility is that the iron chelator deferoxamine treatment may worse functional iron deficiency anaemia and peripheral iron deficiency phenotypes in *Npc1*$^{-/-}$ mice. Other possibilities should also be considered including (i) DFO may have limited BBB permeability (20, 132), (ii) whether DFO specifically chelates lysosomal iron pools and (iii) whether iron is efficiently chelated *in vivo* in mice fed a mouse chow that is rich in iron. Therefore, on the basis of our current findings, it might be of interest to evaluate the potential therapeutic effects of novel iron-modulating reagents or iron ionophores in *Npc1*$^{-/-}$ mice and *Npc1*$^{-/-}$ cells and determine whether these iron-related treatments could correct hematological abnormalities and systemic/cellular iron dysregulation phenotypes in NPC1 disease. In addition, further studies on the combination therapy with substrate reduction therapy using miglustat and iron-dextran would be informative. Although the therapeutic dosage, efficiency, iron formulation and administration routes of iron supplementation remains to be optimized, our current findings suggested the potential beneficial effects of the iron supplementation treatment in *Npc1*$^{-/-}$ mice that could be rapidly translated into the clinic.

Our current studies described in this thesis (**Chapter 2 & 3)** mainly focused on the identification of the mechanistic defects of peripheral iron homeostasis and related hematological defects in *Npc1*$^{-/-}$ mice. However, our proteomic analysis indicated that the dysregulation of brain iron homeostasis with up-regulation of transferrin and IRP-1 was observed from 1-week-of age in *Npc1*$^{-/-}$ mice. There is also growing evidence to suggest that

the brain iron dysregulation may be involved in the underlying pathogenesis of several common neurodegenerative disorders, such as Pakinson's and Alzehimer's diseases and other rare neurodegenerative diseases with brain iron accumulation (NBIA), such as Pantothenate kinase-associated neurodegeneration (PKAN), neuroferritinopathy, aceruloplasminemia, Kufor Rakeb syndromes and fatty acid hydroxylase associated neurodegeneration (FAHN) (79, 133, 134). Therefore, it would be of interest to further investigate the brain iron dysregulation phenotypes in *Npc1*$^{-/-}$ mice. In addition, there is also growing evidence to indicate that NPC1 disease and Alzheimer's disease may share several similar neuro-pathological features, including the formation of neurofibrillary tangles and the accumulation of beta-amyloid, which suggested these two diseases share common biochemical mechanisms involved in their pathogenesis. It has been demonstrated that amyloid precursor protein expression is response to intracellular iron levels and is regulated by the IRP-1 via binding its iron responsive 5'-untranslated region (135). Intriguingly, our current proteomic results indicated that the IRP-1 levels were markedly up-regulated in *Npc1*$^{-/-}$brain. Therefore, our current studies may bring new insights into the mechanistic links between Alzheimer's and NPC1 disease (136). In addition to lipid dyshomeostasis phenotypes, impaired lysosomal function/activity causing cellular iron homeostasis defects in NPC1 pathogenesis may provide a novel model to study the association of lysosomal dysfunction and amyloid precursor protein processing (137). However, it should be noted that the distribution of iron is uneven in the brain and defects in its metabolism could be restricted to certain brain regions (e.g., globus pallidus, substantia nigra), specific cellular types (e.g., astroglia, oligodendrocytes), or subcellular organelles levels (e.g., mitochondria, lysosomes). Furthermore, due to the distinct architectural features and potential metabolic differences in astrocytes, microglia, neurons and oligodendrocytes, cellular iron metabolism may vary regionally which could be another challenge to investigate defects in iron metabolism in the NPC1 disease brain. In addition, the possibility of iron transportation defects across the BBB. Due to the technical issue of obtaining CSF from *Npc1*$^{-/-}$ mice, we only analysed CSF from NPC1 patients and the results indicated that there were undetectable levels of ferritin in the CSF of NPC1 patients. Hence,

there may be CSF iron/ferritin transport defects across the BBB or the brain–cerebrospinal fluid barrier in NPC1 disease. Interestingly, impaired BBB integrity has been demonstrated in another sub-group of lysosomal storage disease, mouse models of the GM1 and GM2 (138). Therefore, it would be of interest to determine the BBB integrity and the efficiency of brain iron/transferrin and CSF ferritin transport across the BBB in *Npc1*$^{-/-}$ mice.

Several lines of evidence have recently demonstrated that (i) lysosomal protease activities and (ii) lysosomal acidification are crucial for the degradation of ferritin complex and utilization of iron from ferritin (73, 74). However, the molecular mechanisms of how iron incorporate into ferritin and how iron export from lysosomes remain poorly understood. Recent studies have suggested that certain candidate metal transporters may be involved in mediating iron transport from lysosomes to the cytosol (51, 73). Intriguingly, peripheral ferritin deficiency has been reported in a small number of NPC1 patients, but did not in patients with other lysosomal storage diseases, including Gaucher, Batten and GM2 gangliosidosis (107, 108). Therefore, these observations suggest that the NPC1 protein may be involved in the regulation of subcellular iron trafficking and ferritin synthesis. NPC1 belongs to a member of RND permease superfamily, a wide range of substrates, including fatty acid, lipophilic drugs, detergents and metal ions, have been suggested to be able to be transported by the NPC1 protein (24). Therefore, it would be of interest to investigate further the potential role of NPC1 on intracellular iron and other metal trafficking in the near future. However, it should be noted that our current studies still cannot rule out other possibilities including (i) impaired systemic and cytosolic iron transport (130), (ii) impaired trafficking/mis-localized of intracellular iron transporters, such as TfR-1, hepcidin/ferroportin complex (139), (iii) defects in lysosomal protease activity and acidification for the extraction of ferritin iron (47). Also, the NPC1 protein could either directly or indirectly interact with other unidentified lysosomal iron transporters. To our knowledge, there are very limited studies regarding the biological function of lysosomes and lysosomal proteins on the regulation of systemic and cellular iron homeostasis. Further studies using novel iron detection probes will be needed to determine subcellular iron levels/distribution, including

cytosolic, mitochondrial and lysosomal compartments The use of biophysical techniques, such as Mössbauer spectroscopy and transmission electron microscopy–energy-dispersive X-ray, will be necessary to get a better understanding of the underlying mechanisms of iron dysregulation in NPC1 disease (73, 131).

In conclusion, we have found systemic and cellular iron dysregulation *in vitro* and *in vivo* in NPC1 disease models. Besides, our results also suggested that systemic iron dyshomeostasis could impair mitochondrial/lysosomal iron trafficking and mitochondrial iron utilization, including impaired heme metabolism and [Fe-S] cluster biosynthesis, in *Npc1*$^{-/-}$ mice. Furthermore, 2-D proteomic analysis also indicated brain iron metabolism defects occur in *Npc1*$^{-/-}$ mice. CSF ferritin deficiency was also observed in NPC1 patients. The potential therapeutic effects of iron supplementation were evaluated in *Npc1*$^{-/-}$ mice. Our studies using genetic, biochemical and pharmacological methods demonstrated the cellular and systemic iron dyshomeostasis in NPC1 disease models and indicated that iron supplementation treatment was of benefit, which could correct peripheral organs iron contents and improve motor functions in *Npc1*$^{-/-}$ mice.

Chapter 4: Defective Copper and Zinc Homeostasis in Niemann-Pick C1 Disease

Chapter 4: Defective Copper and Zinc Homeostasis in Niemann-Pick C1 Disease

4.1 Introduction

4.1.1 Copper/zinc dyshomeostasis and its related diseases

Copper and zinc are crucial trace elements in biological system that are co-factors for many metalloproteins involved in intestinal iron mobilization, biosynthesis and release of neurotransmitters, neuron myelination, melanin formation, blood clotting, mitochondria functions and many other physiologic processes (56, 140). Defective copper and zinc homeostasis is a contributing factor of hepatic and neurotoxicity in several severe hepatic and neurodegenerative diseases, such as Wilson's disease, Menke's disease, amyotrophic lateral sclerosis (ALS), acerulomplasminemia, Alzheimer's disease and Parkinson's disease (141, 142). Dysregulation of systemic copper and zinc homeostasis is a contributing factor to the production of intracellular reactive oxygen species (ROS), which leads to lipid peroxidation, subcellular organelles dysfunction and cellular apoptosis (143). Therefore, intracellular copper and zinc homeostasis is tightly regulated at the level of uptake, intracellular trafficking, subcellular compartmentalization and export.

4.1.2 Systemic and cellular copper homeostasis

Copper absorption is regulated by the plasma membrane transporter, CTR-1, which facilitates cellular copper uptake and delivery to intracellular copper chaperones, (e.g. Atox1, CCS and Cox17) to help copper (i) delivery to *trans*-Golgi (TGN) P-type ATPase transporters, MNK ATP7A and WND ATP7B, to help copper incorporate apo-cuproproteins for holo-cuproproteins, (ii) incorporate into Cu/Zn superoxide dismutases, to help against intracellular/extracellular superoxide damage (iii) and delivery to mitochondrial cytochrome c oxidase, to maintains mitochondrial copper homeostasis (56). However, the mechanisms of how intracellular copper distributes and incorporates into apo-cuproproteins, including the synthesis of ceruloplasmin, remain poorly understood (59).

4.1.3 Systemic and cellular zinc homeostasis

Zinc plays important roles in neurotransmitter biosynthesis/release and may function as an intracellular second messenger (140). The intracellular and extracellular zinc concentration and its distribution is controlled by metallothioneins (MTs) and zinc transporters (140). In general, zinc transporters transport zinc in/out of the cytosol, leading to export or intracellular sequestration, e.g., into zincosomes, which are vesicles that can accumulate high levels of free zinc (140). It has been known that there is considerable cell-specific expression of some of the transporters, which are dynamically regulated in response to zinc status and endocrine and cytokine signaling and expression of these transporters can regulate signal transduction in response to levels of intracellular zinc (144, 145).

4.1.4 Metallothioneins and copper, zinc homeostasis

Metallothionines (MTs) are cysteine-rich, low molecular weight proteins, which have a high affinity for intracellular transition metals, such as copper and zinc (146). MT-1 and MT-2 are expressed in most mammalian tissues, and MT-3 is mainly restricted expression in the central nervous system, which is particularly abundant in zinc-rich neurons (147). MTs are not only involved in the detoxification of tissues heavy metal contaminants, but also help protect against metal dysregulation induced oxidative stress (146, 148). In addition to modulation by transition metal ions, MTs can also be transcriptionally regulated by a number of different molecules, such as corticosteroids, interleukins, interferons and serum growth factors (146). Metallothionines have been suggested to be involved in the regulation of mitochondrial function (146).

4.1.5 Copper and zinc dyshomeostasis disorders

Defects in intracellular copper and zinc homeostasis have been suggested to be associated with several psychiatric and neurological disorders, including Menke's disease, Wilson's disease, amyotrophic lateral sclerosis, Prion diseases and Parkinson's disease (149, 150). Most of our current knowledge of systemic and sub-cellular copper and zinc regulation

mainly relies on (i) certain copper and zinc metabolism genetic knock-out animal models and (ii) rare inborn errors of inherited genetic/metabolic disorders in human patients (141).

4.1.6 The biological function of lysosomes and metal homeostasis

The lysosome plays a crucial role in intracellular catabolic pathways to degrade and redistribute intracellular macromolecules and transition metal ions into cytosolic compartments (1). Lysosomes have been suggested to be involved in the regulation of intracellular copper release into bile or plasma by exocytosis (151). Lysosomes also regulate subcellular zinc distribution, e.g., zinc compartmentalisation, and intracellular zinc signaling (152). Impaired lysosomal function and lysosomal copper accumulation have been observed in LEC rat model for Wilson's disease (151). DMT-1 is one of the postulated divalent metal transporters, which has been suggested to be involved in the regulation of iron, copper, zinc and magnesium transportation within the endosomal/lysosomal system (50, 125). In addition, another postulated bivalent meal transporter, TRPML1, has been recently also suggested to regulate endosomal/lysosomal iron, zinc and calcium homeostasis. Defects in TRPML1 would lead to subcellular iron and zinc compartmentalization and lysosomal calcium flux defects (98, 153).

4.1.7 Acid sphingomyelinase and NPC1 disease

Acid sphingomyelinase (ASM) is a lysosomal phosphodiesterase, which catalyzes the hydrolysis of sphingomyelin to generate phosphorylcholine and ceramide (154). Deficiency of acid sphingomyelinase (ASM) activity results in Niemann Pick type A and B diseases (NPA/B), lysosomal storage diseases characterized by sphingomyelin accumulation (155). It has been demonstrated that copper and zinc are essential co-factors for acid sphingomyelinase (ASM) dimerization and for its enzyme activity (156). Reduced acid sphigomyelinase (ASM) activity has been reported in NPC1 patients fibroblasts and NPC1-null CHO cells (157). It has been suggested that the post-translational modification defects could impair acid

sphingomyelinase in NPC1 disease cells (139, 157); however, the underlying mechanisms of impaired acid sphingomyelinase in NPC1 disease fibroblast remains incompletely understood.

4.1.8 NPC1 disease

The NPC1 protein, is an integral late endosome/lysosome membrane protein that is a member of RND permease superfamily (24). RND proteins in prokaryotic system have been suggested to function as proton sym-porters with a wide range of substrates, including fatty acid, lipophilic drugs and metal ions (111). The role of NPC1 in mediating metal ion movement in eukaryotic cells remains unclear.

4.1.9 Aim of this chapter

In this chapter, we collaborated with Dr. Roman Polishchuk (TIGEM, Italy) and extended our metal ion studies (**Chapter 2 &3**) to copper and zinc ions on the murine model of NPC1 disease. We characterized the systematic/cellular copper and zinc metabolism defects in *in vitro* and *in vivo* NPC1 disease models. Our results indicated that systemic copper and zinc dysregulation could contribute to the pathogenesis cascades in NPC1 disease. These observations also suggested several potential therapeutic strategies for manipulating systemic copper and zinc homeostasis for the developments of potential therapies of NPC1 disease. Furthermore, we have evaluated several copper/zinc manipulation therapies, including (i) copper chelator (D-Penicillamine), (ii) copper/zinc ionophore (clioquinol) and (iii) reduced intestinal copper absorption (zinc acetate), in *Npc1*$^{-/-}$ mice.

4.2 Material & Methods

4.2.1 Animals

Niemann-Pick type C1 mice (BALB/cNctr-*Npc1m1N*/J, *Npc1*$^{-/-}$ mice) were from an established colony. All mice were bred under sterile conditions, with food and water available *ad lib*. All animal studies were conducted using protocols approved by the UK Home Office for the conduct of regulated procedures under license (Animal scientific Procedures Act, 1986).

4.2.2 Administration of copper/zinc manipulation therapies on Npc1$^{-/-}$ *mice*

Npc1$^{-/-}$ mice treated with (i) the copper chelating reagent, using D-Penicillamie (100 mg/kg/day, Sigma); (ii) copper/zinc metal ionophore, using clioquinol (30 mg/kg/day) or (iii) reduced copper absorption therapy, using zinc acetate (300 mg/kg/day), supplemented as dry admix to powdered RM1 mouse chow (SDS, UK). These therapies were administered from 3 weeks of age (P21). The untreated *Npc1*$^{-/-}$ mice were fed on powdered chow as a control group.

4.2.3 Mouse serum samples preparation

Mouse blood samples were collected by cardiac puncture technique as described in **Chapter 2**.

4.2.4 ICP-MS metal analysis for tissue and serum copper and zinc levels

Mouse serum copper and zinc levels were quantified using Inductively Coupled Plasma Mass Spectrometer (ICP-MS) as described in **Chapter 2**.

4.2.5.1 Behavioural analysis - open field

Open field analysis was performed as previously described in **Chapter 2**.

4.2.5.2 Neurological behavioural analysis - tremor

Tremor analysis was performed as previously described in **Chapter 2**.

4.2.5.3 Locomotor Activity: AmLogger and Open Field Rearing

Spontaneous activity of each mouse was recorded weekly using both an automated activity monitor (AmLogger, Linton Instrument, UK) and manual counting as described in **Chapter 3**.

4.2.5.4 Gait Analysis

The CatWalk^{TM} system (Noldus Information Technology, the Netherlands) was used for monitoring changes in movement patters as indicative of any motor complications and to assess any gait improvement patters as indicative of any motor complications and to assess any gait improvement in response to treatment. *Npc1*$^{-/-}$ mice were subjected to CatWalk^{TM} analysis at 9 weeks of age, where a minimum of three "runs" were collected per animal. The data collected were subsequently examined by CatWalk^{TM} XT 10.0 software to produce of 177 inter –paw and intra-paw comparison parameters.

4.2.6 Tissue copper staining (Rhodanine staining)

9-week-old control (*Npc1*$^{+/+}$) and *Npc1*$^{-/-}$ mice were deeply anaesthetized with CO_2 and trans-cardially perfused with 4% paraformaldehyde. Tissues were removed and fixed for at least another 48 hours then dehydrated in 30% sucrose-DPBS solution. For tissue copper rhodanine staining, 20 μm thick tissue sections were cut and incubated at 37°C for 24 hours in rhodanine solution containing 0.2% (w/v) 5-(4-dimethylaminobenzylidene)-2-thioxo-4-thiazolidinone (Wako Pure Chemical Industries), absolute ethanol, and 10% (w/v) sodium acetate trihydrate (Kanto Chemical). Counterstaining was performed with hematoxylin staining. The sections were washed in deionized water, air-dried completely at room temperature, immersed in xylene, and mounted. Images were captured and processed with a Zeiss Axioskop 2 Plus light/fluorescence microscope.

4.2.7 Tissue isolation, RNA extraction, and Microarray hybridization and data analysis

Microarray analysis was performed by Cluzeau *et al.* as described (84).

4.2.8 Cell culture

Human fibroblasts, CHO and astroglial cells were cultured in DMEM medium. RAW 264.7 and HepG2 cells were maintained in RPMI or DMEM-F12, respectively. The culture medium was supplemented with 10% (v/v) fetal bovine serum, 1% penicillin/ streptomycin, and 0.3 μg/mL glutamine in a humidified atmosphere at 37 °C and 5% CO_2.

4.2.9 Immunocytochemistry analysis – Cytosolic copper transporters, MNK ATP7A and WND ATP7B, subcellular localization analysis

Cells were sub-cultured in standard culture medium for 24 hours, then washed with DPBS and treated either with 200 μM copper chloride ($CuCl_2$) or 200 μM D-penicillamine (D-Pen), for 2 hours. Cells were then fixed with 4% paraformaldehyde, washed and blocked with 10% goat serum in DPBS for 1 hour, followed by incubation with the primary antibody in 10% goat serum in DPBS-Triton (0.2%) solution at 4°C overnight. Primary antibodies against MNK ATP7A (1:1000; Abcam, UK) and WND ATP7B (1:1000; Abcam, UK) were used in immunofluorescence assays. Chamber slides were then washed and incubated with either Dylight-594 Red, rabbit anti-mouse (1:3000, Vector Laboratories, UK) or Dylight-488 Green, donkey anti-rat secondary antibodies (1:2000, Invitrogen, UK) for 2 hours at room temperature. Cell nuclei were stained with DAPI (Sigma, UK). Images were captured and processed with a Zeiss Axioskop 2 Plus fluorescence microscope.

4.2.10 Fluorescence Imaging and Flow Cytometric analysis of Free Intracellular Zinc by FluoZin-3 AM Staining.

FluoZin-3 AM is a high affinity, Zn-specific fluorophore which reacts with labile Zn. FluoZin-3 fluorescence was used to visualize labile Zn vesicularization and detection of labile Zn pools in NPC1 human fibroblast, NPC1-null CHO, RAW 264.7 and primary mouse *Npc1*$^{-}$

$^{/-}$ astroglia cells. Cells were seeded onto glass-cover slips. After indicated treatment times, cells were washed with DPBS and incubated with 2.5 μM FluoZin-3 AM (Molecular Probes, Eugene, OR) with 0.02% Pluronic F-127 (Invitrogen, Carlsbad, CA) in serum-free DMEM or DMEM-F12 medium for 30 minutes at room temperature. Subsequently, cells were washed twice with DPBS and immediately imaged to analyse intracellular zinc distribution. Cytosolic zinc labile pool distribution was imaged and processed with a Zeiss Axioskop 2 Plus light/fluorescence microscope. FluoZin-3 was excited at 488 nm, and emission was detected using a 505–550-nm bandpass filter.

4.2.11 Statistics

Data were expressed as the mean ± SEM. Statistical analysis and graph plotting were performed by using GraphPad Prism software. An unpaired two-tailed Student's *t* test was used to determine the significant differences. A *p* value less than 0.05 was considered statistically significant.

4.3 Results:

4.3.1 Defective systemic copper regulation in Npc1$^{-/-}$ mice.

Several studies have previously demonstrated that (i) multi-copper ferroxidase, ceruloplasmin and hephaextin, are crucial to mediate intestinal iron transport and uptake, (ii) copper could substitute for iron in certain mitochondrial iron-containing enzymes, such as mitochondrial cytochromes, when iron deficiency occurs (59, 158, 159). To ascertain whether systemic iron dysregulation in *Npc1*$^{-/-}$ mice could impair homeostasis of other transition metals, such as copper and zinc, *Npc1*$^{-/-}$ peripheral tissues were collected and analysed using the inductively coupled plasma mass spectrometry (ICP-MS). As shown in **Fig. 4.1A**, there was a significant increase in serum copper levels by approximately 1.5 fold in 9-week-old *Npc1*$^{-/-}$ mice, ($p < 0.0001$) compared with age-matched controls, which suggested systemic copper dysregulation in *Npc1*$^{-/-}$ mice.

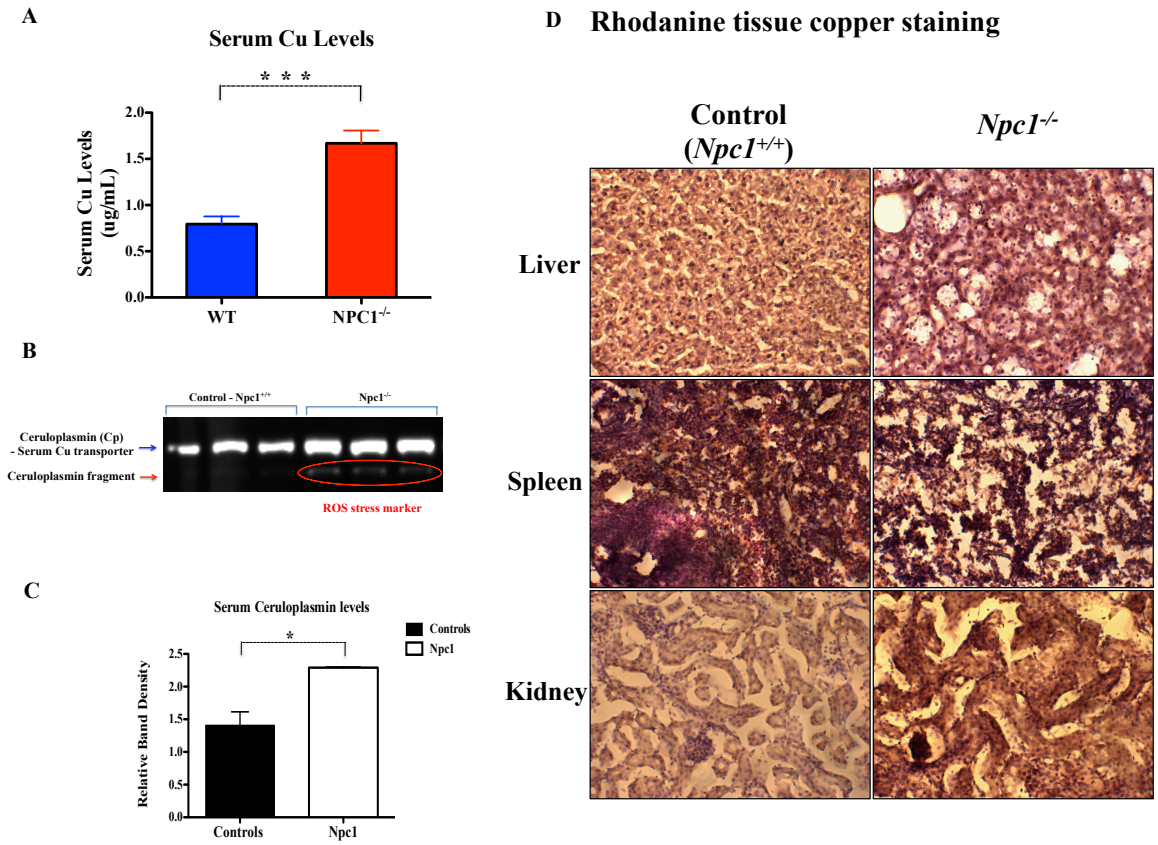

Figure 4.1 System copper dysregulation and increased serum ceruloplasmin in *Npc1*$^{-/-}$ mice. (A) Serum copper levels were anlayzed using ICP-MS technique as described in "Material and Methods". (B) Representative image of immunoblotting of serum ceruloplasmin levels. (C) Quantitative analysis of serum ceruloplasmin levels in control (*Npc1*$^{+/+}$) and *Npc1*$^{-/-}$ mice. (D) Rhodanine tissue copper staining on tissues sections from 9-week-old control and *Npc1*$^{-/-}$ mice. Data represent mean SEM, n = 3, per group, * $p < 0.05$, *** $p < 0.0005$. Scale bar = 100 μm.

Expression levels of the serum copper transporter, ceruloplamsin, were measured by Western blotting. 9-week-old *Npc1*$^{-/-}$ serum ceruloplasmin levels were markedly increased compared with controls **(Fig. 4.1B-C)**. Rhodamine histological copper staining was performed on 9-week-old *Npc1*$^{-/-}$ tissue sections to visualize tissue copper distribution. As shown in **Fig. 4.1D**, tissue copper accumulation (red-brown deposits) were observed in *Npc1*$^{-/-}$ liver and kidney.

4.3.2 Altered hepatic copper metabolism gene expression in Npc1$^{-/-}$ *mice.*

Microarray examination indicated that there were significant down-regulation of hepatic ceruloplasmin mRNA levels in 1-week-old *Npc1*$^{-/-}$ mice compared with age-matched controls then significantly elevated in 5, 9 and 11-week-old of *Npc1*$^{-/-}$ mice (1 week, -1.19 fold, $p = 0.0029$, 5 week, 1.19 fold, $p = 0.0029$, 9 week, 1.25 fold, $p = 0.00018$, 11 week, 1.17 fold, $p = 0.0064$), which suggested hepatic copper dysregulation in *Npc1*$^{-/-}$ mice (**Fig. 4.2A**). We also examined another multi-copper containing ferroxidase, hepaestin, which is also involved in the regulation of iron and copper metabolism. However, there were no significant changes of relative hepatic hephaestin mRNA levels in *Npc1*$^{-/-}$ mice at any age compared with age-matched controls **(Fig. 4.2B)**.

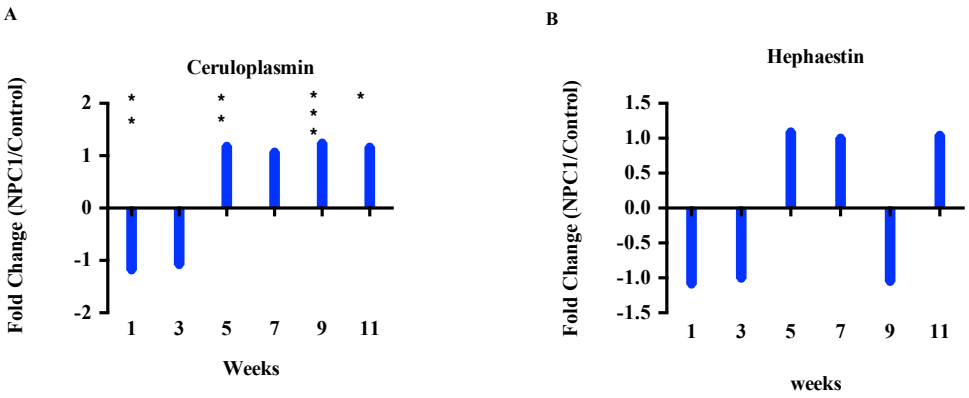

Figure 4.2. Changes in hepatic ceruloplasmin mRNA expressions in *Npc1*$^{-/-}$ mice. (A-B) Hepatic samples from age-matched of control and *Npc1*$^{-/-}$ mice were collected and analyzed through microarray analysis. ANOVA analysis was used to analyze microarray genes expression change. * $p < 0.05$; ** $p < 0.005$; *** $p < 0.0005$; **** $p < 0.0001$. Data represent mean ± SEM, n = 4, per group.

In addition, microarray analysis also indicated that the hepatic plasma copper importer, CTR-1, which mainly facilitates copper uptake across the plasma membrane to intracellular vesicles, was significantly down-regulated from the early pre-symptomatic stage (1-week-old) till the late end stage (11-week-old) of *Npc1*$^{-/-}$ mice relatively to control littermates (1 week, -1.21 fold, $p = 0.00058$, 3 weeks, -1.12 fold, $p = 0.03344$, 7 weeks, -1.32 fold, $p < 0.00001$, 9 week, -1.28 fold, $p < 0.00001$, 11 weeks, -1.84 fold, $p < 0.00001$) (**Fig. 4.3A)**. The observation of down-regulation of hepatic plasma copper importer, CTR1, supported the finding of hepatic copper accumulation phenotypes in *Npc1*$^{-/-}$ mice. Hepatic mRNA levels of another postulated copper transporter, CTR-2, which has been suggested to be involved in the regulation of cellular copper transportation within intracellular vesicles/endosomes and lysosomes, was also examined. There was a significant increase in mRNA expression at 7 & 9 –weeks of age (7 weeks, 1.23 fold, $p = 0.0106$, 11 weeks, 1.51 fold, $p < 0.00001$) **(Fig. 4.3B)**. Therefore, these observations supported our findings and suggested hepatic copper dyshomeostasis in *Npc1*$^{-/-}$ mice.

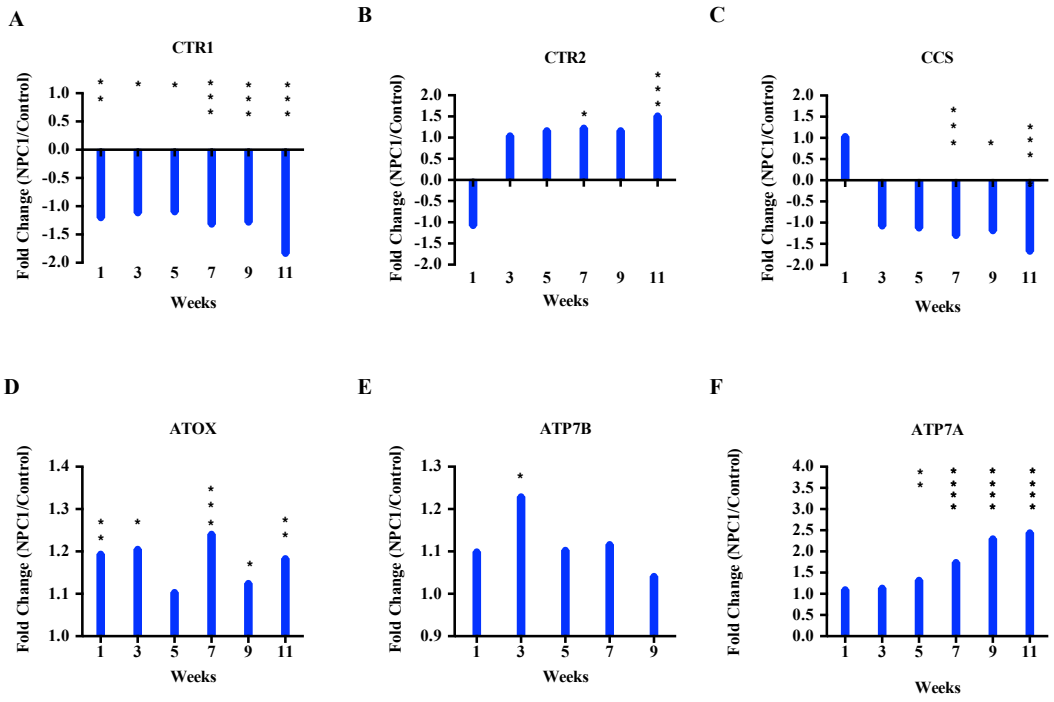

Figure 4.3. Altered hepatic copper metabolism-related gene expression in *Npc1*$^{-/-}$ mice. (A-F) Hepatic samples from age-matched of control (*Npc1*$^{+/+}$) and *Npc1*$^{-/-}$ mice were collected and microarray analysis performed. ANOVA analysis was used to analyze microarray genes expression change. * $p < 0.05$; ** $p < 0.005$; *** $p < 0.0005$; **** $p < 0.0001$. Data represent mean ± SEM, n = 4, per group.

4.3.3 Impaired hepatic cytosolic copper trafficking in Npc1$^{-/-}$ *mice.*

To explore whether NPC1 deficiency could impair hepatic subcellular copper trafficking, the gene expressions of multiple proteins associated with hepatic copper metabolism were examined in *Npc1*$^{-/-}$ mice. Microarray analysis indicated that the expression of the hepatic copper chaperone for Cu/Zn superoxide dismutase (CCS) was significantly reduced from 7-weeks of age in *Npc1*$^{-/-}$ mice (7 week, -1.31 fold, $p = 0.00063$, 9 week, -1.19 fold, $p = 0.0195$, 11 week, -1.68 fold, $p < 0.00001$) **(Figure 4.3C)**. ATOX1, which predominantly mobilises transfers copper to cytosolic copper ATPase transporter, ATP7B, was almost markedly elevated from 1-week of age up to 11-weeks of age in *Npc1*$^{-/-}$ mice (1 week, 1.19 fold, $p = 0.0015$, 3 weeks, 1.21 fold, $p = 0.00090$, 7 weeks, 1.24 fold, $p < 0.00015$, 9 weeks, 1.12 fold, $p = 0.00317$, 11 weeks, 1.18 fold, $p = 0.00255$) **(Figure 4.3D)**. These findings suggested impaired hepatic copper trafficking in *Npc1*$^{-/-}$ mice and this defect could

impair the cupro-enzymes activities of *Npc1*$^{-/-}$, such as Cu/Zn superoxie distumatases. The major hepatic cytosolic Cu ATPase Wilson ATP7B transporter, which mainly functions to efflux excess hepatic copper to bile for elimination, only showed a significant increase in mRNA expression in 3-week-old *Npc1*$^{-/-}$ mice (3 week, 1.23 fold, $p = 0.0086$) **(Figure. 4.3E)**. We also found that the mRNA expressions of another hepatic copper ATPase transporter MNK ATP7A, which has been recently suggested to be involved in systemic copper signalling and possibly functions to mobilize hepatic copper to other peripheral organs (160), were significantly up-regulated from 5-week-old till 11-week-old *Npc1*$^{-/-}$ mice compared with control littermates (5 weeks, 1.32 fold, $p = 0.0023$, 7 weeks, 1.74 fold, $p < 0.00001$, 9 weeks, 2.3 fold, $p < 0.00001$, 11 weeks, 2.4 fold, $p < 0.00001$) **(Fig. 4.3F)**.

4.3.4 Hepatic subcellular copper metabolism defects in Npc1$^{-/-}$ *mice.*

Copper is also required for the activation of the mitochondrial complex IV Cu-dependent enzyme, cytochrome c oxidase (59). Several postulated mitochondrial copper chaperones and mediators, including Cox 23, PET191, CMC1-3, Cox11, Cox17, Cox 19, Sco1 and Sco2, have been suggested to be involved in the mobilization of cytosolic copper into mitochondria and facilitate copper incorporation into mitochondrial cytochrome c oxidase (53). Our microarray examination indicated that there was an age-dependent and significant decrease in mitochondrial Sco1 mRNA expression from 3-weeks of age until late 11-week old *Npc1*$^{-/-}$ mice (3 weeks, -1.17 fold, $p = 0.0019$, 5 weeks, -1.18 fold, $p = 0.01052$, 7 weeks, -1.20 fold, $p = 0.00561$, 9 weeks, -1.41 fold, $p < 0.00001$, 11 weeks, -1.55 fold, $p < 0.0001$) **(Figure 4.4B)**. Other potential mitochondrial copper chaperones and mediators, including Cox11, Cox17, Cox 19 and Cox1, were significantly down-regulated at different time points of *Npc1*$^{-/-}$ mice suggesting that copper dysregulation could impair mitochondrial copper trafficking and cause mitochondrial dysfunction in *Npc1*$^{-/-}$ mice **(Fig. 4.4 A, C-E)**.

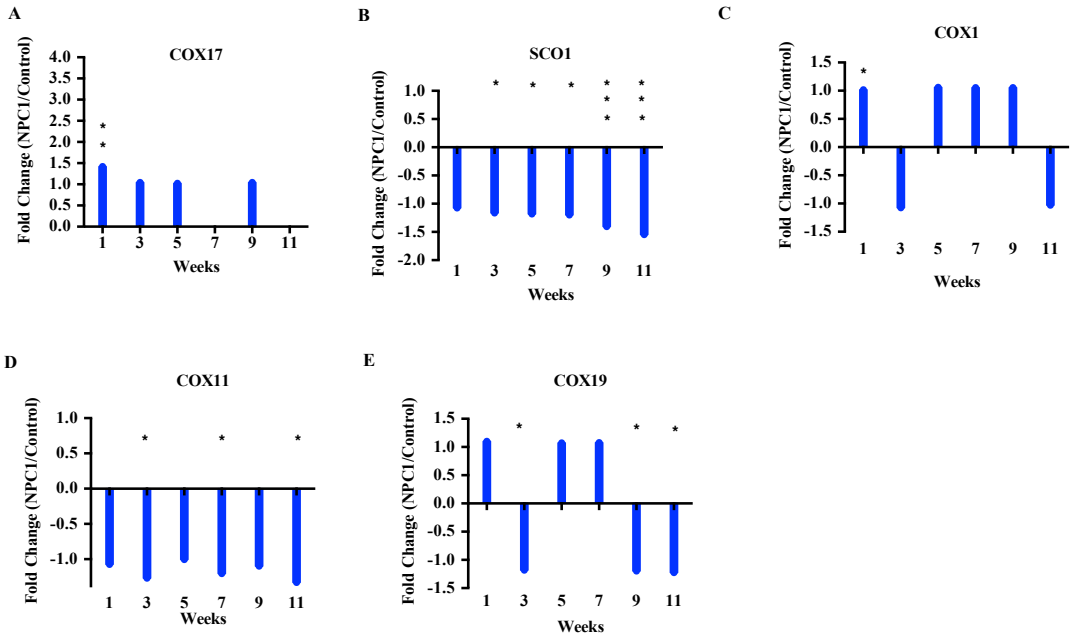

Figure 4.4. Altered hepatic copper metabolism-related gene expression in *Npc1*$^{-/-}$ mice. (A-F) Liver samples from age-matched control (*Npc1*$^{+/+}$) and *Npc1*$^{-/-}$ mice were collected and analyzed by microarray analysis. ANOVA analysis was used to analyze microarray genes expression change. * $p < 0.05$; ** $p < 0.005$; *** $p < 0.0005$; **** $p < 0.00001$. Data represent mean ± SEM, n = 4, per group.

4.3.5 Mislocalization of endogenous WND ATP7B copper transporters in U18666A-treated HepG2 cells.

The intracellular distribution of endogenous hepatic cooper ATPase transporter, WND ATP7B, was firstly examined in U18666A-treated HepG2 cells to induce NPC1 disease cellular phenotypes. As shown in **Fig. 4.6**, under basal conditions, the endogenous Cu transporter, WND ATP7B, was localized within the perinuclear region and partially co-localized with the *trans*-Golgi network (Golgin97) in vehicle (DMSO)-treated HepG2 cells. However, in U18666A-treated cells, WND ATP7B was only found partially co-localized with Golgin97, was mainly distributed within numerous intracellular vesicles and abnormally large subcellular structures/vesicles. Next, HepG2 cells were incubated with the copper chelator, bathocuproine-disulphonate (BPS), overnight. Under cellular copper depletion condition, little endogenous WND ATP7B was detected co-localized with the *trans*-Golgi marker, Golgin97, in vehicle (DMSO)-treated HepG2 cells. On the other hand, under low cellular

copper condition, the distribution of endogenous WND ATP7B resided predominately in perinuclear region and *trans*-Golgi compartments in U18666A-treated HepG2 cells. Some endogenous WND ATP7B localized to some abnormal intracellular giant organelles in U18666A-treated HepG2 cell **(Fig. 4.6)**. In addition, in response to elevated cellular copper content, the endogenous WND ATP7B reversibly re-localized to several cytoplasmic vesicles and distributed widely into other subcellular compartments, including early and late endosomes and plasma membrane in vehicle (DMSO)-treated HepG2 cells **(Fig. 4.6)**. This observation was consistent with the function of WND ATP7B to facilitate uptake of cellular copper and its delivery into cellular secretory networks to facilitate copper incorporation into cupro-enzymes. However, in contrast, in response to elevated cellular copper levels, the WND ATP7B only partially re-localized to the plasma membrane of HepG2 cells and other WND ATP7B transporters were partially co-localized with *trans*-Golgi networks, early endosomes and also intracellular giant granules in U18666A-treated HepG2 cells **(Fig. 4.6)**. Therefore, these observations suggest a potential link between subcellular copper trafficking defects and mis-localization of copper transporters WND ATP7B in pharmacological induced NPC disease phenotypes in HepG2 cells.

Figure 4.6. Endogenous hepatic copper transporter WND ATP7B mis-localized in U18666A-treated HepG2 cells. Immunofluorescence analysis indicated that endogenous WND ATP7B copper transporters mis-localized into intracellular vesicles in U18666A-treated HepG2 cells. Cells were treated with DMSO (vehicle control) or U18666A for 24 hours and were treated with either the copper chelator (200 μM BCS) or copper supplementation (200 μM CuSO4) for 2 hours at 37 °C, prior to fixing and staining for the endogenous WND ATP7B copper transporter. Golgi marker, Golgin 97 (red); endogenous WND ATP7B (green). The immunofluorescence analysis was performed by our collaborator Dr. Roman Polishchuk (TIGEM, Italy).

4.3.6 Mislocalization of exogenous GFP-tagged WND ATP7B copper transporter in NPC1-null CHO-M12 cells.

To further investigate the underlying mechanisms of copper dysregulation in NPC1 disease, NPC1-null CHO-M12 cells were utilized. Chinese hamster ovary (CHO) cells were chosen since CHO cells only express endogenous MNK ATP7A copper transporter, but not the WND ATP7B copper transporter. The CHO cells were transiently transfected with the GFP-tagged cytosolic copper ATPase transporter, Wilson ATP7B protein (GFP-tagged WND ATP7B), to examine its subcellular localization and distribution in response to altered intracellular copper levels. As shown in **Fig. 4.7**, under basal conditions, the subcellular distribution of exogenous GFP-tagged WND ATP7B was mainly localized within the perinuclear region and *trans*-Golgi networks in control CHO-H1 ($Npc1^{+/+}$). This sub-cellular localization is consistent with the function of WND ATP7B to pump copper into cellular secretory networks for help copper incorporate into cupro-enzymes and help maintain their enzymatic activities. However, in NPC1-null CHO-M12 cells, in addition to localizing within the perinuclear region and *trans*-Golgi network, the exogenous GFP-tagged WND ATP7B was retained within the endoplasmic reticulum (ER) and partially co-localized with the early endosomal marker, EEA1 (**Fig. 4.7)**. In addition, when CHO cells were treated with 100 μM of copper chloride, in response to the raised cellular copper contents, the exogenous GFP-tagged WND ATP7B reversible re-localized to subcellular vesicle compartments, including early endosomes, late endosomes, and plasma membrane in control ($Npc1^{+/+}$) CHO-H1 cells. However, in response to elevated copper levels, the exogenous GFP-tagged WND ATP7B redistributed to numerous subcellular cytoplasmic organelles and partially co-localized with

early endosomal marker, EEA1, and was retained close to the plasma membrane in NPC1-null CHO-M12 cells. Next, when the cells were incubated with the copper chelator, bathocuproinedisulfoinc acid (BCS), exogenous GFP-tagged WND ATP7B transporters was found to be mainly restricted to perinuclear regions and *trans*-Golgi network in control CHO-H1 cells (**Figure 4.7)**. However, GFP-tagged WND ATP7B was additionally found within the endoplasmic reticulum (ER) in NPC1-null CHO-M12 cells (**Figure 4.7)**. These observations suggested that mislocalization of exogenous WND ATP7B copper transporters could be associated with the impaired subcellular copper trafficking and impact cellular copper metabolism in NPC1-null CHO-M12 cells.

Figure 4.7. Exogenous GFP-tagged WND ATP7B mislocalized in subcellular compartments in NPC1-null CHO cells. Cultured control (*Npc1*$^{+/+}$) CHO-H1 and NPC1-null CHO-M12 cells were transiently transfected with GFP-tagged WND ATP7B for 16 hours and then where appropriate were treated with either the copper chelator (200 μM BCS) or copper supplementation (200 μM CuSO4) for 2 hours at 37 °C, prior to fixing and staining with subcellular organelles marker antibodies. Early endosomal marker, EEA1 (red); *trans*-Golgi marker, GM130; GFP-tagged ATP7B (green). The immunofluorescence analysis was performed by our collaborator Dr. Roman Polishchuk (TIGEM, Italy).

4.3.7 Transfected exogenous GFP-tagged WND ATP7B copper transporter is not co-localized with LAMP-1 in NPC1-unll CHO-M12 cells.

Next, to explore the possibility whether WND ATP7B copper transporter mediate subcellular copper trafficking into lysosomes, the subcellular localization of GFP-tagged WND ATP7B were double-labeled with lysosomal marker, LAMP-1, in CHO cells. As illustrated in **Figure 4.8**, either in basal conditions, copper depletion or copper supplementation conditions, there were no significant co-localized patterns of exogenous GFP-tagged WND ATP7B and LAMP-1 either in control CHO-H1 or NPC1-null CHO-M12 cells.

Figure 4.8. Exogenous GFP-tagged WND ATP7B is not co-localized with LAMP-1 in NPC1-null CHO-M12 cells. Cultured CHO-H1 and NPC1-null CHO-M12 cells were transiently transfected with GFP-tagged WND ATP7B for 16 hours, and then were incubated either copper supplementation (200 μM CuSO4) or copper chelator (200 μM BCS) for another 2 hours prior to fixing and staining with late endosomal/lysosomal marker, LAMP-1. No significant co-localization of exogenous GFP-tagged WND ATP7B copper transporter and LAMP-1 was observed in control CHO-H1 and NPC1-null CHO-M12 cells. GFP-tagged ATP7B (green); LAMP-1 (red). The immunofluorescence analysis was performed by our collaborator Dr. Roman Polishchuk (TIGEM, Italy).

4.3.8 Cytosolic copper accumulation in NPC1-null CHO-M12 cells

To investigate whether the mislocalization of cytosolic copper transporters, such as WND ATP7B and MNK ATP7A, could impair subcellular copper trafficking and affect cellular copper contents in NPC1-null CHO-M12 cells, an established 4 x MREs (metal response elements) luciferase-based copper biosensor assay was utilized. The assay is based on the transactivation of the metallothionein-1 (MT-1) promoter in response to cytosolic copper content changes. We utilized the 4 x MRE containing luciferase based assay and exogenous GFP-tagged wild type (WT) WND ATP7B copper transporter overexpressing technique to measure bioavailable cytosolic copper content and WND ATP7B-mediated copper transport activity in CHO cells. CHO cells were transiently co-transfected with 4 x MRE containing a luciferase reporter and GFP-tagged WND ATP7B copper transporter, followed by incubation with copper supplementation conditions to induce luciferase-based copper sensor expression. As illustrated in **Fig. 4.9**, when compared with control CHO-H1 cells, the 4 x MREs containing luciferase reporter activity in NPC1-null CHO-M12 cells was increased by 21 %, suggesting cytosolic copper accumulation in NPC1-null CHO-M12 cells. Furthermore, while GFP-tagged WND ATP7B copper transporter was overexpressed, both 4 x MRE luciferase activity in CHO-H1 and NPC1-null CHO-M12 cells were markedly decreased. However, when compared with control groups (ATP7B overexpressing CHO-H1 cells), the 4 x MRE luciferase activity revealed a slight increase (7%) in GFP-tagged WT ATP7B overexpressing NPC1-null CHO-M12 cells, which supported our findings of impaired copper trafficking in NPC1-null CHO-M12 cells. Consistent with our earlier

findings, these results suggested that cytosolic copper accumulation in NPC1-null CHO-M12 cells could be associated with the aberrant subcellular localization of copper transporters and impaired cellular copper trafficking in NPC1 disease.

Figure 4.9. Cytosolic copper accumulation and impaired GFP-tagged WND ATP7B mediated copper export in NPC1-null CHO-M12 cells. CHO cells were transiently transfected with the 4 x MRE containing luciferase copper reporter together with either empty vector (EV) or wild-type GFP-tagged ATP7B constructs. After 16 hours of transfection, cells were incubated with indicated concentration of $CuSO_4$. 4 x MRE containing luciferase copper reporter activities were measured and normalized for *Renilla* luciferase activity as transfection efficiency controls. MRE-luciferase copper reporter activities were expressed as fold induction relative to CHO-H1 EV group. The luciferase cytosolic copper biosensor assay was performed by our collaborator Dr. Roman Polishchuk (TIGEM, Italy).

To confirm the observations of subcellular copper trafficking defects electron microscopy (EM) examination was performed to analyze sub-cellular WND ATP7B distribution in WND ATP7B-overexpressing CHO cells. As shown in **Figure 4.10**, in copper depletion condition (BCS treatment), the subcellular distributions of WND ATP7B was mainly observed within the *trans*-Golgi network in control CHO-H1 ($Npc1^{+/+}$) cells; however, in response to low cellular copper contents, over-expression of WND ATP7B was detected (i) along the plasma membrane, (ii) intracellular vesicles, (iii) endosomes (iv) and endoplasmic reticulum in NPC1-null CHO-M12 cells. In addition, large lysosome-like structures were observed in NPC1-null CHO-M12 cells. However, electron microscopy examination did not reveal significant over-expression of ATP7B localized within the giant lysosome-like structures in CHO-M12 cells. Therefore, these results were consistent with our immunofluorescence studies on NPC1-null CHO-M12 cells and further supported the mislocalization of exogenous copper transporter, WND ATP7B, in NPC1-null CHO-M12 cells.

Figure 4.10. Mis-localization of subcellular distributions of copper transporter WND ATP7B in NPC1-null CHO-M12 cells. CHO-H1 and NPC1-null CHO-M12 cells were transiently transfected with WND ATP7B for 16 hours and then incubated with the copper chelator (BCS) for overnight reaction to reduce cellular copper contents. Subcellular distribution of copper transporter WND ATP7B in CHO-H1 and NPC1-null CHO-M12 cells were examined by electron microscopy. In control CHO-H1 cell, intracellular copper transporter ATP7B mainly resided in the trans-Golgi membrane (upper; black arrow); however, in response to low copper levels, intracellular copper transporter ATP7B was detected along the plasma membrane (empty arrowheads), and intracellular vesicles (arrowheads) along with the early endosomes and the ER profiles (arrows) in NPC1-null CHO-M12 cells. The electron microscopy analysis was performed by our collaborator Dr. Roman Polishchuk (TIGEM, Italy).

4.3.9 Mislocalization of the MNK ATP7A copper transporter in U18666A-treated RAW cells and NPC1 human fibroblasts.

Subcellular copper trafficking is mainly dependent on the cytosolic copper transporters, WND ATP7B and MNK ATP7A, which mediate cellular copper export and help incorporate copper into cupo-enzymes (62). So far, our studies have demonstrated impaired WND ATP7B-mediated subcellular copper trafficking in U18666A-treated HepG2 cells and exogenous GFP-tagged WND ATP7B overexpressing NPC1-null CHO-M12 cells. However, it is still unclear whether the copper metabolism defects in NPC1 disease is cell-type specific or specific to WND ATP7B-mdeiated copper trafficking. To further investigate this hypothesis, we therefore studied another copper transporter, MNK ATPA7A, mediating subcellular copper trafficking. Firstly, we utilized the endogenous MNK ATP7A expressing RAW 264.7 cells (mouse monocyte cell line) to look for potential intracellular copper trafficking defects. As illustrated in **Fig. 4.11**, under basal conditions, the intracellular copper transporter, MNK ATP7A, was mainly localized within perinuclear region and partially localized with early endosomes (EEA-1) in vehicle (DMSO)-treated RAW 264.7 cells. However, in U18666A-treated RAW 264.7 cells, MNK ATP7A was distributed all over the

cytoplasm and there was extensive co-localization with the early endosomal marker, EEA-1. When RAW 264.7 cells were incubated with 100 μM copper chloride ($CuCl_2$) for 2 hours, the MNK ATP7A re-localized to other subcellular compartments and the plasma membrane in both vehicle (DMSO) and U18666A-treated RAW 264.7 cells. However, in copper depletion condition, when the cells were treated with 100 μM copper chelator, D-Penicillamine, MNK ATP7A was mainly localized within the perinuclear region in vehicle (DMSO)-treated RAW 264.7 cells. However, relatively diffuse partial perinuclear staining was observed along with co-localization with the early endosomal marker, EEA-1 in U18666A-treated RAW 264.7 cells. These findings suggested that the mis-localization of the cytosolic MNK ATP7A copper transporter could be associated with subcellular copper trafficking defects in U18666A-treated RAW 264.7 cells

DMSO treated - RAW 264.7 cells

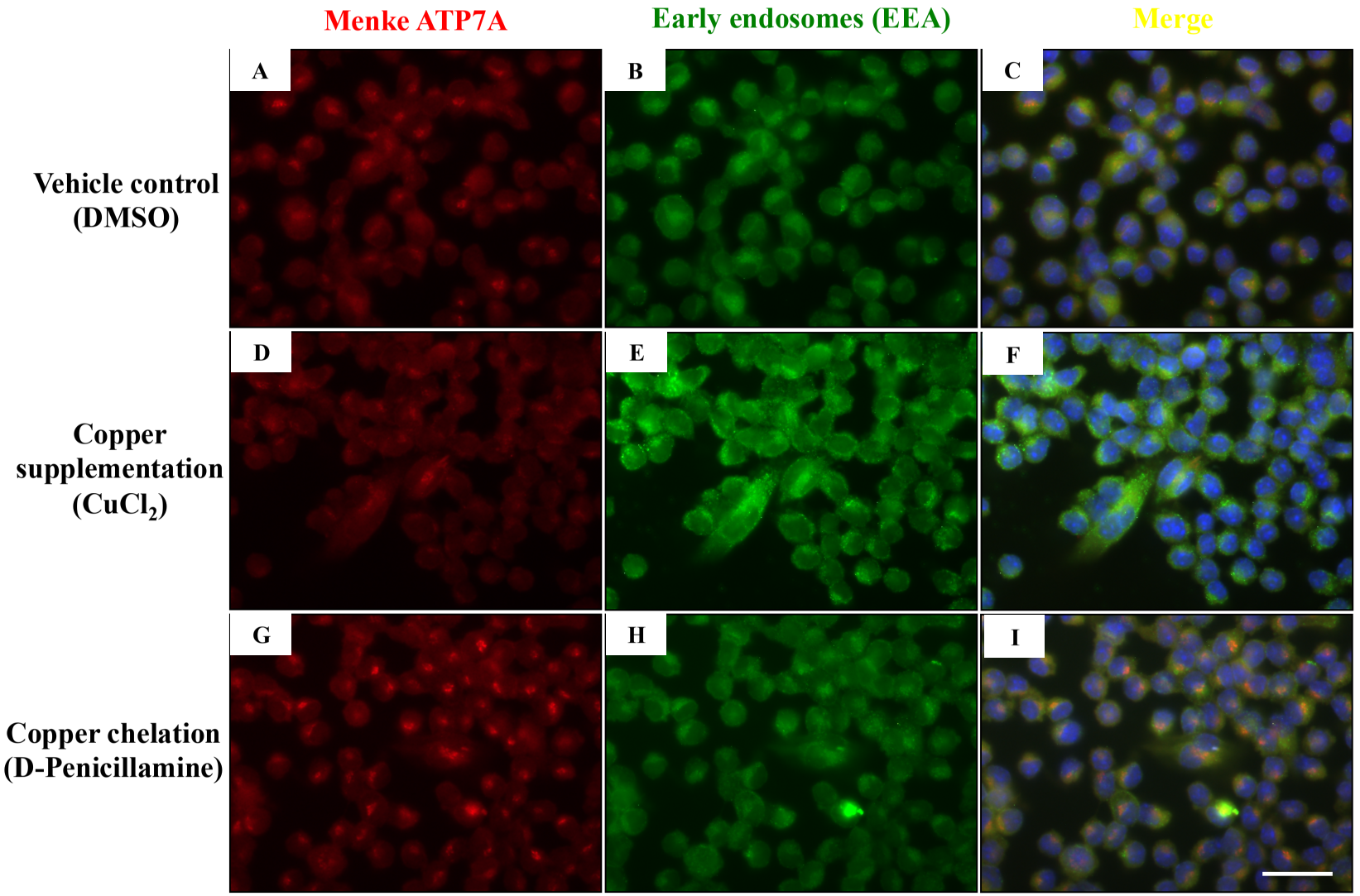

U18666A treated - RAW 264.7 cells

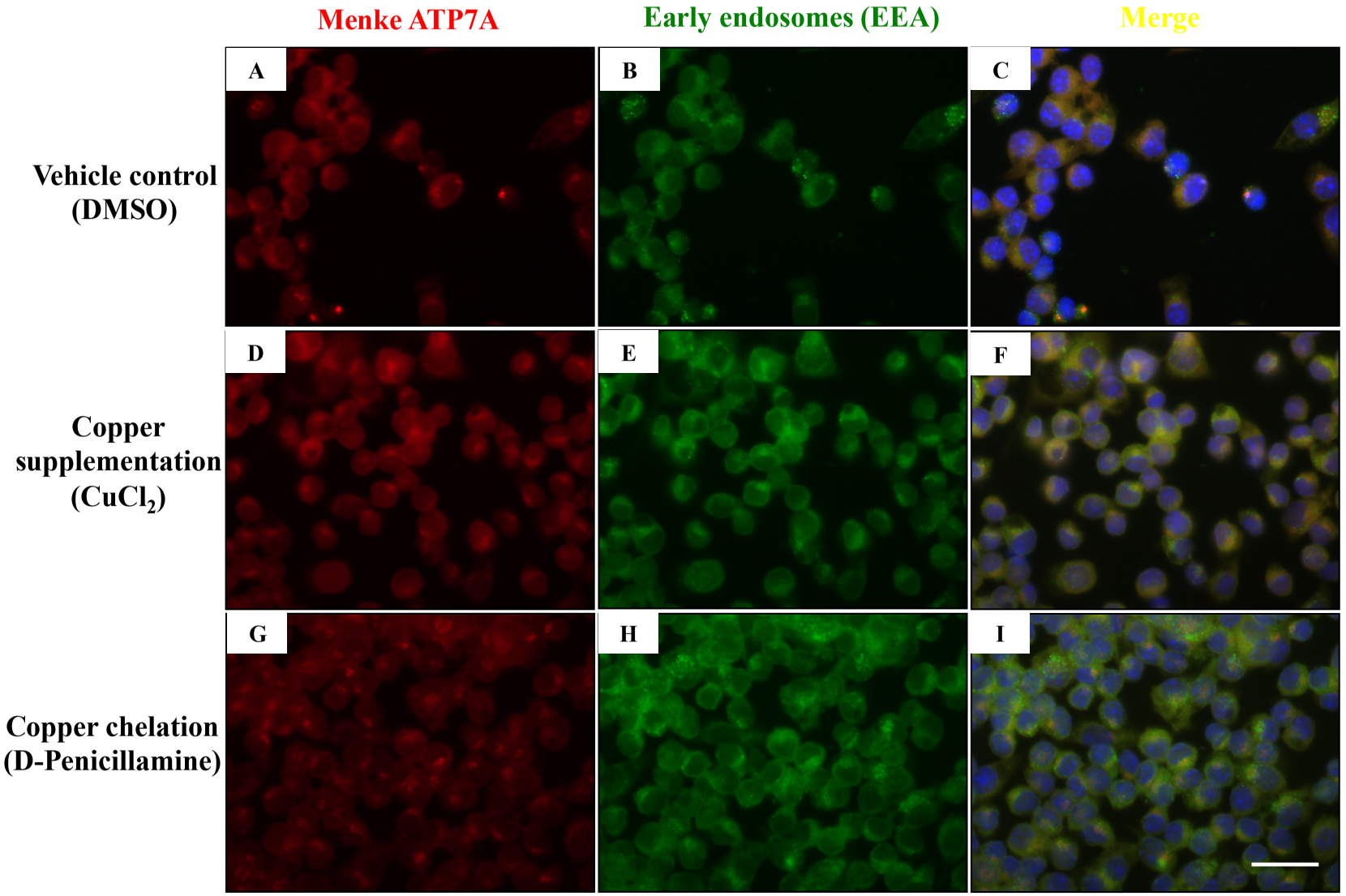

Figure 4.11. Mis-localization of endogenous MNK ATP7A copper transporter in U18666A-treaed RAW 264.7 cells. RAW 264.7 cells were treated either with DMSO (vehicle control) or U18666A (2 μg/mL) for 72 hours to induce NPC1 disease cellular phenotypes. The DMSO and U18666A-treated RAW 264.7 cells were then incubated either with 200 μM $CuCl_2$ or 200 μM D-Penicillamine for 2 hours before fixing and staining with anti-MNK ATP7A (red) and early endosomal marker, EEA1 (green), antibodies. Cell nuclei were counterstained with DAPI. Images were viewed and captured as described in "Materials and Methods". Scale bar = 5 μm. Data are representative of two independent experiments.

In addition, the subcellular localization of endogenous MNK ATP7A copper transporters in control and NPC1 human fibroblasts were also examined. As illustrated in **Fig. 4.12**, the endogenous MNK ATP7A was mainly localized within perinuclear and *trans*-Golgi networks in control and NPC1 human fibroblasts (WF and PH) that were of mild severity. However, mis-localization of MNK ATP7A to subcellular compartments, such as early endosomes (EEA-1), was observed in the severe NPC1 human fibroblast **(161) (Fig. 4.12)**. Therefore, these observations were consistent with our earlier findings and suggested subcellular trafficking defects in NPC1 disease could impair subcellular copper trafficking and cause mis-localization of copper transporters.

100 μM D-Penicillamine

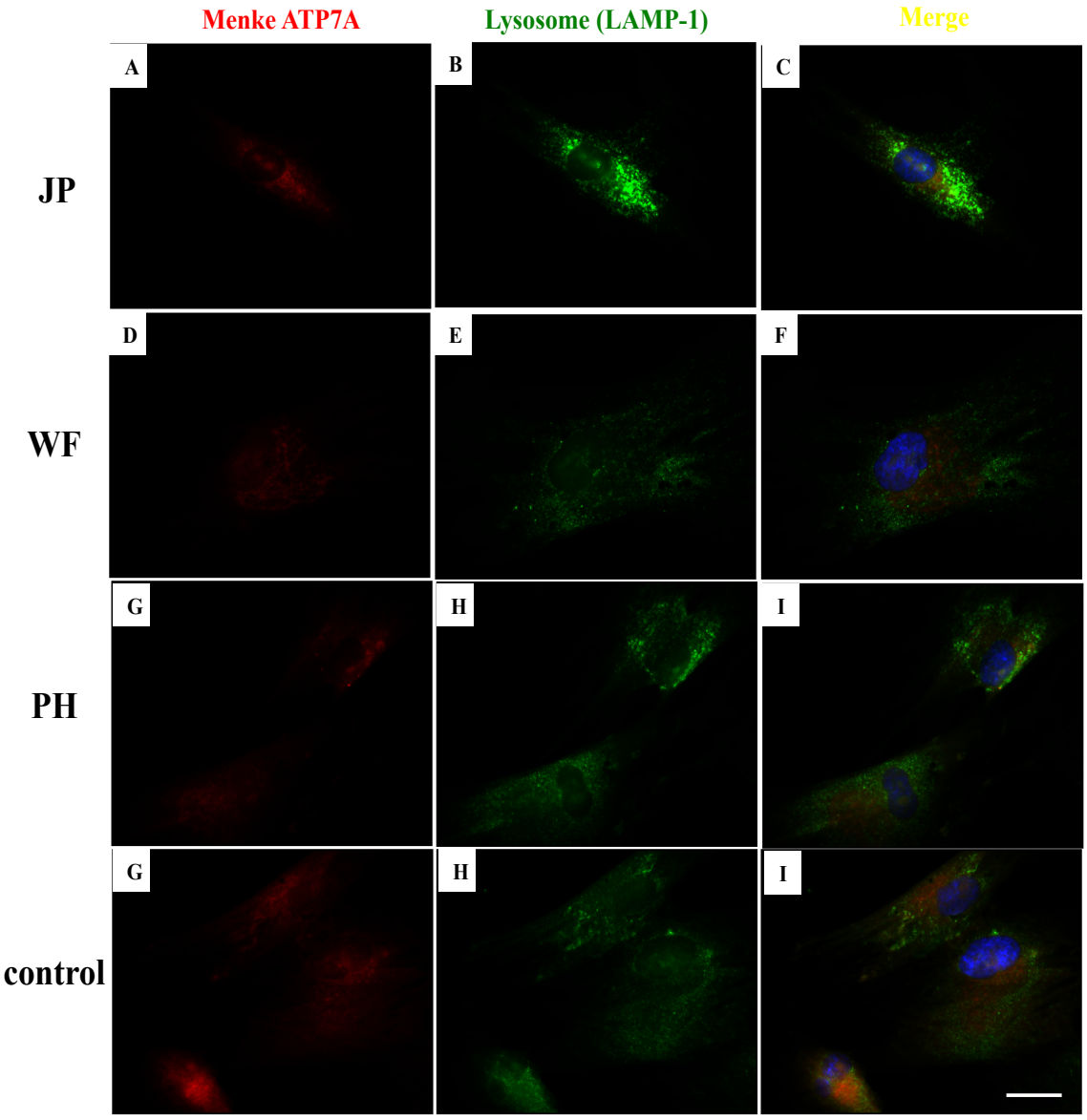

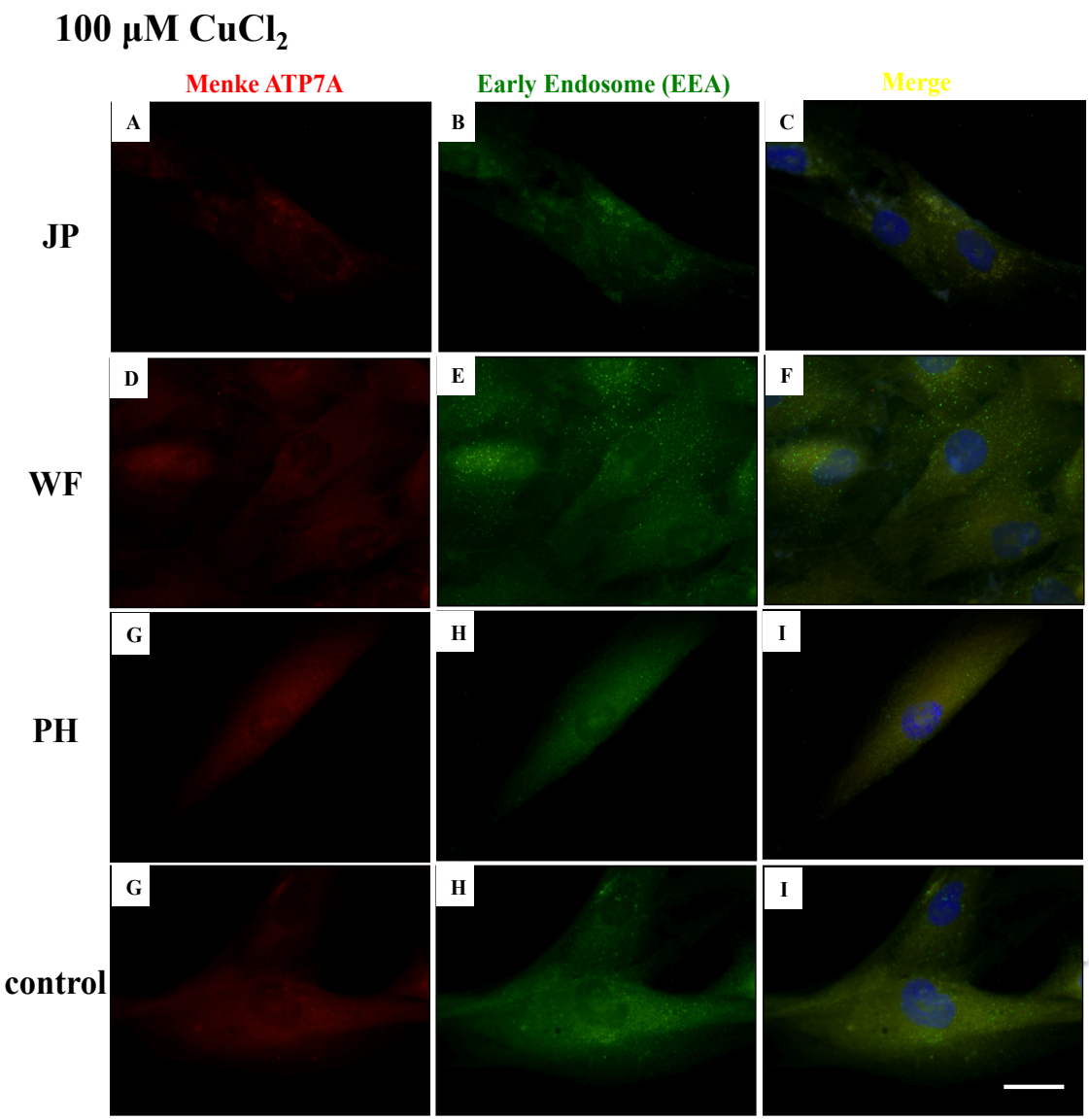

Figure 4.12. Mis-localization of endogenous MNK ATP7A copper transporter in severe NPC1 human fibroblasts. Control and NPC1 human fibroblasts were cultured in basal conditions. Immunofluorescence staining of endogenous MNK ATP7A copper transporter and early endosomal marker, EEA-1, were performed in control and NPC1 disease human fibroblasts (PH, WF, JP). The cells were treated either with 100 µM $CuCl_2$ or 100 µM D-Penicillamine for 2 hours before fixed and staining as described in "Materials & Methods". Menke ATP7A (red), early endosomal marker, EEA1 (green), DAPI. Scale bar = 10 µm. Represent data of one independent experiment. Disease severity score: JP>WF>PH.

4.3.10 Up-regulation of hepatic metallothioneins (MT-1 & MT-2) in Npc1$^{-/-}$ mice.

To determine the effects of impaired hepatic copper homeostasis in *Npc1*$^{-/-}$ mice, we firstly examined expression of hepatic metallothioneins in *Npc1*$^{-/-}$ mice. MT-1 mRNA expression was significantly increased in 7 and 11-week-old *Npc1*$^{-/-}$ mice compared with age-matched control littermates (7 weeks, 2.50 fold, $p = 0.00038$, 11 weeks, 1.71 fold, $p = 0.031$) **(Fig. 4.13A)**. Similarly, *Npc1*$^{-/-}$ hepatic metallothionein-2 (MT-2) mRNA expression was only significantly elevated at 7-weeks of age *Npc1*$^{-/-}$ mice (7 weeks, 2.94 fold, $p = 0.0030$) **(Fig. 4.13B)**. Since metallothioneins are also stress-induced proteins, the up-regulation of MTs at 7-week-old *Npc1*$^{-/-}$ mice could be associated with the initiation of systemic inflammation in *Npc1*$^{-/-}$ mice.

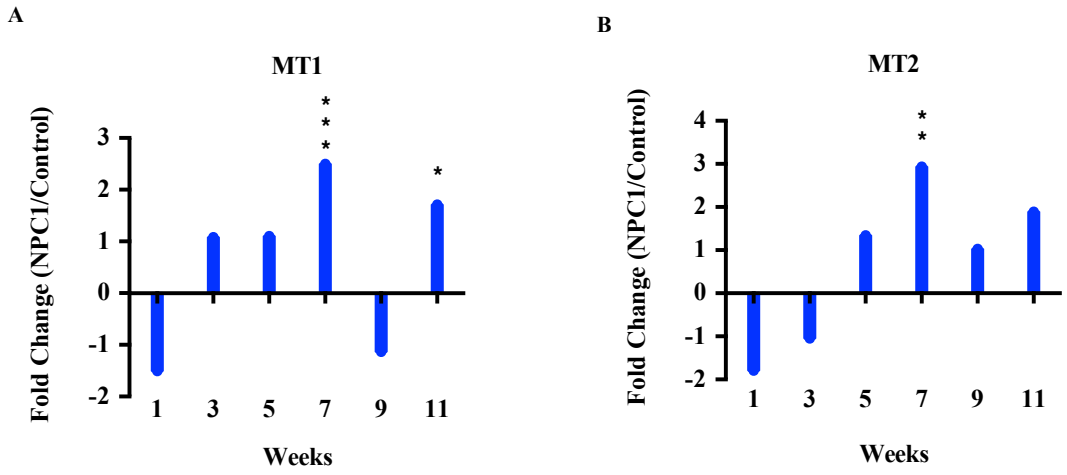

Figure 4.13. Increased hepatic metallothioneins mRNA expressions in *Npc1*$^{-/-}$ mice. (A-B) Hepatic samples from age-matched of control and *Npc1*$^{-/-}$ mice were collected and analyzed through microarray analysis. ANOVA analysis was used to analyze microarray genes expression change. * $p < 0.05$; ** $p < 0.005$; *** $p < 0.0005$; **** $p < 0.0001$. Data represent mean ± SEM, n = 4, per group.

4.3.11 Subcellular zinc compartmentalization defects in vitro in NPC1 disease cells.

Several recent studies have indicated that lysosomes and mitochondria play crucial roles in subcellular zinc compartmentalization (145). In order to test whether subcellular zinc compartmentalization defects occurs in NPC1 disease, the membrane–permeable cytosolic zinc specific fluorescent probe, FluoZin 3-AM, was used to investigate intracellular labile

zinc pool distribution and its subcellular levels in NPC1 disease cells. A punctate distribution was observed in NPC1-null CHO-M12 cells, which suggesting that the intracellular free zinc labile pool was found in membrane–bound organelles not in the cytosol of *Npc1*$^{-/-}$ cells **(Figure 4.15A, D)**. To explore this possibility, cells were co-stained with FluoZin-3 AM and subcellular organelles-specific fluorescence dyes for lysosomes (LysoTracker-Red), mitochondria (MitoTracker-Red). As shown in **Figure 4.15-16**, fluorescence microscopy analysis revealed that FluoZin-3-labeled subcellular vesicles were highly co-localized with LysoTracker-Red positive structures, but not with MitoTracker-Red labeled subcellular compartments in NPC1-null CHO-M12 cells. Similar observations were found in *Npc1*$^{-/-}$ mouse astroglial cells and human fibroblasts derived from NPC1 patients (**Figure 4.17-18**). Therefore, these *in vitro* studies suggested that there were subcellular zinc mis-localization defects in NPC1 disease cell models.

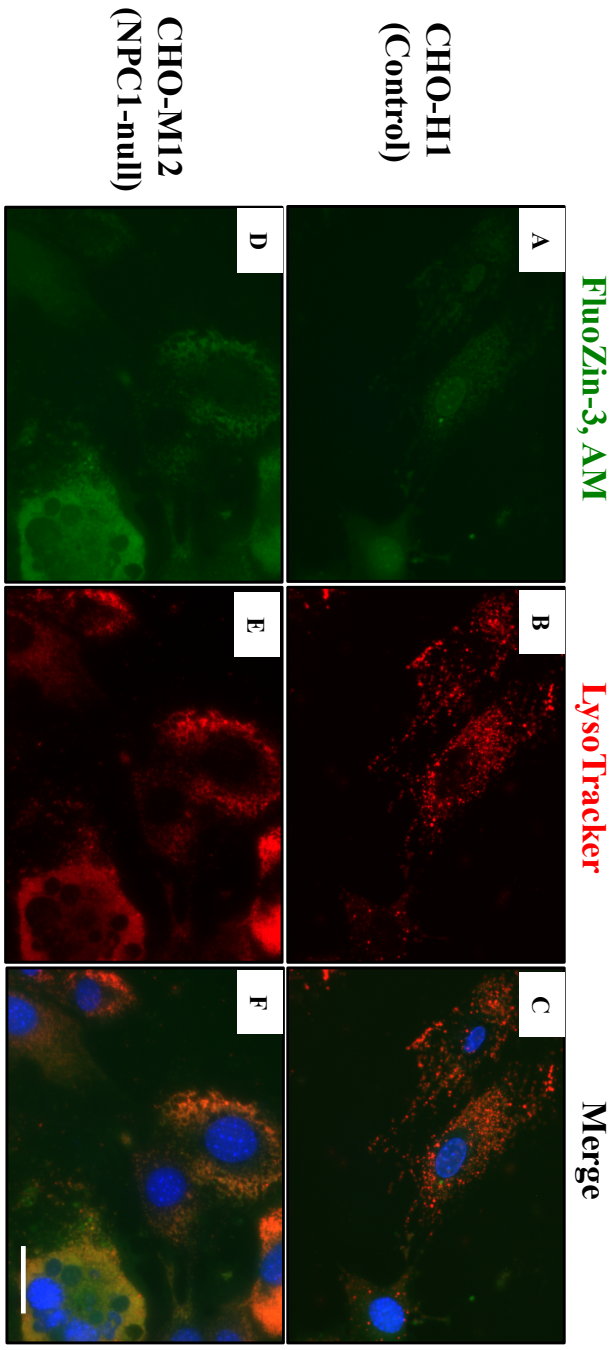

Figure 4.15. Lysosomal zinc accumulation in NPC1-null CHO-M12 cells. Fluorescence images analysis of control (*Npc1*$^{+/+}$) and NPC1-null CHO-M12 cells co-stained with FluoZin-3 (green), LysoTracker (red). Cells nuclei were labeled with DAPI. Images were viewed and captured as described in "Materials and Methods". Scale bar = 10 μm. Represent data of three independent experiments

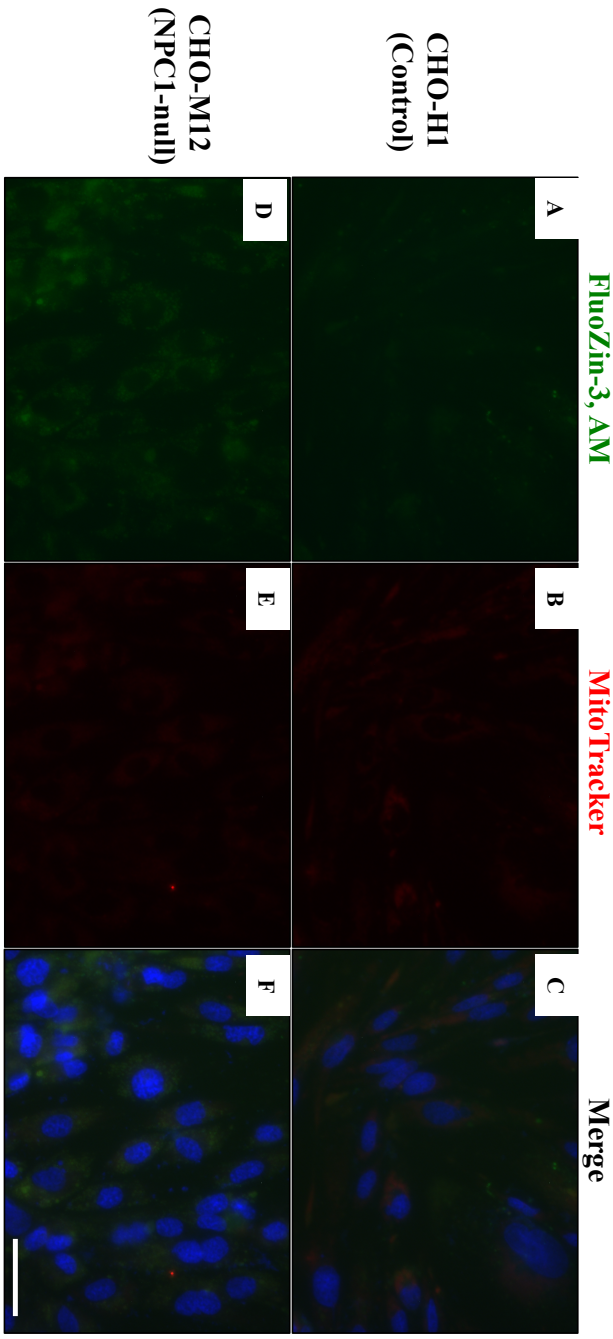

Figure 4.16. Lysosomal zinc accumulation in NPC1-null CHO-M12 cells. Fluorescence images analysis of control (*Npc1*$^{+/+}$) and NPC1-null CHO-M12 cells co-stained with FluoZin-3 (green), MitoTracker (red). Cells nuclei were labeled with DAPI. Images were viewed and captured as described in "Materials and Methods". Scale bar = 10 μm. Represent data of three independent experiments.

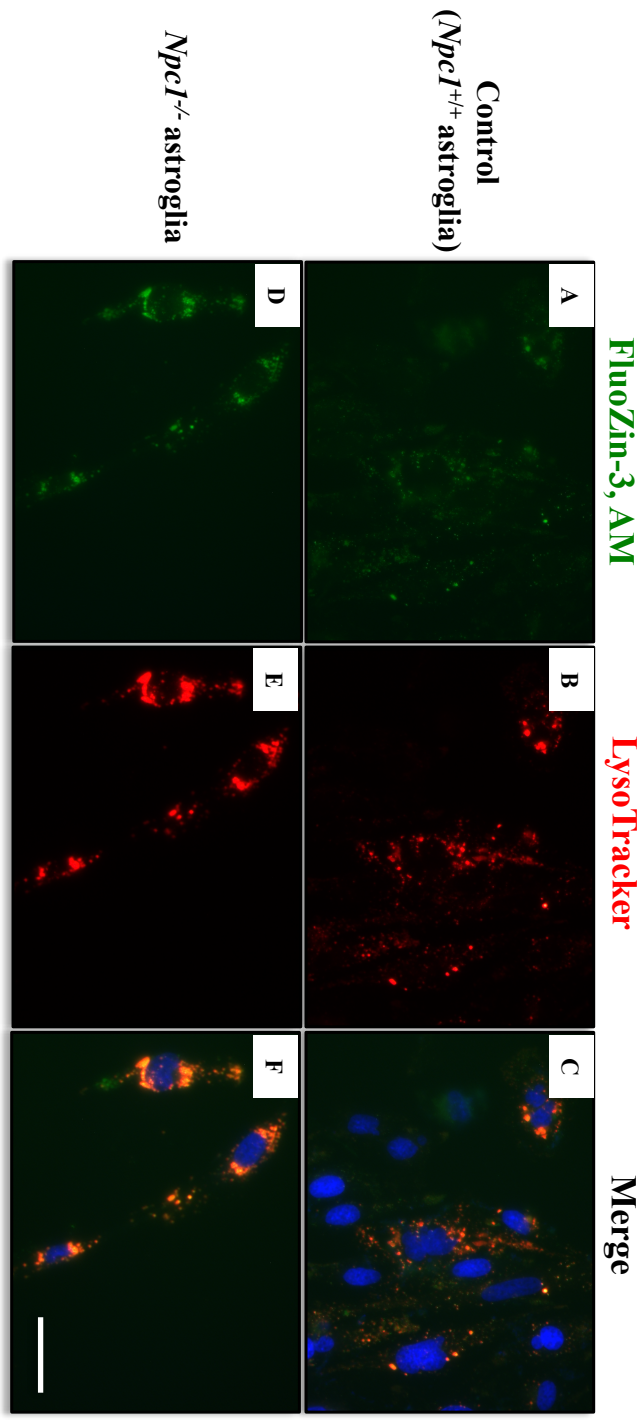

Figure 4.17 Lysosomal zinc accumulation in primary *Npc1*$^{-/-}$ mouse astroglial cells. Fluorescence images analysis of control and *Npc1*$^{-/-}$ mouse primary astroglia cells co-stained with FluoZin-3 (green) LysoTracker (red). Cells nuclei were labeled with DAPI. Scale bar = 10 μm. Represent data of three independent experiments.

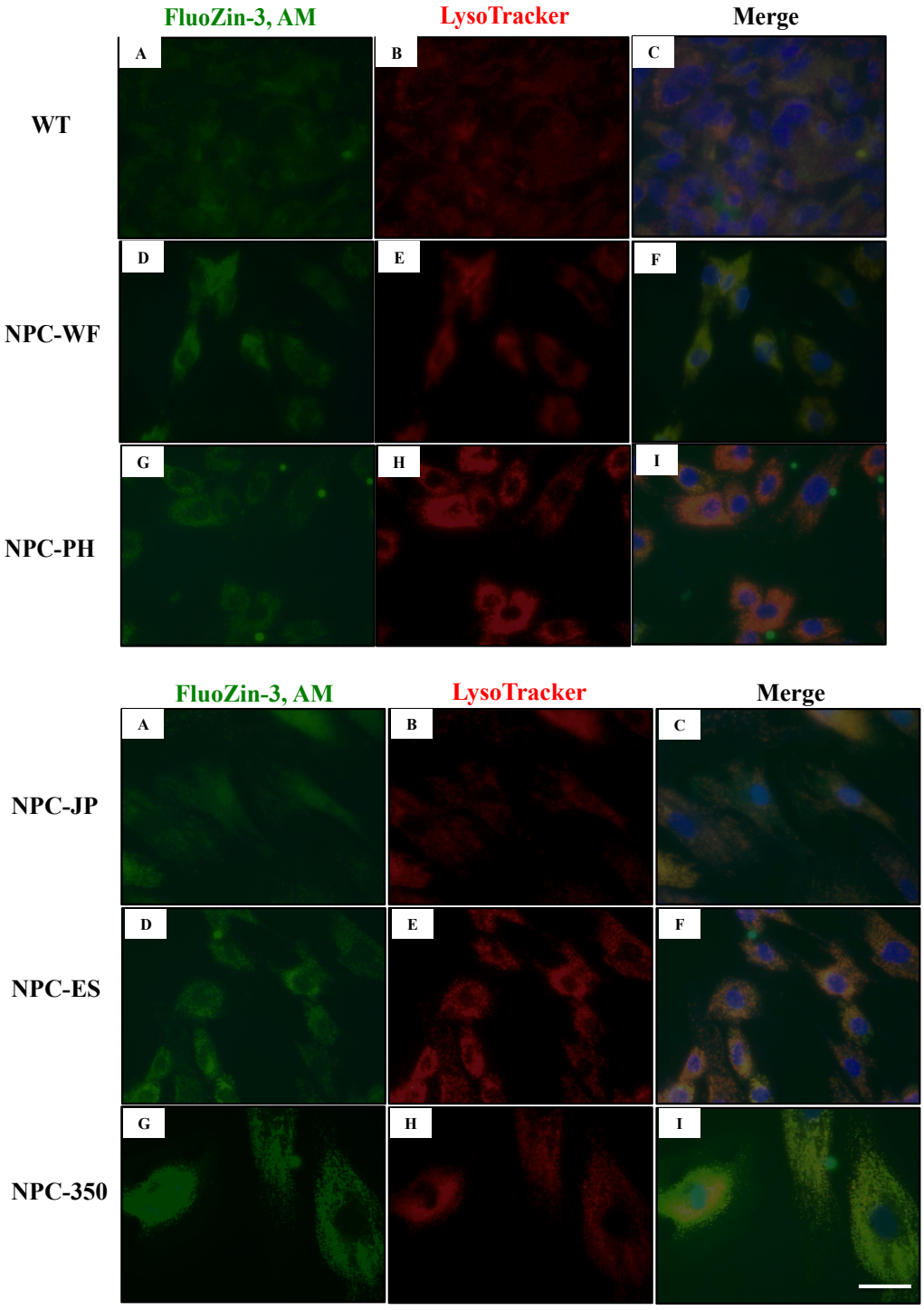

Figure 4.18. Lysosomal zinc accumulation in NPC1 human fibroblasts. Fluorescence images of control and NPC1 human fibroblasts co-stained with FluoZin-3 (green) and LysoTracker (red). One control individual (WT) and five different NPC1 human fibroblasts were used for labile zinc pool analysis. Cell nuclei were labeled with DAPI. Scale bar = 10 µm. Represent data of one independent experiment. Disease severity score: ES> JP>WF>PH>350.

4.3.12 Downregulation of cellular metallothioneins in primary Npc1$^{-/-}$ mouse astroglial cells.

Further, to explore whether *in vitro* cellular copper and zinc dysregulation in NPC1 disease cells could impair cytosolic copper/zinc-dependent enzymes, cellular metallothioneins (MT-1 and MT-2) expression levels were examined. Relatively low fluorescence intensity of cellular metallothioneins was observed in primary *Npc1*$^{-/-}$ mouse astroglia cells, which suggested cytosolic zinc deficiency in *Npc1*$^{-/-}$ astroglia cells **(Figure 4.19)**.

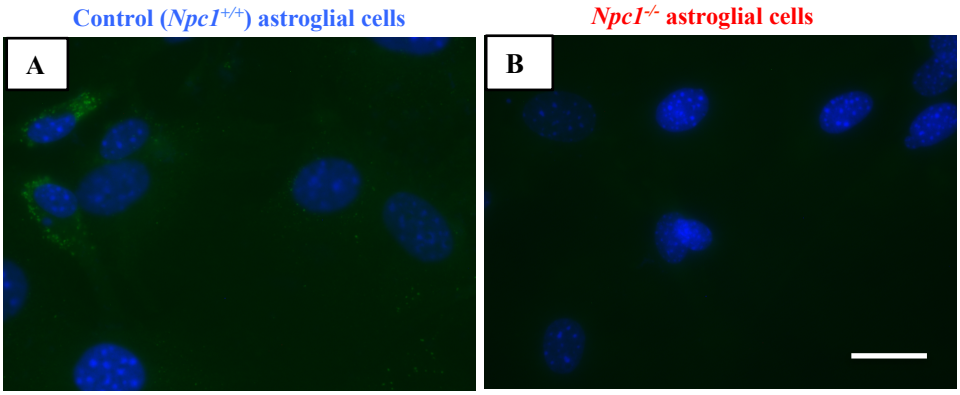

Figure 4.19. Downregulation of cellular metallothioneins (MT-1/MT-2) expression in primary *Npc1*$^{-/-}$ mouse astroglial cells. (A-B) Immunofluorescence analysis of cellular metallothioneins in primary control (*Npc1*$^{+/+}$) and *Npc1*$^{-/-}$ mouse astroglial cells. Cells were cultured in basal conditions and immunostained with anti-metallothioneins (MT1/MT2) antibody. Nuclei were counter-stained with DAPI. Scale bar = 10 µm.

4.3.13 The copper chelator D-Penicillamine, has limited therapeutic effects in Npc1$^{-/-}$ mice.

To further confirm our findings that copper and zinc dyshomeostasis is involved in the pathogenesis of NPC1 disease and to explore whether metal dysregulation could be a potential therapeutic target, we evaluated clinically approved copper-manipulation therapies in *Npc1*$^{-/-}$ mice. Since NPC1 disease shares several common features with copper overload diseases, such as Wilson's disease, we decided to evaluate the potential therapeutic effects of the copper chelator, D-Penicillamine, in *Npc1*$^{-/-}$ mice. To evaluate the potential toxic effects of D-Penicillamine during the course of treatment, the weekly growth rates of D-Penicillamine-treated *Npc1*$^{-/-}$ mice were monitored. There was no significant change in rate of body weight lost on D-Penicillamine-treated *Npc1*$^{-/-}$ mice relative to untreated *Npc1*$^{-/-}$ control littermates (**data not shown**). The effects of treatment on rearing of treated *Npc1*$^{-/-}$ mice were evaluated. Compared with age-matched untreated *Npc1*$^{-/-}$ littermates, D-Penicillamine-treated *Npc1*$^{-/-}$ mice showed significant improvements on side rearing and center rearing counts in the open-field measurement before 6-week-old of age **(data not shown included)**. Locomotor activity was measured by AmLogger measurements. There was no significant improvement on locomotor activity in D-Penicillamine-treated *Npc1*$^{-/-}$ mice **(Fig. 4.20A-F)**. The effects of D-Pencillamine on gait changes were also measured in 9-week-old *Npc1*$^{-/-}$ mice. As illustrated in **Fig. 4.21A-F,** no significant improvements on gait changes were found in D-Penicillamine treated 9-week-old *Npc1*$^{-/-}$ mice. In addition, no significant effect of the D-Penicillamine on survival was observed (**data not shown**). Therefore, these results suggested D-Pencillamine, has no significant therapeutic benefits in treated *Npc1*$^{-/-}$ mice.

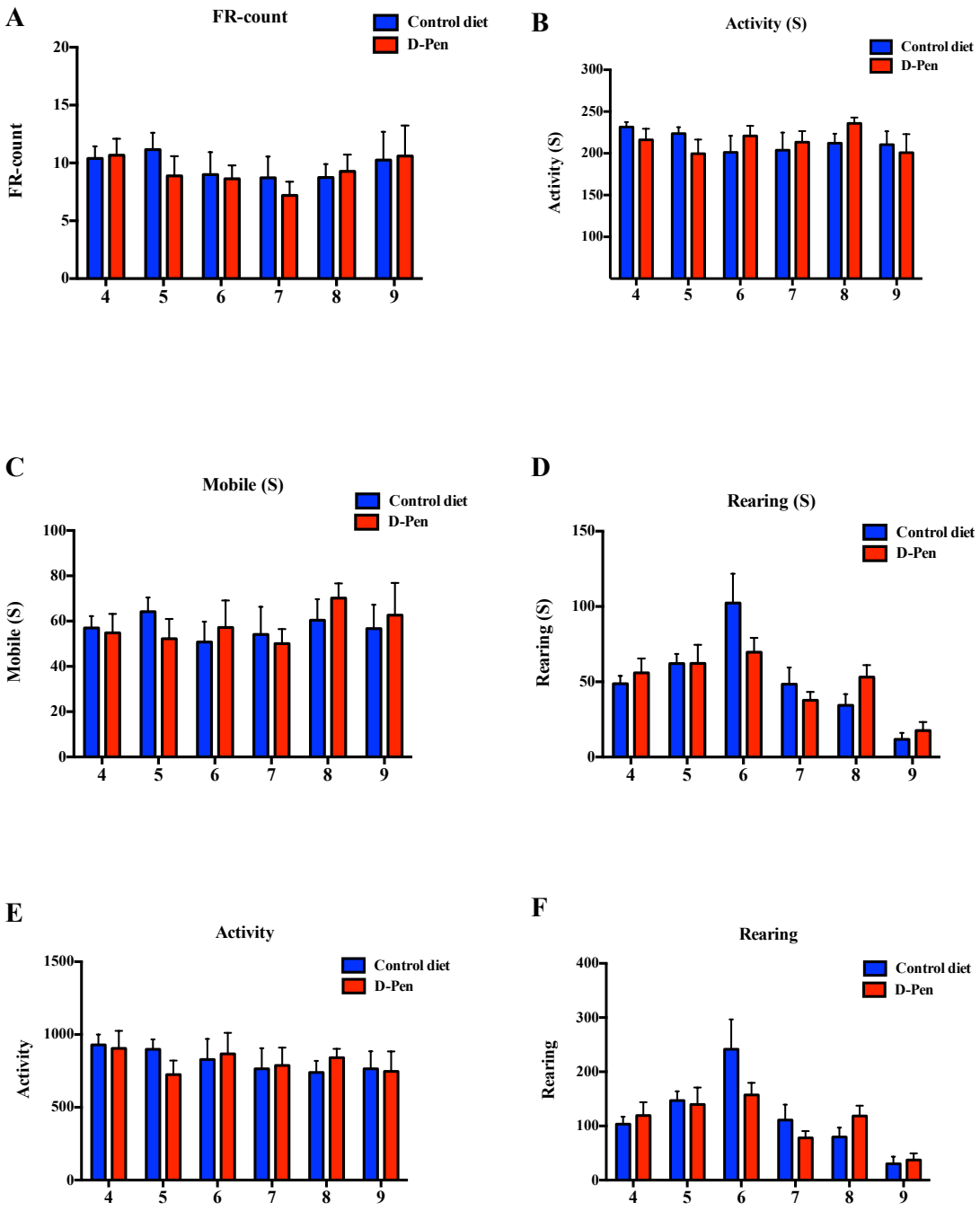

Figure 4.20. A-F. Copper chelating reagent, D-Penicillamine, revealed limited therapeutic effects on locomotor and exploring activities in treated *Npc1*$^{-/-}$ mice. (A-F) D-Penicillamine treatment started at 3 weeks of age (P21). Age-matched *Npc1*$^{-/-}$ mice were fed with normal powdered diet as a control group. Data shown mean ± SEM, n = 4 ~ 8, per group, calculated by an unpaired *t* test using GraphPad Prism v5.

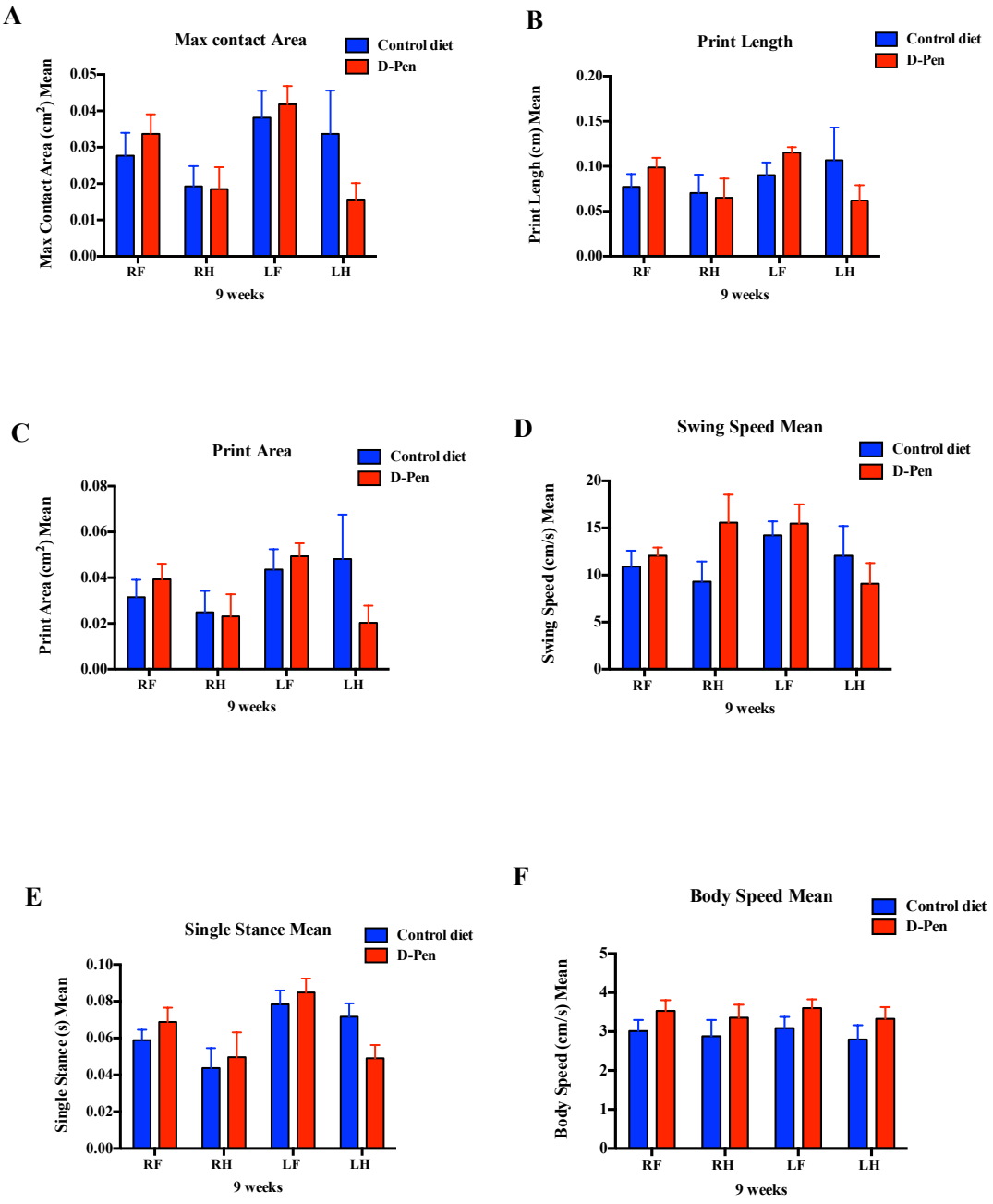

Figure 4.21. D-Penicillamine treatment revealed no significant effects on gait change in treated *Npc1*$^{-/-}$ mice. Intra–paw and inter-paw measurements, including **(A)** max contact area (cm^2) mean, **(B)** print length (cm) mean, **(C)** print area (cm^2) mean, **(D)** swing speed (cm/s) mean, **(E)** single stance (s) mean as well as **(F)** body speed (cm/s) mean were measured from control diet and D-Penicillamine treated 9-week-old *Npc1*$^{-/-}$ mice. Data represent mean ± SEM, n = 4 ~ 6, per group.

4.3.14 Copper/Zinc metal ionophore, clioquinol, treatment significantly improved gait changes and extended life expectancy in treated Npc1$^{-/-}$ mice.

Next, we evaluated another copper-manipulation therapy using a copper/zinc metal ionophore, clioquinol, which could redistribute subcellular copper and zinc distribution and can correct metal homeostasis (162). To evaluate clioquinol treatment in *Npc1*$^{-/-}$ mice, the clioquinol dosing (30 mg/kg/day) was initiated at the pre-symptomatic stage (P21). Growth rates, locomotory activity and tremor were monitored until the animals reached their humane end point. As shown in **Figure 4.22A-B**, clioquinol treatment did not show significant improvements on side rearing and center rearing counts in treated *Npc1*$^{-/-}$ mice. However, clioquinol treatment significantly extended the lifespan of *Npc1*$^{-/-}$ mice from 76.34 ± 1.7 days to 88.71 ± 2.2 days, representing an increase of 16.2 %, compared with un-treated *Npc1*$^{-/-}$ littermates **(Figure 4.22C-D)**. No significant changes in open field activity parameters were found in clioquinol-treated *Npc1*$^{-/-}$ mice **(Figure 4.23A-H)**. However, clioqunionl treatment revealed significantly improvements on several inter-limb and individual paw parameters by CatWalk gait analysis system. As illustrated in **Figure 4.24A-F**, while compared with normal diet treated *Npc1*$^{-/-}$ mice, clioquinol treatment markedly improved (i) max contact area (cm^2) mean (RF, 0.028 v.s. 0.109, p = 0.0009, RH, 0.019 v.s. 0.054, p = 0.0302, LF, 0.038 v.s. 0.105, p = 0.017); (ii) print length (cm) mean (RF, 0.077 v.s. 0.322, $p < 0.0001$, RH, 0.0703 v.s. 0.2293, p = 0.0016, LF, 0.090 v.s 0.322, p = 0.0003, LH, 0.106 v.s. 0.240, p = 0.0118); (iii) print area (cm^2) mean (RF, 0.032 v.s. 0.128, p = 0.0013, LF, 0.044 v.s. 0.124, p = 0.0180); (iv) swing speed (cm/s) mean (RF, 10.91 v.s. 25.39, $p < 0.0001$, RH, 9.30 v.s. 16.98, p = 0.041, LF, 14.23 v.s. 25.60, p = 0.0012); (v) stride length (cm) mean (RF, 1.059 v.s. 2.218, $p < 0.0001$, LF, 1.174 v.s. 2.276, p = 0.0001, LH, 1.150 v.s. 3.050, p = 0.0217); single stance (s) mean (RF, 0.059 v.s. 0.088, p = 0.0168) and (vi) body speed (cm/s) mean (RF, 3.0 v.s. 8.7, $p < 0.0001$, RH, 2.9 v.s. 8.1, p = 0.0006, LF, 3.1 v.s 8.6, $p < 0.0001$, LH, 2.8 v.s. 8.3, p = 0.0003), in 9-week-old *Npc1*$^{-/-}$ mice. Therefore, these findings indicated that the copper/zinc metal ionophore, clioquinol, was of significant benefit in terms of improved gait and life span in *Npc1*$^{-/-}$ mice.

Figure 4.22. The copper/zinc metal ionophore, clioquinol, prolonged the lifespan of treated *Npc1*$^{-/-}$ mice. Mice were treated with copper/zinc metal ionophore, clioquinol (30 mg/kg/day) with normal powdered diet. Clioquinol treatment was started at 3 weeks of age (P21). Age-matched *Npc1*$^{-/-}$ mice were fed with normal powder diet as a control group. **(A-B)** Side and center rearing counts within an open field were measured as described in "Material and Methods". Data are expressed as mean ± SEM, n = 4 ~ 8, per group **(C)** Survival analysis of control powdered diet and clioquinol treated *Npc1*$^{-/-}$ mice. Kaplan-Meier survival curve (%), survival curves were compared using log-rank test. **(D)** Bar diagram showing average survival in days, ** $p < 0.005$.

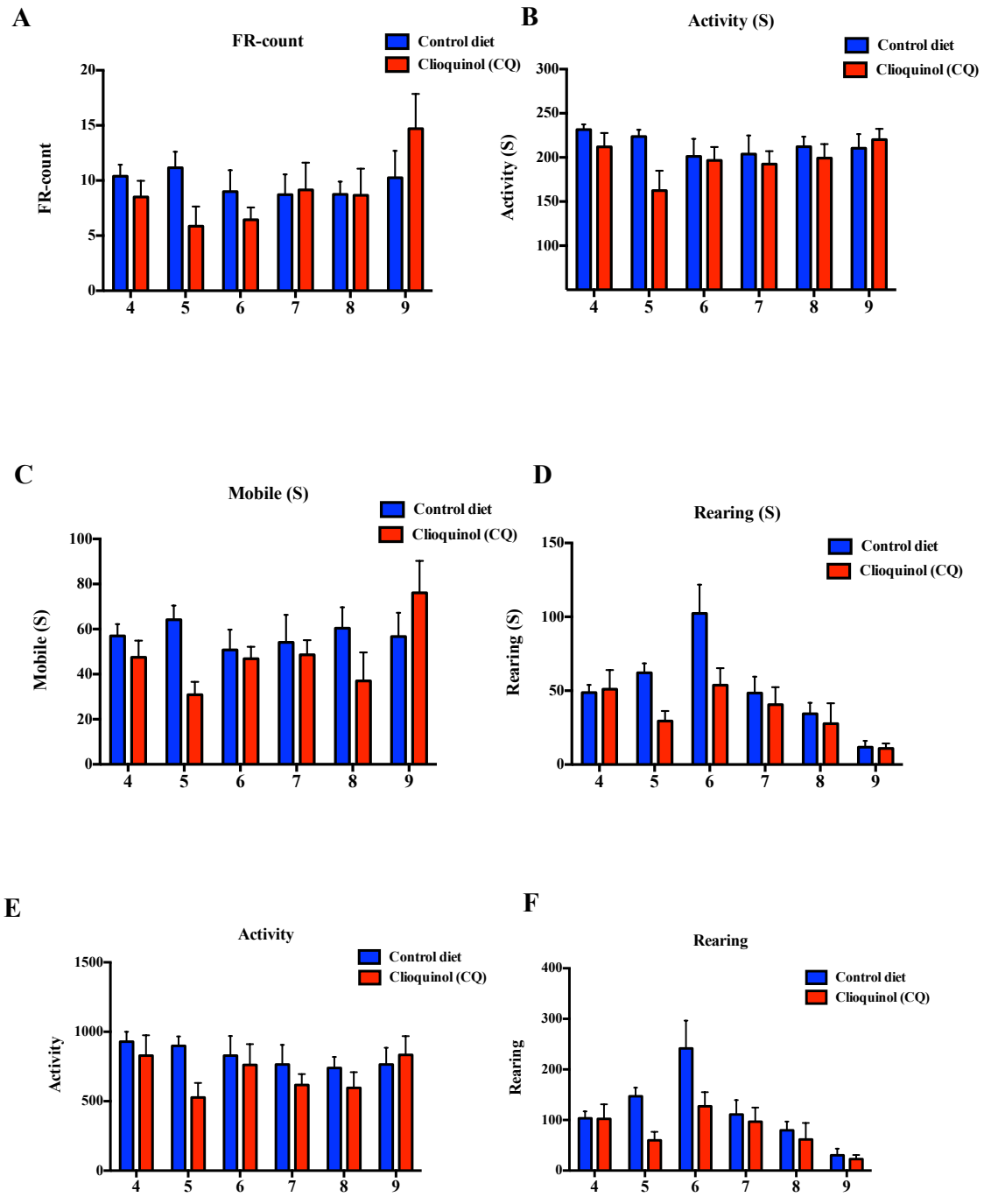

Figure 4.23. Copper/zinc metal ionophore, clioquinol, treatment did not improve locomotor and exploring activities in treated *Npc1*$^{-/-}$ mice. Mice were treated with clioquinol supplementation (30 mg/kg/day) with powdered diet. Clioquinol treatment was started at 3 weeks of age (P21). Age-matched *Npc1*$^{-/-}$ mice were fed with normal powdered diet as a control group. **(A-F)** Locomotor and exploring activities were measured using AmLogger system as described in "Materials and Methods". Data shown mean ± SEM, n = 4 ~ 8, per group, calculated by an unpaired *t* test using GraphPad Prism v5.

Figure 4.24. Copper/zinc metal ionophore, clioquinol, treatment significantly improved gait changes in treated *Npc1*$^{-/-}$ mice. The copper/zinc metal ionophore, clioquinol, significantly improved the gait of 9-week-old *Npc1*$^{-/-}$ mice. **(A-F)** The gait analysis were measured as described in " Materials and Methods" Data represent mean ± SEM, n = 4 ~ 8, per group. * $p < 0.05$, ** $p < 0.005$, *** $p < 0.0005$.

4.3.15 Reduced intestinal copper absorption therapy (zinc acetate) significantly improved motor coordination, gait and extended survival in Npc1$^{-/-}$ *mice.*

Finally, we evaluated the therapeutic effects of zinc acetate on *Npc1*$^{-/-}$ mice. The pharmacological mechanisms of zinc acetate is to induce intestinal/systemic metallothioneins (MTs) expressions and reduce intestinal copper absorption to avoid copper overloaded toxicity (163). The zinc acetate treatment (300 mg/kg/day) was initiated at the beginning of early pre-symptomatic stage (3-week-old, P21) in *Npc1*$^{-/-}$ mice. As illustrated in **Fig. 4.25A-B**, zinc acetate-treated *Npc1*$^{-/-}$ mice maintained center rearing count and exploring activity from 5-9 week-old *Npc1*$^{-/-}$ mice compared with age-matched normal powdered diet treated *Npc1*$^{-/-}$ mice (5 weeks, 6.4 v.s. 17.6, $p < 0.0001$, 6 weeks, 11.8 v.s. 21.0, $p < 0.005$, 7 weeks, 7.4 v.s. 21.3, $p < 0.0005$, 8 weeks, 4.3 v.s. 13.4, $p < 0.0005$, 9 week, 1.8 v.s. 10.0, $p < 0.0001$). Zinc acetate treatment also significantly prolonged the lifespan of treated-*Npc1*$^{-/-}$ mice till 13.5 weeks old, representing an increase by 23.6 %, compared with normal powdered diet treated *Npc1*$^{-/-}$ mice (76.34 v.s. 94.38 days, $p < 0.0005$) **(Fig. 4.25C-D)**. However, there were limited improvements on locomotor activities in zinc acetate treated *Npc1*$^{-/-}$ mice **(Fig. 4.26A-I)**. In addition, CatWalk^{TM} gait analysis revealed that zinc acetate treatment markedly improved several aspects of gait in 9-week-old *Npc1*$^{-/-}$ mice. These improvements in gait included (i) max contact At (%) mean (RF, 34.5 v.s. 47.7, $p < 0.05$); (ii) max contact area (cm^2) mean (RF, 0.028 v.s. 0.058, $p < 0.05$; LF, 0.038 v.s. 0.070, $p < 0.05$); (iii) print length (cm) mean (RF, 0.077 v.s. 0.12, $p < 0.05$; LF, 0.090 v.s. 0.134, $p < 0.05$); (iv)

print area (cm) mean (RF, 0.032 v.s. 0.067, $p < 0.041$ LF, 0.044 v.s. 0.083, $p < 0.026$) and (v) single stance mean (RF, 0.059 v.s. 0.077, $p = 0.0357$), in 9-week-old *Npc1*$^{-/-}$ mice **(Fig. 4.27A-E)**. Therefore, these findings indicated that zinc acetate treatment significantly improved motor coordination, gait and extended survival in *Npc1*$^{-/-}$ mice.

Figure 4.25. Zinc acetate treatment prolonged the lifespan of *Npc1*$^{-/-}$ mice. Mice were treated with zinc acetate (300 mg/kg/day) in powdered diet starting at 3 weeks of age (P21). Age-matched *Npc1*$^{-/-}$ mice were fed with normal powdered diet as a control group. **(A-B)** Side and center rearing counts within an open field were measured weekly for a 5 minutes period. Data shown are mean ± SEM, * $p < 0.05$, ** $p < 0.005$, *** $p < 0.0005$, n = 4 ~ 8, per group. **(C)** Survival analysis of control and zinc acetate treated *Npc1*$^{-/-}$ mice. Kaplan-Meier survival curves were compared using log-rank test. **(D)** Bar diagram showing average survival, **** $p < 0.0001$.

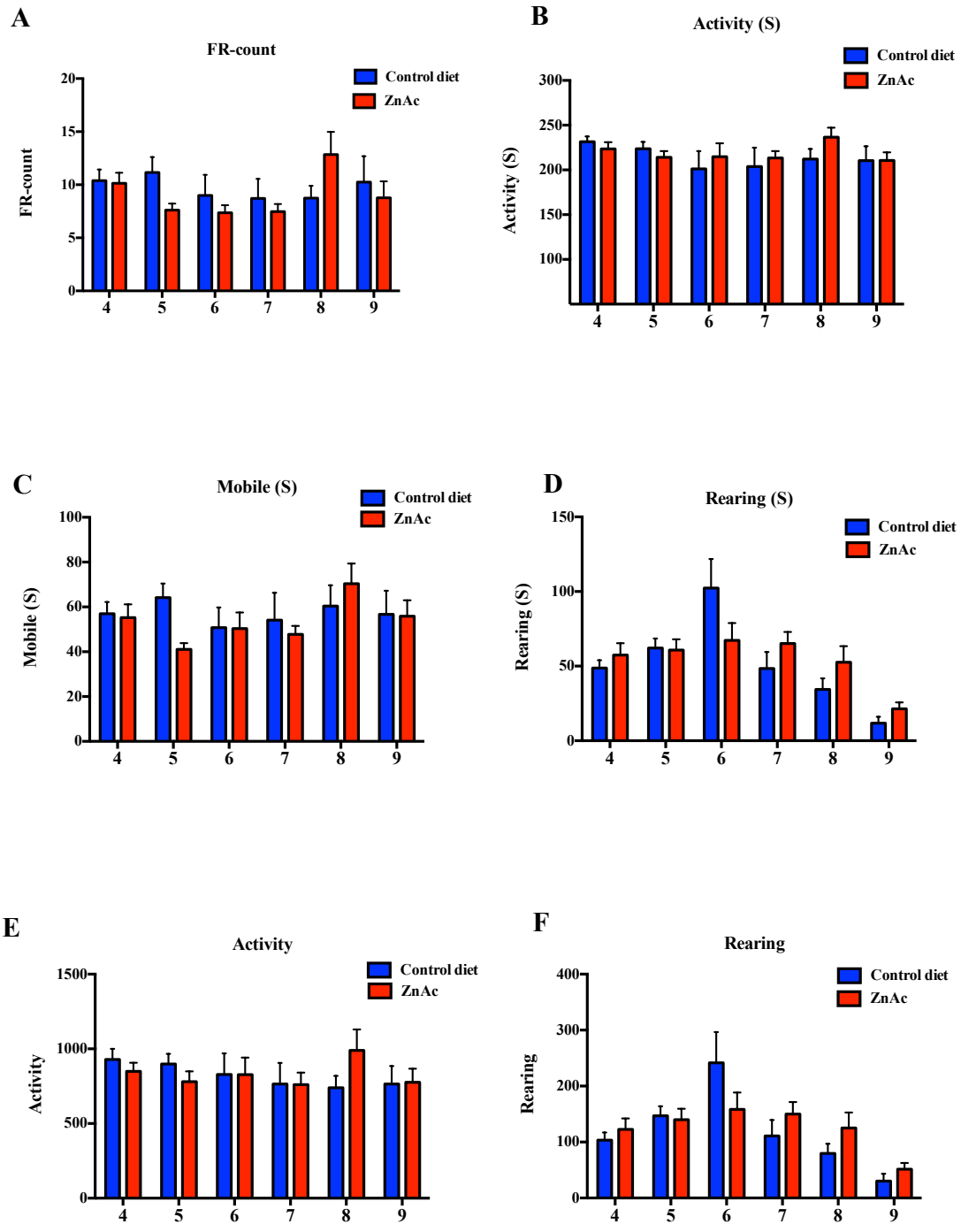

Figure 4.26. Zinc acetate treatment revealed limited improvements on locomotor and exploring activities in treated *Npc1*$^{-/-}$ mice. Mice were treated with zinc acetate supplementation (300 mg/kg/day) in powdered diet. Zinc acetate treatment was started at 3 weeks of age (P21). Age-matched *Npc1*$^{-/-}$ mice were fed with powdered diet as a control group. **(A-F)** The locomotor activity was measured using AmLogger system as described in "Materials and Methods". Data shown are mean ± SEM, n = 4 ~ 10, per group, calculated by an unpaired *t* test using GraphPad Prism v5.

Figure 4.27. Zinc acetate treatment significantly improved gait parameters in treated *Npc1*$^{-/-}$ mice. Reduced copper absorption therapy improved the gait changes of 9-week-old *Npc1*$^{-/-}$ mice. Intra–paw and inter-paw measurements, including **(A)** max contact At (%) mean, **(B)** max contact area (cm^2) mean, **(C)** print length (cm) mean, **(D)** print area (cm^2) mean as well as **(E)** single stance (s) mean were measured from control diet and zinc acetated treated – *Npc1*$^{-/-}$ mice. The gait changes analysis was measured and quantified using the CatWalk^{TM} system as described in "Material and Methods". Data represent mean ± SEM, n = 4 ~ 6, per group. * $p < 0.05$.

4.4 Discussion

In the current study, we have found evidence of altered systemic and cellular copper and zinc homeostasis in NPC1 disease models and investigated the underling mechanistic defects. Our current findings suggested that the systemic copper and zinc homeostasis defects could initiate as early 1 week of age *Npc1*$^{-/-}$ mice. Moreover, our studies indicated that impaired subcellular copper trafficking, mis-localization of cytosolic copper ATPase transporters, MNK ATP7A and WND ATP7B, and sub-cellular zinc compartmentalization defects, in primary mouse *Npc1*$^{-/-}$ astroglia cells, NPC1-null CHO cells, NPC1 patients–derived human fibroblasts and pharmacologically induced (U18666A) NPC1 disease HepG2 and RAW 264.7 cell lines. Since all these findings suggested that systemic and cellular copper and zinc homeostasis defects could be associated with the underlying pathogenesis of NPC1 disease, the development of metal-manipulation therapies may play a role in the future management of NPC1 disease. Therefore, we evaluated several clinically approved compounds with distinct mechanisms of action, including (i) copper chelation with D-penicillamine, (ii) copper/zinc metal ionophore, clioquinol, (iii) and reduced intestinal copper absorption therapy using zinc acetate, in *Npc1*$^{-/-}$ mice. Our results indicated that copper/zinc manipulation therapies can improve exploring activities, gait changes, and prolong survival in treated *Npc1*$^{-/-}$ mice.

Recently, several studies reported abnormal systemic lipid metabolism, especially triglycerides and cholesterol, with significant low levels of TGs and HDL and VLDL-cholesterol, in the *Atp7b*$^{-/-}$ Wilson's disease mouse model and in Wilson's disease patients

(64, 164). These observations suggest that there are mechanistic links between systemic copper dysregulation and abnormal cholesterol metabolism. Furthermore, these studies indicated that abnormal hepatic copper accumulation in *Atp7b*$^{-/-}$ mice could (i) cause the up-regulation of SREBP-2, the major transcription factor involved in regulating expression of genes involved in cholesterol and lipid metabolism (ii) and dysregulate downstream cholesterol metabolism related gene expression, including HMG-CoA reductase (165). Similar findings were made in patients with Wilson's disorder (165). Therefore, these observations highlight the importance of systemic copper homeostasis in the regulation of cellular cholesterol and lipid metabolism more generally. Another enzyme involved in hepatic and hematological pathogenesis of Wilson's disease, is acid sphingomyelinase activity and its relationship to ceramide-mediated signaling in liver cirrhosis and anemia in Wilson's disease (156). This study demonstrated that copper dysregulation in Wilson's disease can up-regulate hepatic acid sphingomyelinase activity and affect ceramide-mediated cellular apoptosis in liver cirrhoss and erythrocytes. These findings therefore emphasize the importance of copper in the regulation of acid sphingomyelinase activity and this could be a novel therapeutic target for the development of treatment for Wilson's disease. Of interest, impaired acid sphingomyelinase (ASM) activity has been documented in human fibroblasts derived from NPC1 patient and in NPC1-null CHO cells (157). Furthermore, it has been suggested that acid sphingomyelinase (ASM) activity defects could be associated with post-translational modification of acid sphingomyelinase in NPC1 cell models (157). Copper and zinc ions have been previously demonstrated to be crucial co-factors to facilitate, *in vitro,* human acid sphingomyelinase dimerization and enzymatic activity (156). Therefore, one would expect if systemic and cellular copper and zinc dysregulation occurs in NPC1 disease, it could affect cellular and systemic acid sphingomyelinase activity. Although the mechanisms of reduced acid sphingomyelinase activity in NPC1 fibroblasts and *Npc1*$^{-/-}$ mice could be complex, our current findings suggested that impaired copper trafficking with mis-localization of cytosolic copper transporters, WND ATP7B and MNK ATPA, and subcellular compartmentalized defects of zinc ions could be associated with acid sphingomyelinase activity defects in NPC1

disease. Our current findings may highlight the importance of copper and zinc ions in the regulation of acid sphinogmyelinase activity in NPC1 disease. Therefore, these observations could provide a new link between metal dysregulation and impaired acid sphingomyelinase activity in NPC1 disease.

Of interest, it has been recently reported that there are a few reported cases of NPC1 patients presenting with systemic copper dyshomeostasis phenotypes with abnormal serum ceruloplasmin levels and hepatic and the CNS copper content (166, 167). Indeed, one of the NPC1 patients was originally mis-diagnosed with Wilson's diseases and was treated with the copper chelator, D-penicillamine, to reduce excess hepatic copper accumulation (167). Similar findings were observed in our current studies in *Npc1*$^{-/-}$ mice, as we also noticed that D-Penicillamine treatment showed modest motor function improvement, in *Npc1*$^{-/-}$ mice. These observations could be explained by either (i) the copper chelation treatment may over-chelate the accumulation of peripheral tissue copper and then cause copper deficiency phenotypes in *Npc1*$^{-/-}$ mice, (ii) or lack of therapeutic efficiency of D-Pencillamine treatment within the endosomal/lysosomal pathway in NPC1 disease. Since most metal chelators only function effectively at neutral pH, it could be possible that the D-Penicillamine, cannot effectively remove excess copper ions from the endo/lysosomal compartment and therefore only have limited therapeutic benefit in -*Npc1*$^{-/-}$ mice.

Our current studies also indicated that the copper/zinc metal ionophore, clioquinol, treatment can significantly prolong the lifespan and revealed modestly motor improvements, such as gait, in *Npc1*$^{-/-}$ mice. Although the clioquinol treatment only achieved modest therapeutic effects, it could be possible that the clioquinol treatment may only correct certain brain regions and certain cellular types in *Npc1*$^{-/-}$ mice. Another possibility should also be kept in mind is the limited blood-brain barrier permeability of clioquinol and this could limit the therapeutic effects of clioquinol in *Npc1*$^{-/-}$ mice. Intriguingly, the potentially clinical application of clioquinol has been evaluated in patients with common neurodegenerative disorders, such as Alzheimer's disease and Parkinson's disease (162). However, due to the potential neurotoxic effects of clioquinol treatment, clioquinol has been withdrawn from

clinical trial (168). Therefore, the potentially future application of clioquinol treatment in patients with NPC1 disease will be limited. In addition, it should be noted that clioquinol has also been suggested to be able to function as a zinc ionophore by targeting zinc into lysosome and cytosolic compartments (169). Therefore, it would be expected that clioquinol treatment could worsen lysosomal zinc accumulation in NPC1 disease cells. Indeed, when we evaluated clioquinol treatment in vitro clioquinol had less toxicity when used as a single agent monotherapy. However, when cells were treated with clioquinol in combination with either copper chloride or zinc acetate, toxicity was significantly increased (**data not shown**). Furthermore, when cells were incubated with zinc acetate and clioquinol, FluoZin-3-AM labelled subcellular lysosomal zinc compartments were elevated as compared to untreated cells. Therefore, our current findings support the hypothesis that clioquinol may function as a copper/zinc ionophore and can target zinc into the lysosomal compartment.

Reduced intestinal copper absorption treatment using zinc acetate has been successfully applied to patients with Wilson's disease or other related copper-overload conditions (153, 170). The advantage of zinc acetate treatment is that it is relatively safe, has low toxicity, and could be used for long-term treatment as a maintenance therapy (163). The pharmacological mechanism of zinc acetate treatment is primarily to induce intestinal and systemic metallothioneins and reduced intestinal copper absorption, prevent free copper and other transition metal ion-mediated tissue/cellular toxicity and prevent copper re-absorption (148, 163). The metallothioneins have been suggested to be able to regulate intracellular copper and zinc distribution and copper/zinc related intracellular signaling (146). Intriguingly, our studies found down-regulation of metallothioneins in *Npc1*$^{-/-}$ astroglia cells. Although the molecule mechanisms of this observation is still unclear, it could be associated with cytosolic zinc deficiency or cellular metallothionein biosynthesis defects in *Npc1*$^{-/-}$ astroglial cells. Therefore, the observations of the functional improvements of zinc acetate-treated *Npc1*$^{-/-}$ mice could be attributable to reduced copper absorption but also by supplementing cytosolic zinc levels and maintaining intracellular zinc mediated signalling in NPC1 disease.

Another potential mechanism to explain the metal ion dysregulation *in vitro* and *in vivo* in NPC1 disease models is that NPC1 protein may function as an intracellular metal transporter/carrier (110). The NPC1 protein is highly homologous to prokaryotic RND permease family proteins(24). In prokaryotic system, RND permease family proteins have been suggested to be involved in the transport of multiple substrates, including metal ions, lipids and amplicatic compounds (111). Therefore, the NPC1 protein may be directly or indirectly involved in the regulation of metal ion transport into or from the endosomal/lysosomal system. Intriguingly, Harada et. al published a series of studies, which reported that copper does not stimulate intracellular redistribution of endogenous WND ATP7B copper transporter in Hu7 hepatocytes or GFP-tagged WND ATP7B in several cell types (171). Harada et. al also postulated a biological function of NPC1 protein to be on intracellular copper trafficking, either directly regulating the biosynthesis of ceruloplasmin or co-operating with lysosomal WND ATP7B to eliminate excess copper into bile and prevent hepatic copper accumulation (110, 172). However, our current findings do not support the Haradda et al findings. Instead, our *in vitro* studies indicated that WND ATP7B and MNK ATP7A were mainly localized within perinuclear and *tran*-Golgi regions and do not co-localize with the late endosomal/lysosomal marker, LAMP-1, in U18666A-treated HepG2 cells, NPC1-null CHO-M12 cells and *Npc1*$^{-/-}$ astroglia cells when intracellular copper content was modulated. Furthermore, our studies suggested that the impaired intracellular copper trafficking and mis-localization of cytosolic copper transporters, MNK ATP7A and WND ATP7B, could be associated with lysosomal trafficking defects in NPC1 disease. The reason for these contradictory results from Harada et. al is unknown. One possibility is that Harada et. al studies used the GFP-tagged WND ATP7B and Flag-tagged NPC1 transfected in Hep3b cells and the protein modifications and overexpression may affect subcellular distribution of protein complexes (110).

It should be noted that our current studies cannot exclude the possibility that other metal dysregulation related pathophysiological factors may be involved in the regulation of NPC1 hepatic and neurodegenerative phenotypes. One intriguing possibility is the potential

interaction of copper and zinc ions and amyloid precursor protein (APP) and the link to neuropathogenesis in NPC1 disease (149). Since the clioquinol and zinc supplementation have been demonstrated to be able to alter amyloid precursor protein metabolism and significantly reduces plaque burden in transgenic Alzheimer's disease mouse model, it might be of interest to determine whether clioquinol and zinc supplementation treatments could alter amyloid precursor protein metabolism and its related signalling in *Npc1*$^{-/-}$ mice (173). Therefore, further studies specifically focussed on neuropathogenesis combined with biophysical techniques to screen whole brain metal distribution, would be valuable to gain a better understanding of copper and zinc dyshomeostasis in relation to neuropathology in NPC1 disease.

Since our microarray examination indicated that several hepatic cytosolic copper and zinc transporters altered mRNA expressions in *Npc1*$^{-/-}$ mice, it is a possibility that hyper-accumulation of cellular copper and zinc ions into lysosomal compartments and cytosolic zinc deficiency occurs in *Npc1*$^{-/-}$ mice. If this hypothesis is correct, the beneficial effects of zinc acetate treatment what we found in this studies may not only be due to reduced intestinal copper absorption but also correction of the cytosolic zinc deficiency phenotypes in *Npc1*$^{-/-}$ mice. Furthermore, if this hypothesis is correct, one would expect that subcellular organelle isolation and metal analysis would be possible to validate this hypothesis. However, it might not be practical to analyze subcellular organelles/fractions of metal distribution in NPC1 disease and other lysosomal storage diseases. Since several cellular substrates mislocalize and accumulate into the endosomal/lysosomal compartments, it would not be practical to use gradient techniques to isolate subcellular organelle fractions from these diseases cells and tissues. Besides, during the samples preparation, it would be highly likely that significant quantities of subcellular metal content would be lost during sample preparation. Another method could be considered is to use metal-specific molecular probes to quantify subcellular organelles metal content. However, it is unclear whether these mole probes could function properly in acidic compartments, such as lysosomes. Therefore, due to these technical issues,

it would be difficult to address metal trafficking and subcellular compartmentalization defects phenotypes in NPC1 and other lysosomal storage diseases.

A potential metal absorption defect in *Npc1*$^{-/-}$ mice should also be considered since it has been suggested that there are certain pathological associations between NPC and Crohn's disease and inflammatory bowel disease (101). Several lines of evidence have indicated that copper, zinc and iron are inter-regulated, one of these transition metal ions dyshomeostasis could affect the others systemic and cellular homeostasis (174). Although the underlying mechanisms of metal absorption defects in NPC1 disease are still under investigation, it seems likely that the altered systemic copper and zinc levels during peripheral iron deficiency in *Npc1*$^{-/-}$ mice was to compensate for decrease tissue iron levels and would be possible a primary physiological response. Therefore, it would be of interest to investigate further the impact of systemic and regional inflammation, such as duodenum inflammation, on systemic metal homeostasis and nutrient absorption in *Npc1*$^{-/-}$ mice.

In conclusion, our current studies identified systemic and cellular copper and zinc dyshomeostasis *in vitro* and *in vivo* in NPC1 disease models. Furthermore, *in vitro* studies indicated that impaired subcellular copper trafficking, mis-localization of cytosolic copper transporters, MNK ATP7A and WND APT7B, and subcellular zinc compartmentalization defects occur in NPC1 disease models. Therefore, several distinct pharmacological mechanisms of copper and zinc manipulation therapy, including copper chelator treatment (D-Penicillamine), copper/zinc ionophore (clioquinol) and reduced intestinal copper absorption therapy (zinc acetate), were evaluated on *Npc1*$^{-/-}$ mice. Our studies indicated that copper/zinc ionophore and zinc acetate treatments can significantly improve motor function, improve gait and prolong the lifespan of *Npc1*$^{-/-}$ mice. These findings, therefore, suggested that systemic copper and zinc dysregulation is involved in the underlying pathogenesis of NPC1 disease and that copper/zinc manipulation therapies may represent useful adjunctive therapies for the treatment of NPC1 disease.

Chapter 5. Investigating the function of lysosome-related organelles in megakaryocytes and platelets in NPC1 disease.

Chapter 5. Investigating the function of lysosome-related organelles in megakaryocytes and platelets in NPC1 disease.

5.1 Introduction.

5.1.1 The biological functions of lysosomes and lysosome-related organelles

Lysosomes are membrane bound, cytosolic, acidic, subcellular organelles, mainly responsible for the catabolism of various intracellular substrates, including lipid, carbohydrates, and proteins (discussed in detail in **Chapter 1**). There is growing evidence that lysosomes not only regulate intracellular substrates degradation but also are involved in the regulation of other cellular events, including membrane repair/fusion, lipid homeostasis, metal distribution, cell death and intracellular signaling (2). LROs belong to a group of tissue/cell type-specific subcellular organelles, which share common features with conventional lysosomes, including acidic pH and lysosomal membrane protein/enzyme contents (5).

5.1.2 The development and function of LROs in megakaryocytes and platelets

Platelets are anucleated cellular bodies derived from the fragmentation of megakaryocytes (175). During megakaryopoiesis, lysosomes and LROs arise from the Golgi apparatus, which form multivesicular bodies (MVB) as intermediate organelles. The early development stages of megarkaryocytes contain numerous MVB but only small numbers of α-granules, δ-granules and lysosomes. Pro-platelets are generated from the fragmentation of the megakaryocytes cytoplasm and released into the circulatory system. There are three different subcellular types of LROs in platelets, including α-, δ-granules and lysosomes (11). Recent studies on the biogenesis of LROs has provided some insights into the molecular mechanisms of LROs biogenesis and suggested that these subcellular organelles may be derived from a common pathway (11). However, platelet LROs have numerous distinctive features from each others, including (i) molecular composition, (ii) ultra-structural morphology (iii) and kinetics of exocytosis and secretory responses to different stimuli (9).

Platelet lysosomes contain a variety of hydrolytic enzymes, such as *hexosaminidase β*, and were postulated to function in elimination of circulating platelet aggregates. In addition to lysosomes, platelets α- and δ-granules are mainly responsible for the storage and secretion of clotting mediators, such as von Willebrand factor (vWF), fibrinogen and non-protein/inorganic small molecules, including calcium, serotonin, poly/pyrophosphate, ADP/ATP, to accelerate platelet adhesion, aggregation upon stimulation (discussed detail in **Chapter I**) (13, 15). In addition, platelet cytosolic compartments also contain different lipid mediators, such as sphingosine-1-phosphate (S1P), which regulates platelet activation and thrombus formation (176). Once activated, platelets secrete cytosolic mediators and release LROs contents to regulate platelet adhesion, recruitment and aggregation. Therefore, platelet LROs not only serve as degradation compartments but also function as secretory compartments (7). However, our knowledge of the cell biology of platelet lysosome/LROs biogenesis, secretion and their potential associations with intracellular lysosomal-mediated signaling in megakaryocytes and platelets remains incompletely understood.

5.1.3 The biological functions of sphingolipids during megakaryopoiesis and thrombopoiesis

S1P plays a role in multiple biological processes, including cell proliferation, migration, apoptosis, morphogenesis and differentiation by binding S1P-specific receptors, mainly G-protein coupled $S1P_1$~$S1P_5$ receptors (177). In addition to regulating various cellular events, S1P has also been demonstrated to play a crucial role in intracellular calcium mobilization and signaling (20). S1P is primarily synthesized by the action of sphingosine kinases that convert sphingosine into S1P. S1P is irreversibly degraded by S1P lyase or reversibly dephosphorylated by S1P phosphatases (177). It has also been demonstrated that S1P gradients drive immune cells trafficking (178). Platelets have highly activated intracellular SPHKs and lack the S1P-degrading enzyme S1P lysase, so they can generate and store high levels of intracellular S1P contents, which is released on stimulation/activation (176). Recent studies have highlighted the novel functions of sphingolipid-mediated signaling

during megakaryopoiesis and thrombopoiesis, which suggested that extracellular S1P gradients, intracellular S1P signaling and its interaction with its multi-functional receptors, $S1P_1$ and $S1P_4$, are crucial for (i) the directional growth of pro-platelets from megarkaryocytes (ii) and pro-platelet formation, extension and release (14, 175). In addition, SPHK2 has recently been identified as a crucial factor in the regulation of platelet biogenesis and its deficiency would lead to the inhibition of megakaryocyte SPHK activity affecting the final stage of thrombopoiesis i.e. pro-platelet shedding (16). However, the details of the physiological functions of S1P and SPHKs on megakaryopoiesis and thrombopoiesis remain largely unknown.

5.1.4 The role of cholesterol in megakaryopoiesis and thrombopoiesis

Cholesterol is a cellular lipid, a major component of lipid rafts and the immediate precursor of steroid hormones and bile acids (179). Intermediates in the cholesterol biosynthetic pathways play essential roles in various cellular functions (180). Pre-squanlene biosynthesis, the isoprenoid intermediates serve as precursors for dolichol, ubiquinone, fanesyl and geranylgeranyl moieties all of which are important in cellular electron transport chain function and prenylation (180). Cholesterol also plays an essential role in development via its addition to Hedgehog signaling proteins that are required for the Hedgehog morphogen gradient (181). Recent studies have revealed that defects in intracellular cholesterol transporters, such as *Abcg4*, *Abcg1*, lead to intracellular cholesterol redistribution and accumulation in subcellular compartments and impaired downstream cholesterol-mediated signaling that affects megakaryocyte production and platelet functions in $Abcg1^{-/-}$ and $Abcg4^{-/-}$ mice (182, 183).

5.1.5 Acidic compartments calcium signaling in megakaryocytes and platelets

Intracellular calcium homeostasis is crucial for several cellular events, including intracellular vesicles trafficking, fusion and fission (184). Since platelet activation, aggregation, adhesion as well as platelet granules release are dependent on intracellular

calcium signaling, impaired intracellular calcium-mediated platelet functions could lead to the development of myocardial infraction, stroke and hemorrhage (185). Nicotinic acid-adenine dinucleotide phosphate (NAADP) is the most potent intracellular calcium mobilizing messenger and targets acidic compartments, e.g., late endosomes and lysosomes and LROs, (184, 186). Recent studies have indicated the importance of NAADP-mediated acidic compartments calcium signaling in human and mouse platelets and its defect would impair platelet spreading, granules release, potent agonists (e.g., thrombin and CRP)-induced platelet aggregation (187). In addition, the postulated NAADP-targeted lysosomal two-pore segment calcium channels, TPC-1 and TPC-2, have recently demonstrated their expressions in human megakaryoblastic MEG-01 cells (188). When expression of TPC-1/TPC-2 is silencing, NAADP-induced acidic compartment calcium release is impaired in MEG-01 cells (188). However, although several calcium-mediated intracellular signaling pathways involved in platelet activation and aggregation have been identified, the links between intracellular calcium signaling and ensosomal/lysosomal trafficking and granule secretion in the platelet field remain poorly understood.

5.1.6 Niemann-Pick type C1 disease

NPC disease is a lysosomal storage disease, is caused by mutations in either the *NPC1* (95% of cases) or *NPC2* genes and occurs at a frequency of approximately 1:120,000 live births (189). NPC1 disease cells have reduced acidic compartments calcium levels and accumulate sphingolipids and un-esterified cholesterol in the endosomal/lysosomal system (22). Clinically, NPC1 disease presents as a lethal neurodegenerative disease of infancy/childhood/adult with variable degrees of transient hepatosplenomegaly involvement (189). In addition to hepatic and neuropathological symptoms, NPC1 patients also present peripheral organs symptoms, including anemia, thrombocytopenia (190, 191) (discussed in detail in **Chapter 1)**.

5.1.7 Aim of this chapter

To investigate whether loss of NPC1 expression and the resulting acidic store calcium defect affects LROs function in megakaryocytes and platelets in a mouse model of NPC1 disease. Our current results suggest that acidic compartment calcium flux defects in *Npc1*$^{-/-}$ megakaryocytes and platelets may cause *Npc1*$^{-/-}$ platelet functional defects.

5.2 Patients, Materials and Methods

5.2.1 Patients for hematological analysis

NPC1 patients were enrolled in an ongoing longitudinal observational study at the National Institutes of Health in Bethesda, Maryland. The NICHD Institutional Review Board approved the study and collection of age-matched control samples as described in **Chapter 2**. The clinical samples and data were kindly provided by Dr. Denny Porter (NIH, USA).

5.2.2 Animals

Niemann-Pick type C1 mice (BALB/cNctr-*Npc1m1N*/J, *Npc1*$^{-/-}$ mice) were from an established colony. All mice were bred under sterile conditions, with food and water available *ad lib* as described in **Chapter 2**. All animal studies were conducted using protocols approved by the UK Home Office for the conduct of regulated procedures under license (Animal scientific Procedures Act, 1986).

5.2.3 Administration of substrate reduction therapy using miglustat on Npc1$^{-/-}$ *mice*

Npc1$^{-/-}$ mice treated with substrate reduction therapy using miglustat (1,200 mg/kg/day, Oxford GlycoSciences/Celltech, UK) were supplemented as dry admix to powdered RM1 mouse chow (SDS, UK). The miglustat treatment was administered from 3 weeks of age (P21). The untreated *Npc1*$^{-/-}$ mice were fed on powdered chow as a control group.

5.2.4 Mice hematological analysis

Mouse blood samples were obtained by cardiac puncture technique and analyzed as described in **Chapter 2**.

5.2.5 Isolation of murine platelets

Mouse platelets were obtained from indicated time points of *Npc1*$^{-/-}$ and age-matched control littermates. For preparation of washed platelets, the mice were anesthetized with CO_2 and blood were obtained by cardiac puncture technique. A total of 400 μL of blood per mouse

was collected in a tube containing 100 μl acid citrate dextrose solution. Platelet-rich plasma (PRP) was obtained by centrifugation at 300*g* for 10 minutes at room temperature. For preparation of washed platelets, PRP was washed at 1000*g* for 8 minutes at room temperature, and the pellet was re-suspended in modified Tyrode-HEPES buffer (134 mM NaCl, 0.34 mM Na2HPO4, 2.9 mM KCL, 12mM $NaHCO_3$, 5 mM HEPES, 5 mM glucose, and 0.35% bovine serum albumin [BSA; pH 7.4]) in the presence of prostacyclin (0.1 ug/mL). Isolated mouse platelets were re-suspended in the same buffer without prostacyclin and incubated at 37°C for 30 minutes before use.

5.2.6 Flow cytometry analysis of granules release

Surface integrin αIIbβ3 levels were assessed with anti-αIIb (CD61) antibody and fibrinogen binding was measured using FITC-labeled fibrinogen. Surface exposure of P-selectin was observed as a measure of α-granules secretion using a PE-conjugated anti-CD62P (P-selectin) antibody. Flow cytometry was carried (FACScan) and analyzed using CellQuest software (Becton Dickinson, Oxford, United Kingdom).

5.2.7 Bleeding assay

Mice were anesthetized with isoflurane and placed onto a heated mat. The tail bleeding time was determined by removing 3 millimeter of the distal tail tip and immersed the tail into sterile DPBS solution. The time to cessation of bleeding was measured up to 5 minutes, after which the assay was terminated.

5.2.8 Platelet Aggregation

Platelet-rich plasma (PRP) was prepared by centrifugation at 250 ug for 10 min at room temperature. The platelet count was adjusted with autologous plasma. Aggregation from PRP platelets was monitored by assessing light transmission in a microplate reader (BMG LabeTec, UK) with continuous stirring at 1100 rpm at 37 °C.

5.2.9 Ferric chloride carotid injury model

Mice were anesthetized with ketamine 100 mg/kg (Vetalar V; Pfizer) and 10 mg/kg xylazine (Rompun; Bayer). Platelets were labeled by intravenous administration of 100 mg/kg Dylight-488 conjugated anti-GPIbβ antibody (Emfret Analytics Gmbh). Right carotid arteries were exposed and 2x1 mm, 15% ferric chloride-soaked filter paper sections were placed on the arterial adventitia for 3 minutes. Time-lapse microscopy of the injury site was performed for 20 minutes and the images were processed using ImageJ. Background fluorescence values were measured upstream of the injury site and subtracted from thrombus-specific fluorescence. The data were expressed as integrated fluorescence density values.

5.2.10 Cell culture

The human megakaryoblastic leukemia MEG-01 cells were obtained from ATCC and cultured in RPMI-1640 supplemented with 10% (v/v) fetal bovine serum, 1% penicillin/ streptomycin, and 0.3 μg/mL glutamine in a humidified atmosphere at 37°C and 5% CO_2.

5.2.11 Immunofluorescence analysis of human megakaryoblastic MEG-01 cell line.

Adherent human MEG-01 cells were fixed with 4% paraformaldehyde, washed and blocked with 10% goat serum in DPBS for 1 hour, followed by incubation with the primary antibody in 10% goat serum in DPBS-Triton (0.2%) solution at 4°C overnight. Primary antibodies against NPC1 (1:1000; Novus, UK), CD63/LAMP-3 (1:1000; Abcam, UK) and P-selectin (CD-62P; 1:1000; Abcam, UK) were used in immunofluorescence assays. Chamber slides were then washed and incubated with either Dylight-594 Red, rabbit anti-mouse (1:3000, Vector Laboratories, UK) or Dylight-488 Green, donkey anti-rat secondary antibodies (1:2000, Invitrogen, UK) for 2 hours at room temperature. Cell nuclei were stained with DAPI (Sigma, UK). Images were captured and processed with a Zeiss Axioskop 2 Plus fluorescence microscope.

5.2.12 Flow cytometric analysis for the measurements of the numbers and volume of platelet acidic compartments.

Washed murine platelets were diluted to 2.5 x 10^7 platelets/ml into modified Tyrode's buffer; MEG-01 cells were re-suspended in HBSS solution. Mouse platelets and MEG-01 cells were incubated with LysoTracker Green DND-26 for 15 minutes at room temperature. Cells were then washed with HBSS solution and flow cytometer analysis was then immediately carried out.

5.2.13 Isolation and culture murine megakaryocytes

For the isolation of murine *Npc1*$^{-/-}$ and *Npc1*$^{+/+}$ megakaryocytes, bone marrow cells were harvested by flushing the femurs with PBS. The obtained cells were cultured in IMDM medium containing 20 ng/ml thrombopoietin. After 5 to 7 days differentiation into mature megakaryocytes had taken place and the cells were purified using a discontinuous bovine serum albumin (BSA) density gradient (0~3% BSA) and analysed by microscopy and flow cytometry.

5.2.14 Megakaryocyte pro-platelet formation assay

Megakaryocytes were enriched from bone marrow aspirates by culturing for 5 days in complete media with 20ng/mL thrombopoietin (PeproTech EC, UK) and 10 units/mL heparin (Sigma Aldrich, UK). Megakaryocytes were harvested and purified through a discontinuous 3/1.5% BSA gradient. Megakaryocytes were seeded onto coverslips coated with 100µg/mL fibrinogen (Sigma Aldrich, UK) and incubated for 5 hours at 37°C and 5% CO_2. Megakaryocytes were fixed with 4% paraformaldehyde and labeled with FITC-conjugated anti-CD41 antibody (AbD Serotec, UK). Pro-platelet-forming cells were manually enumerated in the total adhered, labeled population and were classed as any labeled cell with one or more branched extension.

5.2.15 Statistics

Data were expressed as the mean ± SEM. Statistical analysis and graph plot were performed by using GraphPad Prism software. An unpaired two-tailed Student's *t* test was used to determine the significant differences. A *p* value less than 0.05 was considered statistically significant.

5.3 Results

5.3.1 Increased number of platelets (PLT), plateletcrit (PCT) in Npc1$^{-/-}$ mice.

As shown in **Fig. 5.1A-C**, there was a significant increase in the circulating platelets count (PLT) and plateletcrit (percentage volume of platelets, PCT) in *Npc1*$^{-/-}$ mice; the *Npc1*$^{-/-}$ platelet count (PLT) and plateletcrit (PCT) increased markedly by 40 ~ 42.7 % (7 weeks, 42.7%, p = 0.0082, 9 weeks, 40%, P = 0.0028) and 46.8 ~ 48.3 % (7 weeks, 46.8%, p = 0.0034, 9 weeks, 48.3%, p = 0.0026) from 7 weeks of age, respectively). However, there was no significant change in mean platelet volume (MPV) in *Npc1*$^{-/-}$ platelets while compared with control (*Npc1*$^{+/+}$) platelets.

Figure 5.1 Increased number of platelets (PLT), plateletcrit (PCT) in *Npc1*$^{-/-}$ mice. (A-C) Platelet-related parameter analysis, platelet number (PLT), mean platelet volume (MPV) and plateletcrit (PCT), were determined using an automatic blood analyzer. Data shown are mean ± SEM, n = 5 ~ 7, per group. * $p < 0.05$, ** $p < 0.005$, *** $p < 0.0005$, calculated by an unpaired *t* test using GraphPad Prism v5.

The surface expression of platelet collagen activation receptor GPVI and the αII subunit of the collagen integrin αIIβI were examined and no significant difference between *Npc1*$^{-/-}$ platelets and controls observed (**data not shown**).

5.3.2 Impaired Npc1$^{-/-}$ platelets aggregation in response to thrombin stimulation.

To further explore the functional consequences of the markedly increased of circulating platelet count and the mean platelets volume in *Npc1*$^{-/-}$ mice, we investigated whether there were aggregation defects in *Npc1*$^{-/-}$ platelets stimulated with different agonists. There was a significant decrease of *Npc1*$^{-/-}$ platelets aggregation by 40.7% in response to thrombin stimulation (1 U/mL) while compared with control (*Npc1*$^{+/+}$) mouse platelets (**Figure 5.2A-D)**.

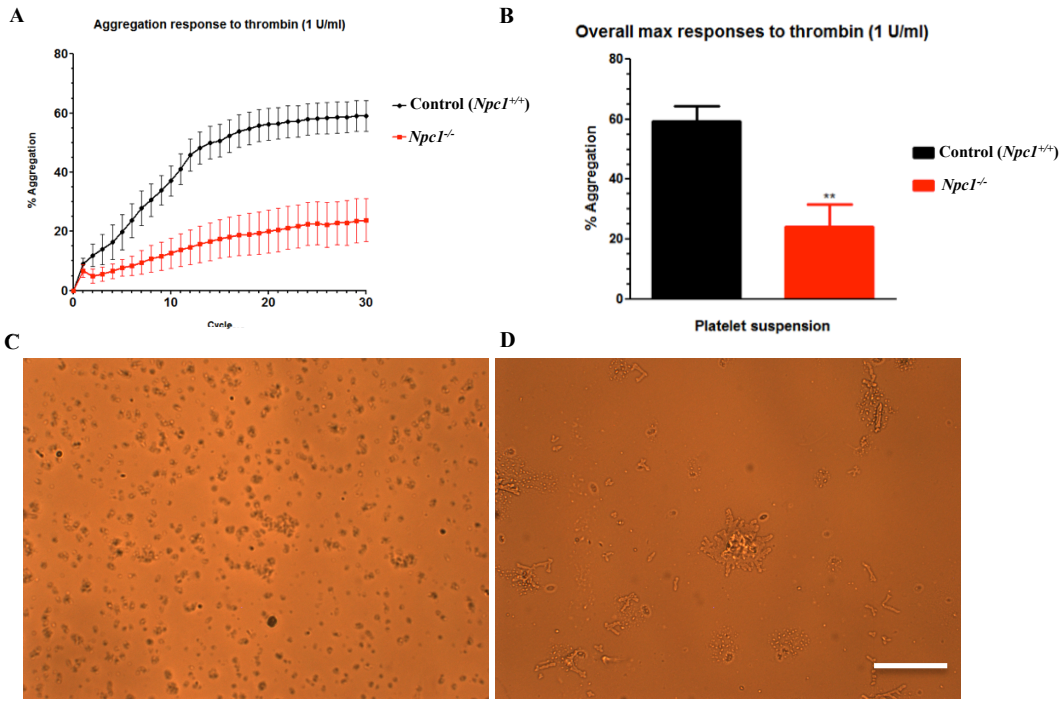

Figure 5.2. Impaired *Npc1*$^{-/-}$ platelets aggregation in response to thrombin (1 unit/ml) stimulation. Mouse platelets were isolated from 10-week-old control (*Npc1*$^{+/+}$) and *Npc1*$^{-/-}$ mice. The aggregation assays were performed with mouse platelets stimulated with thrombin (1 U/ml). **(A-B)** Average maximal *Npc1*$^{-/-}$ mouse platelet aggregation was at 40.7% of the average maximal response relative to control mouse platelets (n = 6). Data presented as mean ± SEM, $p < 0.05$. **(C-D)** Light microscopy analysis of the aggregation response of 10-week-old control (*Npc1*$^{+/+}$) and *Npc1*$^{-/-}$ mouse platelets. Scale bar, 10 µm.

However, there were no significant differences in *Npc1*$^{-/-}$ platelets aggregation in response to while the calcium ionophore A23187 while compared with controls **(Figure 5.3A-B**). These data suggested that the impaired thrombin-induced *Npc1*$^{-/-}$ platelet aggregation could be either associated with (i) the abnormal surface platelet integrin receptors expression; or (ii) impaired intracellular thrombin-induced platelet activation signaling.

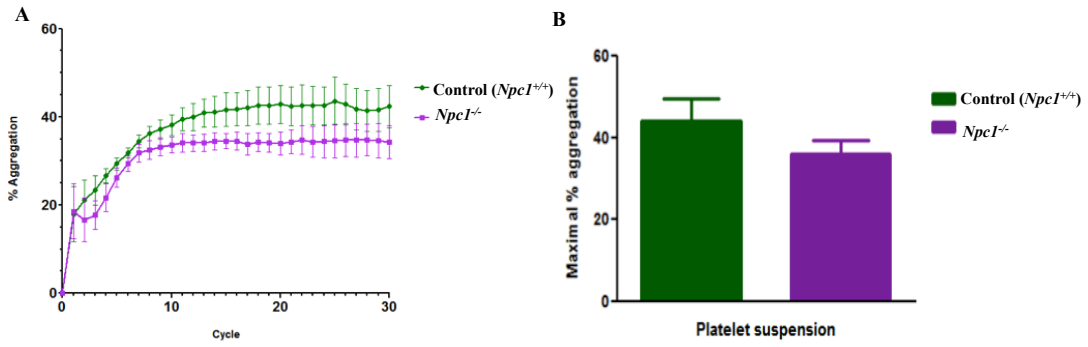

Figure 5.3. *Npc1*$^{-/-}$ platelets do not present any significant difference in aggregation in response to calcium ionophore A23187 stimulation compared with control platelets. Isolated 10-week-old control and *Npc1*$^{-/-}$ platelets were stimulated with the calcium ionophore A23187 (60 uM) in the presence of $CaCl_2$ (1 mM). The platelet aggregation assay was performed as described in "Material & Methods". **(A)** The time-course of the aggregation response. **(B)** The maximal aggregation responses compared to the average platelet aggregation in response to A23187 (60 μM) was 44.2% for control mouse platelets and 36.2% for *Npc1*$^{-/-}$ mouse platelets, respectively. This difference was not statistically significant, n = 4 ~ 5, per group, Data presented as mean ± SEM.

5.3.3. Impaired α-granules release in Npc1$^{-/-}$ *platelets in response to thrombin stimulation.*

Since recent studies have indicated that sphingolipids-mediated signal is crucial for megakaryopoiesis and thrombopoiesis, the impaired intracellular sphingolipids trafficking and its metabolism defects in *Npc1*$^{-/-}$ megakaryocytes and platelets could be a potential explanation for the abnormally high level of circulating platelets in *Npc1*$^{-/-}$ mice. To address this possibility, an *in vitro* pro-platelet formation assay was performed on isolated control (*Npc1*$^{+/+}$) and *Npc1*$^{-/-}$ megakaryocytes. However, there were no significant difference in pro-platelet formation between control (*Npc1*$^{+/+}$) and *Npc1*$^{-/-}$ megakaryocytes **(Figure 5.4A)**. Next, we examined α-granules release by measuring platelet surface P-selectin (CD-62P) exposure. For control (*Npc1*$^{+/+}$) platelets, the mean fluorescence intensity of staining for surface P-selectin exposure increased upon stimulation with thrombin. While stimulated with high concentration of thrombin, the P-selectin exposure levels were significantly decreased in *Npc1*$^{-/-}$ platelets while compared with control (*Npc1*$^{+/+}$) ones. When quantified **(Figure 5.4B)**,

P-selectin staining on *Npc1*$^{-/-}$ platelets was less than 30% of control platelets (*Npc1*$^{+/+}$). These data suggested that thrombin induced α-granules secretion was impaired in *Npc1*$^{-/-}$ platelets. To further investigate whether NPC1 deficiency could also impair δ-dense granules and lysosomes secretion in *Npc1*$^{-/-}$ platelets, the δ-granules and lysosomes secretion were measured using levels of ATP secretion and β-hexosaminidase (*Hex-β*) release by fluorescence analysis. As illustrated in **Figure 5.4C-D**, similar levels of secreted ATP and β-hexosaminidase (*Hex-β)* were detected in control (*Npc1*$^{+/+}$) and *Npc1*$^{-/-}$ platelets, which suggested that thrombin stimulation induced normal levels δ-granules and lysosomes secretion in *Npc1*$^{-/-}$ platelets. Taken together, these findings suggested a specific effect on α-granules release in *Npc1*$^{-/-}$ platelets in response to thrombin.

Figure 5.4 Impaired α-granules release in *Npc1*$^{-/-}$ platelets in response to thrombin stimulation. (A) *In vitro* pro-platelet formation assay was performed on megakaryocytes isolated from 9-week-old control (*Npc1*$^{+/+}$) and *Npc1*$^{-/-}$ mice. **(B-D)** Mouse platelets from control (*Npc1*$^{+/+}$) and *Npc1*$^{-/-}$ mice were stimulated with thrombin. After 30 minutes incubation, reactions were stopped and the extent of secretion from α-granules (**panel B**), δ-granules (**panel C**) and lysosomes (**panel D**) were analyzed and percent secretion was calculated. Data represent the mean ± SEM, n = 3 ~ 4, per group. The assays were performed by our collaborators Dr. Chris Williams and Prof. Alastair Poole (Bristol University, UK).

5.3.4 Increased tail bleeding time in Npc1$^{-/-}$ *mice.*

As there is an abnormal circulating platelets count, impaired thrombin induced-platelet aggregation and platelet activation defects in *Npc1*$^{-/-}$ mice, we next investigated whether this would lead to bleeding abnormalities. To assess this possibility, tail-bleeding assay were performed in 10.5-week-old *Npc1*$^{-/-}$ mice. As shown in **Figure 5.5**, there was a markedly hemostatic defect observed in *Npc1*$^{-/-}$ mice. Whereas bleeding stopped after approximately 2 minutes in control age-matched (*Npc1*$^{+/+}$) mice, tail-bleeding time was markedly increased in 10.5-week-old *Npc1*$^{-/-}$ mice, indeed bleeding did not stop within the observation period of 5 minutes.

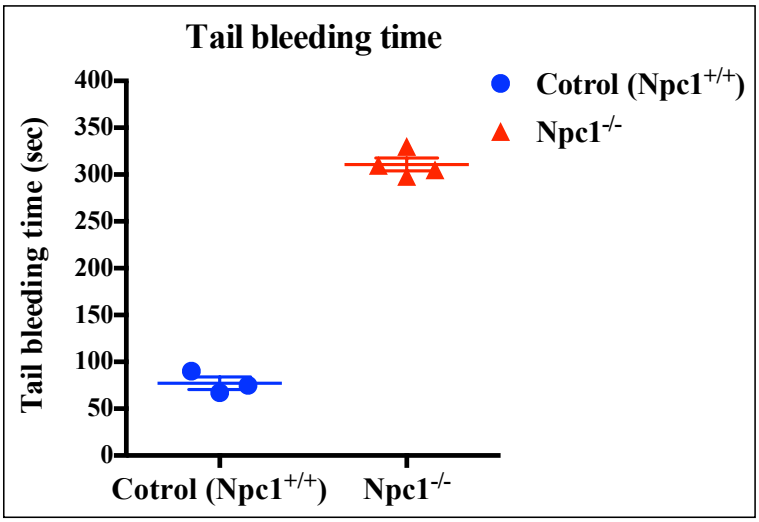

Figure 5.5 Increased tail bleeding time in *Npc1*$^{-/-}$ mice. Tail bleeding assays were performed as described in "Material & Methods" on 10.5-week-old control (*Npc1*$^{+/+}$) and *Npc1*$^{-/-}$ mice. The time from incision to cessation of bleeding was recorded. Data represent mean ± SEM, n = 3 ~ 4, per group. The bleeding assay was stopped at 5 minutes (300 seconds). The data are expressed as mean ± SEM, n = 3 ~ 4, per group

5.3.5 In vivo thrombus formation defects in Npc1$^{-/-}$ *mouse.*

Next, the *in vivo* thrombus formation assay was performed to further evaluate *Npc1*$^{-/-}$ platelets functional defects. As shown in **Figure 5.6A-D**, the size and rate of *in vivo* thrombus formation were significantly reduced in 9-week-old *Npc1*$^{-/-}$ mouse compared with age-matched controls. Collectively, these findings demonstrated that deficiency of NPC1 in platelets results in a bleeding diathesis and a significant reduction *in vivo* thrombus formation in *Npc1*$^{-/-}$ mice. Agonist-induced platelet activation, aggregation and thrombus formation are all directly dependent on intracellular calcium-mediated signaling. Therefore our data suggest that calcium signaling defects in *Npc1*$^{-/-}$ platelets could be associated with *Npc1*$^{-/-}$ platelet dysfunction, but in an agonist specific manner.

Figure 5.6 *In vivo* thrombus formation defect in *Npc1*$^{-/-}$ mouse. (A-D) $FeCl_3$-induced injury was performed in 9-week-old control (*Npc1*$^{+/+}$) and *Npc1*$^{-/-}$ mice and the *in vivo* thrombus formation size was video recorded as described in "Material & Methods". Time courses of the embolus surface area measured by the fluorescence passing through the region of interest downstream of the thrombus. Date represent mean ± SEM. n = 15, $p < 0.05$. The assays were performed by our collaborators Dr. Chris Williams and Prof. Alastair Poole (Bristol University, UK)

5.3.6 Abnormal ultra-structure in Npc1$^{-/-}$ platelets.

Since the NPC1 protein is involved in the regulation of intracellular lipid trafficking, it could be possible that the *in vitro* and *in vivo* platelets functional defects could be associated with lipid storage-induced trafficking defects in *Npc1*$^{-/-}$ platelets. To test this hypothesis, *Npc1*$^{-/-}$ platelets ultra-structure was examined by transmission electron microscopy (52) (52). The TEM examination indicated that there were numerous abnormal electron-dense granules-like storage bodies and increased cytosolic vacuoles in *Npc1*$^{-/-}$ platelets **(Figure 5.7)**.

Figure 5.7 Abnormal ultra-structure in *Npc1*$^{-/-}$ platelets. (A-D) Representative electron microscopy images of platelets collected from 9-week-old control (*Npc1*$^{+/+}$) and *Npc1*$^{-/-}$ mice. Normal ultrastructure in platelets derived from 9-week-old control (*Npc1*$^{+/+}$) mice. **(C-D)** Altered granules ultrastructure in platelets derived from 9-week-old *Npc1*$^{-/-}$ mice. The mouse platelets were isolated and processed for electron microscopy analysis as described in " Materials & Methods". Representative images obtained from one experiment.

5.3.7 Increased LysoTracker-Green fluorescence intensity in Npc1$^{-/-}$ platelets.

In addition, to measure acidic compartments changes, *Npc1*$^{-/-}$ platelets were also collected and incubated with LysoTracker-Green reagent, followed by flow cytometric analysis. The flow cytometric analysis indicated abnormal increase fluorescence intensity peak in 9-week-old *Npc1*$^{-/-}$ platelets while compared with control (*Npc1*$^{+/+}$) mouse platelets. Therefore, consistent with the TEM examination, this result suggested either an increased number or volume of acidic organelles in *Npc1*$^{-/-}$ platelets **(Figure 5.8A-E)**.

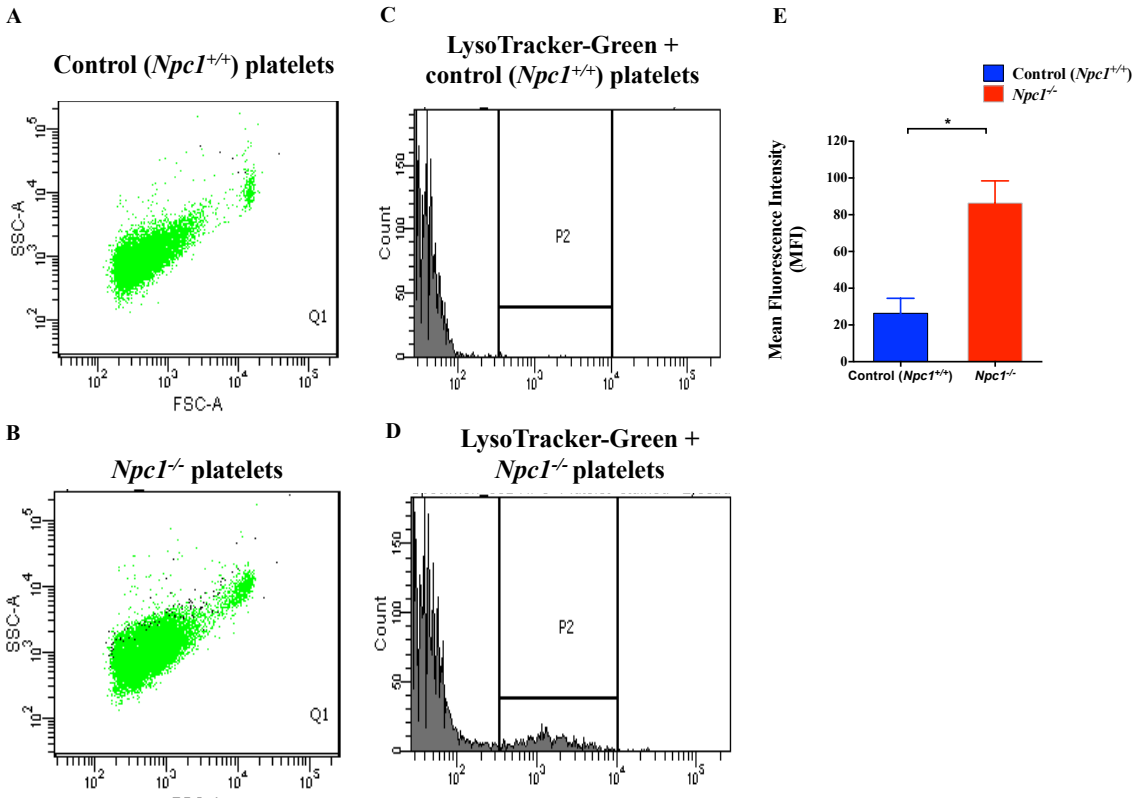

Figure 5.8 Increased LysoTracker-Green fluorescence intensity in *Npc1*$^{-/-}$ platelets. (A-E) Representative images of flow cytometric analysis of the numbers and the volume change of acidic compartments in 9-week-old control (*Npc1*$^{+/+}$) and *Npc1*$^{-/-}$ mouse platelets. Isolated mouse platelets were incubated with LysoTracker-Green reagent and analyzed by flow cytometry as described in " Material and Methods". * $p < 0.05$. Data shown are mean ± SEM, n = 3, per group. Data were calculated and plotted using GraphPad Prism v5.

5.3.8 Increased LysoTracker-Green fluorescence intensity in U18666A-treated human megakaryoblastic MEG-01 cell line.

Next, to further investigate the underlying mechanisms of *Npc1*$^{-/-}$ platelet dysfunction, we utilized the pharmacological compound (U18666A) to induce NPC1 disease cellular phenotypes in human megakaryoblastic MEG-01 cell line, The number and the volume of the intracellular acidic compartments in MEG-01 cells were then measured using LysoTracker-Green staining, followed by flow cytometric analysis. As illustrated in **Figure 5.9A-C**, there was a significant increase in LysosTracker-Green signal intensity in U18666A-

treated MEG-01 cells as predicted compared with vehicle-treated (DMSO) cells.

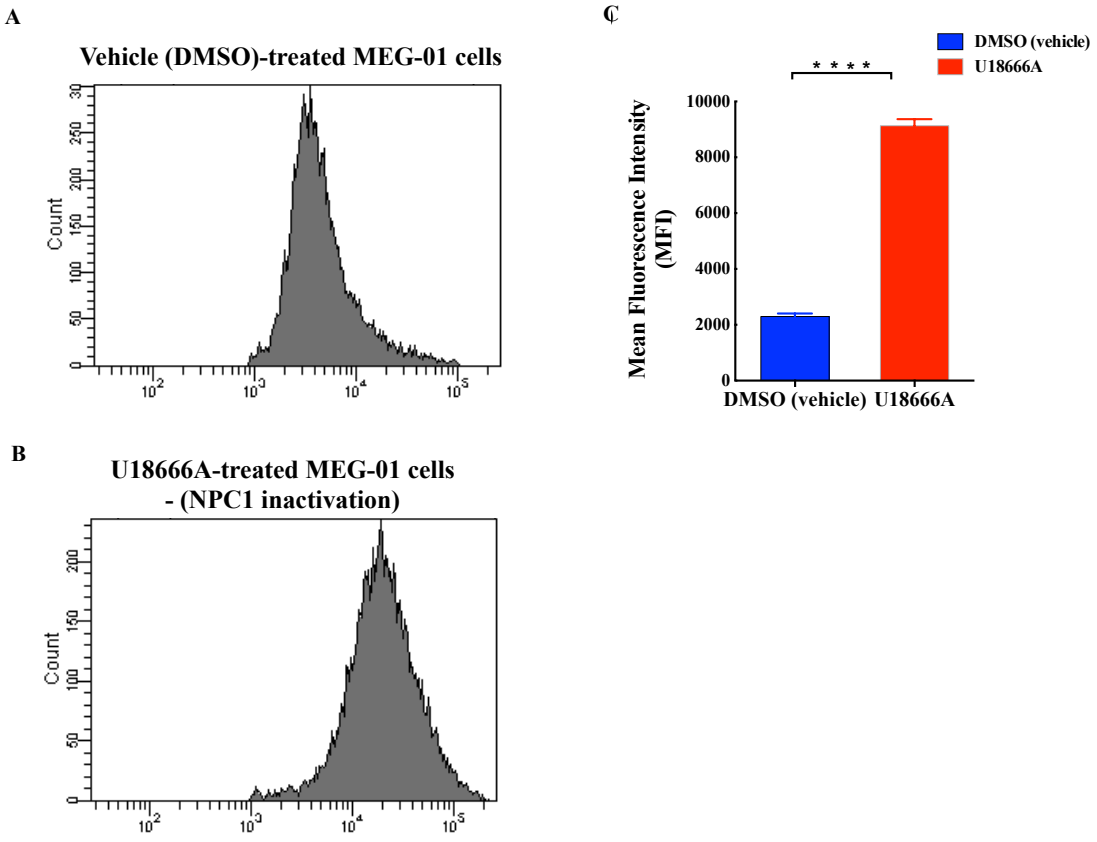

Figure 5.9 Increased LysoTracker-Green fluorescence intensity in U18666A-treated human megakaryoblastic MEG-01 cell line. Representative images of flow cytometric analysis of the numbers or the volume change of acidic compartments in vehicle (DMSO) (panel A) or U18666A-treated MEG-01 cells (panel B). Data were quantified from 3 independent animals (panel C). *** $p < 0.0005$. Data are presented as mean ± SEM, calculated and plotted using GraphPad Prism v5.

5.3.9 Abnormal intracellular storage bodies in U18666A-treated MEG-01 cells.

TEM ultrastructural analysis indicated that numerous enlarged electron dense storage bodies presented in U18666A-treated MEG-01 cells **(Figure 5.10)**.

Figure 5.10.1 Abnormal intracellular storage bodies in U18666A-treated MEG-01 cells. (A-D) Representative images of transmission electron microscopy analysis from vehicle (DMSO) and U18666A treated human megakaryoblastic MEG-01 cell lines. Scale bar = 2 µm. Representative images obtained from one experiment.

Figure 5.10.2 Abnormal subcellular storage bodies in U18666A-treated MEG-01 cells. (A-B) Representative images of transmission electron microscopy analysis from U18666A-treated human megakaryoblastic MEG-01 cell line. Arrows indicated the abnormal morphology of storage bodies presented in U18666A-treated MEG-01 cells. Scale bar = 1 μm. Representative images obtained from one experiment.

5.3.10 NPC1 is co-localized with α-granules marker, P-selectin (CD-62P) and δ- and late endosome/lysosome marker, CD63 (LAMP-3), in U18666A treated MEG-01 cells.

In order to further characterize the subcellular distribution of NPC1 in human megakaryoblasts, U18666A and vehicle (DMSO)-treated MEG-01 cells were co-immunostained with anti-NPC1 and platelet granules markers, including CD62P for α-granules, CD63 for δ-granules and lysosomes. As illustrated in **Figure 5.11.1-2**, immunofluorescence analysis revealed that NPC1 is predominately co-localized with δ-granule and lysosomes marker, CD63/LAMP-3, and partially co-localized with the α-granules marker, CD62P/P-selectin, in U18666A-treated MEG-01 cells, which suggested that NPC1 is potentially involved in the regulation of intracellular cargos transport between granules. Of interest, it has been noted that U18666A-treated MEG-01 cells have abnormal/enlarged $CD62P^{+}$ α-granules morphology compared with DMSO (vehicle)-treated MEG-01 cells. Theses results suggested that NPC1 may be crucial for granules functions in MEG-01 cells.

Figure 5.11.1 NPC1 is co-localized with δ- and late endosome/lysosome marker, CD63 (LAMP-3), in U18666A treated MEG-01 cells. (A-F) Representative images of immunofluorescence analysis of NPC1 subcellular localization in MEG-01 cells. Nuclei were counterstained with DAPI. Images were viewed and captured as described in "Materials & Methods". Scale bar, 10 μm.

Figure 5.11.2 NPC1 is co-localized with α-granules marker, P-selectin (CD-62P), in U18666A treated MEG-01 cells. (A-F) Representative images of immunofluorescence analysis of NPC1 subcellular localization in MEG-01 cells. Nuclei were counterstained with DAPI. Scale bar, 10 μm.

5.3.11 Defects in acidic compartments calcium flux in U18666A-treated MEG-01 cells in response to GPN stimulation.

To investigate whether U18666A-treated MEG-01 cells exhibited reduced acidic store calcium levels as we previously reported in U18666A-treated RAW cells and NPC1 patients-derived human fibroblasts, single cell calcium imaging/mobilization assay was measured in MEG-01 cells (22). Acidic compartments Ca^{2+} release was monitored indirectly by treating Fura-2–loaded MEG-01 cells with Gly–Phe–β-naphtylamide (GPN), a tripeptide causing osmotic lysis of cathepsin C–positive lysosomes. In agreement with our previous studies on NPC1 patients-derived human fibroblasts and RAW 264.7 cells (22), GPN treatment induced a steep increase in the cytosolic Ca^{2+} levels in vehicle (DMSO)-treated MEG-01 cells; whereas GPN-induced acidic compartment Ca^{2+} release was significantly reduced by 30~40% in Fura-2–loaded U18666A-treated MEG-01 cells **(Figure 5.12)**. This result indicated that U18666A-induced NPC1 disease cellular phenotype MEG-01 cells exhibited acidic store calcium efflux defects as predicted.

Figure 5.12 Defects in acidic compartments calcium flux in U18666A-treated MEG-01 cells in response to GPN stimulation. (A-C) Human megakaryoblastic cell line (MEG-01) cells were incubated either with DMSO (vehicle control) or U18666A (2 μg/mL) for 72 hours at to induce NPC1 disease cellular phenotypes. The cells were loaded with Fura-2 AM reagent and then treated with 200 μM GPN to induce acidic compartment calcium release. Single cells calcium images were performed and monitored. The calcium assay was performed and analyzed by Dr. Lianne Davis (Dept. Pharmacology, University of Oxford).

5.3.12 Miglustat (NB-DNJ) treatment improved abnormal circulating platelet count in treated Npc1$^{-/-}$ mice.

Miglustat, a EU-clinically approved substrate reduction therapy for the treatment of NPC1 disease, inhibits intracellular glucoceramide synthase activity and reduces glycosphingolipids accumulation in the endosomal/lysosomal compartments in NPC1 disease (192). However, the potentially therapeutic effects of miglustat treatment on the abnormal megakaryopoiesis and thrombopoiesis phenotypes in *Npc1*$^{-/-}$ mice remain unknown. We therefore evaluated the therapeutic effects of miglustat on platelet related phenotypes in *Npc1*$^{-/-}$ mice. Miglustat treatment (1,200 mg/kg/ day) was started at 3-weeks of age (P21) and continued the treatment for 6 weeks. Hematological analysis revealed that miglustat treatment significantly reduced by 20% the elevated platelet count in *Npc1*$^{-/-}$ mice compared with age-matched control diet-treated *Npc1*$^{-/-}$ littermates **(Figure 5.13A)**. However, no significant changes in mean platelet volume (MPV), and platletcrit (PCT) were noted **(Figure 5.13B-C)**. Therefore, our *in vivo* studies suggested that the miglustat treatment could partially correct abnormal thrombopoiesis phenotype in *Npc1*$^{-/-}$ mice.

Figure 5.13 Miglustat (NB-DNJ) treatment improved abnormal circulating platelet count in treated *Npc1*$^{-/-}$ mice. (A-C) *Npc1*$^{-/-}$ mice were treated with miglustat (1,200 mg/kg/day) from the 3 weeks of age. Age-matched control animals were treated with normal powered diet as control group. Whole Blood from 9-week-old control diet and miglustat treated *Npc1*$^{-/-}$ mice were collected and analysed using an automated blood analyser as described in "Materials and Methods". Data shown are mean ± SEM, n = 3 per group. * $p < 0.05$ calculated by an unpaired *t* test using GraphPad Prism v5.

5.3.13 NPC1 patients present with mild thrombocytopenia

So far, we have demonstrated *Npc1*$^{-/-}$ platelets functional defects with activation/aggregation defects in response to thrombin stimulation. Besides, *in vivo* thrombus assay revealed reduced thrombus formation and thrombus size in *Npc1*$^{-/-}$ mice. Furthermore, the NPC1 inactivation U18666A-treated MEG-01 cells exhibited abnormal subcellular

storage bodies and acidic compartments calcium efflux defects. However, it remains unclear whether the observations of *Npc1*$^{-/-}$ mouse platelet dysfunctional phenotypes reflect similar phenomena in NPC1 patients. Therefore, platelet-related hematological changes were examined in NPC1 patients. As illustrated in **Fig 5.14**, our results revealed that NPC1 patients tend to have low normal range of circulating platelets counts, which suggested thrombocytopenia in NPC1 patients; however, the mean platelet volume (MPV) from NPC1 patients fall within the normal range.

Figure 5.14 NPC1 patients present with mild thrombocytopenia. (A–B) Platelet count (PLT) and mean platelet volume (MPV) were determined using an automated blood analyser. (n = 38 ~ 39, and n = 59, for NPC1 patients and control groups, respectively). Dashed lines indicate the normal range of the platelet related parameters (PLT and MPV) in different groups. Data shown are mean ± SEM, calculated by using GraphPad Prism v5. The data was kindly provided by our collaborator Dr. Denny Porter (NIH, USA).

5.4 Discussion

In the current study, we have found (i) elevated number of circulating platelets, (ii) platelet activation/aggregation defects (iii) and prolonged bleeding times in NPC1 disease murine model. Electron microscopy examination indicated abnormal ultrastructure of cellular storage bodies, evidence of lipid storage, in U18666A-treated MEG-01 cell line and *Npc1*$^{-/-}$ platelets. We also found α-granule secretion defect and impaired *in vivo* thrombus formation in *Npc1*$^{-/-}$ platelets. In addition, *in vitro* studies also identified impaired acidic compartment calcium flux defects in U18666A-treated MEG-01 cells. Taken together, these data suggested that *Npc1*$^{-/-}$ megakaryocytes/platelets LROs have functional defects.

Intriguingly, one recent study indicated that three unrelated NPC1 patients presented with reduced platelet aggregation, P-selectin expression and ATP secretion, which are compatible with the observation of abnormal α- and reduced δ-granules by electron

microscopy and CD63 (LAMP-3) staining after platelet spreading (191). Furthermore, the study indicated that *in vitro* differentiated megakaryocytes from NPC1 patients exhibited hyper-proliferation of immature megakaryocytes (191). However, these observations were not consistent with our current studies on NPC1 disease murine model. The reasons for these differences are unclear at this stage. One possibility is that different platelet activation agonists may stimulate different signaling pathways in NPC1 platelets. Therefore, further studies to test different agonists stimulation on *Npc1*$^{-/-}$ platelets would be crucial to resolve these issues. However, our current studies also cannot exclude the possibility that different molecular mechanisms occur in human and mouse NPC1 deficient platelets.

There could also be a platelet clearance defect and altered physiological distribution of platelets in NPC1 disease, since enlarged and fibrotic spleen can be observed in NPC1 patients and *Npc1*$^{-/-}$ mice. Platelets may be trapped in the spleen and then affect circulating platelets numbers. Therefore, *in vivo* platelet clearance assays will be crucial to help clarify these platelet dysregulation phenotypes. Furthermore, if this hypothesis is correct, it may help explain our observation, which indicated that miglustat-treated *Npc1*$^{-/-}$ mice exhibit normal circulating platelet numbers. However, our studies still cannot exclude a potential platelet production defect in NPC1 disease. Sphingosine-1-phosphate and its associated receptors, especially $S1P_1$ and $S1P_4$ receptors, have been recently suggested to be involved in the regulation of megakaryopoiesis, pro-platelet formation and shedding *in vivo* and *in vitro* models (14). Furthermore, $S1P_4$ receptor-null megakaryocytes exhibited abnormal cellular morphology, which was characterized by cytoplasmic vacuolation and nuclear ploidy changes (193). Interestingly, abnormal platelet formation and megakaryopoieses defects have been recently reported in a few cases of NPC1 and it has been suggested that this could be associated with abnormal lysosomal cholesterol storage in NPC1 disease (191). Since the platelet lipid compositions and its granule contents were mainly determined during megakaryopoiesis and platelet shedding, the abnormal *Npc1*$^{-/-}$ platelet phenotypes could be at least partially associated with abnormal intracellular lipid trafficking and storage phenotypes

observed during megakaryopoiesis and these defects could impair down-stream lipid-mediated intracellular signaling (175).

The main features of platelet storage pool disorders is abnormal numbers or altered morphology of platelet granules, which could be associated with impaired granules formation, packaging, maintenance and secretion (7, 8). Intriguingly, our electron microscopy examination indicated that abnormal electron-dense granules-like structures presented in *Npc1*$^{-/-}$ platelets. One of the possible explanations for these *Npc1*$^{-/-}$ platelet functional phenotypes is that the NPC1 protein is a crucial element for transport intracellular lipid substrates during LROs biogenesis to regulate granules packing, maintaining and secretion. Our current studies demonstrated that the *Npc1*$^{-/-}$ platelets exhibited functional defects, when simulated with thrombin. Of interest, it has been suggested that the platelets lysosomes secretion is only activated by potent agonists, such as thrombin (194, 195). It should also be noted that our previous studies have demonstrated that NPC1 disease is mainly characterized by a lysosomal calcium flux defect that in turn causes LE/lysosome lipid storage (22). Therefore, these findings suggested that *Npc1*$^{-/-}$ platelets functional defects could be associated with acidic compartment calcium signaling in *Npc1*$^{-/-}$ platelet. Although the physiological functions and activation mechanisms of platelets LROs remain unclear in the platelet biology field, our current studies highlight the importance of acidic compartments calcium signaling in the regulation of platelet functions. NAADP is a novel calcium-mobilizing second messenger, which targets acidic (186). Churchill and colleagues recently demonstrated that thrombin and collage-related-peptides (CRP) simulated human platelet aggregation, activation, including fibrinogen binding and granules release, is highly dependent on NAADP-mediated calcium signaling, which suggest a crucial role of NAADP and acidic store calcium release during platelet activation (187). Therefore, we could hypothesize that *Npc1*$^{-/-}$ platelet functional defects could be associated with impaired NAADP-mediated acidic store calcium signaling in *Npc1*$^{-/-}$ platelets. So far, this hypothesis is supported by the following evidence: (i) when *Npc1*$^{-/-}$ platelets were activated with thrombin aggregation was significantly reduced by 30 ~ 50 % compared with age-matched controls. (ii)

However, when *Npc1*$^{-/-}$ platelets were stimulated with calcium ionophore (A23187), *Npc1*$^{-/-}$ platelets did not present aggregation defects. This proposed model would be required further evaluation by using the NAADP-AM and lysosomal two-pore channel antagonist, Ned-19, to measure intracellular calcium responses and determine whether there were NAADP-mediated acidic compartments calcium flux defects in primary *Npc1*$^{-/-}$ megakaryocytes and *in vitro* in U18666A-treated MEG-01 cells (127). In addition, α-granules release defects in thrombin stimulated *Npc1*$^{-/-}$ platelets may raise the question of whether there is any specificity to stimulation with different agonists and this merits future evaluation.

The molecular mechanisms of abnormal granules number and ultra-structure in U18666A-treated MEG-01 cells and in *Npc1*$^{-/-}$ platelets are unclear at this stage. Interestingly, similar observations of abnormal platelet granules morphology and platelet functional defects have been reported in other lysosomes/LROs dysfunctional diseases, such as Tangier disease, Chediak-Higashi syndrome (99) and Hermansky-Pudlak syndrome (HPS) (5, 8, 182). One of the common features of these four disorders is they have intracellular calcium homeostasis defects, either in ER or LE/Lys calcium stores (22, 182, 196). Since intracellular calcium-mediated signaling is crucial for intracellular vesicles fussion and fission events, acidic compartment-mediated calcium homeostasis defects could lead to abnormal intracellular vesicles trafficking and storage in these diseases. Therefore, it would be reasonable to hypothesize that the acidic stores calcium homeostasis defects in NPC1 disease could impair the subcellular trafficking system, affect granules secretion and lead to activation/aggregation defects in *Npc1*$^{-/-}$ megakaryocytes/platelets.

Several studies have addressed the potential biological functions of NPC1 and NPC2 proteins and their presence in LROs in retinal pigment epithelial cells and lamellar-bodies in lung type II cells (91, 197-199). One recent study reported that NPC proteins deficiency leads to abnormal size of lamellar-bodies in lung type II cells in *Npc1*$^{-/-}$ and *Npc2*$^{-/-}$ mice. Also, abnormal cholesterol and phospholipid storage were observed in these specialized LRO containing type II cells in *Npc1*$^{-/-}$ and *Npc2*$^{-/-}$ mice (91). Furthermore, the enlarged and smaller sizes of lamellar-bodies in lung type II cells were noted in *Npc1*$^{-/-}$ and *Npc2*$^{-/-}$ mice,

respectively, which suggested that NPC1 and NPC2 proteins may coordinate each other to regulate the maturation of lamer-bodies in lung type II cells (91). In addition, we recently found defects in cytotoxic granules release from *Npc1*$^{-/-}$ NK cells as a result of reduced lysosome calcium content of (**Speak et al, Blood under revision**). Consistent with this observation, our current studies suggested that α-granules secretion defects in *Npc1*$^{-/-}$ platelets could be associated with the acidic compartment calcium flux defects in NPC1 disease. Furthermore, these observations led to the suggestion that the acidic compartment calcium flux defects may affect secretion of other LROs in *Npc1*$^{-/-}$ mice. If this assumption is correct, it would be of interest to investigate further the potential secretion defects of other LROs, especially Weibel-Palade bodies (WPBs), in *Npc1*$^{-/-}$ mice. For example, while we considered the potential mechanistic links of LROs dysfunction and the reduced thrombus size in *Npc1*$^{-/-}$ mice, one potential mechanism is that *Npc1*$^{-/-}$ platelets acidic compartments calcium signaling defect could affect α-granules secretion and impair thrombus formation in *Npc1*$^{-/-}$ mice. However, another possibility should also be considered is that endothelial cells WPBs secretion could also be affected, which could reduce platelet adhesion to endothelial cells in *Npc1*$^{-/-}$ mice. WPBs are the unique LROs in endothelial cells and harbor a range of bioactive substances that participate in hemostasis, vasomotion, inflammation and fibrinolysis (3). The main constituent protein of WPBs is the haemostatic protein von Willebrand Factor (vWF) and P-selectin, which are involved in haemostasis and inflammation in the development of cardiovascular diseases (200). Intriguingly, it has been reported that trafficking defects of P-selectin and CD63/LAMP-3 and failure to reach WPBs occur in U18666A-treated HUVEC cells (3). Therefore, it would be of interest to investigate potential secretion defects and molecular mechanisms of WPBs secretion *in vitro* and *in vivo* in NPC1 disease models.

Figure 5.17. Working model of impaired thrombus formation in *Npc1*$^{-/-}$ mice.

When vascular injury occurs, endothelial cells secrete Weibel-Palade bodies (WPBs) leading to the surface expression of P-selectin and von Willebrand factor (vWF). Platelets can adhere to the site of injury when GP Ib/IX/V complex expressed on the platelet surface binds to the sub-endothelial vWF. This event can trigger the synthesis and release of TXA_2, serotonin, and ADP and cause activation of several platelet receptors. These events also cause a conformational change in GP IIb/IIIa, enabling the high-affinity binding of fibrinogen resulting in thrombus formation.

- However, the acidic store calcium signaling defect in *Npc1*$^{-/-}$ platelet affects α-granule and potentially endothelial cell Weibel–Palade bodies secretion impairing platelets-endothelial cell interactions and reducing thrombus size and formation in *Npc1*$^{-/-}$ mice.
- *In vitro* studies show that both P-selectin and CD63/LAMP-3 accumulate in late endosomes and fail to reach Weibel–Palade bodies efficiently in U18666A-treated HUVEC cells (3). This figure was adapted from Wagner et al., 2004.

In addition, NAADP is also involved in histamine-induced Ca^{2+} release via the H1R in human endothelial cells (201). Furthermore, this study highlighted a novel pathway for H1 receptor signaling whereby receptor activation leads to intracellular Ca^{2+} release directly and specifically stimulated by NAADP, which in turn regulates the exocytosis of vWF from WPBs (201). Therefore, it would be of interest to investigate any endothelial cells LRO secretion defects in *Npc1*$^{-/-}$ mice. These studies may also help provide a mechanistic link between LROs secretion defects and acidic compartment signaling in NPC1 disease.

Taken together, our current studies have demonstrated that *Npc1*$^{-/-}$ platelets have functional defects, including abnormal circulating platelets counts, platelets activation and *in vivo* thrombus formation defects in the murine model of NPC1 disease. Furthermore, our studies indicated that these *Npc1*$^{-/-}$ platelets functional defects could be associated with the impaired acidic stores calcium signaling in NPC1 disease model.

Chapter 6

General Discussion, Future Prospects and Concluding Remarks

Chapter 6: General Discussion, Future Prospects and Concluding Remarks

6.1 General discussion

In this thesis, we have investigated whether metal dysregulation is involved in the underlying pathogenic cascades in NPC1 disease. In our previous studies, we found progressive systemic iron deficiency in murine models of the GM1 and GM2 gangliosidoses and demonstrated that iron supplementation therapy was of benefit (106). In **chapter 2** of this thesis, we extended our studies to a mouse model of NPC1 disease. We identified a number of hematological abnormalities, including low HGB levels, microcytic erythrocytes and increased circulating platelet counts in *Npc1*$^{-/-}$ mice. Furthermore, our studies indicated that the hematological abnormalities could be related to iron deficiency in *Npc1*$^{-/-}$ mice. Iron homeostasis is affected by many pathophysiological factors, including (i) systemic inflammation, (ii) tissue hypoxia, (iii) anemia, (iv) and abnormal erythropoiesis. The observations of abnormal iron homeostasis in *Npc1*$^{-/-}$ mice could relate to one or more of these pathophysiological factors (26). In our previous studies, we found systemic iron dysregulation induced hematological changes in GM1 (*β-gal*$^{-/-}$) and GM2 gangliosidoses (*Hexb*$^{-/-}$) mice (106). In these two gangliosidoses murine models, there was progressive tissue iron deficiency and iron supplementation therapy was of benefit (106). However, when we compared the functional iron deficiency phenotypes in *Npc1*$^{-/-}$ mice with GM1 and GM2 gangliosidoses mice, we found some similarities but also significant differences between these three related LSDs. As summarized in **Table 6.1**, we previously identified (i) progressively systemic iron deficiency, (ii) inflammatory associated microcytic and macrocytic anemia, (iii) elevated levels of hepatic pro-inflammatory cytokines, such as IL-6 and (iv) up-regulated hepatic hepcidin levels in GM1 and GM2 gangliosidoses mice (106). Similarly, progressive peripheral iron deficiency and more severe microcytic anemia were identified in *Npc1*$^{-/-}$ mice. However, we found that hepatic IL-1β and hepcidin levels were significantly down-regulated in *Npc1*$^{-/-}$ mice, in contrast to upregulation in the GM1 and GM2 gangliosidosis mouse models and this may be the result of dysregulation of the

inflammasome (Platt et al unpublished observation) (106). These findings suggest that there are mechanistic differences in the iron deficiency phenotypes between *Npc1*$^{-/-}$ mice and GM1/GM2 gangliosidosis mice. Since our previous studies found that NPC1 disease is characterized by a unique lysosomal calcium store filling defect and abnormal hepatic expression of two-pore channels (TPC-1 & TPC-2) were observed in *Npc1*$^{-/-}$ mice, these observations suggested that the lysosomal calcium signaling defect characteristic of NPC1 disease is likely involved in the regulation of abnormal hepatic pro-inflammatory cytokines and hepcidin expressions in *Npc1*$^{-/-}$ mice (127, 184, 202). These hypotheses need to further investigate in the future and could potentially reveal the importance of lysosomal calcium-mediated intracellular signaling in the regulation of systemic inflammatory responses and iron homeostasis.

Table 6.1 Comparison of of functional iron deficiency phenotypes in GM1/ GM2 gangliosidoses (*β-gal*$^{-/-}$ *and Hexb*$^{-/-}$) mice and *Npc1*$^{-/-}$ mice.

Laboratory measures	Anemia in NPC1 disease mice	Anemia in GM1/GM2 gangliosidoses mice
Serum ferritin	↑	↑
Serum/hepatic iron	↓	↓
Transferrin	Normal	-
Transferrin saturation	↓	↓
Mean corpuscular volume	↓	↓
Hemoglobin	↓	↓
s - TfR	↑	↑
Hepatic cytokine contents	↑ or ↓	↑
Hepcidin	↓	↑

Lysosomal Ca^{2+} dys-regulation in NPC1 disease ???

In **Chapter 2 & 3** of the thesis, we further investigated the systemic iron dysregulation phenotypes and explored the potential mechanistic links between iron dyshomeostasis and

lysosomal dysfunction in *Npc1*$^{-/-}$ mice. In addition, the potential therapeutic effects of iron supplementation were evaluated in *Npc1*$^{-/-}$ mice. We found peripheral iron deficiency in *Npc1*$^{-/-}$ mice. This observation suggested that iron dysregulation could be associated with defective regulation of subcellular iron compartmentalization. Since cellular iron content can be regulated by different subcellular compartments, including cytosolic, mitochondrial and lysosomal compartments, our microarray data suggested that NPC1 iron dysregulation phenotypes could affect all of these subcellular compartments (44, 52, 98). However, the detailed mechanisms of systemic iron dysregulation remain to be further explored. It will be of interest to investigate lysosomal iron content and bioimaging of metal distribution in *Npc1*$^{-/-}$ cells and *Npc1*$^{-/-}$ tissue samples using novel lysosomal iron probes and biophysical techniques, such as laser ablation inductively coupled plasma mass spectrometry (LA-ICP-MS) to screen whole brain metal distribution imaging (203-205). We also need to evaluate the potential therapeutic effects of novel intracellular iron-modulating agents on the NPC1 disease murine model and determine whether these compounds could correct the hematological abnormalities and systemic/cellular iron dysregulation phenotypes that we have defined in NPC1 disease models.

Interestingly, subcellular iron compartmentalization defects have been recently reported in certain mitochondrial and lysosomal iron metabolism defect disorders, including Friedreich's ataxia, siderocytic anemia and transient receptor potential cation channel Mucolipin1 (TRPML1) disorders (52, 98, 206). Since subcellular iron compartmentalization defects have been identified in these human genetic disorders, further studies on these diseases could provide new therapeutic strategies to treat multiple disorders. The first potential iron-targeting therapeutic strategy is to supply cytosolic iron with the aim of ameliorating the cytosolic iron deficiency in these disorders. The second strategy is to remove excess iron from organelles, for example, using mitochondrial targeting iron chelators, e.g. pyridoxal isonicotinoyl hydrazine (130) and salicylaldehyde isonicotinoyl hydrazone (SIH) (128, 207, 208). Finally, iron ionophores could also be considered, which aim to redistribute subcellular iron contents from different subcellular compartments to achieve a more

physiologically balanced distribution of iron (209). However, one potential difficulty is that delivering exogenous iron through supplementation may worsen the hepatic disease and neuropathology if it is not targeted to the appropriate molecular machinery. Hence, a delicate balance using combined therapies that replenish the iron-deficient cytosol and chelate subcellular-compartment iron pools could theoretically be the optimal therapeutic strategy**.** However, in terms of systemic and cellular iron metabolism, it might be a very complicated issue in LSDs or non-LSDs iron metabolism disorders as the lysosome is involved in many different aspects of iron homeostasis. These defects could affect enterocyte mediated iron absorption, hepatocyte-mediated iron storage, bone marrow and splenic reticuloendothelial system-mediated iron utilization and recycling and further impair systemic iron homeostasis **(Figure 6.1)** (26, 117).

Figure 6.1. Proposed working model of systemic and cellular lysosomal dysfunction causing defects in iron metabolism, including iron uptake, storage, utilization and recycling in LSDs. In LSDs, systemic lysosomal dysfunction and inflammatory cytokines could impair enterocytes and macrophage mediated iron absorption and recycling. In addition, Tf uptake/TfR-1 recycling defects and impaired cellular ferritin synthesis could also affect iron metabolism at the cellular level.

Although in **Chapter 2 & 3** we mainly focused on the hematological abnormalities and peripheral iron dysregulation phenotypes in NPC1 disease, our preliminary results from proteomic analysis indicated that iron dysregulation phenotypes also occurs in the CNS of *Npc1*$^{-/-}$ mice and NPC1 patients. In the CNS, dysregulation of trace metal homeostasis has been considered to be one of the major contributing factors of neurotoxicity in several severe neurodegenerative diseases, such as Menke's, Wilson's, Alzheimer's, Parkinson's, Friedreich's ataxia and prion diseases (79, 142, 210, 211). Furthermore, systemic metal dysregulation has been suggested to be involved in the production of intracellular reactive oxygen species (ROS), which leads to lipid peroxidation, mitochondrial, lysosomal dysfunction and DNA damage **(Figure 6.2)** (113).

Figure 6.2. Proposed working model of iron dyshomeostasis in LSDs. In LSDs, lysosomal dysfunction could affect intracellular iron homeostasis, including cellular iron uptake, subcellular iron distribution, storage and utilization. These cellular iron dyshomeostasis could lead to intracellular free radical production via the Fenton reaction, which could further increase cellular oxidative stress, cause mitochondrial dysfunction, lipid peroxidation and DNA damage.

However, it should be noted that several studies have suggested that there are separated iron regulatory systems in peripheral organs versus the CNS. Therefore, further studies would be needed to investigate the metal dysregulation phenotypes in the CNS in NPC1 disease, which could provide important mechanistic insights into metal dysregulation in NPC1 and other neurodegenerative LSDs (149).

There is increasing evidence that systemic iron metabolism is closely linked to copper and zinc regulation, so in **Chapter 4** we extended our studies to other transition metal ions in *Npc1*$^{-/-}$ mice (146). We found altered cellular and systemic copper and zinc homeostasis *in vitro* and *in vivo* in NPC1 disease cellular/murine models. Furthermore, mis-trafficking of cytosolic copper ATPase transporters, MNK ATP7A and WND ATP7B, were observed along with subcellular compartmentalization defects of intracellular zinc, in NPC1 disease cell line models **(Table 6.2)**. Therefore, several different copper/zinc manipulation therapies, including (i) copper chelator with D-penicillamine, (ii) copper/zinc ionophore with clioquinol (iii) and reduced intestinal copper absorption treatment using zinc acetate were evaluated in *Npc1*$^{-/-}$ mice and demonstrated that these metal-related treatments differentially improved function and/or survival in *Npc1*$^{-/-}$ mice.

When we compared the copper dysregulation phenotypes of Wilson's disease and NPC1 disease, it was unclear what the subcellular copper distribution was in *Npc1*$^{-/-}$ disease cells (165). Interestingly, lysosomal dysfunction associated copper metabolism defects have been reported in a mouse model of one of the LRO diseases, Chediak-Higashi syndrome (Beige

mouse) (212). In the beige mouse, it has been suggested that lysosomal dysfunction and phagocytic defects restricted the ability of hepatocytes to store excess amounts of copper in the lysosomal system when beige mice were given a copper supplement (i.p) (212). Furthermore, the studies also suggested that the endosomal/lysosomal functional defects could cause hepatic subcellular copper distribution changes in Beige mice (212). Therefore, on the basis of our current findings and other previous studies from other groups, these observations may raise an intriguing possibility that (i) impaired subcellular copper trafficking (ii) and mis-localization of MNK ATP7A and WND ATP7B transporters may belong to one of the unidentified common pathogenesis cascades in most LSDs. If this hypothesis is correct, it may provide some novel therapeutic targets and several potential copper-related therapeutic strategies to modulate disease progression of lysosome and LROs dysfunctional diseases.

In **Chapter 5**, we investigated the molecular mechanisms leading to platelet dysfunction in NPC1 disease. The NPC1 protein appears to be crucial for megakaryocytes/platelets LROs function and its deficiency would impair platelet aggregation and activation when stimulated with thrombin. Since our previous studies have shown that NPC1 dysfunction would lead to disrupt acidic store calcium content, which accounts for the failure of late endosomes/lysosomes fusion and the complex pattern of downstream, lipid storage observed in this disease (22). Therefore, these findings suggested that acidic compartment calcium flux defects from *Npc1*$^{-/-}$ megakaryocytes/platelets and U18666A induced NPC1 disease phenotypes in MEG-01 cells could provide the potential mechanistic link with the platelet dysfunctional phenotypes observed in NPC1 disease (196). Since platelet activation and aggregation are highly dependent of intracellular calcium-mediated signaling, the thrombin-induced platelets aggregation and granules release defects in *Npc1*$^{-/-}$ mice could result from intracellular calcium signaling defects (213). NAADP is a novel calcium-mobilizing second messenger, which targets intracellular acidic stores (127). Since Churchill and colleagues recently demonstrated that thrombin and collagen-related-peptide (CRP) mediate human platelet aggregation, activation are highly dependent on NAADP-

mediated calcium signaling, it would be of interest to further investigate the potential role of NAADP-mediated signaling in *Npc1*$^{-/-}$ megakaryocytes/platelets (187).

It should also be noted that several recent studies have made some interesting observations about the potential biological functions of NPC1 and NPC2 proteins and their presence in LROs of certain specialized cellular types, such as lamellar-bodies in lung type II cells (197). Consistent with this hypothesis and other findings, our current studies suggest that the NPC1 protein may play a crucial role in granule secretion in megakaryocytes and platelets, although the exact molecular mechanisms remain to be elucidated (91). So far, our findings indicated that NPC1 deficiency would lead to the development of abnormal granules morphology and increased intracellular vacuolation in *Npc1*$^{-/-}$ platelets. Interestingly, when we compared the *Npc1*$^{-/-}$ platelet dysfunctional phenotypes with other LSDs or LRO dysfunctional disorders, such as Tangier disease, Hermansky–Pudlak syndrome (HPS) and Chediak–Higashi Syndrome (99) (99), we found certain similarities and differences among these three disorders (8, 182, 196). One of the common features is that these disorders all have intracellular calcium homeostasis defects, either ER or LE/Lys (196). Since intracellular calcium-mediated signaling is crucial for intracellular vesicles fusion and fission events, defects in acidic compartments calcium homeostasis could lead to abnormal intracellular vesicles trafficking, storage and impair the cellular trafficking system (196). In addition, we also found that melanin/melanosomes formation defect occur in U18666A-treated murine melanocytes, which suggested that NPC1 might be crucial for melanin/melanosome formation (**data not shown**) (198). This observation is supported by a recent study, which indicated the in retinal pigment epithelial cells melanin formation defects occur in *Npc1*$^{-/-}$ mice (199). However, another intriguing possibility should also be considered that the impaired subcellular copper trafficking in U18666A-treated melanocytes could cause copper ion incorporation defects into tyrosinase. Interestingly, mis-localization of MNK ATP7A copper transporter into early endosomes and hypo-pigmentation have been recently reported in one of the LROs dysfunctional diseases, Hermansky-Pudlak syndrome (HPS) BLOC-1$^{-/-}$ cells (6). Therefore, these observations may again indicate that disruption of intracellular

copper and other metal ions trafficking may be affected in other LSDs or LROs dysfunctional disorders. If our hypothesis is correct, intracellular copper trafficking efficiency should be studied in other LSDs. In addition, we also plan to study TPC-2 human skin melanocytes or Ned-19-treated melanocytes (Ned-19 is a drug that inhibits TPCs function blocking acidic store calcium release (187)) since hypo-pigmentation has been reported in humans with TPC-2 mutations and also these disease cells have impaired intracellular substrates trafficking and lysosomal calcium flux defects shared with NPC1 disease (214). Therefore, on the basis of our current findings and studies from other groups, these observations suggest that the NPC1 protein may not only be involved in the regulation of lysosome functions but is also involved in LROs functions in certain specialized cell types **(Figure 6.3)**.

Figure 6.3. Summarized of LROs dysfunction in NPC1 disease. This figure summarized the LROs functional defects identified in NPC1 disease murine model. The intracellular substrates trafficking defects and impaired acidic compartment calcium signaling could affect LROs secretion, such as melanosomes, lamellar bodies, lytic granules and platelet α-, δ- granules, in NPC1 disease.

We will therefore investigate whether NPC1 deficiency results in functional defects in (i) mast cell basophilic granules, (ii) Weibel Palade bodies of endothelial cells, (iii) azurophilic granules of neutrophils and eosinophils, (iv) osteoclast granules (v) and renin granules of juxtaglomerular cells **(Table 6.3) (6)**. These investigations may help gain further insight into the regulation of LROs and provide a better understanding of the underlying molecular mechanisms that drive pathogenesis in NPC1 disease and in other LROs dysfunctional disorders.

6.2. Future work and implications

Future work: Lysosomal Storage Diseases and Iron Metabolism

A key question is whether metal dysregulation is a common feature of LSDs and LROs dysfunctional disorders **(Table 6.4)** (98, 106, 168, 212, 215-217). Since LSDs are mainly characterized by (i) impaired autophagy, (ii) intracellular signaling/trafficking defects, (iii) altered lysosomal number, volume and lysosomal membrane permeability, all these lysosome dysfunctional defects could be involved in the regulation of systemic and cellular iron and other transition metal ions homeostasis (18, 97). Therefore, broader studies of systemic and cellular transition metal metabolism would be needed in the LSDs field.

Table 6.4 Summary of metal dysregulation identified in LSDs and LRO dysfunctional diseases

Lysosomal Sotrgae Diseases		Fe	Cu	Zn	Mn
Kufor-Rakeb disease, PARK9	***PARK9*$^{-/-}$**	+			+
GM1 gangliosidosis	***B-gal*$^{-/-}$**	+	**?**	**?**	
GM2 ganglisidosis	***Hexb*$^{-/-}$**	+	**?**	**?**	
Fucosidosis		+			
Mucolipidosis type IV	***Mucoln*$^{-/-}$**	+		+	
Niemann-Pick type C 1	***Npc1*$^{-/-}$**	+	+	+	+
CLN6 Neuronal Ceroid lipofuscinosis	***CLN6*$^{-/-}$**			+	+
Chediak–Higashi syndrome	***Chs1*$^{-/-}$**		+		

Copper manipulation therapies in NPC1 disease

In Chapter 4, we demonstrated the potential therapeutic value of copper-manipulation therapies in NPC1 disease murine model, which could be trialed in patients with NPC1 disease. So far, we have evaluated three different clinically approved copper manipulation therapies in *Npc1*$^{-/-}$ mice, including copper chelator (D-Penicillamine), copper/zinc ionophore (clioquinol) and reducing intestinal copper absorption therapy using zinc acetate (163, 169, 218). Since the *in vivo* animal studies were encouraging, it would be worth evaluating other clinically approved copper chelating reagents, such as Trientine and Teterthiomolybdate, in

Npc1$^{-/-}$ mice and testing different administration routes/therapeutic dosages to determine which copper manipulation therapy could provide the greatest potential clinical benefit **(Table 6.5)**.

Drug	Dosage (mg/kg/day)	Age started	Pharmacological Mechanism	Note
Trientine	**0.8~1.0 w/w, mix with diet**	**3 weeks**	**Cu2+ chelator and urinary excretion**	**Chelate free Cu^{2+}** **- Clinically approved treatment for Wilson's disease (copper overload disease)**
Teterthiomolybdate	**5 mg/kg, i.p (7 times/per week)**	**3 weeks**	**Blocking the intestinal absorption of copper and a copper chelator**	**- Clinically approved treatment for Wilson's disease**
Galzin (Zinc acetate)	**30 ~ 150 mg/ kg/day, mix with diet**	**3 weeks**	**Inhibition intestinal copper absorption**	**Induce intestinal metallothioneins (MTs) expression to bind free Cu^{2+}** **- Clinically approved treatment for Wilson's disease** **- Optimized the therapeutic dosage for combination treatment with miglustat**

In addition, it would also be an attractive option to combine these metal-related treatments with other existing clinically approved therapies, such as substrate reduction therapy with miglustat, to determine if this combination provides synergistic benefit **(Figure 6.4)**.

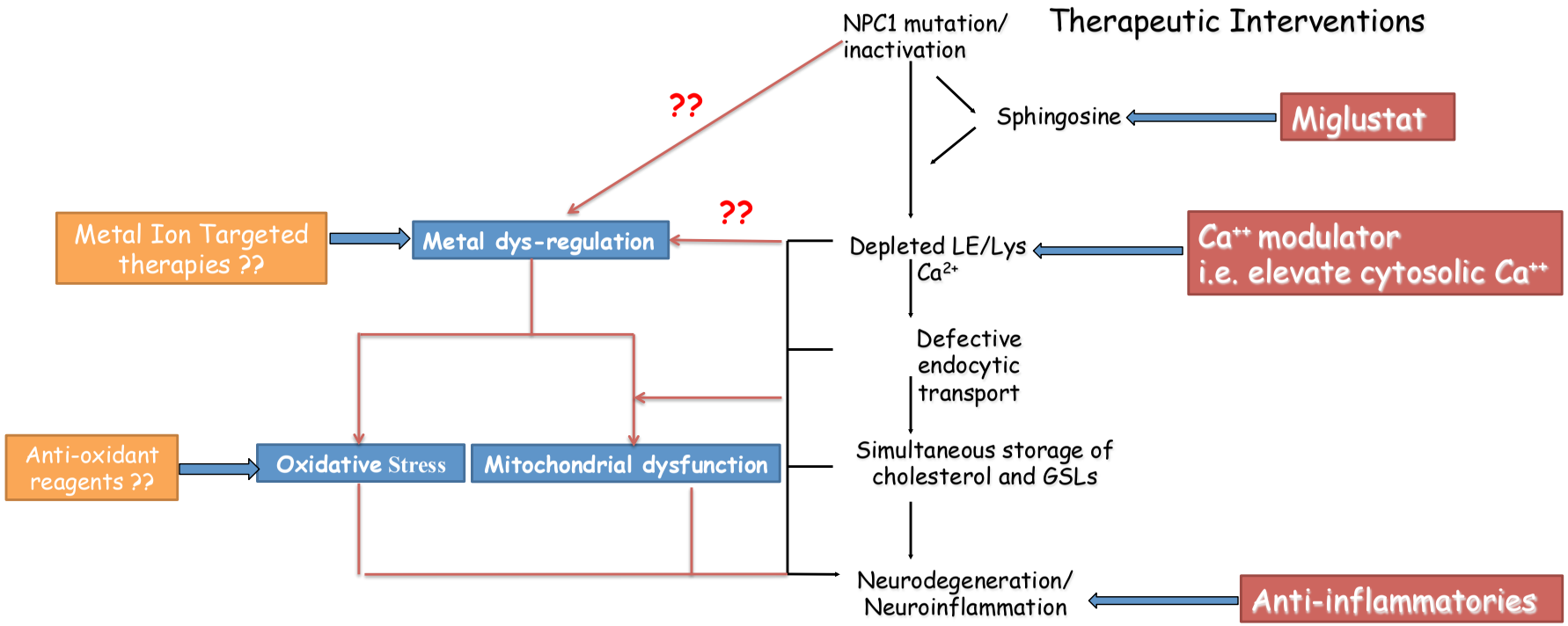
NPC1 mutation/
inactivation
Therapeutic Interventions
??
Sphingosine
Miglustat
Metal Ion Targeted
therapies ??
Metal dys-regulation
??
Depleted LE/Lys
Ca2+
Ca++ modulator
i.e. elevate cytosolic Ca++
Defective
endocytic
transport
Anti-oxidant
reagents ??
Oxidative Stress
Mitochondrial dysfunction
Simultaneous storage of
cholesterol and GSLs
Neurodegeneration/
Neuroinflammation
Anti-inflammatories

Figure 6.4. Proposed working model of the underlying pathogenesis of NPC1 disease and its related potential therapies. (i) Substrate reduction therapy (e.g., miglustat), (ii) Ca^{2+} modulator (e.g., curcumin), (iii) metal manipulation therapies (e.g., iron supplementation, copper/zinc metal ionophore), (iv) anti-oxidants (e.g., N-acetylcysteine), (v) anti-inflammatory reagents (e.g., ibuprofen, anti-TNF-α antibodies) could be potential therapies or adjunctive therapies for the treatments of NPC1 disease.

6.3 Concluding Remarks

In this thesis, we have demonstrated that metal dysregulation is involved in the pathogenesis of NPC1 disease in *in vitro* and *in vivo* models. Similar findings were also observed in NPC1 patients, especially the iron dysregulation and hematological abnormalities. We have investigated the mechanisms leading to these defects and uncovered a highly complex set of factors that may contribute to these disease phenotypes. These studies also identified several metal-related peripheral blood and CSF biomarkers, which could have practical utility for monitoring disease progression and response to therapies. In addition, we have also evaluated several metal manipulation and combination therapies in *Npc1*$^{-/-}$ mice. Several of these therapies revealed functional improvements and improved survival in treated animals paving the way for clinical studies in the future **(Table 6.6)**.

In addition, we also demonstrated the importance of the NPC1 protein in the regulation of LROs functions in megakaryocytes and platelets. Moreover, our findings indicated that impaired acidic compartment calcium release may affect platelet aggregation, activation and α-granules release in *Npc1*$^{-/-}$ mice. However, there are still several crucial questions that need to be answered including

- Is metal dysregulation involved in other LSDs?
- Do NAADP-mediated acid compartment calcium flux defects occur in primary *Npc1*$^{-/-}$ megakaryocytes and *Npc1*$^{-/-}$ platelets?
- Could the NPC1 disease murine model provide a system to study the regulated secretion of LROs contents and provide new insights into the molecular mechanisms of LROs biogenesis?

This knowledge will be critical to better understand fundamental cell biological processes, the molecular basis for pathogenesis in LSDs and lead to the development of novel therapeutic strategies for this group of devastating disorders.

References

References

1. Luzio JP, Pryor PR, Bright NA. Lysosomes: fusion and function. Nat Rev Mol Cell Biol 2007;8(8):622-632.

2. Saftig P, Klumperman J. Lysosome biogenesis and lysosomal membrane proteins: trafficking meets function. Nat Rev Mol Cell Biol 2009;10(9):623-635.

3. Kobayashi T, Vischer UM, Rosnoblet C, Lebrand C, Lindsay M, Parton RG, Kruithof EKO, Gruenberg J. The Tetraspanin CD63/lamp3 Cycles between Endocytic and Secretory Compartments in Human Endothelial Cells. Molecular Biology of the Cell 2000;11(5):1829-1843.

4. Roczniak-Ferguson A, Petit CS, Froehlich F, Qian S, Ky J, Angarola B, Walther TC, Ferguson SM. The transcription factor TFEB links mTORC1 signaling to transcriptional control of lysosome homeostasis. Sci Signal 2012;5(228):ra42.

5. Dell'Angelica EC, Mullins C, Caplan S, Bonifacino JS. Lysosome-related organelles. The FASEB Journal 2000;14(10):1265-1278.

6. Marks MS, Heijnen HFG, Raposo G. Lysosome-related organelles: unusual compartments become mainstream. Current Opinion in Cell Biology 2013;25(4):495-505.

7. Huizing M, Helip-Wooley A, Westbroek W, Gunay-Aygun M, Gahl WA. Disorders of lysosome-related organelle biogenesis: Clinical and molecular genetics. 2008. p. 359-386.

8. Li W, Rusiniak ME, Chintala S, Gautam R, Novak EK, Swank RT. Murine Hermansky–Pudlak syndrome genes: regulators of lysosome-related organelles. BioEssays 2004;26(6):616-628.

9. Fitch-Tewfik JL, Flaumenhaft R. Platelet granule exocytosis: a comparison with chromaffin cells. Front Endocrinol (Lausanne) 2013;4:77.

10. Flaumenhaft R. Molecular Basis of Platelet Granule Secretion. Arteriosclerosis, Thrombosis, and Vascular Biology 2003;23(7):1152-1160.

11. King SM, Reed GL. Development of platelet secretory granules. Seminars in Cell & Developmental Biology 2002;13(4):293-302.

12. Srivastava PC, Powling MJ, Nokes TJC, Patrick AD, Dawes J, Hardisty RM. Grey platelet syndrome: studies on platelet alpha-granules, lysosomes and defective response to thrombin. British Journal of Haematology 1987;65(4):441-446.

13. Whiteheart SW. Platelet granules: surprise packages. Blood 2011;118(5):1190-1191.

14. Zhang L, Orban M, Lorenz M, Barocke V, Braun D, Urtz N, Schulz C, von Brühl M-L, Tirniceriu A, Gaertner F, Proia RL, Graf T, Bolz S-S, Montanez E, Prinz M, *et al.* A novel role of sphingosine 1-phosphate receptor S1pr1 in mouse thrombopoiesis. The Journal of Experimental Medicine 2012;209(12):2165-2181.

15. Ambrosio AL, Boyle JA, Di Pietro SM. Mechanism of platelet dense granule biogenesis: study of cargo transport and function of Rab32 and Rab38 in a model system. Blood 2012;120(19):4072-4081.

16. Zhang L, Urtz N, Gaertner F, Legate KR, Petzold T, Lorenz M, Mazharian A, Watson SP, Massberg S. Sphingosine kinase 2 (Sphk2) regulates platelet biogenesis by providing intracellular sphingosine 1-phosphate (S1P). Blood 2013;122(5):791-802.

17. Roh Hyun C, Collier S, Guthrie J, Robertson JD, Kornfeld K. Lysosome-Related Organelles in Intestinal Cells Are a Zinc Storage Site in C. elegans. Cell Metabolism 2012;15(1):88-99.

18. Jeyakumar M, Dwek RA, Butters TD, Platt FM. Storage solutions: treating lysosomal disorders of the brain. Nat Rev Neurosci 2005;6(9):713-725.

19. Platt FM, Boland B, van der Spoel AC. Lysosomal storage disorders: The cellular impact of lysosomal dysfunction. The Journal of Cell Biology 2012;199(5):723-734.

20. Lloyd-Evans E, Platt FM. Lipids on Trial: The Search for the Offending Metabolite in Niemann-Pick type C Disease. Traffic 2010;11(4):419-428.

21. Daniel S O. The Niemann-Pick Disease Genes: Regulators of Cellular Cholesterol Homeostasis. Trends in Cardiovascular Medicine 2004;14(2):66-72.

22. Lloyd-Evans E, Morgan AJ, He X, Smith DA, Elliot-Smith E, Sillence DJ, Churchill GC, Schuchman EH, Galione A, Platt FM. Niemann-Pick disease type C1 is a sphingosine storage disease that causes deregulation of lysosomal calcium. Nat Med 2008;14(11):1247-1255.

23. Patterson MC, Hendriksz CJ, Walterfang M, Sedel F, Vanier MT, Wijburg F. Recommendations for the diagnosis and management of Niemann-Pick disease type C: an update. Mol Genet Metab 2012;106(3):330-344.

24. Scott C, Ioannou YA. The NPC1 protein: structure implies function. Biochimica et Biophysica Acta (BBA) - Molecular and Cell Biology of Lipids 2004;1685(1-3):8-13.

25. Vanier MT, Millat G. Structure and function of the NPC2 protein. Biochimica et Biophysica Acta (BBA) - Molecular and Cell Biology of Lipids 2004;1685(1-3):14-21.

26. Hentze MW, Muckenthaler MU, Galy B, Camaschella C. Two to Tango: Regulation of Mammalian Iron Metabolism. Cell 2010;142(1):24-38.

27. Andrews NC. Disorders of Iron Metabolism. New England Journal of Medicine 1999;341(26):1986-1995.

28. Ganz T, Nemeth E. Hepcidin and Disorders of Iron Metabolism. Annual Review of Medicine 2011;62(1):347-360.

29. Zhang D-L, Senecal T, Ghosh MC, Ollivierre-Wilson H, Tu T, Rouault TA. Hepcidin regulates ferroportin expression and intracellular iron homeostasis of erythroblasts. Blood 2011;118(10):2868-2877.

30. De Freitas JM, Meneghini R. Iron and its sensitive balance in the cell. Mutation Research/Fundamental and Molecular Mechanisms of Mutagenesis 2001;475(1–2):153-159.

31. De Domenico I, Ward DM, Langelier C, Vaughn MB, Nemeth E, Sundquist WI, Ganz T, Musci G, Kaplan J. The Molecular Mechanism of Hepcidin-mediated Ferroportin Down-Regulation. Molecular Biology of the Cell 2007;18(7):2569-2578.

32. White C, Yuan X, Schmidt Paul J, Bresciani E, Samuel Tamika K, Campagna D, Hall C, Bishop K, Calicchio Monica L, Lapierre A, Ward Diane M, Liu P, Fleming Mark D, Hamza I. HRG1 Is Essential for Heme Transport from the Phagolysosome of Macrophages during Erythrophagocytosis. Cell Metabolism 2013;17(2):261-270.

33. Qiao B, Sugianto P, Fung E, del-Castillo-Rueda A, Moran-Jimenez M-J, Ganz T, Nemeth E. Hepcidin-Induced Endocytosis of Ferroportin Is Dependent on Ferroportin Ubiquitination. Cell Metabolism 2012;15(6):918-924.

34. De Domenico I, Ward DM, Kaplan J. Hepcidin regulation: ironing out the details. The Journal of Clinical Investigation 2007;117(7):1755-1758.

35. Schmidt PJ, Toran PT, Giannetti AM, Bjorkman PJ, Andrews NC. The Transferrin Receptor Modulates Hfe-Dependent Regulation of Hepcidin Expression. Cell Metabolism 2008;7(3):205-214.

36. Peyssonnaux C, Zinkernagel AS, Schuepbach RA, Rankin E, Vaulont S, Haase VH, Nizet V, Johnson RS. Regulation of iron homeostasis by the hypoxia-inducible transcription factors (HIFs). The Journal of Clinical Investigation 2007;117(7):1926-1932.

37. Gao J, Chen J, Kramer M, Tsukamoto H, Zhang A-S, Enns CA. Interaction of the Hereditary Hemochromatosis Protein HFE with Transferrin Receptor 2 Is Required for Transferrin-Induced Hepcidin Expression. Cell Metabolism 2009;9(3):217-227.

38. De Domenico I, Zhang TY, Koening CL, Branch RW, London N, Lo E, Daynes RA, Kushner JP, Li D, Ward DM, Kaplan J. Hepcidin mediates transcriptional changes that modulate acute cytokine-induced inflammatory responses in mice. The Journal of Clinical Investigation 2010;120(7):2395-2405.

39. Silvestri L, Pagani A, Nai A, De Domenico I, Kaplan J, Camaschella C. The Serine Protease Matriptase-2 (TMPRSS6) Inhibits Hepcidin Activation by Cleaving Membrane Hemojuvelin. Cell Metabolism 2008;8(6):502-511.

40. Ganz T. Hepcidin, a key regulator of iron metabolism and mediator of anemia of inflammation. Blood 2003;102(3):783-788.

41. Robach P, Cairo G, Gelfi C, Bernuzzi F, Pilegaard H, Viganò A, Santambrogio P, Cerretelli P, Calbet JAL, Moutereau S, Lundby C. Strong iron demand during hypoxia-induced erythropoiesis is associated with down-regulation of iron-related proteins and myoglobin in human skeletal muscle. Blood 2007;109(11):4724-4731.

42. Rouault TA, Tong W-H. Tangled Up In Red: Intertwining of the Heme and Iron-Sulfur Cluster Biogenesis Pathways. Cell Metabolism 2009;10(2):80-81.

43. Takahashi-Makise N, Ward DM, Kaplan J. On the mechanism of iron sensing by IRP2: new players, new paradigms. Nat Chem Biol 2009;5(12):874-875.

44. Kon K, Kim J-S, Uchiyama A, Jaeschke H, Lemasters JJ. Lysosomal Iron Mobilization and Induction of the Mitochondrial Permeability Transition in Acetaminophen-Induced Toxicity to Mouse Hepatocytes. Toxicological Sciences 2010;117(1):101-108.

45. Kurz T, Eaton JW, Brunk UT. The role of lysosomes in iron metabolism and recycling. The International Journal of Biochemistry & Cell Biology 2011;43(12):1686-1697.

46. Uchiyama A, Kim J-S, Kon K, Jaeschke H, Ikejima K, Watanabe S, Lemasters JJ. Translocation of iron from lysosomes into mitochondria is a key event during oxidative stress-induced hepatocellular injury. Hepatology 2008;48(5):1644-1654.

47. Kidane TZ, Sauble E, Linder MC. Release of iron from ferritin requires lysosomal activity. American Journal of Physiology - Cell Physiology 2006;291(3):C445-C455.

48. De Domenico I, McVey Ward D, Kaplan J. Autophagy, ferritin and iron chelation. Autophagy 2010;6(1):157-157.

49. Kurz T, Eaton JW, Brunk UT. The role of lysosomes in iron metabolism and recycling. The International Journal of Biochemistry & Cell Biology 2011;43(12):1686-1697.

50. Foot NJ, Dalton HE, Shearwin-Whyatt LM, Dorstyn L, Tan S-S, Yang B, Kumar S. Regulation of the divalent metal ion transporter DMT1 and iron homeostasis by a ubiquitin-dependent mechanism involving Ndfips and WWP2. Blood 2008;112(10):4268-4275.

51. Cheng X, Shen D, Samie M, Xu H. Mucolipins: Intracellular TRPML1-3 channels. FEBS Letters 2010;584(10):2013-2021.

52. Stemmler TL, Lesuisse E, Pain D, Dancis A. Frataxin and Mitochondrial FeS Cluster Biogenesis. Journal of Biological Chemistry 2010;285(35):26737-26743.

53. Xu W, Barrientos T, Andrews NC. Iron and Copper in Mitochondrial Diseases. Cell Metabolism 2013;17(3):319-328.

54. Babady NE, Carelle N, Wells RD, Rouault TA, Hirano M, Lynch DR, Delatycki MB, Wilson RB, Isaya G, Puccio H. Advancements in the pathophysiology of Friedreich's Ataxia and new prospects for treatments. Molecular Genetics and Metabolism 2007;92(1–2):23-35.

55. Whitnall M, Rahmanto YS, Sutak R, Xu X, Becker EM, Mikhael MR, Ponka P, Richardson DR. The MCK mouse heart model of Friedreich's ataxia: Alterations in iron-regulated proteins and cardiac hypertrophy are limited by iron chelation. Proceedings of the National Academy of Sciences 2008;105(28):9757-9762.

56. Polishchuk R, Lutsenko S. Golgi in copper homeostasis: a view from the membrane trafficking field. Histochem Cell Biol 2013;140(3):285-295.

57. Forbes JR, Cox DW. Copper-dependent trafficking of Wilson disease mutant ATP7B proteins. Human Molecular Genetics 2000;9(13):1927-1935.

58. Holloway ZG, Velayos-Baeza A, Howell GJ, Levecque C, Ponnambalam S, Sztul E, Monaco AP. Trafficking of the Menkes copper transporter ATP7A is regulated by clathrin-, AP-2–, AP-1–, and Rab22-dependent steps. Molecular Biology of the Cell 2013;24(11):1735-1748.

59. Prohaska JR. Role of copper transporters in copper homeostasis. The American Journal of Clinical Nutrition 2008;88(3):826S-829S.

60. Martinelli D, Travaglini L, Drouin CA, Ceballos-Picot I, Rizza T, Bertini E, Carrozzo R, Petrini S, de Lonlay P, El Hachem M, Hubert L, Montpetit A, Torre G, Dionisi-Vici C. MEDNIK syndrome: a novel defect of copper metabolism treatable by zinc acetate therapy. Brain 2013;136(3):872-881.

61. Lönnerdal B. Intestinal regulation of copper homeostasis: a developmental perspective. The American Journal of Clinical Nutrition 2008;88(3):846S-850S.

62. Linz R, Lutsenko S. Copper-transporting ATPases ATP7A and ATP7B: cousins, not twins. J Bioenerg Biomembr 2007;39(5-6):403-407.

63. Weiss KH, Wurz J, Gotthardt D, Merle U, Stremmel W, Füllekrug J. Localization of the Wilson disease protein in murine intestine. Journal of Anatomy 2008;213(3):232-240.

64. Wilmarth PA, Short KK, Fiehn O, Lutsenko S, David LL, Burkhead JL. A systems approach implicates nuclear receptor targeting in the Atp7b-/- mouse model of Wilson's disease. Metallomics 2012;4(7):660-668.

65. Moos T, Trinder D, Morgan EH. Effect of iron status on DMT1 expression in duodenal enterocytes from β2-microglobulin knockout mice. American Journal of Physiology - Gastrointestinal and Liver Physiology 2002;283(3):G687-G694.

66. Lu Y, Kim C, Collins JF. Multiple Menkes copper ATPase (Atp7a) transcript and protein variants are induced by iron deficiency in rat duodenal enterocytes. Journal of Trace Elements in Medicine and Biology 2012;26(2–3):109-114.

67. Lutsenko S, Barnes NL, Bartee MY, Dmitriev OY. Function and Regulation of Human Copper-Transporting ATPases. Physiological Reviews 2007;87(3):1011-1046.

68. Stein J, Hartmann F, Dignass AU. Diagnosis and management of iron deficiency anemia in patients with IBD. Nat Rev Gastroenterol Hepatol 2010;7(11):599-610.

69. Goodnough LT, Nemeth E, Ganz T. Detection, evaluation, and management of iron-restricted erythropoiesis. Blood 2010;116(23):4754-4761.

70. Drakesmith H, Prentice A. Viral infection and iron metabolism. Nat Rev Micro 2008;6(7):541-552.

71. De Domenico I, McVey Ward D, Kaplan J. Regulation of iron acquisition and storage: consequences for iron-linked disorders. Nat Rev Mol Cell Biol 2008;9(1):72-81.

72. Dycke C, Charbonnier P, Pantopoulos K, Moulis J-M. A role for lysosomes in the turnover of human iron regulatory protein 2. The International Journal of Biochemistry & Cell Biology 2008;40(12):2826-2832.

73. Asano T, Komatsu M, Yamaguchi-Iwai Y, Ishikawa F, Mizushima N, Iwai K. Distinct Mechanisms of Ferritin Delivery to Lysosomes in Iron-Depleted and Iron-Replete Cells. Molecular and Cellular Biology 2011;31(10):2040-2052.

74. Radisky DC, Kaplan J. Iron in cytosolic ferritin can be recycled through lysosomal degradation in human fibroblasts. Biochem J 1998;336(1):201-205.

75. Richardson DR, Lane DJR, Becker EM, Huang ML-H, Whitnall M, Rahmanto YS, Sheftel AD, Ponka P. Mitochondrial iron trafficking and the integration of iron metabolism between the mitochondrion and cytosol. Proceedings of the National Academy of Sciences 2010;107(24):10775-10782.

76. Walkley SU, Suzuki K. Consequences of NPC1 and NPC2 loss of function in mammalian neurons. Biochimica et Biophysica Acta (BBA) - Molecular and Cell Biology of Lipids 2004;1685(1-3):48-62.

77. Frolov A, Zielinski SE, Crowley JR, Dudley-Rucker N, Schaffer JE, Ory DS. NPC1 and NPC2 Regulate Cellular Cholesterol Homeostasis through Generation of Low Density Lipoprotein Cholesterol-derived Oxysterols. Journal of Biological Chemistry 2003;278(28):25517-25525.

78. Holmes C, Cunningham C, Zotova E, Woolford J, Dean C, Kerr S, Culliford D, Perry VH. Systemic inflammation and disease progression in Alzheimer disease. Neurology 2009;73(10):768-774.

79. Zecca L, Youdim MBH, Riederer P, Connor JR, Crichton RR. Iron, brain ageing and neurodegenerative disorders. Nat Rev Neurosci 2004;5(11):863-873.

80. Eltzschig HK, Carmeliet P. Hypoxia and Inflammation. New England Journal of Medicine 2011;364(7):656-665.

81. Pentchev PG, Gal AE, Booth AD, Omodeo-Sale F, Fours J, Neumeyer BA, Quirk JM, Dawson G, Brady RO. A lysosomal storage disorder in mice characterized by a dual deficiency of sphingomyelinase and glucocerebrosidase. Biochimica et Biophysica Acta (BBA) - Lipids and Lipid Metabolism 1980;619(3):669-679.

82. Smith D, Wallom K-L, Williams IM, Jeyakumar M, Platt FM. Beneficial effects of anti-inflammatory therapy in a mouse model of Niemann-Pick disease type C1. Neurobiology of Disease 2009;36(2):242-251.

83. Yanjanin NM, Vélez JI, Gropman A, King K, Bianconi SE, Conley SK, Brewer CC, Solomon B, Pavan WJ, Arcos-Burgos M, Patterson MC, Porter FD. Linear clinical progression, independent of age of onset, in Niemann–Pick disease, type C. American Journal of Medical Genetics Part B: Neuropsychiatric Genetics 2010;153B(1):132-140.

84. Cluzeau CV, Watkins-Chow DE, Fu R, Borate B, Yanjanin N, Dail MK, Davidson CD, Walkley SU, Ory DS, Wassif CA, Pavan WJ, Porter FD. Microarray expression analysis and identification of serum biomarkers for Niemann-Pick disease, type C1. Hum Mol Genet 2012;21(16):3632-3646.

85. Jelkmann W. Regulation of erythropoietin production. The Journal of Physiology 2011;589(6):1251-1258.

86. Schofield CJ, Ratcliffe PJ. Oxygen sensing by HIF hydroxylases. Nat Rev Mol Cell Biol 2004;5(5):343-354.

87. Giordano FJ. Oxygen, oxidative stress, hypoxia, and heart failure. The Journal of Clinical Investigation 2005;115(3):500-508.

88. Liu Q, Berchner-Pfannschmidt U, Möller U, Brecht M, Wotzlaw C, Acker H, Jungermann K, Kietzmann T. A Fenton reaction at the endoplasmic reticulum is involved in the redox control of hypoxia-inducible gene expression. Proceedings of the National Academy of Sciences 2004;101(12):4302-4307.

89. Muralidhar A, Borbon IA, Esharif DM, Ke W, Manacheril R, Daines M, Erickson RP. Pulmonary function and pathology in hydroxypropyl-beta-cyclodextin-treated and untreated Npc1−/− mice. Molecular Genetics and Metabolism 2011;103(2):142-147.

90. Ramirez CM, Lopez AM, Le LQ, Posey KS, Weinberg AG, Turley SD. Ontogenic changes in lung cholesterol metabolism, lipid content, and histology in mice with Niemann-Pick type C disease. Biochim Biophys Acta 2013(0).

91. Roszell BR, Tao J-Q, Yu KJ, Gao L, Huang S, Ning Y, Feinstein SI, Vite CH, Bates SR. Pulmonary Abnormalities in Animal Models Due to Niemann-Pick Type C1 (NPC1) or C2 (NPC2) Disease. PLoS ONE 2013;8(7):e67084.

92. Fischer R, Simmerlein R, Huber RM, Schiffl H, Lang SM. Lung disease severity, chronic inflammation, iron deficiency, and erythropoietin response in adults with cystic fibrosis. Pediatric Pulmonology 2007;42(12):1193-1197.

93. Ginzburg Y, Rivella S. β-thalassemia: a model for elucidating the dynamic regulation of ineffective erythropoiesis and iron metabolism. Blood 2011;118(16):4321-4330.

94. Simons K, Ikonen E. Functional rafts in cell membranes. Nature 1997;387(6633):569-572.

95. Takamura A, Sakai N, Shinpoo M, Noguchi A, Takahashi T, Matsuda S, Yamamoto M, Narita A, Ohno K, Ohashi T, Ida H, Eto Y. The useful preliminary diagnosis of Niemann-Pick disease type C by filipin test in blood smear. Mol Genet Metab 2013(0).

96. Zhou S, Davidson C, McGlynn R, Stephney G, Dobrenis K, Vanier MT, Walkley SU. Endosomal/Lysosomal Processing of Gangliosides Affects Neuronal Cholesterol Sequestration in Niemann-Pick Disease Type C. The American Journal of Pathology 2011;179(2):890-902.

97. Futerman AH, van Meer G. The cell biology of lysosomal storage disorders. Nat Rev Mol Cell Biol 2004;5(7):554-565.

98. Dong X-P, Cheng X, Mills E, Delling M, Wang F, Kurz T, Xu H. The type IV mucolipidosis-associated protein TRPML1 is an endolysosomal iron release channel. Nature 2008;455(7215):992-996.

99. Nicholson AG, Florio R, Hansell DM, du Bois RM, Wells AU, Hughes P, Ramadan HK, Mackinlay CI, Brambilla E, Ferretti GR, Erichsen A, Malone M, Lantuejoul S. Pulmonary involvement by Niemann–Pick disease. A report of six cases. Histopathology 2006;48(5):596-603.

100. Field FJ, Watt K, Mathur SN. TNF-α decreases ABCA1 expression and attenuates HDL cholesterol efflux in the human intestinal cell line Caco-2. Journal of Lipid Research 2010;51(6):1407-1415.

101. Steven L, Driver C. Niemann-Pick Disease Type C and Crohn's Disease. Scottish Medical Journal 2005;50(2):80-81.

102. Chua E, Clague JE, Sharma AK, Horan MA, Lombard M. Serum transferrin receptor assay in iron deficiency anaemia and anaemia of chronic disease in the elderly. QJM 1999;92(10):587-594.

103. Suominen P, Punnonen K, Rajamäki A, Irjala K. Serum Transferrin Receptor and Transferrin Receptor-Ferritin Index Identify Healthy Subjects With Subclinical Iron Deficits. Blood 1998;92(8):2934-2939.

104. Punnonen K, Irjala K, Rajamäki A. Serum Transferrin Receptor and Its Ratio to Serum Ferritin in the Diagnosis of Iron Deficiency. Blood 1997;89(3):1052-1057.

105. Cohen LA, Gutierrez L, Weiss A, Leichtmann-Bardoogo Y, Zhang D-l, Crooks DR, Sougrat R, Morgenstern A, Galy B, Hentze MW, Lazaro FJ, Rouault TA, Meyron-Holtz EG.

Serum ferritin is derived primarily from macrophages through a nonclassical secretory pathway. Blood 2010;116(9):1574-1584.

106. Jeyakumar M, Williams I, Smith DA, Cox TM, Platt FM. Critical role of iron in the pathogenesis of the murine gangliosidoses. Neurobiology of Disease 2009;34(3):406-416.

107. Christomanou H, Kellermann J, Link RP, Harzer K. Deficient Ferritin Immunoreactivity in Visceral Organs from Four Patients with Niemann-Pick Disease Type C. Biochemical and Molecular Medicine 1995;55(2):105-115.

108. Christomanou H, Vanier MT, Santambrogio P, Arosio P, Kleijer WJ, Harzer K. Deficient Ferritin Immunoreactivity in Tissues from Niemann–Pick Type C Patients: Extension of Findings to Fetal Tissues, H and L Ferritin Isoforms, but also One Case of the Rare Niemann–Pick C2 Complementation Group. Molecular Genetics and Metabolism 2000;70(3):196-202.

109. Christomanou H, Harzer K. Ouchterlony Double Immunodiffusion Method Demonstrates Absence of Ferritin Immunoreactivity in Visceral Organs from Nine Patients with Niemann-Pick Disease Type C. Biochemical and Molecular Medicine 1996;58(2):176-183.

110. Yanagimoto C, Harada M, Kumemura H, Koga H, Kawaguchi T, Terada K, Hanada S, Taniguchi E, Koizumi Y, Koyota S, Ninomiya H, Ueno T, Sugiyama T, Sata M. Niemann-Pick C1 protein transports copper to the secretory compartment from late endosomes where ATP7B resides. Experimental Cell Research 2009;315(2):119-126.

111. Nikaido H, Takatsuka Y. Mechanisms of RND multidrug efflux pumps. Biochimica et Biophysica Acta (BBA) - Proteins and Proteomics 2009;1794(5):769-781.

112. Eaton JW, Qian M. Molecular bases of cellular iron toxicity. Free Radical Biology and Medicine 2002;32(9):833-840.

113. Arosio P, Levi S. Ferritin, iron homeostasis, and oxidative damage. Free Radical Biology and Medicine 2002;33(4):457-463.

114. Kühn LC. How Iron Controls Iron. Cell Metabolism 2009;10(6):439-441.

115. Andrews NC. Closing the Iron Gate. New England Journal of Medicine 2012;366(4):376-377.

116. Zhang Y, Mikhael M, Xu D, Li Y, Soe-Lin S, Ning B, Li W, Nie G, Zhao Y, Ponka P. Lysosomal Proteolysis Is the Primary Degradation Pathway for Cytosolic Ferritin and Cytosolic Ferritin Degradation Is Necessary for Iron Exit. Antioxidants & Redox Signaling 2010;13(7):999-1009.

117. Camaschella C. Treating Iron Overload. New England Journal of Medicine 2013;368(24):2325-2327.

118. Simpson RJ, McKie AT. Regulation of Intestinal Iron Absorption: The Mucosa Takes Control? Cell Metabolism 2009;10(2):84-87.

119. Kimber C, Weintraub LR. Malabsorption of Iron Secondary to Iron Deficiency. New England Journal of Medicine 1968;279(9):453-459.

120. Dunn LL, Rahmanto YS, Richardson DR. Iron uptake and metabolism in the new millennium. Trends in Cell Biology 2007;17(2):93-100.

121. Vitner EB, Platt FM, Futerman AH. Common and Uncommon Pathogenic Cascades in Lysosomal Storage Diseases. Journal of Biological Chemistry 2010;285(27):20423-20427.

122. Spiegel R, Raas-Rothschild A, Reish O, Regev M, Meiner V, Bargal R, Sury V, Meir K, Nadjari M, Hermann G, Iancu TC, Shalev SA, Zeigler M. The clinical spectrum of fetal Niemann–Pick type C. American Journal of Medical Genetics Part A 2009;149A(3):446-450.

123. Vruchte Dt, Lloyd-Evans E, Veldman RJ, Neville DCA, Dwek RA, Platt FM, van Blitterswijk WJ, Sillence DJ. Accumulation of Glycosphingolipids in Niemann-Pick C Disease Disrupts Endosomal Transport. Journal of Biological Chemistry 2004;279(25):26167-26175.

124. Yiannis A I. The Structure and Function of the Niemann–Pick C1 Protein. Molecular Genetics and Metabolism 2000;71(1-2):175-181.

125. Mims MP, Prchal JT. Divalent metal transporter 1. Hematology 2005;10(4):339-345.

126. Hansen JB, Tonnesen MF, Madsen AN, Hagedorn PH, Friberg J, Grunnet LG, Heller RS, Nielsen Aÿ, St¯rling J, Baeyens L, Anker-Kitai L, Qvortrup K, Bouwens L, Efrat S, Aalund M*, et al.* Divalent Metal Transporter 1 Regulates Iron-Mediated ROS and Pancreatic ≤ Cell Fate in Response to Cytokines. Cell Metabolism 2012;16(4):449-461.

127. Ruas M, Rietdorf K, Arredouani A, Davis LC, Lloyd-Evans E, Koegel H, Funnell TM, Morgan AJ, Ward JA, Watanabe K, Cheng X, Churchill GC, Zhu MX, Platt FM, Wessel GM*, et al.* Purified TPC Isoforms Form NAADP Receptors with Distinct Roles for Ca^{2+} Signaling and Endolysosomal Trafficking. Current Biology 2010;20(8):703-709.

128. Li K, Besse EK, Ha D, Kovtunovych G, Rouault TA. Iron-dependent regulation of frataxin expression: implications for treatment of Friedreich ataxia. Human Molecular Genetics 2008;17(15):2265-2273.

129. Friedreich's ataxia: iron chelators that target the mitochondrion as a therapeutic strategy? Expert Opinion on Investigational Drugs 2003;12(2):235-245.

130. Blom TS, Linder MD, Snow K, Pihko H, Hess MW, Jokitalo E, Veckman V, Syvänen A-C, Ikonen E. Defective endocytic trafficking of NPC1 and NPC2 underlying infantile Niemann–Pick type C disease. Human Molecular Genetics 2003;12(3):257-272.

131. Whitnall M, Rahmanto YS, Huang ML-H, Saletta F, Lok HC, Gutiérrez L, Lázaro FJ, Fleming AJ, St. Pierre TG, Mikhael MR, Ponka P, Richardson DR. Identification of nonferritin mitochondrial iron deposits in a mouse model of Friedreich ataxia. Proceedings of the National Academy of Sciences 2012;109(50):20590-20595.

132. Hider RC, Roy S, Ma YM, Le Kong X, Preston J. The potential application of iron chelators for the treatment of neurodegenerative diseases. Metallomics 2011;3(3):239-249.

133. Oshiro S, Morioka MS, Kikuchi M. Dysregulation of iron metabolism in Alzheimer's disease, Parkinson's disease, and amyotrophic lateral sclerosis. Advances in Pharmacological Sciences 2011;2011:378278.

134. Schneider S, Bhatia K. Excess iron harms the brain: the syndromes of neurodegeneration with brain iron accumulation (NBIA). J Neural Transm 2013;120(4):695-703.

135. Cho H-H, Cahill CM, Vanderburg CR, Scherzer CR, Wang B, Huang X, Rogers JT. Selective Translational Control of the Alzheimer Amyloid Precursor Protein Transcript by Iron Regulatory Protein-1. Journal of Biological Chemistry 2010;285(41):31217-31232.

136. Rodrıguez-Rodrıguez E, Vázquez-Higuera JL, Sánchez-Juan P, Mateo I, Pozueta A, Martínez-García A, Frank A, Valdivieso F, Berciano J, Bullido MJ, Combarros O. Epistasis Between Intracellular Cholesterol Trafficking-Related Genes (NPC1 and ABCA1) and Alzheimer's Disease Risk. Journal of Alzheimer's Disease 2010;21(2):619-625.

137. Zorzi G, Zibordi F, Chiapparini L, Nardocci N. Therapeutic Advances in Neurodegeneration With Brain Iron Accumulation. Seminars in Pediatric Neurology 2012;19(2):82-86.

138. Jeyakumar M, Thomas R, Elliot‐Smith E, Smith DA, van der Spoel AC, d'Azzo A, Hugh Perry V, Butters TD, Dwek RA, Platt FM. Central nervous system inflammation is a hallmark of pathogenesis in mouse models of GM1 and GM2 gangliosidosis. Brain 2003;126(4):974-987.

139. Devlin C, Pipalia NH, Liao X, Schuchman EH, Maxfield FR, Tabas I. Improvement in Lipid and Protein Trafficking in Niemann-Pick C1 Cells by Correction of a Secondary Enzyme Defect. Traffic 2010;11(5):601-615.

140. Maret W. Zinc biochemistry: from a single zinc enzyme to a key element of life. Adv Nutr 2013;4(1):82-91.

141. Barnes N, Tsivkovskii R, Tsivkovskaia N, Lutsenko S. The Copper-transporting ATPases, Menkes and Wilson Disease Proteins, Have Distinct Roles in Adult and Developing Cerebellum. Journal of Biological Chemistry 2005;280(10):9640-9645.

142. Siggs OM, Cruite JT, Du X, Rutschmann S, Masliah E, Beutler B, Oldstone MBA. Disruption of copper homeostasis due to a mutation of Atp7a delays the onset of prion disease. Proceedings of the National Academy of Sciences 2012;109(34):13733-13738.

143. Ding X, Xie H, Kang YJ. The significance of copper chelators in clinical and experimental application. The Journal of Nutritional Biochemistry 2011;22(4):301-310.

144. Foster M, Samman S. Zinc and Regulation of Inflammatory Cytokines: Implications for Cardiometabolic Disease. Nutrients 2012;4(7):676-694.

145. McCormick NH, Kelleher SL. ZnT4 provides zinc to zinc-dependent proteins in the trans-Golgi network critical for cell function and Zn export in mammary epithelial cells. American Journal of Physiology - Cell Physiolog 2012;303(3):C291-C297.

146. Babula P, Masarik M, Adam V, Eckschlager T, Stiborova M, Trnkova L, Skutkova H, Provaznik I, Hubalek J, Kizek R. Mammalian metallothioneins: properties and functions. Metallomics 2012;4(8):739-750.

147. Klaassen CD, Liu J, Choudhuri S. METALLOTHIONEIN: An Intracellular Protein to Protect Against Cadmium Toxicity. Annual Review of Pharmacology and Toxicology 1999;39(1):267-294.

148. Medici V, Santon A, Sturniolo G, D'Incà R, Giannetto S, Albergoni V, Irato P. Metallothionein and antioxidant enzymes in Long-Evans Cinnamon rats treated with zinc. Arch Toxicol 2002;76(9):509-516.

149. Ayton S, Lei P, Bush AI. Metallostasis in Alzheimer's disease. Free Radical Biology and Medicine 2013;62(0):76-89.

150. Tokuda E, Okawa E, Ono S. Dysregulation of intracellular copper trafficking pathway in a mouse model of mutant copper/zinc superoxide dismutase-linked familial amyotrophic lateral sclerosis. J Neurochem 2009;111(1):181-191.

151. Klein, Lichtmannegger, Heinzmann, Müller H, Michaelsen, Summer. Association of copper to metallothionein in hepatic lysosomes of Long–Evans cinnamon (LEC) rats during the development of hepatitis. European Journal of Clinical Investigation 1998;28(4):302-310.

152. Lopez V, Foolad F, Kelleher SL. ZnT2-overexpression represses the cytotoxic effects of zinc hyper-accumulation in malignant metallothionein-null T47D breast tumor cells. Cancer letters 2011;304(1):41-51.

153. Eichelsdoerfer JL, Evans JA, Slaugenhaupt SA, Cuajungco MP. Zinc Dyshomeostasis Is Linked with the Loss of Mucolipidosis IV-associated TRPML1 Ion Channel. Journal of Biological Chemistry 2010;285(45):34304-34308.

154. Jenkins RW, Idkowiak-Baldys J, Simbari F, Canals D, Roddy P, Riner CD, Clarke CJ, Hannun YA. A novel mechanism of lysosomal acid sphingomyelinase maturation: requirement for carboxyl-terminal proteolytic processing. J Biol Chem 2011;286(5):3777-3788.

155. Dodge JC, Clarke J, Treleaven CM, Taksir TV, Griffiths DA, Yang W, Fidler JA, Passini MA, Karey KP, Schuchman EH, Cheng SH, Shihabuddin LS. Intracerebroventricular infusion of acid sphingomyelinase corrects CNS manifestations in a mouse model of Niemann–Pick A disease. Experimental Neurology 2009;215(2):349-357.

156. Qiu H, Edmunds T, Baker-Malcolm J, Karey KP, Estes S, Schwarz C, Hughes H, Van Patten SM. Activation of human acid sphingomyelinase through modification or deletion of C-terminal cysteine. J Biol Chem 2003;278(35):32744-32752.

157. Reagan JW, Hubbert ML, Shelness GS. Posttranslational Regulation of Acid Sphingomyelinase in Niemann-Pick Type C1 Fibroblasts and Free Cholesterol-enriched Chinese Hamster Ovary Cells. J Bio Chem 2000;275(48):38104-38110.

158. Hellman NE, Gitlin JD. Ceruloplasmin metabolism and function. Annu Rev Nutr 2002;22(1):439-458.

159. Harris ZL, Durley AP, Man TK, Gitlin JD. Targeted gene disruption reveals an essential role for ceruloplasmin in cellular iron efflux. Proceedings of the National Academy of Sciences 1999;96(19):10812-10817.

160. Kim B-E, Turski ML, Nose Y, Casad M, Rockman HA, Thiele DJ. Cardiac Copper Deficiency Activates a Systemic Signaling Mechanism that Communicates with the Copper Acquisition and Storage Organs. Cell Metabolism 2010;11(5):353-363.

161. Pappu R, Schwab S, Cornelissen I, Pereira J, Regard J, Xu Y, Camerer E, Zheng Y, Huang Y, Cyster J, Coughlin S. Promotion of lymphocyte egress into blood and lymph by distinct sources of sphingosine-1-phosphate. Science 2007;316:295 - 298.

162. Ding W-Q, Liu B, Vaught JL, Yamauchi H, Lind SE. Anticancer Activity of the Antibiotic Clioquinol. Cancer Research 2005;65(8):3389-3395.

163. Zinc acetate for the treatment of Wilson's disease. Expert Opinion on Pharmacotherapy 2001;2(9):1473-1477.

164. Sauer SW, Merle U, Opp S, Haas D, Hoffmann GF, Stremmel W, Okun JG. Severe dysfunction of respiratory chain and cholesterol metabolism in Atp7b−/− mice as a model for Wilson disease. Biochimica et Biophysica Acta (BBA) - Molecular Basis of Disease 2011;1812(12):1607-1615.

165. Huster D, Purnat TD, Burkhead JL, Ralle M, Fiehn O, Stuckert F, Olson NE, Teupser D, Lutsenko S. High Copper Selectively Alters Lipid Metabolism and Cell Cycle Machinery in the Mouse Model of Wilson Disease. Journal of Biological Chemistry 2007;282(11):8343-8355.

166. Goez HR, Jacob FD, Fealey RD, Patterson MC, Ramaswamy V, Persad R, Johnson ES, Yager JY. An unusual presentation of copper metabolism disorder and a possible connection with Niemann-Pick type C. J Child Neurol 2011;26(4):518-521.

167. Connemann BJ, Gahr M, Schmid M, Runz H, Freudenmann RW. Low ceruloplasmin in a patient with Niemann-Pick Type C disease. Journal of clinical neuroscience : official journal of the Neurosurgical Society of Australasia 2012;19(4):620-621.

168. Li X, Jankovic J, Le W. Iron chelation and neuroprotection in neurodegenerative diseases. J Neural Transm 2011;118(3):473-477.

169. Park M-H, Lee S-J, Byun H-r, Kim Y, Oh YJ, Koh J-Y, Hwang JJ. Clioquinol induces autophagy in cultured astrocytes and neurons by acting as a zinc ionophore. Neurobiology of Disease 2011;42(3):242-251.

170. Anderson L, Hakojarvi S, Boudreaux S. Zinc acetate treatment in Wilson's disease. The Annals of Pharmacotherapy 1998;32(1):78-87.

171. Harada M, Kawaguchi T, Kumemura H, Terada K, Ninomiya H, Taniguchi E, Hanada S, Baba S, Maeyama M, Koga H, Ueno T, Furuta K, Suganuma T, Sugiyama T, Sata M. The Wilson Disease Protein ATP7B Resides in the Late Endosomes with Rab7 and the Niemann-Pick C1 Protein. The American Journal of Pathology 2005;166(2):499-510.

172. Yanagimoto C, Harada M, Kumemura H, Abe M, Koga H, Sakata M, Kawaguchi T, Terada K, Hanada S, Taniguchi E, Ninomiya H, Ueno T, Sugiyama T, Sata M. Copper incorporation into ceruloplasmin is regulated by Niemann–Pick C1 protein. Hepatology Research 2011;41(5):484-491.

173. Grossi C, Francese S, Casini A, Rosi MC, Luccarini I, Fiorentini A, Gabbiani C, Messori L, Moneti G, Casamenti F. Clioquinol Decreases Amyloid-β Burden and Reduces Working Memory Impairment in a Transgenic Mouse Model of Alzheimer's Disease. Journal of Alzheimer's Disease 2009;17(2):423-440.

174. Domellöf M, Hernell O, Abrams SA, Chen Z, Lönnerdal B. Iron supplementation does not affect copper and zinc absorption in breastfed infants. The American Journal of Clinical Nutrition 2009;89(1):185-190.

175. Hla T, Galvani S, Rafii S, Nachman R. S1P and the birth of platelets. The Journal of Experimental Medicine 2012;209(12):2137-2140.

176. Yatomi Y, Igarashi Y, Yang L, Hisano N, Qi R, Asazuma N, Satoh K, Ozaki Y, Kume S. Sphingosine 1-phosphate, a bioactive sphingolipid abundantly stored in platelets, is a normal constituent of human plasma and serum. J Biochem 1997;121:969 - 973.

177. Spiegel S, Milstien S. Sphingosine-1-phosphate: an enigmatic signalling lipid. Nat Rev Mol Cell Biol 2003;4:397 - 407.

178. Olivera A, Allende ML, Proia RL. Shaping the landscape: Metabolic regulation of S1P gradients. Biochimica et Biophysica Acta (BBA) - Molecular and Cell Biology of Lipids 2013;1831(1):193-202.

179. Khurana S, Raufman J-P, Pallone TL. Bile Acids Regulate Cardiovascular Function. Clinical and Translational Science 2011;4(3):210-218.

180. Edwards PA, Ericsson J. STEROLS AND ISOPRENOIDS: Signaling Molecules Derived from the Cholesterol Biosynthetic Pathway. Annual Review of Biochemistry 1999;68(1):157-185.

181. Robbins DJ, Fei DL, Riobo NA. The Hedgehog signal transduction network. Sci Signal 2012;5(246):re6.

182. Nofer J-R, Herminghaus G, Brodde M, Morgenstern E, Rust S, Engel T, Seedorf U, Assmann G, Bluethmann H, Kehrel BE. Impaired Platelet Activation in Familial High Density Lipoprotein Deficiency (Tangier Disease). Journal of Biological Chemistry 2004;279(32):34032-34037.

183. Schmitz G, Schambeck CM. Molecular Defects in the ABCA1 Pathway Affect Platelet Function. Pathophysiology of Haemostasis and Thrombosis 2006;35(1-2):166-174.

184. Morgan AJ, Platt FM, Lloyd−Evans E, Galione A. Molecular mechanisms of endolysosomal Ca2+ signalling in health and disease. Biochemical Journal 2011;439(3):349-374.

185. Nesbitt WS, Giuliano S, Kulkarni S, Dopheide SM, Harper IS, Jackson SP. Intercellular calcium communication regulates platelet aggregation and thrombus growth. The Journal of Cell Biology 2003;160(7):1151-1161.

186. Galione A, Parrington J, Funnell T. Physiological roles of NAADP-mediated Ca^{2+} signaling. Sci China Life Sci 2011;54(8):725-732.

187. Coxon CH, Lewis AM, Sadler AJ, Vasudevan SR, Thomas A, Dundas KA, Taylor L, Campbell RD, Gibbins JM, Churchill GC, Tucker KL. NAADP regulates human platelet function. Biochemical Journal 2012;441(1):435-442.

188. Dionisio N, Albarrán L, López JJ, Berna-Erro A, Salido GM, Bobe R, Rosado JA. Acidic NAADP-releasable Ca2+ compartments in the megakaryoblastic cell line MEG01. Biochimica et Biophysica Acta (BBA) - Molecular Cell Research 2011;1813(8):1483-1494.

189. Wraith JE, Baumgartner MR, Bembi B, Covanis A, Levade T, Mengel E, Pineda M, Sedel F, Topçu M, Vanier MT, Widner H, Wijburg FA, Patterson MC. Recommendations on the diagnosis and management of Niemann-Pick disease type C. Molecular Genetics and Metabolism 2009;98(1–2):152-165.

190. Imrie J, Wraith JE. Isolated splenomegaly as the presenting feature of Niemann–Pick disease type C. Archives of Disease in Childhood 2001;84(5):427-429.

191. Louwette S, Régal L, Wittevrongel C, Thys C, Vandeweeghde G, Decuyper E, Leemans P, De Vos R, Van Geet C, Jaeken J, Freson K. NPC1 defect results in abnormal platelet formation and function: studies in Niemann–Pick disease type C1 patients and zebrafish. Human Molecular Genetics 2013;22(1):61-73.

192. Patterson MC, Vecchio D, Prady H, Abel L, Wraith JE. Miglustat for treatment of Niemann-Pick C disease: a randomised controlled study. The Lancet Neurology 2007;6(9):765-772.

193. Golfier S, Kondo S, Schulze T, Takeuchi T, Vassileva G, Achtman AH, Gräler MH, Abbondanzo SJ, Wiekowski M, Kremmer E, Endo Y, Lira SA, Bacon KB, Lipp M. Shaping of terminal megakaryocyte differentiation and proplatelet development by sphingosine-1-phosphate receptor S1P4. The FASEB Journal 2010;24(12):4701-4710.

194. Silverstein R, Febbraio M. Identification of lysosome-associated membrane protein-2 as an activation-dependent platelet surface glycoprotein. Blood 1992;80(6):1470-1475.

195. Febbraio M, Silverstein RL. Identification and characterization of LAMP-1 as an activation-dependent platelet surface glycoprotein. Journal of Biological Chemistry 1990;265(30):18531-18537.

196. Lloyd-Evans E, Platt FM. Lysosomal Ca2+ homeostasis: Role in pathogenesis of lysosomal storage diseases. Cell Calcium 2011;50(2):200-205.

197. Roszell BR, Tao J-Q, Yu KJ, Huang S, Bates SR. Characterization of the Niemann-Pick C pathway in alveolar type II cells and lamellar bodies of the lung. American Journal of Physiology - Lung Cellular and Molecular Physiology 2012;302(9):L919-L932.

198. Hall AM, Krishnamoorthy L, Orlow SJ. Accumulation of Tyrosinase in the Endolysosomal Compartment is Induced by U18666A. Pigment Cell Research 2003;16(2):149-158.

199. Claudepierre T, Paques M, Simonutti M, Buard I, Sahel J, Maue RA, Picaud S, Pfrieger FW. Lack of Niemann–Pick type C1 induces age-related degeneration in the mouse retina. Molecular and Cellular Neuroscience 2010;43(1):164-176.

200. Wagner DD. New Links Between Inflammation and Thrombosis. Arteriosclerosis, Thrombosis, and Vascular Biology 2005;25(7):1321-1324.

201. Esposito B, Gambara G, Lewis AM, Palombi F, D'Alessio A, Taylor LX, Genazzani AA, Ziparo E, Galione A, Churchill GC, Filippini A. NAADP links histamine H1 receptors to secretion of von Willebrand factor in human endothelial cells. Blood 2011;117(18):4968-4977.

202. Schieder M, Rötzer K, Brüggemann A, Biel M, Wahl-Schott CA. Characterization of Two-pore Channel 2 (TPCN2)-mediated Ca^{2+} Currents in Isolated Lysosomes. Journal of Biological Chemistry 2010;285(28):21219-21222.

203. Fakih S, Podinovskaia M, Kong X, Collins HL, Schaible UE, Hider RC. Targeting the Lysosome: Fluorescent Iron(III) Chelators To Selectively Monitor Endosomal/Lysosomal Labile Iron Pools. Journal of Medicinal Chemistry 2008;51(15):4539-4552.

204. Fakih S, Podinovskaia M, Kong X, Schaible UE, Collins HL, Hider RC. Monitoring intracellular labile iron pools: A novel fluorescent iron(III) sensor as a potential non-invasive diagnosis tool. Journal of Pharmaceutical Sciences 2009;98(6):2212-2226.

205. Becker JS, Matusch A, Palm C, Salber D, Morton KA, Becker JS. Bioimaging of metals in brain tissue by laser ablation inductively coupled plasma mass spectrometry (LA-ICP-MS) and metallomics. Metallomics 2010;2(2):104-111.

206. Ye H, Rouault TA. Human Iron−Sulfur Cluster Assembly, Cellular Iron Homeostasis, and Disease. Biochemistry 2010;49(24):4945-4956.

207. Huang ML-H, Becker EM, Whitnall M, Rahmanto YS, Ponka P, Richardson DR. Elucidation of the mechanism of mitochondrial iron loading in Friedreich's ataxia by analysis of a mouse mutant. Proceedings of the National Academy of Sciences 2009;106(38):16381-16386.

208. Armstrong JS, Khdour O, Hecht SM. Does oxidative stress contribute to the pathology of Friedreich's ataxia? A radical question. The FASEB Journal 2010;24(7):2152-2163.

209. Byrne SL, Krishnamurthy D, Wessling-Resnick M. Pharmacology of Iron Transport. Annual Review of Pharmacology and Toxicology 2013;53(1):17-36.

210. Singh I, Sagare AP, Coma M, Perlmutter D, Gelein R, Bell RD, Deane RJ, Zhong E, Parisi M, Ciszewski J, Kasper RT, Deane R. Low levels of copper disrupt brain amyloid-β homeostasis by altering its production and clearance. Proceedings of the National Academy of Sciences 2013;110(36):14771-14776.

211. Park S-J, Kim N-H, Jeong B-H, Jin J-K, Choi J-K, Park Y-J, Kim J-I, Carp RI, Kim Y-S. The effect of Fenton reaction on protease-resistant prion protein (PrPSc) degradation and scrapie infectivity. Brain Research 2008;1238(0):172-180.

212. Helman RG, Adams LG, Pierce KR, Bridges CH, Bailey EM. The role of lysosomes in the pathogenesis of copper-induced hepatotoxicity: Morphological studies. Journal of Comparative Pathology 1985;95(1):25-35.

213. Rosado JA. Acidic Ca2+ stores in platelets. Cell Calcium 2011;50(2):168-174.

214. Zhu MX, Ma J, Parrington J, Galione A, Mark Evans A. TPCs: Endolysosomal channels for Ca^{2+} mobilization from acidic organelles triggered by NAADP. FEBS Letters 2010;584(10):1966-1974.

215. Cox TM, Cachón-González MB. The cellular pathology of lysosomal diseases. The Journal of Pathology 2012;226(2):241-254.

216. Dusek P, Jankovic J, Le W. Iron dysregulation in movement disorders. Neurobiology of Disease 2012;46(1):1-18.

217. Lopez V, Kelleher SL. Zinc transporter-2 (ZnT2) variants are localized to distinct subcellular compartments and functionally transport zinc. Biochemical Journal 2009;422(1):43-52.

218. Treiber C, Simons A, Strauss M, Hafner M, Cappai R, Bayer TA, Multhaup G. Clioquinol Mediates Copper Uptake and Counteracts Copper Efflux Activities of the Amyloid Precursor Protein of Alzheimer's Disease. Journal of Biological Chemistry 2004;279(50):51958-51964.